MASTER

BAW-120, Rev. 1

CONSOLIDATED EDISON THORIUM REACTOR
PHYSICS DESIGN

Issued March 1960
Revised July 1960
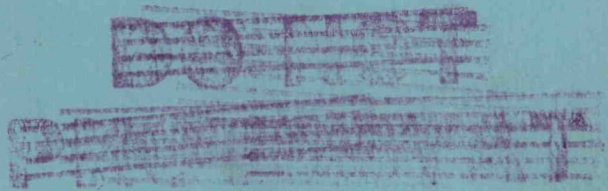
540    001

# THE BABCOCK & WILCOX COMPANY

## ATOMIC ENERGY DIVISION

## DISCLAIMER

This report was prepared as an account of work sponsored by an agency of the United States Government. Neither the United States Government nor any agency Thereof, nor any of their employees, makes any warranty, express or implied, or assumes any legal liability or responsibility for the accuracy, completeness, or usefulness of any information, apparatus, product, or process disclosed, or represents that its use would not infringe privately owned rights. Reference herein to any specific commercial product, process, or service by trade name, trademark, manufacturer, or otherwise does not necessarily constitute or imply its endorsement, recommendation, or favoring by the United States Government or any agency thereof. The views and opinions of authors expressed herein do not necessarily state or reflect those of the United States Government or any agency thereof.
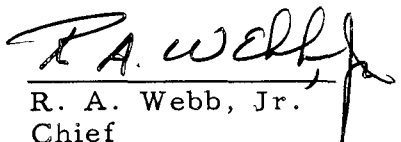
BAW-120, Rev. 1

CONSOLIDATED EDISON THORIUM REACTOR
PHYSICS DESIGN

Issued March 1960
Revised July 1960

By
H. S. Barringer
R. B. Flickinger
S. W. Spetz

Approved by: *R. A. Webb, Jr.*
R. A. Webb, Jr.
Chief
Reactor Physics Section

Approved by: *M. C. Edlund*
M. C. Edlund
Manager
Development Department

PREPARED FOR
THE CONSOLIDATED EDISON COMPANY OF NEW YORK
BY
THE BABCOCK & WILCOX COMPANY
ATOMIC ENERGY DIVISION
Lynchburg, Virginia

# CROSS REFERENCE INDEX

This Cross Reference Index has been prepared to key the supplementary material to the information which is contained in the Hazards Summary Report dated January, 1960, Exhibit K-5 (Rev-1) filed with Amendment No. 10 to Consolidated Edison's Application for Licenses.

## SECTION 2 - REACTOR DESIGN

2.1 - REACTOR DESCRIPTION        EXHIBIT NO.

### 2.1.1 Reactor Vessel and Its Internal Structure

Consolidated Edison Thorium Reactor Reactor Vessel Internal Components Design (Report BAW-136)      K-5A1

### 2.1.2 Fuel Element Design

Fuel Element Structural Design and Manufacture for the Consolidated Edison Thorium Reactor Plant (Report BAW-133)      ˎK-5A2

### 2.1.3 Control Rods, Fixed Shim Rods and Flux Depressors

Design of the Movable and Fixed Control Components for the Consolidated Edison Thorium Reactor (Report BAW-147)      K-5A3

## 2.2 - THERMAL AND HYDRAULIC DESIGN

### 2.2.1 General Design Data

Thermal and Hydraulic Design of the Consolidated Edison Thorium Reactor (Report BAW-132)      K-5A4

### 2.2.2 Design Methods and Correlations

Thermal and Hydraulic Design of the Consolidated Edison Thorium Reactor (Report BAW-132)      K-5A4

Irradiation Test Program for the Consolidated Edison Thorium Reactor (Report BAW-134)      K-5A5

3. 1. 3 Seal Water and Primary Makeup System

Supplementary Information on Plant
Design of Consolidated Edison Nuclear
Steam Generating Station                    K-5A11

3. 1. 4 Primary Relief System

Supplementary Information on Plant
Design of Consolidated Edison Nuclear
Steam Generating Station                    K-5A11

3. 1. 5 Primary Vent System

Supplementary Information on Plant
Design of Consolidated Edison Nuclear
Steam Generating Station                    K-5A11

3. 2 - SECONDARY SYSTEMS

Exhibit K-5A11 contains an introductory section
entitled, "Conventional Plant Features Contributing
to Nuclear Plant Safety." In addition, this exhibit
contains supplementary data on the following systems:

3. 2. 1   Steam Piping System
3. 2. 2   Secondary Relief System
3. 2. 3   Boiler Feed System
3. 2. 4   Boiler Blowdown System

3. 3 - SUPPORTING SYSTEMS

3. 3. 1 Chemical Processing Systems

Supplementary Information on Plant
Design of Consolidated Edison Nuclear
Steam Generating Station                    K-5A11

The Effects of Fuel Rod Fission Product
Leakage on the Consolidated Edison Thorium
Reactor Plant (Report BAW-85 Rev. 1)        K-5A13

Corrosion Product Activity Distribution
Across the Chemical Process System
for the Consolidated Edison Thorium Reactor
(Report BAW-142 Rev. 1)                     K-5A14

3. 3. 2   Boron Addition System
3. 3. 3   Decay Heat Cooling System
3. 3. 4   Component Drain System
3. 3. 5   Sampling System
3. 3. 6   Fresh Water Cooling System
3. 3. 7   Electrical System

Additional data on these six supporting
systems described in the Hazards Summary
Report is contained in the report, "Supplementary
Information on Plant Design of Consolidated
Edison Nuclear Steam Generating Station"     K-5A11

## 3.4 - INSTRUMENTATION AND CONTROL

### 3.4.1 Nuclear Instrumentation

### 3.4.3 Reactor Control System

### 3.4.5 Radiation Monitoring

## 3.7 - HANDLING SYSTEMS

## SECTION 4 - INCIDENT ANALYSIS

## 4.4 - MECHANICAL INCIDENTS

### 4.4.2 Incidents Involving Reduction or Loss of Forced Coolant Flow

CONTENTS

CONTENTS (Cont'd)

# LIST OF TABLES

# LIST OF FIGURES

LIST OF FIGURES (Cont'd)

# LIST OF FIGURES (Cont'd)

# SECTION 1
## INTRODUCTION

### 1.1 SCOPE OF REPORT

This repórt describes the nuclear characteristics of the Consolidated Edison Thorium Reactor (CETR). The CETR is a pressurized water reactor with nuclear fuel composed of thorium and fully enriched uranium oxides contained in stainless steel tubes. The reactor power output is 585 MW of heat. Major aspects of design that are discussed in this report are the core operating lifetime, control rod worth, and the power density distribution. The objectives of the nuclear design have been to maximize the core operating life, to minimize the power density variation, and to assure control of the reactor. The results of the design calculations give the reactor lifetime of 600 days, the power density maximum less than 4.1 times the average and assurance that the control rods keep the reactor at least 2% subcritical under the worst normal conditions.

### 1.2 METHODS OF DESIGN

The fundamental design work has been done using four group, 2-dimensional diffusion theory. Core lifetimes were calculated taking into account the effects of epithermal absorptions on the buildup of higher isotopes. Criticality, control rod worth, and power density distributions were determined experimentally for a variety of core lattices. Calculations matched critical conditions at room temperature and agreed with effects of temperature variation measured in exponential experiments. Calculations of control rod worth were matched to experiments at room temperature. Experimental flux shapes around control rods at room and operating temperatures were matched well with computed flux shapes. Power density distributions obtained from calculations agreed well with the experimental data. On the basis of these studies, a sound foundation was formed for the use of the methods to extrapolate to the characteristics of the CETR under operating conditions.

## 1.3 COMPUTER CODES

A large number of the design calculations for the CETR were sufficiently complex that the aid of large digital computers was necessary. Use was made of computer codes which were already available whenever possible. A number of these are mentioned specifically in this report, and they are described here for convenient reference. The proprietary (Babcock and Wilcox Company) codes written for use on the ElectroData 205 Computer are:

(a)  Spectral Code - A 40-group, bare reactor calculation is made to determine criticality, neutron balance, flux variation with energy, and flux weighted effective cross sections for 2-group or 4-group calculations. The Selengut-Goertzel approximation is used for slowing down, and the effects of inelastic scattering are taken into account. Cross sections generally are those given in BNL-325.[1]

(b)  SLEUTH - This code solves the two group diffusion equations in one dimension to determine criticality $(k_{eff})$ and flux shape. The concentrations of materials (fission products, higher isotopes, etc.) flux shapes, and criticality of the reactor at later times are computed in a succession of steps.

(c)  Four Group Code - This code solves the 4-group diffusion equations in one dimension to obtain criticality $(k_{eff})$ and flux shapes.

(d)  Multigroup Code - The diffusion equation is solved in this code in one dimension for either 20 or 40 groups to obtain criticality $(k_{eff})$ and flux shapes. Cross sections are generally those given in BNL-325. The Selengut-Goertzel approximation is used for slowing down, and the effects of inelastic scattering are taken into account.

(e)  Two Group Adjoint Code - This code calculates the flux and adjoint flux distributions and the effective multiplication constant of multi-region, 1-dimensional systems, using the 2-group diffusion equations.

(f)  Temperature Coefficient Code - Using 2-group perturbation theory equations and the results of the Two-Group Adjoint Code, the value of $\delta k_{eff}$ is computed for given changes in temperature. The effects of spatial variation in one dimension are calculated.

The codes generally available and written for use on the IBM-704 computer are:

(g)  PDQ - This is a 2-dimensional diffusion equation code for 1 to 4 groups, which calculates criticality and flux shape.  For details, see the program report, WAPD-TM-70.[2]

(h)  TKO - This is a 3-dimensional diffusion equation code for 2 or 4 groups which calculates criticality and flux shape.  The code is patterned after PDQ.  For details, see the program report WAPD-TM-143.[3]

## 1.4  EXPERIMENTAL BASIS OF DESIGN

The basic experimental information used to verify the calculational model was obtained from critical experiments at room temperature, exponential experiments over a range of temperatures up to 500 F, and resonance integral measurements over a much larger range of temperatures.  These data are reported in other documents which are referred to in the body of this report.  These other documents are:

BAW-31,  Consolidated Edison Thorium Reactor - Critical Experiment on Plate Fuel Elements.[4]

BAW-116,  Consolidated Edison Thorium Reactor - Hot Exponential Experiment.[5]

BAW-119,  Consolidated Edison Thorium Reactor - Critical Experiments with Oxide Fuel Pins.[6]

BAW-144,  Geometric and Temperature Effects in Thorium Resonance Capture.[7]

## SECTION 2
## CORE DESCRIPTION

2..1   GENERAL DESCRIPTION

The Consolidated Edison Thorium Reactor is a pressurized water reactor with nuclear fuel composed of thorium and fully enriched uranium oxides. The fuel is in pellet form and is contained in 0.304 in. OD stainless steel tubes. These fuel rods (pins) are spaced by ferrules. The complete assembly is brazed to form bundles of 195 pins in the form of a square lattice. Each fuel bundle is placed in a Zircaloy-2 fuel element can 5.7 in. square. The active reactor core consists of 120 fuel elements. These form a cylinder with a height of 98.5 inches and a mean diameter of 77.7 inches. Twenty-one movable control rods are mounted between the fuel element cans. Fixed control rods and flux depressor plates are also located between fuel elements. The core and the positions of fuel elements and control members are shown in Figure 2.1. A cross section of a fuel element in Figure 2.2 shows one bundle.

The loading of U-235 in the core is 1100 kg. Three zones within the core are composed of fuel elements with three different fuel loadings. The arrangement of the three zones is shown in Figure 2.1, where Zone I is composed of elements 1-32, Zone II of elements 33-76, and Zone III of elements 77-120.

Internally, each fuel element is composed of fuel rods of several different U-235 concentrations. The core contains fuel pellets of six different thorium to uranium ratios. Figure 2.3 shows the loading arrangement for each of the three different types of fuel elements. This loading arrangement has been determined to satisfy the criteria of the reactor core relative to power distribution, control rod programming, control rod adequacy, and the operating life of the reactor.

## 2.2 ThO$_2$-UO$_2$ OXIDE FUEL

The core contains 1100 kg of U-235 (1344 kg of 93% enriched UO$_2$) and 17,207 kg of ThO$_2$ in the form of UO$_2$-ThO$_2$ pellets of six different thorium to uranium ratios. Table 2.1 shows the loading of the various fuel rods in the core. A summary of the U-235 loadings in each type of fuel element is given in Table 2.2.

The average fuel pellet density is 9.25 gm/cm$^3$. Fuel pellet diameter is 0.260 in. The pellets are stacked to an active fuel length of 98.5 in. at 68 F (99.2 in. at full power) and are placed in stainless steel tubes (clad) to make fuel rods.

## 2.3 FUEL RODS

Fuel clad is 304 stainless steel containing 200-225 ppm natural boron. (The use of this burnable poison is described in Section 4.) The density of the clad is 7.93 gm/cc. The outside diameter of the fuel rod is 0.304 in. and the clad thickness is 0.0205 in. Between the fuel pellets and the clad there is a gap (at room temperature) nominally 0.0015 in. thick. This gap is filled with helium gas.

## 2.4 FUEL BUNDLES

Fuel rods are assembled into 14 x 14 square arrays with one corner fuel rod omitted. The 195 fuel rods are spaced by ferrules (short, thin, tubular sections) and the whole assembly is brazed together to form a bundle 5.2 in. square. Figure 2.2 shows the arrangement of a fuel bundle. Fuel rods are on a square pitch of 0.374 in. Volume fractions for this lattice structure are given in Table 2.3. The metal/water ratio for the lattice only, (defining "metal" as being everything except moderator) is equal to 1.116. (The volume fractions for the complete core are given in Table 3.3.)

The lattice spacing is maintained by the ferrules, which are 304 stainless steel, 0.225 in. OD, 0.189 in. ID, and 0.750 in. long. The ferrules are spaced axially 9 in. center-to-center in planes perpendicular to the longitudinal axis of the bundle. Rows of smaller ferrules (0.125 in. OD x 0.095 in. ID) are spaced around the outside of the bundle to support the outer row of fuel rods and to separate the fuel rods from the can wall. The ferrules are brazed to the outer row of fuel rods.

## TABLE 2.1
### FUEL ROD LOADING SUMMARY

| Rod Type | Pellet Loading (gms U-235/axial in.) | No. Rods/Bundle Zone I | Zone II | Zone III | No. Rods/Zone Zone I | Zone II | Zone III | No. Rods in Core |
|---|---|---|---|---|---|---|---|---|
| A | 0.2049 | 19 | 4 | 2 | 608 | 176 | 88 | 872 |
| B | .2928 | 34 | 25 | 7 | 1088 | 1100 | 308 | 2496 |
| C | .3904 | 139 | 40 | 22 | 4448 | 1760 | 968 | 7176 |
| D | .5292 | 0 | 123 | 24 | 0 | 5412 | 1056 | 6468 |
| E | .6610 | 0 | 0 | 137 | 0 | 0 | 6028 | 6028 |
| F* | 1/3 ThO$_2$ plus 2/3 Type A (0.2049) | 3 | 3 | 3 | 96 | 132 | 132 | 360 |
| Totals | | 195 | 195 | 195 | 6240 | 8580 | 8580 | 23400 |

*Center 32.5 ± 1 in. filled with ThO$_2$ pellets; 33 ± 1 in. at each end filled with Type A pellets.

## TABLE 2.2
### FUEL ELEMENT LOADING SUMMARY

| Rod Type | Mass/Rod in grams | Mass/Bundle in Grams Zone I | Zone II | Zone III |
|---|---|---|---|---|
| A | 20.2 ± 0.4 | 384 | 81 | 40 |
| B | 28.8 ± 0.6 | 981 | 721 | 202 |
| C | 38.5 ± 0.8 | 5,345 | 1,538 | 846 |
| D | 52.1 ± 1.0 | 0 | 6,411 | 1,251 |
| E | 65.1 ± 1.3 | 0 | 0 | 8,921 |
| F | 13.5 ± 0.3 | 40 | 40 | 40 |
| Total Mass of U-235/Bundle | | 6,750 | 8,791 | 11,300 |
| No. of Bundles/Zone | | x 32 | x 44 | x 44 |
| Total Mass U-235 Per Zone | | 216 kg | 387 kg | 497 kg |
| Total Mass of U-235 in Core | 1100 kg | | | |

TABLE 2.3

VOLUME FRACTIONS IN LATTICE

| | | |
|---|---|---|
| Fuel | - | 0.3796 |
| Gap | - | 0.0088 |
| Clad | - | 0.1306 |
| Moderator | - | 0.4727 |
| Ferrules | - | 0.0083 |

The three different fuel bundles that are required for zone loading of the core are described in Table 2.2 and in Fig. 2.1. The figure shows where each rod type is placed in the bundles of Zones I, II and III. Atom concentrations for a unit cell with the volume fractions of Table 2.3 are given for each fuel rod type in Table 2.4.

TABLE 2.4

ATOM CONCENTRATIONS FOR CLEAN LATTICE

(Tabulated Numbers x $10^{24}$ = Atoms/cm$^3$)

| Material | A | B | C | D | E | F |
|---|---|---|---|---|---|---|
| Thorium | .007660 | .007553 | .007454 | .007266 | .007105 | .007743 |
| U-235 | .0002292 | .0003275 | .0004367 | .0005919 | .0007394 | .0001528 |
| U-238 | .0000173 | .0000247 | .0000329 | .0000446 | .0000557 | .0000115 |

| Material | | |
|---|---|---|
| Hydrogen ( 68 F) | .03158 | |
| (500 F) | .02495 | |
| Boron | .0000125 | Identical in all types of rods |
| Oxygen ( 68 F) | .0316 | |
| (500 F) | .0283 | |
| Stainless Steel | .01176 | |

## 2.5 FUEL ELEMENT CANS

The can is made of Zircaloy-2 in the form of an envelope surrounding the fuel bundle and is shown in Fig. 2.2. Cans are 5.711 in. square and 0.155 in. thick. Radius of curvature at the corners is 0.25 in. inside. Zone loading requires specific fuel bundle orientation in the core. This is accomplished by orienting the bundle within the can and orienting the can within the core. The missing corner fuel rod in the bundle and an index strip in one corner of the can insure proper rotational orientation within the can. Two Zircaloy-2 flow blocks are attached to each element to reduce power peaking and distribute coolant flow in the fixed shim rod channel.

## 2.6   THE COMPLETE ACTIVE CORE

One hundred twenty fuel elements comprise the active core.   These are arranged on a pitch of 6.32 in. in the pattern shown in Fig. 2.1. Zone I contains 32 elements; Zones II and III contain 44 elements each. Elements in these zones have a 3:3:9:5 mass ratio of U-235 loaded as shown in Table 2.2.   The equivalent core diameter of this arrangement is 77.7 in. (197.3 cm); the core height is 98.5 in. (250.2 cm) cold and 99.2 in. (252.0 cm) at full power.

The use of the Zircaloy-2 flow blocks on the periphery of the can assures correct orientation of the bundle in core.   And the use of index strips permits the proper orientation of the fuel rods within each bundle. The combination of both centering devices assures positive location of individual fuel rods in the active core.

## 2.7   CONTROL RODS, FIXED SHIM RODS AND FLUX DEPRESSORS

The 21 movable control rods are located in a square pattern as shown in Fig. 2.1.   They are cruciform hafnium rods of density 12.65 gms/cc.   Rod composition is 95.4% Hf, 4.5% Zr, and assorted impurities equivalent to $1.04 \times 10^{19}$ atoms of boron/cc.   Movable rods are 0.300 in. thick and have 10 in. blade width.   They are spaced at 12.645 in. intervals.   The rods are attached to cruciform Zircaloy-2 follower rods of the same dimensions.   The hafnium rods are 96.5 in. long and travel 91 in. between the full in and full out positions.

The design allows for the use of as many as 24 fixed shim rods of boron containing stainless steel to adjust core reactivity.   Determination of the required number of shims must await final calibration tests of the core.   These rods are also cruciform shape and are 10 in. wide by 0.125 in. thick.   The stainless steel, base type 304, contains 1% boron by weight enriched to 80% B-10 by weight.   Rod density is 7.87 gms/cc.   Spaces not occupied by fixed shims will be filled with Zircaloy-2 fixed filler rods of the same geometry and dimensions as the shim rods.

There are other water channels at the periphery of the core not occupied by either fixed or movable rods.   In order to avoid localized power peaking in the fuel rods next to these channels, they are filled

with flux depressors made of type 304 stainless steel plates. These plates vary in shape to conform to the geometry of the channels occupied and are 0.125 in. thick with 4.875 in. arms. The flux depressors occupy all but the top two feet of the active core.

## 2.8   IMMEDIATE SURROUNDINGS OF ACTIVE CORE

Twenty-eight hold down columns are placed around the perimeter of the core as shown in Fig. 2.1. These are stainless steel cans which do not contain fuel rods. The first annular thermal shield comes at a distance of 47 in. from the axial center line of active core and is 1 in. thick type 304 stainless steel. The upper and lower reflectors consist of the fuel rod end caps and transition pieces. For nuclear purposes they are 90% water and 10% stainless steel.

# SECTION 3
# CORE LIFETIME AND RELATED REACTIVITY EFFECTS

## 3.1  GENERAL DISCUSSION

The operation of the CETR at full power involves the burnup of U-235 and at the same time the conversion of thorium to new U-233 fuel. Since the burnup of U-235 is faster than the formation of U-233, extra U-235 fuel is built into the reactor core initially. The reactivity (excess multiplication) associated with this fuel is controlled with the control rods. As the fuel is burned, the control rods are removed from the core. After an extended period, the control rods are completely removed from the core and criticality no longer can be maintained at full power. The length of time until this happens is called the core lifetime, or reactivity lifetime. The reactivity lifetime of the CETR core was determined by analytical methods. Critical experiments were used to develop the methods of calculation of initial reactivity. The estimates of possible errors in the reactivity of the initial full power core were determined by comparisons of experimental results with the results of the calculational methods.

Many reactivity factors affect the lifetime of the CETR core. Some of these factors have been determined experimentally. Measurements were made at the Critical Experiment Laboratory to determine the temperature deficit, the power doppler effect, and the reactivity and rod worth of zone loaded cores. Generally, the experiments did not mock up the exact fuel concentrations, geometries, and temperatures present in the reference design. In order to determine reactivity effects in the CETR reference design, analytical treatment of the measured situation was used as the basis for development of adequate calculational methods. Comparisons of measured and calculated results provided a basis for the estimation of possible errors in the calculation of various reactivity effects of the reference core with temperature and power level.

Two dimensional, four group calculations were used to determine the initial reactivity of the core. The estimated maximum error in the calculation of $k_{eff}$ by this method is $\pm 0.03 \Delta k_{eff}$ for the initial hot operating core. This estimate is based on comparison of calculations with critical experiments, hot exponential experiments, and measurements of the Doppler effect as a function of temperature. The loading of the CETR has been set to give an expected core lifetime of 600 full power days. If the reactivity of the core is three percent lower than expected, the core lifetime would be no less than 350 full power days. If the reactivity is three percent higher than expected, the core lifetime would be greater than 750 full power days.

The reactivity requirements for equilibrium xenon and samarium, temperature, Doppler effect in thorium, burnup of fuel, and buildup of fission product poisons are shown in Table 3.1.

TABLE 3.1

REACTIVITY REQUIREMENTS

| Effect | $\Delta k_{eff}$ |
|---|---|
| Equilibrium Xenon-135 | 2.3 |
| Equilibrium Samarium-149 | 0.7 |
| Temperature (68 F - 501 F) | 3.4 |
| Power Doppler (hot, zero to full power) | 2.1[*] |
| Burnup of Fuel and Buildup of Fission Products (shim) | 5.4[**] |
| | 13.9 |

[*] Based on an average fuel temperature of 1870 F.
[**] Includes complete transient xenon override for about 600 full power days of operation.

The core contains boron which is alloyed with the stainless steel cladding of the fuel rods. As the core is operated at power, the boron is consumed resulting in a substantial increase in the life of the core. The initial reactivity worth of the initial boron concentration (200-225

parts per million in the cladding) is 0.021 to 0.024 $\Delta k_{eff}$. Core lifetime studies show a continuous decrease in the reactivity of the core during full power operation. The negative reactivity effects associated with fuel depletion and fission products poisoning were greater than the positive reactivity effect that results from burnable poison depletion.

## 3.2  REACTIVITY LIFETIME

The reactivity lifetime of the reference core was computed by a combination of one dimensional two group lifetime calculations. Lifetime calculations were made using SLEUTH, and both radial and axial flux variation were investigated. The calculational model for the radial lifetime was based on a three region zone loaded, reflected core. The initial material concentrations and nuclear parameters are given in Table 3.2. The subscript notation for heavy isotopes in this table and other portions of the report is defined by: 25 = U-235, 28 = U-238, 23 = U-233, 02 = Th-232, 13 = Pa-233.

One dimensional radial lifetime computations assume that the flux and burnup in the transverse or axial direction is uniform. In the physical case, however, the burnup in the axial direction is nonuniform. Nonuniform burnup leads to reactivities different from the uniform burnup case primarily because burnup is concentrated in the regions of high importance, and secondarily because the flux distribution is perturbed causing changes in leakage. The net reactivity change is a balance between competing effects. Reactor produced poisons build in nonuniformly, depressing reactivity more than in the uniform case. This effect predominates early in life with the build up xenon and samarium. The late life is dominated by the nonuniform burnup of fuel. Since the fuel burns faster in the high importance regions, reactivity falls more rapidly than if the core were burned uniformly. A competing effect is in operation if a burnable poison is present since reactivity increases as it burns. Therefore, one dimensional lifetime calculations are in error by the difference between the uniform and nonuniform transverse calculations. Two dimensional burnup is treated exactly in the "Turbo" Code, but this program will not handle the thorium chain. As an alternate, an accurate solution can be obtained by synthesis methods. An estimate of the effect of nonuniform axial burnup has been obtained in this fashion.

TABLE 3.2

## NUCLEAR DATA FOR THE HOMOGENIZED
## CETR REFERENCE CORE

| | Core Region | | | Reflector |
|---|---|---|---|---|
| | 1 | 2 | 3 | |
| Outer Radius, cm | 51.26 | 78.99 | 99.25 | 120 |
| $k_{\infty}$ | 1.0885 | 1.159 | 1.220 | ---- |
| $k_{1\infty}$ | .2693 | .339 | .410 | ---- |
| $k_{2\infty}$ | .8192 | .820 | .810 | ---- |
| $D_1$, cm | 1.49 | 1.50 | 1.51 | 2.05 |
| $D_2$, cm | .350 | .340 | .330 | .247 |
| $\tau$, cm$^2$ | 56.8 | 56.6 | 55.1 | 53.0 |
| $\xi\Sigma_s$, cm$^{-1}$ | .532 | .529 | .550 | 1.095 |
| $\epsilon_{02}$ | 1.01 | 1.01 | 1.01 | ---- |
| $\eta_{res}$ | 1.618 | 1.618 | 1.618 | ---- |
| $\eta_{th}$ | 2.07 | 2.07 | 2.07 | ---- |
| $\bar{\eta}$ | 1.936 | 1.915 | 1.901 | ---- |
| $P_{02}$ | .796 | .798 | .814 | ---- |
| $P_{25}$ | .782 | .725 | .672 | ---- |
| $P_{SS}$ | .959 | .959 | .953 | ---- |
| $P_{28}$ | .991 | .988 | .985 | ---- |
| $P_{Zr-2}$ | .998 | .998 | .998 | ---- |
| $P_{total}$ | .587 | .544 | .510 | ---- |
| f | .667 | .722 | .759 | ---- |
| $\Sigma_{25}^a$, cm$^{-1}$ | .115 | .150 | .192 | ---- |
| $\Sigma_{total}^a$, cm$^{-1}$ | .172 | .207 | .254 | .0115 |
| $B^2$, cm$^{-2}$ | .00064 | .00064 | .00064 | .00064 |
| $N_{25}$, cm$^{-3}$ x $10^{-24}$ | .000268 | .000349 | .000449 | ---- |
| $N_{02}$, cm$^{-3}$ x $10^{-24}$ | .00511 | .00502 | .00491 | ---- |
| $N_{H_2O}$, cm$^{-3}$ x $10^{-24}$ | .0127 | .0127 | .0132 | .0264 |
| $N_{SS}$, cm$^{-3}$ x $10^{-24}$ | .0080 | .0080 | .0096 | ---- |
| $N_{Zr-2}$, cm$^{-3}$ x $10^{-24}$ | .00678 | .00678 | .00522 | ---- |
| $N_{28}$, cm$^{-3}$ x $10^{-24}$ | .000020 | .000026 | .000034 | ---- |
| $N_{B_{10}}$, cm$^{-3}$ x $10^{-24}$ | .0000016 | .0000016 | .0000016 | ---- |

## TABLE 3.2

### NUCLEAR DATA FOR THE HOMOGENIZED
### CETR REFERENCE CORE (CONT'D)

|  | Core Region 1 | Core Region 2 | Core Region 3 | Reflector |
|---|---|---|---|---|
| $R_{02}$, barns | 23.8 | 23.8 | 23.0 | - - - - |
| $R_{25}$, barns | 487 | 487 | 487 | - - - - |
| $R_{SS}$, barns | 2.75 | 2.75 | 2.75 | - - - - |
| $R_{Zr-2}$, barns | .17 | .17 | .17 | - - - - |
| $R_{28}$, barns | 240 | 240 | 240 | - - - - |

The difference between the uniform and nonuniform axial burnup was calculated using SLEUTH. The scheme required the running of a single region uniform burnup axial case for direct comparison with the multiregion nonuniform axial burnup cases. The result of the radial lifetime calculation with uniform axial burnup is shown in Fig. 3.1 where the multiplication constant, $k_{eff}$, as a function of time is plotted. Fig. 3.2 shows the axial calculations used to adjust the radial lifetime curve to give the best estimate of the reactivity lifetime of the core. The uniform burnup curve has the same assumption made in the radial lifetime calculation. The cosine burnup curve shows the axial lifetime with nonuniform burnup based on no control rod motion. If the core contained no rods, the difference between these curves would be the correction to be made on the radial lifetime. The third curve is the best calculational estimate of the axial burnup of the reactor core. This curve was generated by using three groups of control rods simu-lated by homogenized poison, and by withdrawing one group of rods at a time to keep the system critical throughout core life. Life ended when all three groups of rods were withdrawn. The details of this study are discussed more completely in Section 5. The curve of Fig. 3.1 was adjusted by the difference between the curves of Fig. 3.2 to give the expected reactivity curve for the reference core. The re-sultant reactivity-life curve is shown in Fig. 3.3. This figure does not include the effects of the fixed shim rods.

### 3.2.1 Nominal Core Lifetime

The nominal or best estimate of the operating lifetime curve of the reference core is shown in Fig. 3.4. The figure shows $k_{eff}$ of the core as a function of temperature and time of full power operation. This nominal case has four fixed shim rods controlling 1% in reactivity. At 450 F the core has an excess reactivity 0.101 $\Delta k_{eff}$, which is .034 $\Delta k_{eff}$ less than that controlled by the movable rods. Thus the shutdown margin at 450 F is .034 $\Delta k_{eff}$. The lifetime of the core is 530 days for full xenon override. Following this period the reactor still can be run to 600 days if partial xenon override is acceptable. Also the core life can be increased beyond 530 days if the four fixed shim rods are removed. In this situation the core life will be 600 days for full xenon override, and 640 days if it is not necessary to override peak xenon.

It is expected in the nominal case that .010 $\Delta k_{eff}$ will be held by the fixed shim rods, and these calculations have been made with the rods in the core. Other core lifetime calculations have been performed assuming that these rods were not in the core. These other results must be corrected before they can be compared directly with the nominal case. Table 3.3 gives the nuclear performance characteristics and the balances of fertile and fissionable material at startup and the end of 600 full power days.

### 3.2.2 Effect of Possible Errors on Reactivity Lifetime

The initial reactivity and the lifetime of the core can be calculated within certain limits of error. These errors that may effect the lifetime arise as follows:

(a) The reactivity of the cold clean core can be computed within $\pm$ .01 $\Delta k_{eff}$.

(b) Hot exponential experiments indicate that the decrease in core reactivity with temperature between 68 F and 501 F can be computed to within $\pm$ .005 $\Delta k_{eff}$. For this analysis the more conservative limit of $\pm$ .01 $\Delta k_{eff}$ is used. The error on the reactivity change between 68 F and 450 F is $\pm$ .007 $\Delta k_{eff}$.

TABLE 3.3

NUCLEAR DESIGN CHARACTERISTICS

| Initial Loadings | kg (total) |
|---|---|
| Uranium-235 | 1,100 |
| Thorium Oxide (fertile material) | 17,207 |

| Loadings at End of 600 Days of Full Power Operation | kg (total) |
|---|---|
| Uranium-233 | 147 |
| Uranium-234 | 9 |
| Uranium-235 | 695 |
| Uranium-236 | 76 |
| Protactinium-233 | 14 |
| Thorium Oxide | 16,950 |

| | |
|---|---|
| Average Thermal Neutron Flux at 585 MW | $1.5 \times 10^{13} n/cm^2\text{-sec}$ |
| Conversion ratio* | 0.46 |
| Equivalent Core Diameter | 197.3 cm |
| Core Height (Full Power) | 252.0 cm |
| Total Core Volume | 7,705 liters |

Core Volume Fractions

| Material | Volume Fraction |
|---|---|
| Water | 0.48597 |
| Fuel | 0.26435 |
| Stainless Steel | 0.09020 |
| Zr-2 | 0.10084 |
| Helium | 0.00405 |
| Control Rods | 0.03672 |
| Fixed Rods | 0.01787 |
| Metal/Water Ratio | 1.0577 |

*The conversion ratio is defined as the ratio of the total fuel produced to the total fuel consumed during the core life.

- 17 -

(c) The loss of reactivity caused by the power coefficient (doppler effect) may be calculated to within $\pm .01 \Delta k_{eff}$. The margin of error is due to the uncertainties in the doppler coefficient and the fuel temperature.

(d) Uncertainties in the burnup analysis are not expected to contribute appreciably to the total error in computed core life. The reason for this is that a large fraction of the possible error in reactivity of the full power core is caused by error in the resonance integral of thorium. An error in the resonance integral of thorium tends to compensate over the core life for the error in initial reactivity that it causes. Thus if the initial reactivity is lower than calculated the core life would be reduced, except that this would be caused in part by a thorium resonance integral higher than computed. The higher resonance absorption means a higher conversion ratio, causing the curve of $k_{eff}$ vs time to drop more slowly, and thus compensating for the reduced initial $k_{eff}$. In a similar fashion, initial reactivity higher than computed would be caused by a resonance integral lower than computed. The longer life caused by the larger initial $k_{eff}$ is compensated by the faster $k_{eff}$ decrease resulting from the lower conversion ratio.

(e) The fission product poisoning that has been used for calculations are such that the poisoning is more likely to be overestimated than underestimated. A thermal poisoning of 65 barns per fission and a resonance poisoning of 248 barns resonance integral per fission for U-235 were used in the calculations. The respective cross section for U-233 poisoning was 52 barns and the resonance integral was 180 barns.

The errors of (a), (b) and (c) may be combined in many ways. The maximum possible variation from the expected core would be

$\pm .01 \Delta k_{eff}$ at 68 F clean, zero power;

$\pm .017 \Delta k_{eff}$ at 450 F clean, zero power;

$\pm .02 \Delta k_{eff}$ at 501 F clean, zero power;

$\pm\,.03\ \Delta k_{eff}$ at 501 F clean full power, initial;

$<\ \pm\,.03\ \Delta k_{eff}$ full power, after significant operation.

### 3.2.3 Possible Reactivity Lifetime Situations

The error estimates must be considered in terms of the variation permitted by the performance specifications of the CETR. These are concerned mainly with the shutdown margin and the lifetime. The maximum and minimum lifetime situations of the CETR that are reasonably possible have been studied. The extreme cases are presented below.

For safety of the reactor, the control rod worth was designed to be always at least $.02\ \Delta k_{eff}$ greater than the excess reactivity of the core. The crucial conditions occur at the 450 F, clean, zero power stage. Since the error estimates show a possible deviation in $k_{eff}$ at this point of $\pm\,.017\ \Delta k_{eff}$, the rod worth may have to be $.037\ \Delta k_{eff}$ greater than the computed excess reactivity. This is not the case for the nominal core, which has a shutdown margin of only $.034\ \Delta k_{eff}$. The $k_{eff}$ of the actual core will be measured, and if the value is sufficiently higher than the nominal value, eight additional fixed shim rods worth $.02\ \Delta k_{eff}$ will be placed in the core to assure the safe shutdown margin.

If $k_{eff}$ at 450 F falls $.017\ \Delta k_{eff}$ lower than the nominal case, there is certainly no question of the adequacy of shutdown margin, but the core lifetime will be reduced. The minimum possible lifetime of 350 days is very unlikely. This minimum lifetime results if $k_{eff}$ at the full power condition falls $.03\ \Delta k_{eff}$ lower than expected. The 350 day life results since end of life occurs at $k_{eff}$ equal to 1.03 in Fig. 3.3, which is the reactivity curve for the case without fixed shim rods.

## 3.3 STUDIES OF SIGNIFICANT REACTIVITY EFFECTS

Experimental measurements of the criticality of single region lattices and of multi-zone cores served as the bench mark for calculations of excess reactivity. The constants of the Spectral Code, the Four Group Code, and SLEUTH were adjusted to fit the experimental data before extrapolation to the CETR core. Calculations using these codes with the adjusted constants were then compared with experimental buckling data from a series of exponential experiments over the expected CETR range

of temperature. There is good agreement between theory and experiment. Measurements of the doppler coefficient of the thorium resonance integral were used in a 2 group, 3 dimensional (synthesized) calculation to determine the power coefficient of the CETR. In this manner, the excess reactivity of the CETR core between 68 F and 501 F, and between zero and full power, was determined by careful comparison with experimental data.

### 3.3.1 Cold, Clean Reactivity Determination

The object of this study was to obtain a consistent set of constants in the present calculational model for the various CETR pin critical cores that have been operated.[6] Only cores that had no control rod inserted were used in these calculations. The nuclear parameters measured in the cores were used in the calculations. Four infinite lattice and three canned cores were chosen for this study. The four infinite lattice cores use their common designation of 9A, 9B, 7A and 7B. The infinite lattice cores are four combinations of two $ThO_2$-U-235 ratios and two metal-water ratios. The two $ThO_2$-U-235 cores considered have atomic ratios of 15/1 and 25.76/1 respectively; the two metal-water ratios and the corresponding center to center pin spacings are M/W = 1.119 for 0.3805 in. spacing and M/W = 0.892 for 0.4027 in. spacing. The canned cores are: 1) complete inner zone and partial middle zone, 2) complete inner and middle zones, and 3) complete inner, middle and outer zones.

Each of the infinite lattice cores consisted of an assembly of fuel pins and four control rods and rod guides. The rod and rod guide area occupied the space of 60 pins per guide. In these small cores this corresponded to about 10% of the core volume. For a homogeneous calculation, the fuel in the pins and the aluminum guides and water channel would normally be smeared out over the entire core volume. However, in calculating these cores the fuel number densities used were those corresponding to an infinite lattice of unit pin cells. This procedure is backed by experiment since the local guide area of aluminum and water was determined experimentally to have approximately the same reactivity effects as fuel pins in the same area.

The Spectral Code was used to determine the two group diffusion coefficients for SLEUTH. Measured flux depression factors were used when available, and all others inferred from those measured. The cores were also investigated using thermal cross section averaged over a Wigner-Wilkins spectrum. In these cases $k_{eff}$ was approximately 0.005 lower than the value obtained with the Maxwell averaged spectrum. The thorium resonance integrals used were 20 and 18 barns for lattices with metal-water ratios of 0.892 and 1.119 respectively. These values agree with data from single pin resonance integral measurements (BAW-144),[7] and also with the results of cadmium ratio measurements in the experimental lattice (BAW-119).[6] To obtain a best fit to the four single region critical experiments the age was varied in SLEUTH by adding a constant to all the ages computed from the Spectral Code, so that $\tau^{**} = \tau^* +$ constant. This constant was adjusted to obtain $k_{eff}$ as close to 1 as possible for all four cores. Table 3.4 shows the values of $k_{eff}$ computed directly with the Spectral Code, with SLEUTH using constants from the Spectral Code, and with SLEUTH using the adjusted best fit ages. The parameters for the calculations are listed in Table 3.5.

TABLE 3.4

COMPUTED $k_{eff}$ OF SINGLE REGION CRITICAL EXPERIMENTS

| Core | | | | |
|---|---|---|---|---|
| $ThO_2/U$-235 Atomic Ratio | Metal/Water Ratio | Spectral Code | SLEUTH* | SLEUTH** |
| 15/1 | 0.892 | 1.0108 | 1.0114 | 1.0041 |
| 15/1 | 1.119 | 1.0113 | 1.0162 | 1.0094 |
| 25.76/1 | 0.892 | 0.9981 | 0.9940 | 0.9889 |
| 25.76/1 | 1.119 | 1.0035 | 1.0076 | 1.0027 |

* Values using Spectral Code age.

** Values using "best fit" age.

# TABLE 3.5

## PARAMETERS USED IN CALCULATIONS OF $k_{eff}$

|  | 9A | 9B | 7A | 7B |
|---|---|---|---|---|
| $\phi_{water}/\phi_{fuel}$ | 1.17 | 1.13 | 1.14 | 1.09 |
| $\phi_{clad}/\phi_{fuel}$ | 1.14 | 1.11 | 1.12 | 1.07 |
| $D_1$ | 1.452 | 1.439 | 1.471 | 1.452 |
| $D_2$ | 0.222 | 0.235 | 0.229 | 0.214 |
| $\tau^*$ | 43.75 | 46.32 | 44.16 | 46.71 |
| $\tau^{**}$ | 46.0 | 48.5 | 46.4 | 48.9 |
| $R_{02}$ | 20 | 18 | 20 | 18 |
| $R_{25}$ | 485 | 485 | 485 | 485 |

\* Age obtained from Spectral Code.

\*\* "Best fit" age.


A critical lattice with aluminum cans was built to simulate the full CETR core. This multi-zone pin critical core consisted of three zones of 32, 44, and 44 fuel elements. While building up the core to the full three zones, the laboratory obtained two other critical cores of interest. The geometry of the core arrangements is given in Table 3.2 of BAW-119. The three cases which were calculated are:

Case 1 - Minimum Critical

      32 inner zone elements

      22 middle zone elements

Case 2 - Two Zone Critical

      32 inner zone elements

      44 middle zone elements

Case 3 - Three Zone Critical

      32 inner zone elements

      44 middle zone elements

      44 outer zone elements.

The number densities used in a unit element cell were based on the oxide critical experiment information (BAW-119),[6] and the following volume fractions in a unit canned element cell:

| | |
|---|---|
| Lattice | 0.7582 |
| Can | 0.1089 |
| Water Channel | 0.1329 |

The inner zone fuel elements contained 206 fuel pins per can having a thorium-to-uranium ratio of 25.76/1. In each of these fuel elements 137 pins had gadolinium impurity in excess of the specified limits. In order to account for this added neutron poison, a boron equivalent number density was used. The boron equivalent number density for pins having specified thermal poisons was $1.8992 \times 10^{18}$ atoms/cc, while the boron equivalent number density for the pins having excess thermal poisons was $1.3725 \times 10^{19}$ atoms/cc. These numbers applied to a unit pin cell. The U-235 concentration ratio for the three zones, as assembled in the critical experiment, is 3.00, 3.93, and 4.81.

The Four Group Code was used to homogenize the cross sections over a fuel element, including the can. Two four group calculations were made on a unit element cell from each zone in slab geometry. One case had an infinite lattice of fuel pins (Case A), while the other case shows the can wall and water channel surrounding the lattice for one dimension (Case B). In each case the vertical buckling was zero and $\frac{\phi'}{\phi}$ was zero at the cell boundary. The value of the thorium resonance integral in the lattice was 20.13 barns in both calculations. Values of $k_{eff}$ for infinite arrays of fuel elements were calculated, and the difference between this effective $k_\infty$ and the $k_\infty$ of the lattice without cans was the contribution of the cans and water channel. This difference was doubled to approximate the two dimensional geometry effect of the unit element cell, thus giving an effective $k_\infty$ for a homogenized unit element cell. These values are shown on Table 3.6. Other calculations, comparing PDQ 2-dimensional results with equivalent 1-dimensional calculations, indicate that this 2-dimensional approximation is valid.

## TABLE 3.6

## $k_\infty$ OF ELEMENT CELL

|  | Zone 1 | Zone 2 | Zone 3 |
|---|---|---|---|
| Infinite Pin Cell Lattice (Case A) | 1.0893 | 1.2078 | 1.2722 |
| Can, Water and Lattice (one direction) (Case B) | 1.0839 | 1.2056 | 1.2734 |
| $\Delta k_\infty$, Difference Between Cases B and A | -0.0054 | -0.0022 | 0.0012 |
| Can, Water, Lattice (two directions) | 1.0785 | 1.2034 | 1.2746 |

In order to fit these calculations with homogenized data, curves of $k_\infty$ vs $R_{02}$ were calculated using the Spectral Code and the volume fractions of the fuel element including the cans. It was found that a value of $R_{02}$ = 23.85 barns gave a best fit to the values of $k_\infty$ for the three zones. On the surface the choice of $R_{02}$ as a fitting parameter seems arbitrary. However, one of the most important nuclear effects of cans and water channels is the change in the Dancoff (resonance shadowing) effect. Thus in a channel fuel element, the effective resonance integral of a pin next to a water channel is larger than that of a pin in the interior of the fuel bundle. The change in $R_{02}$ from 20.13 barns to 23.85 barns in the fitting procedure above includes this Dancoff effect as well as the effects of spatial flux variation. This value of $R_{02}$ and values of the other constants averaged with the Spectral Code for the fuel element cell were used in SLEUTH to compute $k_{eff}$ for the three experimental cores. In order to obtain a best fit to the experimental criticalities, the age was then used as a parameter in SLEUTH to obtain curves of $k_{eff}$ vs $\tau$. Table 3.7 gives the values of $k_{eff}$ for the three cases studied. The age for criticality is approximately 54 $cm^2$. The spectral calculated age for the homogenized element is 49 $cm^2$. This change in the age for critical matching of the multi-zone cores is in the same direction as for the infinite lattice cores.

TABLE 3.7

k_eff OF MULTI-ZONE CORES

|         | $k_{eff}$* | $k_{eff}$** |
|---------|------------|-------------|
| Case 1  | 1.0075     | 1.0000      |
| Case 2  | 1.0105     | 1.0010      |
| Case 3  | 1.0155     | 1.0008      |

\* Age obtained from the spectral
   code = 49.2 cm$^2$
\*\* "Best fit" age = 54.2 cm$^2$


3.3.2   Change of Reactivity with Moderator Temperature

Exponential assemblies were used to measure the material buckling of a specific lattice as a function of temperature and boric acid concentration. The specific lattice considered has a $ThO_2$/U-235 atomic ratio of 15/1 and a metal-water ratio of 1.119. A full description of the experiment and the experimental results are given in the report on the Hot Exponential Experiment (BAW-116).[5] The material buckling of each of the exponential assembly conditions was calculated using the Spectral Code to determine the $k_\infty$ and migration area of the lattice. A comparison of calculated and measured buckling for various temperatures and boron concentrations in the core is shown in Table 3.8. This table also gives the calculated infinite multiplication constant of the lattice material for the various cases. Figure 3.5 shows the measured and calculated change in material buckling between 450 F and 68 F as a function of boron in the core. The change of reactivity with temperature was also computed using the Temperature Coefficient Code. The results obtained from this code were compared with measured data of temperature vs material buckling obtained from hot exponential experiments. It was concluded that the calculational method would adequately determine temperature coefficients for the CETR core. The results of the calculation on the CETR core give the coefficients of Table 3.9, and the effective multiplication ($k_{eff}$) vs moderator temperature curve is shown in Fig. 3.6.

TABLE 3.8

COMPARISON OF MEASURED AND CALCULATED MATERIAL BUCKLING
AS A FUNCTION OF BORON AND TEMPERATURE

| Temp., F | $N_B$* | $B_m^2$ Measured | $B_m^2$ Calc. | $k_\infty$ Calc. | $\tau$ Calc. | $L^2$ Calc. |
|---|---|---|---|---|---|---|
| 68 | 0 | .00665 | .00643 | 1.3037 | 46.43 | .75 |
| 450 | 0 | .00482 | .00429 | 1.2498 | 58.40 | 1.42 |
| 68 | 2.638 | .00548 | .00505 | 1.2380 | 46.38 | .71 |
| 450 | 2.163 | .00344 | .00343 | 1.2018 | 57.74 | 1.31 |
| 450 | 4.265 | .00294 | .00266 | 1.1570 | 57.74 | 1.25 |

*Boron concentration, atoms boron/cc of core x $10^{-19}$.

TABLE 3.9

TEMPERATURE COEFFICIENTS OF THE CETR, $\Delta k/F$

| Coefficient | 68 F (Initial) | 500 F (Initial) | 500 F (600 Days) |
|---|---|---|---|
| Doppler | $-4.1 \times 10^{-5}$ | $-3.3 \times 10^{-5}$ | $-3.1 \times 10^{-5}$ |
| Moderator | $-3.1 \times 10^{-5}$ | $-1.4 \times 10^{-4}$ | $-0.8 \times 10^{-4}$ |
| Total | $-7.2 \times 10^{-5}$ | $-1.7 \times 10^{-4}$ | $-1.1 \times 10^{-4}$ |

3.3.3   Reactivity Effect Due to Power Doppler

The reactivity decrease in the CETR core between 500 F zero power and 500 F full power has been calculated to be 0.021 $\Delta k_{eff}$. The power coefficient of reactivity occurs as a result of the Doppler broadening of thorium resonances as the fuel heats up to operating conditions. The coefficient at the beginning of core life has been calculated as $-1 \times 10^{-5}$ $\Delta k/F$ at full power, and $-3.3 \times 10^{-5}$ $\Delta k/F$ at 500 F, zero power. The change in this coefficient during core life is insignificant. These calculations used the measured temperature dependence of the thorium resonance integral reported in BAW-144.[7] The two dimensional distribution of the

resonance integral was based on the temperature distribution obtained from a two dimensional power shape synthesized from one dimensional radial and axial power plots. The one dimensional calculations were performed using SLEUTH.

The methods of calculating multi-dimensional cores by synthesizing few dimensional calculations have received considerable attention in the Naval Reactor program. The methods proposed resolve into simulation of transverse dimension effects through the use of the proper space and lifetime dependent transverse buckling. The particular scheme used here was "SPOT" (synthesis from a point traverse) which employs traverses based on local material properties in contrast to "SCAT" (synthesis from a core average traverse) which employs flux weighted material properties. The validity of the "SPOT" method based on axial traverses at different radii was verified with two trial cases.

For the CETR calculation the core model was cylindrical with 20 regions (9 fuel) radially and 11 regions (9 fuel) axially. Two control rod rings were fully inserted. The calculational scheme consisted of the following steps:

(a) An initial power distribution in three dimensions was assumed.

(b) The temperature distribution was determined from the power distribution using the fuel temperature vs power density curve of Fig. 3.7. A gap of .003 in. was assumed, and the temperature distribution values were extrapolated from Fig. 3.7.

(c) The distribution of the thorium resonance integral, $R_{02}$, was computed from the temperature distribution employing the measured temperature dependence of the resonance integral given in BAW-144.[7] The value of $R_{02}(68\ F)$ was taken to be 20.13 barns. The Dancoff correction used was $R_{02}(500\ F)/R_{02}(68\ F) = 0.919$.

(d) The two dimensional criticality and power distribution was synthesized by the "SPOT" method from one dimensional radial and axial (r = 0) computations utilizing the two dimensional $R_{02}$ distribution.

(e) Steps (b) through (d) were repeated until $k_{eff}$ and the power distribution converged.

The converged value of $k_{eff}$ was 1.005 for the full power core. The value of $k_{eff}$ at 500 F zero power was computed to be 1.026 using a uniform $R_{02}$ of 20.27. The difference between this and the full power $k_{eff}$, which is the $\Delta k_{eff}$ change due to the doppler effect, is 0.021. For comparison, the equivalent uniform full power $R_{02}$, which gives the same $\Delta k_{eff}$ (.021) as the two dimensionally distributed $R_{02}$, was calculated to be 22.58 barns. The uniform $R_{02}$ calculations are summarized in Table 3.10.

TABLE 3.10

EQUIVALENT $k_{eff}$ FOR UNIFORM $R_{02}$ CORES

| Uniform $R_{02}$ at 500 F | $k_{eff}$ |
|---|---|
| 20.27 | 1.026 |
| 22.00 | 1.010 |
| 22.50 | 1.006 |
| 23.00 | 1.001 |

## 3.4 FACTORS EFFECTING THE CORE REACTIVITY AND OPERATION DURING LIFE

Several reactivity effects during the core life are important from the operational and excess reactivity standpoint. The relative reactivity importance of U-235 distribution was studied to obtain information on the reactivity effects of zone fuel loading and the fine structure fuel depletion near water channels. The reactivity effects of transient xenon and of equilibrium xenon and samarium were calculated, and the question of possible xenon oscillation was investigated. The effective delayed neutron fraction and the half-life of the delayed neutrons were calculated as a basis for the design of the control system.

### 3.4.1 The Relative Reactivity Importance of U-235 in the CETR

The CETR consists of three fuel zones. Within each of these zones, located within the fuel bundles adjacent to the water gap

regions, are several rows of low enriched fuel pins to reduce the power peaking within each fuel can next to the water gap. In order to determine the fuel loading of these zones and regions, it was necessary to determine the effect upon the reactivity that results from varying the concentration of U-235 within a portion of the core. This can be done by expressing the reactivity by:

$$\frac{\delta k_e}{k_e} = \int_V F(v, N_{25}) \delta N_{25} dv$$

where V denotes integration over the reactor volume, or

$$\frac{\delta k_e}{k_e} = \int_R F(r, N_{25}) \delta N_{25} dr$$

where R denotes integration over the reactor radius.

The function $F(r, N_{25})$ is the relative importance (percentage change in $k_{eff}$) in a cylindrical reactor, per unit change in radius and unit change in the U-235 atom concentration, for the portion of the reactor located at the radial coordinate r. The function $F(v, N_{25})$ is similarly defined except that the parameter of radius is replaced by the parameter of volume.

The reactivity expression was derived from 2-group perturbation theory. Two-group constants were computed using the Spectral Code, and the relative importance functions were computed using the Two Group Adjoint Code. The importance functions are related by

$$F(v, N_{25}) = \frac{1}{r} F(r, N_{25}).$$

For the case that was studied the core arrangement sketched in Fig. 3.8 was used in cylindrical geometry. The values for the radii shown are the exact numbers that were used in the calculations, and do not represent the accuracy of the measured dimensions. The assumed reactor temperature was 68 F for the calculations. The number densities of the constituents in the various regions are listed in Table 3.11

TABLE 3.11

MATERIAL COMPOSITION FOR CALCULATION OF RELATIVE
IMPORTANCE OF U-235 AS A FUNCTION OF RADIUS

| Region | Constituent | Number Density $cm^{-3} \times 10^{-24}$ |
|---|---|---|
| Core Lattice I | H | 0.0328 |
| | O | 0.0269 |
| | Al | 0.0068 |
| | SS-304 | 0.00806 |
| | Th-232 | 0.0049 |
| | U-235 | 0.0001931 |
| Core Lattice II | H | 0.0328 |
| | O | 0.0269 |
| | Al | 0.0068 |
| | SS-304 | 0.00806 |
| | Th-232 | 0.0049 |
| | U-235 | 0.0002525 |
| Core Lattice III | H | 0.0328 |
| | O | 0.0269 |
| | Al | 0.0068 |
| | SS-304 | 0.00806 |
| | Th-232 | 0.0049 |
| | U-235 | 0.0003098 |
| Water | $H_2O$ | 0.03327 |
| Boral | B | 0.021745 |
| | C | 0.005436 |
| | Al | 0.0325 |
| Aluminum | Al | 0.060275 |

The physical and adjoint fluxes are plotted in Figs. 3.9 through 3.12.
The relative importance factors are plotted in Figs. 3.13 through 3.16.
Two distinct cases were considered, one with the boral control rods
inserted, and the other with the boral control rods withdrawn and re-
placed by aluminum followers.

The curves were used to find the change in reactivity of
the critical experiment caused by variation of the loading ratio in a
portion of the core. The curves indicate that a considerable increase
occurs in the relative importance of the core regions adjacent to the
water gaps when the boral control rods are withdrawn and replaced with
aluminum followers. Figs. 3.13 through 3.16 provide quantitative
estimates of the magnitude of this change.

### 3.4.2 Lifetime Calculation With Partitioned Fuel Regions

Two lifetime calculations were made for the CETR core
to determine if partitioning of the fuel zones had a significant effect on
$k_{eff}$ during the course of life. In calculations using SLEUTH the code
requires each region to burn up uniformly independent of the flux shape
through that region. If there are actually large local power peaks, such
as are encountered in the CETR core adjacent to water gaps, SLEUTH
underestimates the burnup in these local regions. If these are regions
of high importance a uniform burnup calculation would overestimate $k_{eff}$
late in life.

The first lifetime calculation was on a twelve region basic
core with three fuel zones, two rod rings, and high $k_\infty$ pins adjacent to
rod rings. The second was on the same basic core, but with the fuel
zones partitioned into an additional seven regions for a total of nineteen.
The partitioned regions were one centimeter thick and were located in
the areas of local peaks adjacent to high $k_\infty$ regions, zone interfaces, and
the core-reflector interface. The $k_{eff}$ values during life for the two cases
appear in Table 3.12.

The difference between the two cases is appreciable. This
indicates that the local variations of fuel burnup are important to the life
of the reactor.

TABLE 3.12

COMPARISON OF $k_{eff}$ DURING LIFE WITH AND WITHOUT
FUEL PARTITIONING

| Time (days) | $k_{eff}$ Basic Core | $k_{eff}$ Partitioned Core | Difference |
|---|---|---|---|
| 0 | 1.1355 | 1.1355 | 0 |
| 100 | 1.0746 | 1..0740 | .0006 |
| 200 | 1.0597 | 1.0585 | .0012 |
| 300 | 1.0443 | 1.0424 | .0019 |
| 400 | 1.0280 | 1.0255 | .0025 |
| 500 | 1.0114 | 1.0084 | .0030 |
| 600 | .9945 | .9914 | .0031 |

3.4.3   Reactivity Effects of Xenon and Samarium

The reduction of core reactivity caused by the buildup of
Xe-135 to its equilibrium value depends upon the operating power level.
This effect in the CETR was studied using SLEUTH.   The power levels
chosen for calculational purposes are 15%, 30%, 60%, and 100% of the
full power operating level of 585 MW.   $k_{eff}$ and the number densities of
Xe-135 for each power level were calculated for the first few days of
operation.   The results are shown in Figs. 3.17 and 3.18.   Fig. 3.17
shows the change in reactor reactivity as a function of reactor life for
the various power levels.   Fig. 3.18 shows the accumulation of Xe-135
within each core region as the CETR operates at full power.   The amount
that the reactor reactivity is decreased during the period that the Xe-135
concentration climbs to its equilibrium value is distorted because some
U-235 depletion and some Sm-149 accumulation takes place.   To obtain
the net reactivity loss caused solely by the Xe-135 formation, a small
correction was applied to each of the curves given in Fig. 3.17.   The
results are plotted in Figs. 3.19 and 3.20.

When power is reduced after the equilibrium Xe-135 con-
centration has been established a reactivity transient occurs.   Initially
the Xe-135 concentration increases, with a concurrent decrease in the

- 32 -

reactor reactivity. Shortly afterwards the Xe-135 decays to a smaller equilibrium concentration than existed at the original power level. The reactivity decrease associated with the transient rise in Xe-135 concentration is called the xenon override. To study this phenomenon in the CETR core two separate power changes were used: full power to 15 percent full power, and full power to zero power. The atomic concentrations and the reactivity of the core were computed as functions of time after the power level change, using SLEUTH. The power level change was made at 10 days of reactor life. The reactor behavior was studied in detail during the following day of reactor operation at reduced power. At ten days of reactor life the equilibrium Xe-135 concentration established is responsible for a decrease in reactor reactivity equal to .023 $\Delta k_{eff}$. The absorption cross sections used were obtained by averaging over a Wigner-Wilkins neutron energy spectrum at 500 F. The results for Xe-135 and Sm-149 are given in Table 3.13.

TABLE 3.13

WIGNER-WILKINS AVERAGED Xe-135 AND Sm-149 CROSS SECTIONS

| Radial Zone | Xe-135, $\sigma_a$(barns) | Sm-149, $\sigma_a$(barns) |
|---|---|---|
| I | 1.59 ($10^6$) | 5.55 ($10^4$) |
| II | 1.50 ($10^6$) | 5.28 ($10^4$) |
| III | 1.42 ($10^6$) | 5.04 ($10^4$) |

The behavior of the reactor reactivity after the power level is reduced is shown in Figs. 3.21 and 3.22. These figures indicate that for the power change of 585 MW to 87.75 MW the maximum extra reactivity needed for xenon override is 0.555% and for the power change of 585 MW to 0 MW the maximum xenon override is 0.720%.

- 33 -

Calculations have shown that in the CETR core the equilibrium Sm-149 concentration is reached after about 50 full power days of operation. The reactivity reduction due to Sm-149 poisoning is approximately constant at $.007 \Delta k_{eff}$ throughout core life.

### 3.4.4 Delayed Neutrons in the CETR

For the study of transient behavior of the core it is necessary to determine the effective fraction of delayed neutrons in the core and their effective half life. The absolute yield of delayed neutrons per thermal fission for U-235 has been found by experiment to be 0.0158. No dependence of this yield on the energy of the neutrons that induce the fissions in a reactor has been observed. Since the total number of neutrons per fission is $\nu_{25} = 2.47$ for U-235, the fraction of these that are delayed is $\beta_{25} = .0064$. Table 3.14 gives pertinent information for each delayed neutron group of U-235.

TABLE 3.14

DELAYED NEUTRON GROUPS OF U-235

| Group Index i | Half-life $T_i$ | Absolute Group Yield | $\beta_i$ |
|---|---|---|---|
| 1 | 55.72 sec | 0.00052 | 0.000211 |
| 2 | 22.72 | 0.00346 | 0.001401 |
| 3 | 6.22 | 0.00310 | 0.001255 |
| 4 | 2.30 | 0.00624 | 0.002526 |
| 5 | 0.610 | 0.00182 | 0.000737 |
| 6 | 0.230 | 0.00066 | 0.000267 |

The total delayed neutron fraction is the sum of the fractions with different half lives:

$$\beta_{25} = \sum_i \beta_i .$$

The effective half-life of the delayed neutrons is the average

$$\overline{T}_{25} = \frac{\sum\limits_{i} \beta_i T_i}{\beta_{25}} \ ,$$

which gives $\overline{T}_{25} = 9.0$ seconds.

For U-233 the absolute yield of delayed neutrons per thermal fission is 0.0070. The total number of neutrons per fission is $\nu_{23} = 2.52$, and the delayed neutron fraction is $\beta_{23} = .0028$. Delayed neutron group data are given in Table 3.15.

## TABLE 3.15
## DELAYED NEUTRON GROUPS OF U-233

| Group Index i | Half-life $T_i$ | Yield per Group | $\beta_i$ |
|---|---|---|---|
| 1 | 55.11 sec | 0.00060 | 0.000238 |
| 2 | 20.74 | 0.00192 | 0.000762 |
| 3 | 5.30 | 0.00159 | 0.000631 |
| 4 | 2.29 | 0.00222 | 0.000881 |
| 5 | 0.546 | 0.00051 | 0.000202 |
| 6 | 0.221 | 0.00016 | 0.000064 |

The effective half-life of the U-233 delayed neutrons is

$$\overline{T}_{23} = \frac{\sum\limits_{i} \beta_i T_i}{\beta_{23}}$$

which gives $\overline{T}_{23} = 12.4$ seconds.

At the end of 600 days of life the reactor core consists of a mixture of U-235 and U-233 nonuniform concentration. Thus it

is necessary to perform a suitable averaging process in order to obtain a value for the reactor $\beta$ and $\overline{T}$. The reactor delayed neutron fraction $\beta$ is found from a neutron balance:

$$\beta_{core}(\overline{\Sigma_{f23}\phi} + \overline{\Sigma_{f25}\phi}) = \beta_{23}\overline{\Sigma_{f23}\phi} + \beta_{25}\overline{\Sigma_{f25}\phi}.$$

$\overline{\Sigma_{f23}\phi}$ and $\overline{\Sigma_{f25}\phi}$ are averaged over the reactor core volume and represent contributions to the fission reaction rate from both resonance and thermal fissions. At 600 days of full power operation the values

$$\overline{\Sigma_{f23}^{23}\phi} = 0.512 \text{ and } \overline{\Sigma_{f25}^{25}\phi} = 1.284$$

were determined from a core lifetime calculation using SLEUTH. Thus $\beta_{core} = 0.0054$ after 600 days of full power operation. The half-life of the delayed neutron emitters averaged over reactor volume and groups of emitters is $\overline{T}_{core} = 9.52$ sec after 600 days of full power operation.

### 3.4.5 The Stability of the CETR Against Xenon Oscillations

It has been established, based on the theory of Randall and St. John,[8] that the CETR will not be subject to xenon induced power oscillations. The magnitude of the Doppler power coefficient of this reactor precludes oscillations under any conditions of size and power level. Furthermore, the CETR is stable under operating conditions even without the benefit of a negative power coefficient.

In the theory, the flux threshold for instability is the value of the flux which satisfies the relation:

$$\frac{M^2 B_g^2}{\alpha_x} \Lambda_j - \frac{\alpha_T}{\alpha_x} \phi = \frac{\dfrac{1}{1 + \dfrac{\lambda_x}{\sigma_x \phi}} - \beta_x}{1 + \dfrac{\lambda_x + \lambda_i}{\sigma_x \phi}},$$

where:

$M^2$ = migration area

$B_g^2$ = geometric buckling

$\alpha_x$ = xenon coefficient of reactivity at very high flux

- 36 -

$\alpha_T$ = power coefficient of reactivity in terms of reactivity per unit flux

$\phi$ = average flux

$\lambda_x$, $\lambda_i$ = decay constants of $Xe^{135}$ and $I^{135}$

$\beta_x$ = fraction of xenon formed directly from fission $= \dfrac{\gamma_x}{\gamma_x + \gamma_i}$

$\Lambda_j = \dfrac{\mu_j^2}{B_g^2}$

The values of $\mu_j^2$ are determined from:

$$(\nabla^2 + B^2)g_j + \mu_j^2 g_j = 0$$

with $\mu_o^2 = 0$.

$g_j$ = orthonormal eigenfunctions of the boundary value problem that has the unperturbed flux shape as its fundamental solution

$B^2$ = material buckling.

The higher eigenfunctions $g_j$ and eigenvalues $B_j^2 = (\mu_j^2 + B^2)$ are determined once the unperturbed (fundamental) flux shape is specified. They may be obtained immediately for two unperturbed flux shapes of practical importance:

$$\phi(z, r) = \sin \frac{\pi z}{H} J_o(\frac{2.405r}{R}) \quad \text{and} \quad \phi(z, r) = \sin \frac{\pi z}{H}.$$

The second distribution is the case of flat radial flux. The first harmonic eigenfunctions and eigenvalues for these fundamental shapes are summarized in Table 3.16. The properties of the CETR which are pertinent to the stability computations are tabulated in Table 3.17.

TABLE 3.16

EIGENFUNCTIONS AND EIGENVALUES RELATED
TO XENON STABILITY

| $g_{00}$(unperturbed) | $\sin \dfrac{\pi z}{H} J_o \dfrac{2.405r}{R}$ | $\sin \dfrac{\pi z}{H}$ |
|---|---|---|
| $B_{00}^2$ | $\left(\dfrac{\pi}{H}\right)^2 + \left(\dfrac{2.405}{R}\right)^2$ | $\left(\dfrac{\pi}{H}\right)^2$ |

TABLE 3.16

## EIGENFUNCTIONS AND EIGENVALUES RELATED
### TO XENON STABILITY (CONT'D)

$g_{10}$      $\sin \dfrac{2\pi z}{H} J_o \dfrac{(2.405r)}{R}$      $\sin \dfrac{2\pi z}{H}$

$B_{10}^2$      $4\left(\dfrac{\pi}{H}\right)^2 + \left(\dfrac{2.405}{R}\right)^2$      $4\left(\dfrac{\pi}{H}\right)^2$

$g_{01}$      $\sin \dfrac{\pi z}{H} J_1 \dfrac{(3.832r)}{R} \cos\theta$      $\sin \dfrac{\pi z}{H} J_1 \dfrac{(1.841r)}{R} \cos\theta$

$B_{01}^2$      $\left(\dfrac{\pi}{H}\right)^2 + \left(\dfrac{3.832}{R}\right)^2$      $\left(\dfrac{\pi}{H}\right)^2 + \left(\dfrac{1.841}{R}\right)^2$

## TABLE 3.17
### REACTOR PROPERTIES RELATED TO XENON STABILITY

| | |
|---|---|
| H, cm | 266 |
| R, cm | 107 |
| $a_x$ | 0.0325 |
| $a_T/a_x$, $(n/cm^2\ sec)^{-1}$* | $0.138 \times 10^{-13}$ |
| $M^2$, $cm^2$ | 47 |
| $\phi$, $n/cm^2\ sec$ | $1.4 \times 10^{13}$ |

*Doppler coefficient only.

The xenon coefficient was calculated, using SLEUTH, as the difference between the reactivities with xenon concentrations of:

$$x = 0 \quad \text{and} \quad x = (\gamma_x + \gamma_i) \frac{f_1\phi_1 + f_2\phi_2}{\nu\sigma_x\phi_2} .$$

In the second equation above, $f_2\phi_2$ is the neutron production rate from thermal fissions and $f_1\phi_1$ is the neutron production rate from epithermal

fissions. The second xenon concentration is that present at very high flux levels and includes resonance production of xenon but not resonance burnup. The threshold flux levels for xenon instability were determined for the CETR under the two conditions of unperturbed flux distribution and with a zero power coefficient. These results are summarized in Table 3.18.

TABLE 3.18

THRESHOLD FLUXES FOR XENON OSCILLATIONS

(ZERO POWER COEFFICIENT)

| Type of Oscillation | Flux, $n/cm^2$ sec |
|---|---|
| Axial About Midplane | $6.2 \times 10^{13}$ |
| Radial About Diameter | |
| Unperturbed Radial Shape: | |
| $J_o \dfrac{(2.405r)}{R}$ | $\infty$ |
| Unperturbed Radial Shape: | |
| Flat | $3.9 \times 10^{13}$ |

The values of the threshold fluxes were read from the curve presented by Randall and St. John.[8] This curve was constructed using $\sigma_x = 3.08 \times 10^6$ barns. The threshold fluxes were corrected to $\sigma_x = 2.0 \times 10^6$ barns by multiplying the graph values by $3.08/2.0$. The susceptibility of a given mode to oscillation is dependent on the mode buckling, which exerts its influence through $\Lambda_j$. Susceptibility increases with decreasing buckling. For instance, the flat radial flux reactors would oscillate about a diameter first as the flux was increased. If the flux was raised further, they would also begin to oscillate about the midplane. Note that all oscillation thresholds for the CETR are above the actual flux. This reactor is thus stable against xenon oscillations even discounting the stabilizing effect of the power coefficient.

If the power coefficient is larger than some critical value, this mechanism will in itself be enough to assure stability for any reactor size and flux level. This critical value is $\frac{a_T}{a_x} = 0.134 \times 10^{-13}$ for $\sigma_x = 2 \times 10^6$ barns. The Doppler power coefficient of CETR is therefore large enough to assure stability under all conditions.

A study was also made of the behavior of power oscillations in the CETR arising from the non-equilibrium xenon condition that results from a change in control rod position. The calculations were made for a core operating at 585 MW. The study demonstrated that the power oscillations vary slowly, attenuating with time, and reaching steady state approximately 30 hrs after the perturbation. Axial power profiles during core life were calculated using SLEUTH. In these "window shade" calculations rod group position was represented by a smeared poison distribution. In order to demonstrate the effect of an extreme xenon non-equilibrium state, a rod group was withdrawn from a partially inserted position at a time in life when the equilibrium xenon was the only effective poison with a nonuniform distribution. Results from a "window shade" lifetime calculation indicated that these conditions were satisfied about eleven days after initial start up. At this time the xenon concentration varies by a factor of three along the core axis with the concentration being higher in the bottom half of the core. Figs. 3.23 and 3.24 indicate the axial power shape at 11 days of core life before and after an instantaneous change in rod group position. The positions of the three rod groups are shown at the bottom of the figures. Figs. 3.25 and 3.27 show the power profiles at 0.75, 1.25 and 1.75 days after the instantaneous motion of the control rod group. At the end of 1.25 days the power distribution is the fundamental steady state shape, and no further change in shape occurs with time. Thus the system is stable to the severe rod withdrawal case that was studied.

# SECTION 4
# REACTIVITY CONTROL AND CONTROL ROD
# WORTH IN THE CETR

## 4.1 CONTROL SUMMARY

Twenty-one movable hafnium control rods, a variable number of fixed boron steel shim rods and soluble poison in the coolant are used to compensate for the reactivity requirements of the CETR. Changes in concentrations of soluble poison compensate for the change in reactivity between 68 F and 450 F. The number of fixed shim rods in the core is flexible in order that adjustments can be made in the final core for possible variations of the core reactivity from the expected value.

This section presents the reactivity control distributions, the reference and possible sequences of control rod programming, and the worth of the various control rod groups in various programming sequences for the CETR. Experimental data relative to the worths of control rod materials and patterns of control rods in the CETR mockup is reported in BAW-119.[6] These data were analyzed, and the results of the comparisons of experimental and calculated rod worths were used to establish and modify calculational methods. These comparisons provided a basis for uncertainty estimates on the analytical methods.

With no control rods in the core the effective multiplication factor at full power is $1.084 \pm .03$. At 450 F, the shutdown temperature of the primary system and the point at which most of the soluble poison is removed from the coolant, the multiplication factor is $1.111 \pm .017$. The 450 F point is considered to be the control point, the point at which the shutdown margin due to insertion of the movable rods is a minimum. The 21 movable hafnium control rods in the CETR core are worth $0.112 \Delta k_{eff}$ at 68 F, $0.135 \Delta k_{eff}$ at 450 F and $0.140 \Delta k_{eff}$ at 501 F. To insure a minimum subcritical margin of $0.02 \Delta k_{eff}$ at 450 F with all

hafnium rods inserted, three cases of starting conditions were computed. Each case involves a different number of fixed shim rods in the core. A control rod programming sequence was established for each of the three cases.

## 4.2   EXPECTED INITIAL REACTIVITY CONTROL DISTRIBUTION

The reactivity control of the CETR core is distributed among three control mechanisms. The control mechanisms are 21 movable hafnium control rods, a variable number of fixed shim rods, and boric acid concentration in the reactor coolant. The initial distribution of reactivity control between movable rods, fixed rods, and soluble poisons is given in Table 4.1. The core contains boron which is alloyed with the stainless steel clad of the fuel rods. As the core is operated at power the boron is consumed, resulting in a substantial increase in the life of the core. The initial reactivity worth of the boron concentration (200-225 ppm in the clad) is 0.021 to 0.024 $\Delta k_{eff}$. This reactivity is not considered in Table 4.1 because the negative reactivity effects associated with fuel depletion and fission product poisoning were determined to be greater during the operation of the reactor than the positive reactivity effect that results from burnable poison depletion.

TABLE 4.1

NOMINAL INITIAL REACTIVITY CONTROL DISTRIBUTION, $\Delta k_{eff}$

| Effect | Movable Rods | Fixed Rods | Soluble Poison | Total |
|---|---|---|---|---|
| Shim | .044 | .010 | | .054 |
| Temp. 68-450 F | | | .028 | .028 |
| Temp. 450-501 F | .006 | | | .006 |
| Power Doppler | .021 | | | .021 |
| Equilib. Xenon | .023 | | | .023 |
| Equilib. Samarium | .007 | | | .007 |
| | .101 | .010 | `.028 | .139 |

## 4.3  BASIS OF CONTROL ROD WORTH

The reactivity worth of the CETR control rods was determined using 2-dimensional, 4-group calculations (PDQ code). Comparison of computed with measured rod worth indicated a correction factor which was used to obtain the best estimate of rod worth.

The PDQ code was used to calculate the $k_{eff}$ of the CETR core with 21 hafnium control rods inserted. A similar calculation was performed with the control rods removed and replaced with zirconium followers. The difference between these calculations was the computed worth of the rods: 0.143 $\Delta k_{eff}$ at 68 F, 0.173 $\Delta k_{eff}$ at 450 F, and 0.179 $\Delta k_{eff}$ at 501 F. Best estimates of the rod worth were obtained by multiplying each of the computed values by the factor 0.78. Thus the quoted rod worths are: 0.112 $\Delta k_{eff}$ at 68 F, 0.135 $\Delta k_{eff}$ at 450 F, and 0.140 $\Delta k_{eff}$ at 501 F. These values are unchanged when fixed shim rods are added, based on calculations for the three possible patterns: no fixed rods; 4 fixed rods; and 12 fixed rods. The uncertainties in the calculations were estimated to be $^{+\ .03}_{-\ .01}$ $\Delta k_{eff}$ at 68 F. This means that the movable rod worth at 68 F is more than 0.10 $\Delta k_{eff}$ and less than 0.15 $\Delta k_{eff}$.

The correction factor 0.78 was determined as a result of the various measured and computed factors that could affect the calculated rod worth values. These considerations are listed:

(a)  In the critical mockup of CETR, 21 boral control rods of 7-1/2 in. blade length were worth .075 $^{+\ .01}_{-\ .005}$ $\Delta k_{eff}$. The PDQ calculations on this critical assembly core gave a worth of 0.097 $\Delta k_{eff}$. The ratio of measured worth to calculated worth gives a factor of 0.78.

(b)  Critical experiments measured the relative worth of equal size 0.300 in. thick hafnium and boral samples. The ratio of hafnium worth to boral worth was 1.04. Multigroup calculations of the relative worth of the hafnium to boral gave a ratio of 1.03.

(c)  The standard four group method used to calculate the CETR gives a worth of hafnium rod material 14% less than that given by multigroup calculations.

(d) Calculations of flux shapes in the vicinity of control rods and rod followers have agreed well with measurement. This implies that the four group programs should compute control rod worths accurately.

(e) Four group calculations fitted the experimental data obtained from hot exponential experiments. These data included flux shapes around control rods at various temperatures. The calculations are described in Section 5.

Factors (b), (c), and (d), and (e) indicate that the four group PDQ calculations compute relative rod worth accurately. Factor (a) indicates that the PDQ calculations overestimate the absolute rod worth by a $\frac{1}{0.78}$ factor. In determining the nominal reference rod worth a conservative approach justifies the use of the 0.78 factor to reduce the calculated rod worth. Errors were estimated by considering the maximum rod worth to be the calculated $\Delta k_{eff}$ from PDQ computations and the minimum rod worth to be .01 $\Delta k_{eff}$ less than the nominal worth.

### 4.3.1 Rod Worth in the Zone Loaded Critical Assembly

Rod worths were measured by the $\frac{d\rho}{dh}$ water height method in a zone loaded mockup of the CETR. The concentration of boron to make the core critical at full water height was also measured. Section 8 of BAW-119[6] gives a full description of these measurements. Several determinations of $\frac{d\rho}{dh}$ over a wide range of water heights were made for the multizone pin critical assembly. Integration of the curve of $\frac{d\rho}{dh}$ vs critical water height yields the total reactivity of the assembly. From these experiments the total rod worth of the multizone critical was $\Delta k_{eff} = 0.075 \begin{smallmatrix} +0.01 \\ -0.005 \end{smallmatrix}$. These values are the experimental uncertainty.

The amount of soluble boron necessary to hold the excess reactivity of the system was also measured. Boron concentration for the just critical, no rod, infinite water reflected reactor is 0.6393 gm B/liter of water. The excess reactivity associated with this boron concentration is equal to the rod worth. The reactivity of the system with and without boron was calculated using SLEUTH. Two-group constants were generated from the Spectral Code. Thermal flux disadvantage factors based on a $P_3$ transport solution of the flux in a single element were applied to each fuel region. Rod worth as calculated from the critical boron concentration was $\Delta k_{eff} = 0.072$.

The PDQ program was used to calculate the rod worth of Core A mocked up in the Critical Experiment Laboratory. This core included cans, several concentrations of fuel, water gaps, and control rods; a detailed description is given in Section 8.2.2 of BAW-119.[6] With the PDQ program it was possible to correctly picture the square boundaries of the core, and to show control rods, water gaps, cans, and fuel pin matrices as finite regions. Four group coefficients were generated by the Spectral Code. The effective multiplication was calculated with and without control rods inserted. The $k_{eff}$ with rods was 1.005; the $k_{eff}$ with no rods was 1.102. The difference gives a calculated rod worth of 0.097 $\Delta k_{eff}$.
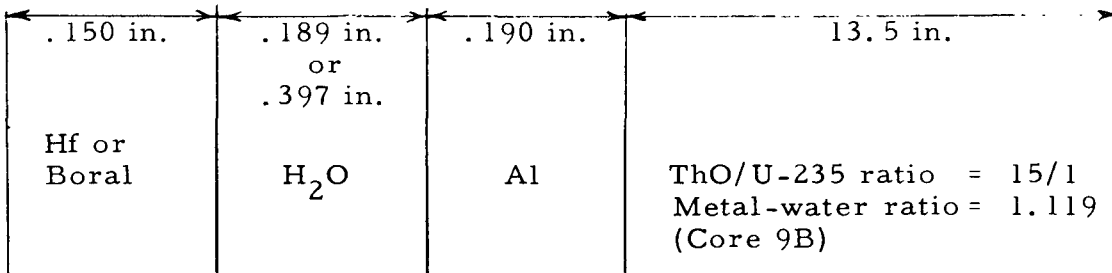
### 4.3.2 Comparison of Hafnium and Boral Worth

The reactivity worth of hafnium and boral was compared experimentally in a single region lattice core. The core consisted of fuel pins with a $ThO_2$/U-235 atom ratio of 15/1 and a metal-water ratio of 1.119. The core and experiment are described as Core 9B in Section 8.8 of BAW-119.[6] The results of the experiment showed that hafnium is worth 1.04 times as much as boral. Table 4.2 gives the experimental results.

TABLE 4.2

EXPERIMENTAL REACTIVITY WORTH OF BORAL AND HAFNIUM

| Water Gap | Sample | Thickness | Reactivity Worth, cents | | |
| --- | --- | --- | --- | --- | --- |
| | | | Thermal | Epi-Cd | Total |
| 0.189 in. | Boral | .300 in. | 52.2 | 40.5 | 92.7 |
| | Hafnium | | 52.2 | 40.8 | 96.0 |
| 0.379 in. | Boral | .300 in. | 71.5 | 27.3 | 98.8 |
| | Hafnium | | 72.1 | 30.7 | 102.8 |

Several different calculations were made in an attempt to match the experimental ratio of hafnium worth to boral worth of 1.04. The model used for calculations was:

| .150 in. | .189 in. or .397 in. | .190 in. | 13.5 in. |
|---|---|---|---|
| Hf or Boral | $H_2O$ | Al | ThO/U-235 ratio = 15/1 Metal-water ratio = 1.119 (Core 9B) |

The results of the various calculations are shown in Table 4.3.

TABLE 4.3

COMPARISON OF CALCULATED ROD WORTHS

| Code | Sample | Water Gap, in. | $k_{eff}$ | $\Delta k$ | Ratio, Hf Worth Boral Worth |
|---|---|---|---|---|---|
| Multigroup | Boral | 0.189 | 0.989 | | |
| | Al | .189 | 1.061 | 0.072 | 1.03 |
| | Hf | .189 | .987 | .074 | |
| | Boral | .397 | .986 | | |
| | Al | .397 | 1.062 | .076 | 1.03 |
| | Hf | .397 | .984 | .078 | |
| Four Group | Boral | .189 | .992 | | |
| | Al | .189 | 1.056 | .064 | 1.00 |
| | Hf | .189 | .992 | .064 | |
| | Boral | .397 | .998 | | |
| | Al | .397 | 1.057 | .069 | .99 |
| | Hf | .397 | .989 | .068 | |
| SLEUTH | Boral | .189 | 1.020 | | |
| | Al | .189 | 1.058 | .038 | .88 |
| | Hf | .189 | 1.024 | .034 | |
| | Boral | .397 | 1.013 | | |
| | Al | .397 | 1.059 | .046 | .91 |
| | Hf | .397 | 1.017 | .042 | |

The Multigroup Code gives good agreement with the experiment. The attempt to match the results of the Multigroup Code with the Four Group Code and with SLEUTH was not successful when all input coefficients were generated by the Spectral Code. Better agreement between Multigroup Code results and those from the Four Group Code were obtained with hafnium as the control rod material by modifying the four group coefficients for the hafnium epithermal group. These modified coefficients were obtained by transmission theory. The method is shown in Appendix A. Fig. 4.1 shows the improvement in flux distribution obtained by using the modified coefficients.

The Multigroup Code was used in a study of the worth of a hafnium slab at 68 F and 500 F. Change in reactivity suppression is determined by comparison with Zircaloy under similar conditions. The slab geometry shown below was used with symmetry on the left boundary. Leakage contributions to rod worth are minimiaed by using a large system. The worth of the hafnium slab was 0.0367 $\Delta k_{eff}$ at 68 F and 0.0449 $\Delta k_{eff}$ at 500 F, computed using the Multigroup Code. The increase in worth of the hafnium slab from cold to hot is 22%. PDQ four group calculations independently predict an increase in worth from cold to hot for all 21 rods of 25%.

| 0.397 cm | 0.806 cm | 86 cm |
|---|---|---|
| Hf | $H_2O$ | Homogenized outer zone of CETR |
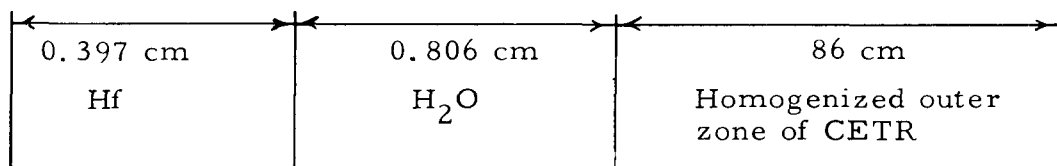
### 4.3.3 Comparison of Worth of 7-1/2 In. and 10 In. Rods

A direct comparison was made between the reactivity worth of a 7-1/2 in. cruciform rod and a 10 in. cruciform rod. Section 8.6 of BAW-119[6] describes the experiment. The results of the experiment indicate that the 10 in. rods are worth between 23% and 29% more than the 7-1/2 in. rods. Considering tip and corner effects to remain constant as the blade length increases by 33%, absorption area theory predicted an increased rod worth of about 25%. This is within the range that was measured.

### 4.3.4 Effect on Rod Worth of Fuel Loading Near Control Rod Channels

The PDQ program was used extensively to study the behavior of control rods and control rod patterns in the reference design.

- 47 -

A mesh of points utilizing the maximum number permitted by code and machine limitations was used. Control rods, water gaps, cans and outer rows of pins were considered as finite regions. All data except for the group coefficients in hafnium was generated by the Spectral Code. A fission source was used for all regions containing moderator. The leakage from adjacent moderator regions was used as a source in solid metal regions such as rod or cans. The mesh spacing and group constants are tabulated in Appendix B.

A large number of PDQ cases were run in order to evaluate a variety of rod patterns. Six cases were used to determine the effect of $k_\infty$ of the pins adjacent to the rod. PDQ reference design results (10 in. Hf rods) for three different types of adjacent pins are tabulated in Table 4.4. Special pin locations are shown in Fig. 4.2. Experiments which also show the dependence of rod worth on the fuel loading of the pins adjacent to the rod are described in Section 8.4 of BAW-119.[6]

## TABLE 4.4
## ROD WORTH DEPENDENCE ON FUEL LOADING NEAR CONTROL ROD CHANNEL

| Special Pins | $k_\infty$ of Special Pins | No Rods | Rods | $\Delta k$ | Mass Holddown, kg |
|---|---|---|---|---|---|
| Regular | 1.05 | 1.0904 | .9583 | .1321 | 350 |
| Light Loaded | 0.95 | 1.0811 | .9517 | .1294 | 360 |
| No Thorium | 1.25 | 1.1301 | .9707 | .1594 | 320 |

## 4.4  ROD PROGRAMMING IN THE CETR

Movable hafnium rods, fixed boron steel shim rods and soluble poison in the coolant are used to compensate for reactivity requirements of the core. Changes in concentrations of soluble poison compensate for

the reactivity change between 68 F and 450 F. The number of shim rods required is maintained flexible in order to adjust for possible variation of the core reactivity from the expected value. With no control rods in the core the effective multiplication at full power is computed in Section 3 to be $1.084 \pm .03$. To insure satisfactory performance three cases of starting conditions must be considered, each involving a different number of fixed rods. The three possibilities at full power are:

    (a)  Nominal $k_{eff}$ of 1.084 (1.111 @ 450 F)

    (b)  High $k_{eff}$ of 1.114 (1.128 @ 450 F)

    (c)  Low $k_{eff}$ of 1.054 (1.094 @ 450 F).

Control rod worth at 450 F is $0.135 \, {}^{+.03}_{-.01} \, \Delta k_{eff}$. A control rod margin greater than $.02 \, \Delta k_{eff}$ is needed at 450 F to insure the shut down safety of the reactor. Thus the excess reactivity of the core at 450 F must be limited to less than $0.105 \, \Delta k_{eff}$. To do this for the nominal case (a), four fixed shim rods worth $0.01 \, \Delta k_{eff}$ are required to be inserted in the core. Twelve fixed shim rods worth $0.03 \, \Delta k_{eff}$ are required for case (b). No fixed shims are needed for case (c). A rod programming sequence has been established for these three possible fixed rod situations. The three are: the nominal four fixed rods, the high $k_{eff}$ case with 12 fixed rods, and the low $k_{eff}$ case with no fixed rods. The choice of fixed rod situation will be made when the $k_{eff}$ of the core is determined more accurately by critical tests on the actual fuel elements. Table 4.5 contains the worth of each rod group as determined by two dimensional analysis. Table 4.6 defines the movable (CR) and fixed rod (FSR) groups.

      Control rod worth as a function of insertion distance has been calculated for a group worth $0.02 \, \Delta k$ and one worth $0.042 \, \Delta k$. SLEUTH was used in a series of "window shade" calculations described in Section 5.3. The results of the study are compared with a $\sin^2 x$ relationship in Fig. 4.3.

TABLE 4.5

## SEQUENCE OF CONTROL ROD WITHDRAWAL IN THE CETR

| Fixed Shims | Movable Rod In Groups | $k_{eff}$ | Group Removed | $\Delta k_{eff}$ | $k_{eff}$ | Group Removed | $\Delta k_{eff}$ |
|---|---|---|---|---|---|---|---|
| 12 | A B C D E | 0.914 | E | 0.028 | 0.950 | E | 0.027 |
| 12 | A B C D | .942 | D | .025 | .977 | D | .024 |
| 12 | A B C | .967 | C | .026 | 1.001 | C | .025 |
| 12 | A B | .993 | B | .025 | 1.026 | B | .024 |
| 12 | A | 1.018 | A | .036 | 1.050 | A | .035 |
| 12 | | 1.054 | 12 FSR's | .030 | 1.085 | 12 FSR's | .029 |
| No fixed, no movable | | 1.084 | | | 1.114 | | |
| 4 | A B C D E | 0.934 | E | .032 | 0.969 | E | .031 |
| 4 | A B C D | .966 | D | .029 | 1.000 | D | .028 |
| 4 | A B C | .995 | A | .028 | 1.028 | A | .027 |
| 4 | B C | 1.023 | B | .027 | 1.055 | B | .026 |
| 4 | C | 1.050 | C | .024 | 1.081 | C | .023 |
| 4 | | 1.074 | 4 FSR's | .010 | 1.104 | 4 FSR's | .010 |
| No fixed, no movable | | 1.084 | | | 1.114 | | |
| None | A B C D E | 0.944 | E | .039 | 0.979 | E | .038 |
| None | A B C D | .983 | D | .036 | 1.017 | D | .035 |
| None | A B C | 1.019 | A | .022 | 1.052 | A | .021 |
| None | B C | 1.041 | B | .022 | 1.073 | B | .021 |
| None | C | 1.063 | C | .021 | 1.094 | C | .020 |
| No fixed, no movable | | 1.084 | | | 1.114 | | |

5 40 062

## TABLE 4.6

## DEFINITION OF ROD GROUPS

| Group | Rod Numbers that Make Up Group (Ref: Fig. 2.1) |
|---|---|
| A | CR's 6, 10, 12, 16 |
| B | CR's 5, 7, 15, 17 |
| C | CR's 2, 9, 13, 20 |
| D | CR's 1, 8, 14, 21 |
| E | CR's 3, 4, 18, 19, 11 |
| 4 Fixed | FSR's 3, 6, 19, 22 |
| 12 Fixed | FSR's 1, 2, 3, 6, 7, 12, 22, 23, 24 |

# SECTION 5
# POWER DISTRIBUTION STUDIES

## 5.1   RATIO OF PEAK TO AVERAGE POWER DENSITY

This section describes the power distribution in the CETR core, the methods used to determine this power distribution, and the design innovations used to keep the power distribution as uniform as practicable. The power distribution in the core was determined as initially loaded with fuel. Then estimates were made of the effects of fuel burnup using special lifetime studies. For the CETR the highest localized power density that might occur during core life was calculated to be 4.1 times the average core power density. The total power peaking consists of three separate factors.

(a) The gross radial factor $(P_R)$ is a result of the gross shaping of the power distribution in the radial direction. It is chiefly influenced by control rod positions and variation of fuel concentration over comparatively large volumes of the core. There is some variation of the gross radial peaking factor with azimuth. The maximum of the combination of radial and azimuthal power density variation is used to define the gross radial factor.

(b) The local factor $(P_L)$ is the additional fine structure peaking superimposed on the gross radial distribution. It is a highly localized peaking which occurs in fuel pins located near water regions or core regions of low neutron absorption. It is chiefly influenced by the size of water gaps in the core which cause increased thermalization of neutrons. This increased local supply of neutrons causes increased fission rates in adjacent fuel pins.

(c) The axial factor $(P_A)$ is a result of the variation of power along the core length. For a bare core loaded uniformly in the axial direction and with rods fully inserted or fully withdrawn the power distribution is a cosine. For the CETR reflected core the axial peaking factor is 1.5 under the above conditions. The axial power distribution and in turn the axial power peaking factor is influenced by the insertion or withdrawal of control rods.

The product of $P_R$, $P_L$, and $P_A$ is defined as the total power peaking factor ($P_T$). Normally, all three of these peakings will not occur at the same point in the reactor. However, it has not been possible to determine that the three peaking factors will not occasionally pile up. The thermal rating of the core has, therefore, been based on the assumption that they will.

## 5.2  DETERMINATION OF RADIAL AND LOCAL PEAKING

The radial and local peaking factors were studied in two main phases. The first phase was to choose the type of calculation, the method of approximating core geometry, and the nuclear parameters to match calculated results with experimental data. The second phase consisted of calculations to determine the peaking factors for the design core. The method that resulted uses the PDQ Code in four groups. The Four Group Code was used to study the best geometrical and nuclear representation of the core. Group constants were obtained from the Spectral Code. Power distributions determined by experiment were matched adequately with this method.

### 5.2.1  Fine Structure Verification

Comparison of the thermal flux profiles in a typical CETR core lattice as given by calculations and as taken from experimental measurement is shown in Figs. 5.1 and 5.2. Dysprosium foil measurements were made in the critical assembly to determine the flux shapes near control rod regions and control rod follower regions. To determine the adequacy of calculational methods comparisons were made between four group two dimensional calculations, four group one dimensional calculations, and experimental measurements. Fig. 5.1 shows the thermal flux profiles near a control rod and Fig. 5.2 shows the same profiles near a control rod follower. The experimental points plotted are from Figs. 9.26 and 9.27 of BAW-119.[6] The calculated thermal flux profiles were determined using the Four Group and PDQ codes. The two dimensional four group coefficients are by definition identical to those of the one dimensional four group.

## 5.2.2 Coarse Structure Verification

Fig. 5.3 maps the power distribution of the CETR zone-loaded critical assembly as given by experimental measurement and by PDQ two dimensional calculation. The comparison is made for a horizontal cross section through the critical core. The numbers quoted in the figure are the ratios of the local radial power density to the volume averaged radial power density. The critical assembly core consisted of three zones with approximate relative U-235 concentrations of 3:4:4.8. These ratios were arranged by using low loaded (25/1 Th-to U-235 ratio) pins in the inner zone, high loaded (15/1 Th-to U-235 ratio) pins in the outer zone, and a mixture of high loaded and low loaded pins in the middle zone. Since this assembly is symmetric by octants about the central vertical axis, Fig. 5.3 shows only an octant of the assembled core. The experimental results are from Fig. 9.3 of BAW-119.[6]

## 5.2.3 Temperature Effects

The exponential assembly was used to measure the fine structure distributions of the thermal flux through simulated control rod and rod follower regions at 68 F and 495 F. Slab geometry calculations were compared with experimental measurements of the fine structure thermal flux distributions. The Four Group Code, where the four group coefficients were generated by the Spectral Code, was used for the calculations.

A sketch of the geometrical arrangement of the exponential assembly is shown at the top of Fig. 5.4. The experimental data are shown in Figs. 16 through 20 of BAW-116.[5] A valuable comparison results from a study of the changes in fine structure flux distributions between 68 F and 495 F. Since calculations on the critical assembly showed that the calculated distributions agreed well with critical experiments at room temperature, these comparisons of the changes in flux distribution between 68 F and 495 F were good checks of the calculational model. This method of comparison minimizes the importance of knowing the exact water gap thicknesses in the exponential. This comparison is shown in Fig. 5.4.

A comparison of the calculated curve and the experimentally determined curve at 68 F is shown in Fig. 5.5. A similar comparison

at 495 F is shown in Fig. 5.6. Agreement between the computed curves and experimental curves is good except in the vicinity of the right side of the control rod simulation. Most of the irregularities of experimental points in the lattice region were fine structure effects in the fuel pin lattice.

### 5.2.4 Gross Radial Peaking Calculations

Two dimensional PDQ calculations in x - y geometry were performed on the reference core. The objective was finding the most flexible and effective control rod arrangements consistent with satisfactory power distributions. The results for several of these calculations are shown in Figs. 5.7 through 5.11. The actual geometry and all material coefficients used in the calculations are given in Appendix B. Fig. B.1 in this Appendix shows the geometric details and power distribution details for a representative case. Since the CETR reference core is symmetric, all figures except 5.11 show only one-quarter of the core cross section. Fig. 5.11 shows the complete core cross section to illustrate the power distribution when only two rods of a group of four are inserted. The numbers reported on the figures are the ratios of the average power density in the fuel element to the average core power density. When making the calculations, power density was calculated for many points within the bundle. However, due to subsequent preferential loading of pins in the element to reduce the local peaking factor, the numbers quoted are the only ones applicable to the final core design. The results of these gross power distribution calculations were studied to arrive at a control rod program for the CETR. The control rod program as finally developed is given in detail in Section 4.4, and the effect of the rod program on power density is given in Section 5.6.

### 5.2.5 Local Peaking Calculations

Local peaking factors were obtained by calculating the power density in one bundle at a time. This made it possible to include enough points of calculated power density in a bundle to obtain a true picture of local peaking. Local peaking calculated for an inner, middle, and outer zone bundle for the core as designed is shown in Figs. 5.12, 5.13 and 5.14. Fig. 5.15 shows the result of a calculation performed

- 55 -

to determine the power density gradient across a bundle when it is adjacent to a hafnium rod. The preferential pin loading scheme for each type of element is shown in Fig. 2.3.

## 5.3 AXIAL PEAKING STUDIES

The axial power peaking factors that result from partially inserted control rod groups were studied using SLEUTH in slab geometry. A set of "window shade" calculations were made. This technique consists of simulating a group of symmetrically spaced control rods by a homogenized poison. The poison is introduced into the core until it reduces the core reactivity by the same amount as the group of rods being simulated. The poison is then withdrawn from segments of the core leaving the original concentration of poison in the balance of the core. This technique simulated control rod withdrawal. Following each removal step, the changes in the one dimensional power distributions were calculated. The resulting curves of the axial power distribution as a function of rod withdrawal distance are shown on Fig. 5.16.

The axial power distribution is adversely affected by partially withdrawn rod groups. Fig. 5.16 shows that the axial power peaking is 1.5 times the average based on an approximate cosine distribution. This is exceeded for partial withdrawal of a rod group worth $0.042\Delta k_{eff}$ (solid curves). The resultant distribution departs significantly from a cosine. Partial withdrawal of a rod group worth $0.020 \Delta k_{eff}$ (broken curve) also departs significantly from a cosine distribution but does not exceed the factor of 1.5 by as great a margin. For insertion greater than 75% the curve is essentially cosine. All of the group reactivity worths for the CETR linear power range groups lie in the range of 0.02 to $0.036 \Delta k_{eff}$. Based on the maximum rod group worth of $0.036 \Delta k_{eff}$, these calculations predict that the axial power peak may approach 1.9 times the average.

## 5.4 THREE DIMENSIONAL CALCULATION

A three dimensional calculation was performed to determine the total gross peaking in the CETR with a group of control rods partially withdrawn. The TKO code with the four group option was used. For the case studied, a rod group was withdrawn from the core to a position

that was expected to result in the maximum axial peaking. The results
of the three dimensional calculation are shown in Figs. 5.17 and 5.18.
In Fig. 5.17, fully inserted rods are identified by the solid cross symbol
and rods inserted 168 cm are identified by the open cross symbol.
Fig. 5.17 shows that the maximum gross radial power density and the
maximum axial power density do not occur at the same point. The three
dimensional picture in Fig. 5.18 shows the normalized power distribution
for the core.

There were limitations in the number of calculation points that
could be included in this three dimensional calculation. Thus it was
necessary to make many approximations concerning the core geometry
and homogenized material regions. Although the results from the
calculations are believed to be substantially correct, they were used
only to observe in a qualitative manner the power distribution within
the core when a rod group is partially withdrawn.

## 5.5  EFFECT OF BURNUP ON THE POWER DISTRIBUTION

Two types of special lifetime studies were performed to determine
the effects of core burnup and rod programming on power distribution.
One of these studies estimates the effect of burnup on axial power distri-
bution. The other simulates the fine structure effect on local power
peaking caused by various burnup situations.

### 5.5.1  Fine Structure Effects

It was necessary to determine whether withdrawal of a
control rod late in life would create a high local peaking factor. A
highly unfavorable xenon distribution or low fuel burnup near the rod
would be expected to cause this. Analysis shows that neither of these
conditions will take place.

For this study an outer zone element was calculated with
pellets with fuel concentration (D) in the pheripheral row of pins and
with concentration (E) pellets in all other pins (see Fig. 2.3 and
Table 2.2). Lifetime calculations using SLEUTH in slab geometry
were performed with the element pessimistically operated at 160%
of average power. Calculated local peaking was higher than in the
reference element loading at full power, but the results show qualita-
tively what will occur in the operating core. Local xenon distribution

- 57 -

is shown to be relatively insensitive to the presence of control rod or Zr follower. Fig. 5.19 illustrates the xenon distribution with and without the control rod. Reduced fuel burnup near a control rod did not cause a high local peaking factor when the rod was eventually withdrawn. It was found that the thermal flux provides adequate burnup in the fuel pins next to a control rod.

A given rod channel will most probably have one of two histories. Either a Zr follower will enter early in life and remain in, or a control rod will repose in the channel until displaced at some point later in life by a Zr follower. Figs. 5.20, 5.21 and 5.22 show the power peaking effects of control rod removal at various stages of reactor operation. Fig. 5.23 shows the power history for fuel next to a rod channel where the control rod was removed early in core life. The discontinuities in the figures are caused by the seven discrete regions of the calculational model, rather than by the actual physical situation. Note that removal of the control rod during life will actually cause a lower peaking factor than is obtained by placing a Zr follower in the channel at startup. High burnup of the first row of low loaded pins occurs in the presence of the Zr follower. The resulting high flux creates increased burnup in the more heavily loaded second row of pins. With the control rod in place during life, burnup immediately is shifted more toward the second row of pins but there is still adequate burnup of the fuel near the rod. Substitution of the Zr follower does not increase the flux sufficiently to produce an unfavorable peaking factor.

## 5.5.2 Gross Axial Effects

A study was made to determine axial power distribution as a function of rod position and core burnup. Figs. 5.24 through 5.45 are axial power profiles calculated at various times during life for the rod configuration shown at the bottom of each graph at the time that is noted on the graph. The rod configurations were simulated with "window shade" boron poison concentrations. Calculations were performed using SLEUTH. The amount of rod insertion was chosen to keep $k_{eff} = 1$ during core life. Tables 5.1 through 5.5 exhibit the variation of fuel and poison concentration along with the infinite multiplication factor during core life.

The maximum axial peaking factor calculated was 1.88. This peaking occurred in the lower portion of the core after 25 full power days of operation. The maximum axial peaking factor that occurred above the midplane of the core was 1.63. This occurred after 590 days of full power operation. On the basis of these calculations it was concluded that the maximum axial peaking factor of 1.9 established for the core as initially loaded would not be exceeded during its operating life.

## 5.6  EFFECTS OF ROD PROGRAMMING ON POWER DISTRIBUTION

The power distribution studies of the core were used to establish the preferential pin loading required to obtain a practical minimum local peaking factor and the control rod programming to keep the gross peaking within tolerable limits. The rod programming for the core was established for the three possible fixed rod situations that may exist in the core at startup; the expected case with four fixed shim rods in the core, the high $k_{eff}$ case with twelve fixed shim rods in the core, and the low $k_{eff}$ case with no fixed shim rods in the core. Table 4.6 defines the movable rod groups A, B, C, D and E, the 4 fixed shim rods, and the 12 fixed shim rods. The sequence of control rod removal for each case is as follows:

Expected case:  E, D, A, B, C

High $k_{eff}$ case:  E, D, C, B, A

Low $k_{eff}$ case:  E, D, A, B, C.

Table 5.6 shows the radial peaking factor for the combination of movable control rods and fixed shim rods that may be in the core at rated power operation. These radial factors were calculated using the PDQ code as described in Section 5.2. A maximum axial factor of 1.9 was determined by steady state calculations and by core lifetime calculations using SLEUTH. The resultant total power peaking factor for the CETR is 4.1.

TABLE 5.1

INFINITE MULTIPLICATION CONSTANT DURING CORE LIFE WITH CONTROL ROD SIMULATION

| TIME | CORE REGION | | | | | | | | | |
|---|---|---|---|---|---|---|---|---|---|---|
| (days) | 1 | 2 | 3 | 4 | 5 | 6 | 7 | 8 | 9 | 10 |
| 0 | 1.0350 | 1.0350 | 1.0350 | 1.0350 | 1.0350 | 1.0350 | 1.0350 | 1.0350 | 1.0350 | 1.0350 |
| 1 | 1.0267 | 1.0222 | 1.0193 | 1.0178 | 1.0171 | 1.0445 | 1.0453 | 1.0471 | 1.0502 | 1.0551 |
| 10 | 1.0248 | 1.0189 | 1.0413 | 1.0369 | 1.0346 | 1.0337 | 1.0342 | 1.0363 | 1.0406 | 1.0480 |
| 50 | 1.0501 | 1.0425 | 1.0365 | 1.0319 | 1.0278 | 1.0236 | 1.0386 | 1.0449 | 1.0472 | 1.0578 |
| 100 | 1.0461 | 1.0379 | 1.0314 | 1.0259 | 1.0499 | 1.0435 | 1.0399 | 1.0407 | 1.0471 | 1.0594 |
| 200 | 1.0384 | 1.0574 | 1.0469 | 1.0399 | 1.0363 | 1.0353 | 1.0366 | 1.0409 | 1.0499 | 1.0630 |
| 300 | 1.0634 | 1.0508 | 1.0407 | 1.0341 | 1.0300 | 1.0277 | 1.0272 | 1.0296 | 1.0800 | 1.0934 |
| 420 | 1.0676 | 1.0544 | 1.0419 | 1.0323 | 1.0235 | 1.0565 | 1.0448 | 1.0416 | 1.0524 | 1.0775 |
| 500 | 1.0630 | 1.0466 | 1.0309 | 1.0605 | 1.0468 | 1.0377 | 1.0337 | 1.0365 | 1.0509 | 1.0782 |
| 630 | 1.0852 | 1.0573 | 1.0378 | 1.0295 | 1.0272 | 1.0273 | 1.0289 | 1.0347 | 1.0511 | 1.0802 |

- 60 -

TABLE 5.2

FUEL CONCENTRATION DURING CORE LIFE

(Atoms/cm$^3$ (x $10^{-21}$) of U-235, U-233, and Pa-233)

| TIME | CORE REGION | | | | | | | | | |
|------|--------|--------|--------|--------|--------|--------|--------|--------|--------|--------|
| (days) | 1 | 2 | 3 | 4 | 5 | 6 | 7 | 8 | 9 | 10 |
| 0 | 0.3591 | 0.3591 | 0.3591 | 0.3591 | 0.3591 | 0.3591 | 0.3591 | 0.3591 | 0.3591 | 0.3591 |
| 1 | .3590 | .3589 | .3588 | .3588 | .3587 | .3587 | .3588 | .3588 | .3589 | .3590 |
| 10 | .3587 | .3584 | .3581 | .3576 | .3573 | .3570 | .3570 | .3572 | .3576 | .3582 |
| 50 | .3572 | .3557 | .3540 | .3525 | .3513 | .3502 | .3491 | .3483 | .3497 | .3529 |
| 100 | .3549 | .3519 | .3488 | .3461 | .3435 | .3406 | .3383 | .3380 | .3414 | .3476 |
| 200 | .3495 | .3428 | .3355 | .3292 | .3320 | .3215 | .3205 | .3223 | .3290 | .3396 |
| 300 | .3413 | .3300 | .3201 | .3131 | .3086 | .3061 | .3057 | .3084 | .3169 | .3307 |
| 420 | .3352 | .3209 | .3090 | .3008 | .2949 | .2899 | .2853 | .2847 | .2929 | .3123 |
| 500 | .3305 | .3140 | .3005 | .2908 | .2826 | .2761 | .2719 | .2725 | .2824 | .3047 |
| 630 | .3184 | .2957 | .2785 | .2684 | .2625 | .2589 | .2572 | .2597 | .2714 | .2964 |

TABLE 5.3

$\Sigma_a(cm^{-1})$ OF BORON-10 DURING CORE LIFE

| TIME | CORE REGION | | | | | | | | | |
|------|------|------|------|------|------|------|------|------|------|------|
| (days) | 1 | 2 | 3 | 4 | 5 | 6 | 7 | 8 | 9 | 10 |
| 0 | 0.005465 | 0.005465 | 0.005465 | 0.005465 | 0.005465 | 0.005465 | 0.005465 | 0.005465 | 0.005465 | 0.005465 |
| 1 | .005455 | .005447 | .004440 | .005435 | .005432 | .005432 | .005435 | .005440 | .005448 | .005456 |
| 10 | .005405 | .005353 | .005291 | .005221 | .005167 | .005126 | .005120 | .005153 | .005225 | .005324 |
| 50 | .005162 | .004923 | .004670 | .004459 | .004291 | .004142 | .004011 | .003920 | .004093 | .004553 |
| 100 | .004823 | .004380 | .003974 | .003644 | .003351 | .003049 | .002838 | .002815 | .003144 | .003882 |
| 200 | .004111 | .003283 | .002588 | .002098 | .001787 | .001611 | .001556 | .001663 | .002095 | .003045 |
| 300 | .003209 | .002170 | .001542 | .001203 | .001021 | .000930 | .000917 | .001017 | .001389 | .002307 |
| 420 | .002654 | .001597 | .001044 | .000769 | .000612 | .000503 | .000420 | .000412 | .000577 | .001263 |
| 500 | .002292 | .001258 | .000764 | .000525 | .000378 | .000287 | .000240 | .000248 | .000381 | .000970 |
| 630 | .001548 | .000645 | .000322 | .000208 | .000160 | .000135 | .000125 | .000141 | .000242 | .000724 |

TABLE 5.4

$\Sigma_a(cm^{-1})$ OF Xe-135 DURING CORE LIFE

| TIME (days) | CORE REGION | | | | | | | | | |
|---|---|---|---|---|---|---|---|---|---|---|
| | 1 | 2 | 3 | 4 | 5 | 6 | 7 | 8 | 9 | 10 |
| 1 | 0.002586 | 0.003959 | 0.004838 | 0.005318 | 0.005527 | 0.005518 | 0.005288 | 0.004786 | 0.003888 | 0.002491 |
| 10 | .002776 | .004281 | .005439 | .006283 | .006611 | .006608 | .006384 | .005932 | .005116 | .003639 |
| 50 | .002207 | .003299 | .004051 | .004637 | .005207 | .005806 | .006423 | .006893 | .006799 | .005724 |
| 100 | .002382 | .003581 | .004447 | .005139 | .005796 | .006351 | .006493 | .006347 | .005887 | .004668 |
| 200 | .003506 | .004971 | .005819 | .006041 | .005990 | .005840 | .005640 | .005362 | .004848 | .003674 |
| 300 | .003716 | .004796 | .005196 | .005330 | .005393 | .005455 | .005535 | .005609 | .005578 | .004991 |
| 420 | .002664 | ..003671 | .004184 | .004523 | .004904 | .005407 | .005876 | .005959 | .005799 | .005027 |
| 500 | .003040 | .004107 | .004672 | ..005142 | .005553 | .005569 | .005415 | .005251 | .005030 | .004256 |
| 630 | .004916 | .005855 | .005764 | .005420 | .005033 | .004656 | .004324 | .004061 | .003771 | .003027 |

# TABLE 5.5

$\Sigma_a(cm^{-1})$ OF GROSS FISSION PRODUCTS DURING CORE LIFE

(Xe-135 and Sm-149 are not included)

| TIME | CORE REGION | | | | | | | | | |
|---|---|---|---|---|---|---|---|---|---|---|
| (days) | 1 | 2 | 3 | 4 | 5 | 6 | 7 | 8 | 9 | 10 |
| 1 | 0.000004 | 0.000007 | 0.000010 | 0.000012 | 0.000013 | 0.000013 | 0.000011 | 0.000009 | 0.000007 | 0.000004 |
| 10 | .000023 | .000043 | .000067 | .000094 | .000116 | .000132 | .000134 | .000122 | .000093 | .000054 |
| 50 | .000117 | .000213 | .000319 | .000411 | .000486 | .000556 | .000619 | .000664 | .000581 | .000370 |
| 100 | .000254 | .000446 | .000636 | .000801 | .000959 | .001133 | .001264 | .001279 | .001078 | .000681 |
| 200 | .000570 | .000999 | .001433 | .001799 | .002067 | .002235 | .002289 | .002182 | .001798 | .001137 |
| 300 | .001042 | .001744 | .002312 | .002701 | .002948 | .003084 | .003104 | .002952 | .002479 | .001636 |
| 420 | .001389 | .002259 | .002922 | .003365 | .003678 | .003938 | .004174 | .004200 | .003766 | .002633 |
| 500 | .001649 | .002642 | .003379 | .003889 | .004308 | .004635 | .004839 | .004804 | .004297 | .003035 |
| 630 | .002313 | .003626 | .004513 | .005007 | .005285 | .005452 | .005529 | .005409 | .004836 | .003456 |

- 64 -

TABLE 5.6

RADIAL POWER PEAKING FACTORS IN ROD PROGRAMMING

| Movable Rods in Core | Radial Peaking Factor[*] |
|---|---|
| Expected Case With 4 Fixed Shim Rods in Core | |
| Group ABC | 2.09 |
| Group BC | 2.05 |
| Group C | 1.98 |
| None | 1.88 |
| High $k_{eff}$ Case With 12 Fixed Shim Rods in Core | |
| Group ABC | 2.17 |
| Group AB | 2.17 |
| Group A | 1.99 |
| Only Central Rod | 2.10 |
| Low $k_{eff}$ Case With No Fixed Shim Rods in Core | |
| Group ABC | 2.11 |
| Group BC | 1.98 |
| Group C | 1.98 |
| None | 1.67 |

[*]Includes local peaking.

APPENDICES

# APPENDIX A
## METHOD OF OBTAINING MODIFIED
## COEFFICIENTS FOR A THIN HIGHLY ABSORBING SLAB

At the boundary of an infinite black absorber, diffusion theory uses the flux extrapolation condition

$$\left(\frac{D\phi'}{\phi}\right) = \frac{1}{2} \, .$$

If the absorbing region is thin rather than infinite and is heavily absorbing rather than black, the extrapolation condition can be used in the altered form

$$\left(\frac{D\phi'}{\phi}\right)_{\substack{\text{at edge} \\ \text{of slab}}} = \frac{1}{2} \cdot \frac{1 - T}{1 + T} = \alpha$$

where

$\quad T \;=\; 2E_3(\Sigma t)$

$\quad \Sigma \;=\;$ macroscopic absorption cross section

$\quad t \;=\;$ slab thickness

$$E_n(x) \;=\; \int_1^\infty \frac{e^{-xu}}{u^n}\, du.$$

Inside the absorbing slab the neutron balance equation assuming zero source is

$$D_i\phi_i'' - \Sigma_i\phi_i \;=\; 0$$

Solution is

$$\phi_i \;=\; A \cos h\left(\sqrt{\frac{\Sigma_i}{D_i}}\, x\right)$$

so

$$\left(\frac{D_i \phi_i'}{\phi_i}\right)_{\frac{t}{2}} = \frac{D_i A \sqrt{\frac{\Sigma_i}{D_i}} \sin h \left(\sqrt{\frac{\Sigma_i}{D_i}} \frac{t}{2}\right)}{A \cos h \left(\sqrt{\frac{\Sigma_i}{D_i}} \frac{t}{2}\right)} = D_i \sqrt{\frac{\Sigma_i}{D_i}} \tan h \left(\sqrt{\frac{\Sigma_i}{D_i}} \cdot \frac{t}{2}\right) = a \ .$$

For a region with large absorption cross section, the value of the diffusion constant makes little difference in the total absorptions in the region. For simplicity the value of $D_i$ was chosen to be the same as $\Sigma_i$. Then the equation becomes

$$D_i \tan h \frac{t}{2} = a$$

or

$$D_i = \frac{a}{\tan h \frac{t}{2}} = \frac{1}{2} \cdot \frac{1 - 2E_3(\Sigma t)}{1 + 2E_3(\Sigma t)} \cdot \frac{1}{\tan h \frac{t}{2}} \ .$$

Values of $D_i$ and $\Sigma_i$ are then found to fit this equation. This recipe was used to generate the constants for hafnium control regions. In the 4-group representations (Four Group Code, PDQ) the group 3 (just above thermal energy) constants were calculated in this manner. Constants for all other groups and for all other regions were generated directly from the Spectral Code.

# APPENDIX B
## PDQ INPUT FOR REFERENCE CORE CALCULATIONS

The $PDQ^2$ mesh lines and the corresponding distance from the center of the reactor are tabulated in Table B-1.

The PDQ coefficients for four operating conditions are tabulated for each of the twelve different material regions required to describe the core. The tabulations are presented in Tables B-2 through B-5.

Figure B. 1 shows the typical mesh spacing and material arrangement for one pattern of control rods.

## TABLE B. 1
## PDQ MESH FOR CETR REFERENCE CORE CALCULATIONS

| Line | Inches From Center Line | Centimeters From Center Line |
|------|-------------------------|------------------------------|
| 0 | -0. 150 | -0. 381 |
| 1 | 0. 150 | 0. 381 |
| 2 | 0. 450 | 1. 143 |
| 3 | 0. 6825 | 1. 734 |
| 4 | 1. 0565 | 2. 684 |
| 5 | 1. 3225 | 3. 359 |
| 6 | 3. 160 | 8. 026 |
| 7 | 5. 000 | 12. 7 |
| 8 | 5. 5445 | 14. 083 |
| 9 | 5. 9185 | 15. 033 |
| 10 | 6. 151 | 15. 624 |
| 11 | 6. 260 | 15. 900 |
| 12 | 6. 385 | 16. 218 |
| 13 | 6. 494 | 16. 495 |
| 14 | 6. 7265 | 17. 085 |
| 15 | 7. 1005 | 18. 035 |
| 16 | 7. 645 | 19. 418 |
| 17 | 9. 485 | 24. 092 |
| 18 | 11. 3225 | 28. 759 |
| 19 | 11. 5885 | 29. 435 |
| 20 | 11. 9625 | 30. 385 |
| 21 | 12. 195 | 30. 975 |

| Line | Inches<br>From Center Line | Centimeters<br>From Center Line |
|---|---|---|
| 22 | 12.495 | 31.737 |
| 23 | 12.795 | 32.499 |
| 24 | 13.095 | 33..261 |
| 25 | 13.3275 | 33.852 |
| 26 | 13.7015 | 34.802 |
| 27 | 13.9675 | 35.477 |
| 28 | 15.805 | 40.145 |
| 29 | 17.645 | 44.818 |
| 30 | 18.1895 | 46.201 |
| 31 | 18.5635 | 47.151 |
| 32 | 18.796 | 47.742 |
| 33 | 18.905 | 48.019 |
| 34 | 19.030 | 48.336 |
| 35 | 19.139 | 48.613 |
| 36 | 19.3715 | 49.204 |
| 37 | 19.7455 | 50.154 |
| 38 | 20.29 | 51.537 |
| 39 | 22.13 | 56.210 |
| 40 | 23.9675 | 60.877 |
| 41 | 24.2335 | 61.553 |
| 42 | 24.514 | 62.266 |
| 43 | 24.6075 | 62.503 |
| 44 | 24.84 | 63.094 |
| 45 | 25.14 | 63.856 |
| 46 | 25.44 | 64.618 |
| 47 | 25.74 | 65.380 |
| 48 | 25.9725 | 65.970 |
| 49 | 26.066 | 66.208 |
| 50 | 26.3465 | 66.920 |
| 51 | 26.6125 | 67.596 |
| 52 | 28.45 | 72.263 |
| 53 | 30.29 | 76.937 |
| 54 | 30.8345 | 78.320 |
| 55 | 31.2085 | 79.270 |
| 56 | 31.441 | 79.860 |
| 57 | 31.55 | 80.137 |
| 58 | 31.675 | 80.455 |
| 59 | 31.784 | 80.731 |
| 60 | 32.0165 | 81.322 |
| 61 | 32.3905 | 82.272 |
| 62 | 34.5015 | 87.634 |
| 63 | 36.6125 | 92.996 |
| 64 | 36.8785 | 93.671 |
| 65 | 37.2525 | 94.621 |
| 66 | 37.485 | 95.212 |
| 67 | 37.6725 | 95.688 |
| 68 | 37.86 | 96.164 |
| 69 | 38.36 | 97.434 |
| 70 | 39.36 | 99.974 |
| 71 | 41.86 | 106.324 |
| 72 | 45.86 | 116.484 |
| 73 | 49.85 | 126.619 |

TABLE B-2

PDQ COEFFICIENTS FOR 501 F AND FULL POWER

| Material Number | Material | Group | $D$ | $\Sigma_a$ | $\Sigma_R$ | $\nu\Sigma_f$ |
|---|---|---|---|---|---|---|
| 1 | Lattice of Zone I Central and Zone II and III Peripheral Fuel Pins | 1 | 2.0203991 | 0.002743789 | 0.042189445 | 0.002333 |
| | | 2 | 0.66344871 | 0.023908825 | 0.085913846 | 0.01344886 |
| | | 3 | 0.6231046 | 0.05483162 | 0.095811148 | 0.051736559 |
| | | 4 | 0.3303093 | 0.247945987 | | 0.36061582 |
| 2 | Lattice of Zone II Central Fuel Pins | 1 | 2.0209829 | 0.002982737 | 0.042101381 | 0.0029174102 |
| | | 2 | 0.66452786 | 0.0260717 | 0.084925547 | 0.018124301 |
| | | 3 | 0.62126848 | 0.06605206 | 0.09335379 | 0.06964662 |
| | | 4 | 0.32310275 | 0.30403802 | | 0.47881604 |
| 3 | Lattice of Zone III Central Fuel Pins | 1 | 2.0221945 | 0.003209374 | 0.04202863 | 0.0034720966 |
| | | 2 | 0.6656913 | 0.028104418 | 0.084050914 | 0.022517156 |
| | | 3 | 0.61976689 | 0.076627663 | 0.091220731 | 0.086472044 |
| | | 4 | 0.3166158 | 0.35627173 | | 0.58868865 |
| 4 | Lattice of Zone I Peripheral Fuel Pins | 1 | 2.0200794 | 0.002609213 | 0.042245963 | 0.0020040363 |
| | | 2 | 0.66285712 | 0.022681299 | 0.086504776 | 0.010794795 |
| | | 3 | 0.62421275 | 0.0484747 | 0.097300615 | 0.041560761 |
| | | 4 | 0.33477627 | 0.214191452 | | 0.28997149 |
| 5 | Lattice of Corner Pins Containing $ThO_2$ Pellets | 1 | 2.0231532 | 0.002069735 | 0.042560456 | 0.00068806301 |
| | | 2 | 0.66137787 | 0.017691451 | 0.089292864 | |
| | | 3 | 0.62992712 | 0.022646561 | 0.10431439 | |
| | | 4 | 0.35413446 | 0.074961903 | | |
| 6 | Hafnium Control Rod | 1 | 0.9840825 | 0.00049323 | | |
| | | 2 | 0.98408248 | 0.000534436 | | |
| | | 3 | 1.16 | 1.15983528 | | |
| | | 4 | 0.3568865 | 2.93240782 | | |

| Material Number | Material | Group | D | $\Sigma_a$ | $\Sigma_R$ | $\nu \Sigma_f$ |
|---|---|---|---|---|---|---|
| 7 | Boron Steel Control Rod | 1 | 1.3050602 | 0.003012946 | 0.0013248423 | |
| | | 2 | 0.4051895 | 0.049015293 | 0.00073654669 | |
| | | 3 | 0.38035182 | 0.79759712 | 0.0011765489 | |
| | | 4 | 0.10928394 | 10.16824248 | | |
| 8 | Water | 1 | 2.7953089 | 0.000330829 | 0.060355096 | |
| | | 2 | 0.73489355 | 0.000490186 | 0.20246255 | |
| | | 3 | 0.72311216 | -0.000156741 | 0.22554059 | |
| | | 4 | 0.24719869 | 0.01153107 | | |
| 9 | SS-304 | 1 | 1.2619985 | | 0.0033309907 | |
| | | 2 | 0.41116892 | | 0.0068052977 | |
| | | 3 | 0.38280854 | 0.02374718 | 0.00028993276 | |
| | | 4 | 0.38063111 | 0.165861581 | | |
| 10 | Zr-2 | 1 | 1.144997 | | 0.0014042092 | |
| | | 2 | 1.15288 | | 0.0009272515 | |
| | | 3 | 1.2749498 | 0.009329562 | 0.0000210832 | |
| | | 4 | 1.2924531 | 0.006674719 | | |
| 11 | Homogenized Water and Zr-2 Ratio 1:2 | 1 | 1.7299774 | 0.000128908 | 0.023821799 | |
| | | 2 | 0.96898091 | 0.000161988 | 0.068022717 | |
| | | 3 | 1.0173638 | 0.016178052 | 0.068469805 | |
| | | 4 | 0.53615305 | 0.008291319 | | |
| 12 | Homogenized Water and Zr-2 Ratio 1:1 | 1 | 1.9297955 | 0.000182641 | 0.033538664 | |
| | | 2 | 0.8967502 | 0.000244312 | 0.10169949 | |
| | | 3 | 0.92325758 | 0.012421408 | 0.10754281 | |
| | | 4 | 0.41468844 | 0.009103 | | |

TABLE B-3

PDQ COEFFICIENTS FOR 501 F AND NO POWER

| Material Number | Material | Group | D | $\Sigma_a$ | $\Sigma_R$ | $\nu\Sigma_f$ |
|---|---|---|---|---|---|---|
| 1 | Lattice of Zone 1 | 1 | 2.0195506 | 0.002566597 | 0.042271403 | 0.0023327425 |
|  | Central and Zone II | 2 | 0.66326055 | 0.022346606 | 0.086614424 | 0.013507611 |
|  | and III Peripheral | 3 | 0.62300416 | 0.053273401 | 0.095858839 | 0.05176367 |
|  | Fuel Pins | 4 | 0.3303093 | 0.24794599 |  | 0.36061581 |
| 2 | Lattice of Zone II | 1 | 2.0201115 | 0.002809574 | 0.042181231 | 0.0029178054 |
|  | Central Fuel Pins | 2 | 0.66435397 | 0.024561869 | 0.085595771 | 0.018201978 |
|  |  | 3 | 0.62115279 | 0.064499385 | 0.093390435 | 0.069681265 |
|  |  | 4 | 0.32310275 | 0.30403802 |  | 0.47881604 |
| 3 | Lattice of Zone III | 1 | 2.0213474 | 0.003040098 | 0.042106482 | 0.0034727032 |
|  | Central Fuel Pins | 2 | 0.66552652 | 0.026643058 | 0.084693382 | 0.022610491 |
|  |  | 3 | 0.61965192 | 0.075082041 | 0.091248169 | 0.08651242 |
|  |  | 4 | 0.3166158 | 0.35627174 |  | 0.58868864 |
| 4 | Lattice of Zone I | 1 | 2.0191679 | 0.002429646 | 0.042329111 | 0.0020040589 |
|  | Peripheral Fuel Pins | 2 | 0.66266744 | 0.021088963 | 0.08722297 | 0.010843589 |
|  |  | 3 | 0.62409693 | 0.046914167 | 0.097355193 | 0.04158378 |
|  |  | 4 | 0.33477627 | 0.21419146 |  | 0.28997149 |
| 5 | Lattice of Corner | 1 | 2.0221859 | 0.001881015 | 0.04264835 | 0.0006874984 |
|  | Pins Containing | 2 | 0.66116397 | 0.015973661 | 0.090085679 |  |
|  | ThO$_2$ Pellets | 3 | 0.6298138 | 0.02108284 | 0.10440224 |  |
|  |  | 4 | 0.35413446 | 0.07496191 |  |  |
| 6-12 | All constants for material regions 6 through 12 are identical with those shown for the 501 F, full power core in Table B-2. | | | | | |

## TABLE B-4

### PDQ COEFFICIENTS FOR 425 F AND NO POWER

| Material Number | Material | Group | D | $\Sigma_a$ | $\Sigma_R$ | $\nu\Sigma_f$ |
|---|---|---|---|---|---|---|
| 1 | Lattice and Zone I Central and Zone II and III Peripheral Fuel Pins | 1 | 1.9756989 | 0.002593215 | 0.044541193 | 0.0023434974 |
| | | 2 | 0.64338735 | 0.022683165 | 0.093208775 | 0.013573382 |
| | | 3 | 0.60513763 | 0.05353728 | 0.10326994 | 0.051942883 |
| | | 4 | 0.30527202 | 0.26008985 | | 0.37878006 |
| 2 | Lattice of Zone II Central Fuel Pins | 1 | 1.9764948 | 0.00283513 | 0.04444613 | 0.0029268396 |
| | | 2 | 0.64448589 | 0.02491178 | 0.092170878 | 0.018295609 |
| | | 3 | 0.60358019 | 0.06478464 | 0.10074139 | 0.06994117 |
| | | 4 | 0.29893272 | 0.31895319 | | 0.50288627 |
| 3 | Lattice of Zone III Central Fuel Pins | 1 | 1.9776693 | 0.00306471 | 0.044369644 | 0.0034805571 |
| | | 2 | 0.64560803 | 0.02700743 | 0.09125671 | 0.022734045 |
| | | 3 | 0.60227553 | 0.075390216 | 0.098545541 | 0.086854383 |
| | | 4 | 0.2931949 | 0.37375851 | | 0.61834344 |
| 4 | Lattice of Zone I Peripheral Fuel Pins | 1 | 1.9755525 | 0.002456806 | 0.044601238 | 0.0020150951 |
| | | 2 | 0.64283673 | 0.021417778 | 0.093830432 | 0.010893376 |
| | | 3 | 0.60612753 | 0.04716599 | 0.10480022 | 0.041719257 |
| | | 4 | 0.30920188 | 0.22466505 | | 0.30456373 |
| 5 | Lattice of Corner Pins Containing $ThO_2$ Pellets | 1 | 1.9781572 | 0.001910619 | 0.04493527 | 0.00070153293 |
| | | 2 | 0.64127333 | 0.01627822 | 0.096754854 | |
| | | 3 | 0.61108702 | 0.0221754 | 0.11197004 | |
| | | 4 | 0.32607841 | 0.07858263 | | |
| 6 | Hafnium Control Rod | 1 | 0.9840825 | 0.00049323 | | |
| | | 2 | 0.98408248 | 0.000534436 | | |
| | | 3 | 1.16 | 1.15983528 | | |
| | | 4 | 0.35259942 | 2.92857614 | | |

## TABLE B-4

### PDQ COEFFICIENTS FOR 425 F AND NO POWER (CONT'D)

| Material Number | Material | Group | D | $\Sigma_a$ | $\Sigma_R$ | $\nu\Sigma_f$ |
|---|---|---|---|---|---|---|
| 7 | Boron Steel Control Rod | 1 | 1.3054651 | 0.003011858 | 0.00132442 | |
| | | 2 | 0.40519132 | 0.049018728 | 0.00073684 | |
| | | 3 | 0.38035208 | 0.797639955 | 0.0011768245 | |
| | | 4 | 0.1060631 | 10.5958539 | | |
| 8 | Water | 1 | 2.6033343 | 0.000355348 | 0.064827027 | |
| | | 2 | 0.68386438 | 0.00052719 | 0.21759172 | |
| | | 3 | 0.67290064 | -0.00016795 | 0.24239034 | |
| | | 4 | 0.21887282 | 0.01291267 | | |
| 9 | SS-304 | 1 | 1.2623732 | | 0.0033300595 | |
| | | 2 | 0.41116839 | | 0.00680573 | |
| | | 3 | 0.3828088 | 0.024357998 | 0.00029011312 | |
| | | 4 | 0.3799747 | 0.17283667 | | |
| 10 | Zr-2 | 1 | 1.145094 | | 0.0014039224 | |
| | | 2 | 1.1528769 | | 0.0009271846 | |
| | | 3 | 1.2749498 | 0.009329175 | 0.0000210747 | |
| | | 4 | 1.2921416 | 0.006955419 | | |
| 11 | Homogenized Water and Zr-2 Ratio 1:2 | 1 | 1.7063937 | 0.000137615 | 0.025407271 | |
| | | 2 | 0.93817512 | 0.000174382 | 0.073059836 | |
| | | 3 | 0.98302337 | 0.016234639 | 0.074029924 | |
| | | 4 | 0.49030842 | 0.008938362 | | |
| 12 | Homogenized Water and Zr-2 Ratio 1:1 | 1 | 1.8822216 | 0.00019532 | 0.035850125 | |
| | | 2 | 0.85765005 | 0.00026289 | 0.10926524 | |
| | | 3 | 0.8812809 | 0.01244102 | 0.11594761 | |
| | | 4 | 0.37407146 | 0.009934047 | | |

TABLE B-5

PDQ COEFFICIENTS FOR 68 F AND NO POWER

| Material Number | Material | Group | D | $\Sigma_a$ | $\Sigma_R$ | $\nu\Sigma_f$ |
|---|---|---|---|---|---|---|
| 1 | Lattice of Zone I Central and Zone II and III Peripheral Fuel Pins | 1 | 1.8575326 | 0.00258451 | 0.050823246 | 0.0023734975 |
| | | 2 | 0.59318765 | 0.02278574 | 0.1119527 | 0.013774234 |
| | | 3 | 0.55970951 | 0.05353604 | 0.12396239 | 0.05247546 |
| | | 4 | 0.2295857 | 0.33685993 | | 0.49400658 |
| 2 | Lattice of Zone II Central Fuel Pins | 1 | 1.8577165 | 0.00282657 | 0.050724464 | 0.002955242 |
| | | 2 | 0.59407147 | 0.02507512 | 0.11087094 | 0.018580098 |
| | | 3 | 0.55854251 | 0.06486487 | 0.12130235 | 0.070706607 |
| | | 4 | 0.22483802 | 0.41669894 | | 0.6625084 |
| 3 | Lattice of Zone III Central Fuel Pins | 1 | 1.8583719 | 0.00305625 | 0.050644221 | 0.003507461 |
| | | 2 | 0.59499741 | 0.02723018 | 0.10991663 | 0.023102928 |
| | | 3 | 0.55758697 | 0.07555218 | 0.1189739 | 0.08785201 |
| | | 4 | 0.22050696 | 0.49155473 | | 0.82043953 |
| 4 | Lattice of Zone I Peripheral Fuel Pins | 1 | 1.8573396 | 0.00244823 | 0.050890661 | 0.0020460957 |
| | | 2 | 0.59266458 | 0.02148817 | 0.11261184 | 0.011050232 |
| | | 3 | 0.56038142 | 0.04712373 | 0.12557536 | 0.042130062 |
| | | 4 | 0.23220789 | 0.29319009 | | 0.40068361 |
| 5 | Lattice of Corner Pins Containing ThO$_2$ Pellets | 1 | 1.8615233 | 0.00190225 | 0.05125205 | 0.0007365384 |
| | | 2 | 0.59147684 | 0.01622608 | 0.11571323 | |
| | | 3 | 0.56418454 | 0.02112315 | 0.13305159 | |
| | | 4 | 0.24406654 | 0.10307068 | | |
| 6 | Hafnium Control Rod | 1 | 0.95052585 | 0.000627 | | |
| | | 2 | 0.95089379 | 0.000609884 | | |
| | | 3 | 1.16 | 1.159835 | | |
| | | 4 | 0.2971951 | 3.7915013 | | |

TABLE B-5

PDQ COEFFICIENTS FOR 68 F AND NO POWER (CONT'D)

| Material Number | Material | Group | D | $\Sigma_a$ | $\Sigma_R$ | $\nu\Sigma_f$ |
|---|---|---|---|---|---|---|
| 7 | Boron Steel Control Rod | 1 | 1.0911954 | 0.00350252 | 0.001295066 | |
| | | 2 | 0.39617577 | 0.04088969 | 0.000262984 | |
| | | 3 | 0.38034417 | 0.7969522 | 0.0012577I | |
| | | 4 | 0.087281293 | 13.71799561 | | |
| 8 | Water | 1 | 2.2177913 | 0.00041735 | 0.076138371 | |
| | | 2 | 0.58172936 | 0.00062067 | 0.25583733 | |
| | | 3 | 0.57240268 | -0.00019642 | 0.28498651 | |
| | | 4 | 0.15021718 | 0.01965249 | | |
| 9 | SS-304 | 1 | 1.0639234 | | 0.00349517 | |
| | | 2 | 0.41199223 | | 0.0059236952 | |
| | | 3 | 0.38245444 | 0.02245502 | 0.0000840642 | |
| | | 4 | 0.37524947 | 0.22376418 | | |
| 10 | Zr-2 | 1 | 1.1452696 | | 0.001403405 | |
| | | 2 | 1.1528712 | | 0.000927063 | |
| | | 3 | 1.2749498 | 0.00932846 | 0.0000210589 | |
| | | 4 | 1.2898721 | 0.00900488 | | |
| 11 | Homogenized Water and Zr-2 Ratio 1:2 | 1 | 1.6481985 | 0.00015948 | 0.029392226 | |
| | | 2 | 0.86834589 | 0.00020568 | 0.085800688 | |
| | | 3 | 0.90567795 | 0.01634884 | 0.08811773 | |
| | | 4 | 0.3654756 | 0.01254949 | | |
| 12 | Homogenized Water and Zr-2 Ratio 1:1 | 1 | 1.7712542 | 0.00022724 | 0.041671769 | |
| | | 2 | 0.7724913 | 0.00030977 | 0.12839732 | |
| | | 3 | 0.79040510 | 0.0124777 | 0.13721266 | |
| | | 4 | 0.26892821 | 0.01432884 | | |

- 79 -

# REFERENCES

1.  Hughes, D. J. and Schwartz, R. B., Neutron Cross Sections, BNL-325, Second Edition, July 1, 1958.

2.  Bilodeau, G. G., et al., PDQ - An IBM-704 Code to Solve the Two-Dimensional Few-Group Neutron-Diffusion Equations, WAPD-TM-70, August 1957.

3.  Cadwell, W. R., TKO - A Three-Dimensional Neutron-Diffusion Code for the IBM-704, WAPD-TM-143, July 1958.

4.  Barringer, H. S. and Snidow, N. L., Consolidated Edison Thorium Reactor - Critical Experiment on Plate Fuel Elements, BAW-31, Rev. 1, August 1960.

5.  Clark, R. H., Barrett, L. G. and Funderburg, J. M., Consolidated Edison Thorium Reactor - Hot Exponential Experiment, BAW-116, Rev. 1, July 1960.

6.  Batch, M. L. and Snidow, N. L., Consolidated Edison Thorium Reactor - Critical Experiments with Oxide Fuel Pins, BAW-119, Rev. 1, August 1960.

7.  Pettus, W. G., Geometric and Temperature Effects in Thorium Resonance Capture, BAW-144, June 1960.

8.  Randall, D. and St. John, D. S., "Xenon Spatial Oscillations", Nucleonics 16, No. 3, March 1958.

FIGURES

FIG. 2.1: CETR CORE HARDWARE POSITION DESIGNATIONS

LEGEND

FUEL ELEMENT POSITION ZONE I

FUEL ELEMENT POSITION ZONE II

FUEL ELEMENT POSITION ZONE III

HOLD DOWN COLUMN POSITION

MOVABLE ROD POSITION

FIXED ROD POSITION

T-SHAPED FLUX DEPRESSOR

ANGLE-SHAPED FLUX DEPRESSOR

CRUCIFORM SHAPED FLUX DEPRESSOR
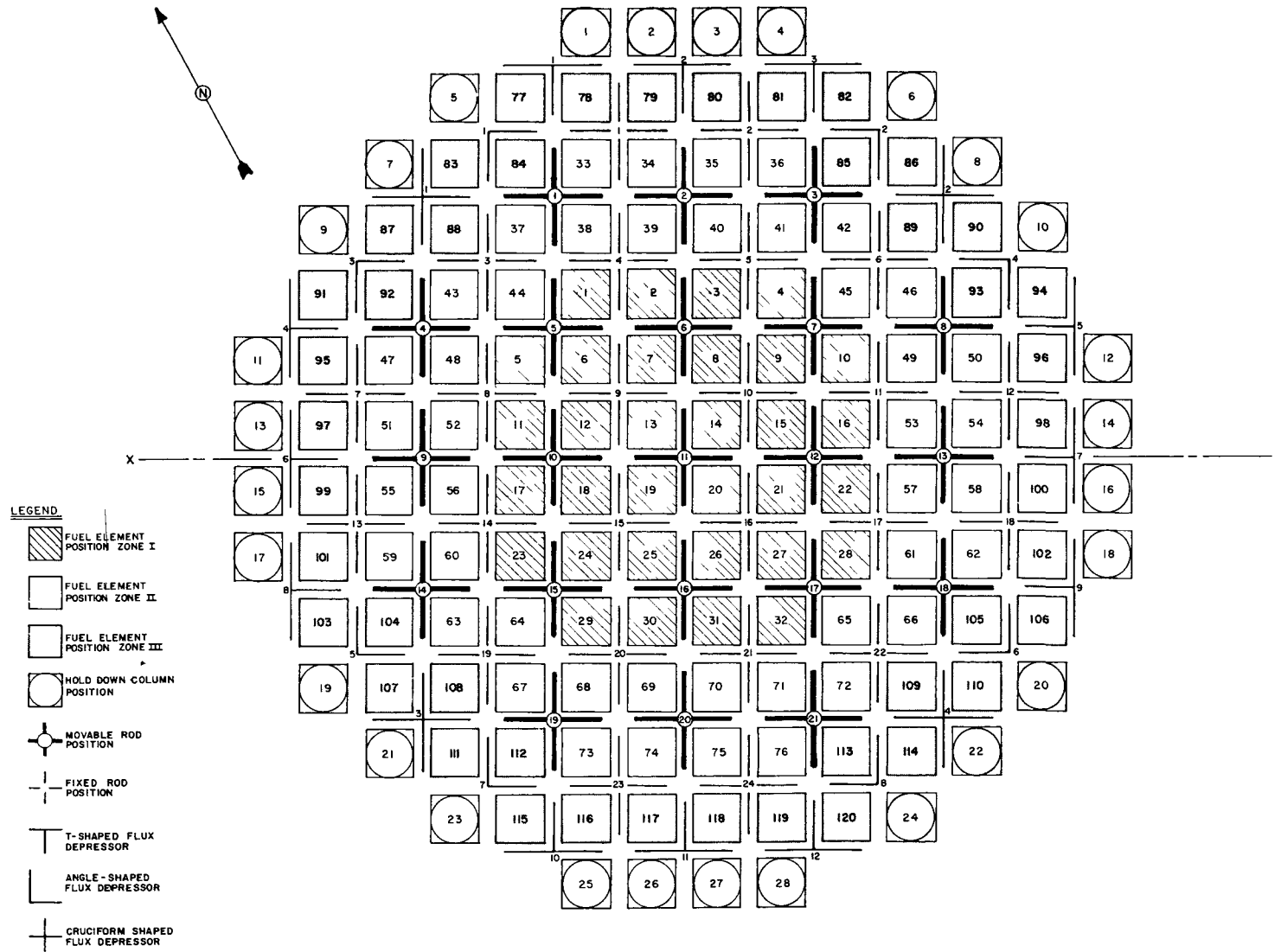
FIG. 2.2:  FUEL ELEMENT CROSS SECTION



INDEX STRIP

.445"

.374"

.374"

FLOW BLOCK

5.401"

.155"

5.711"
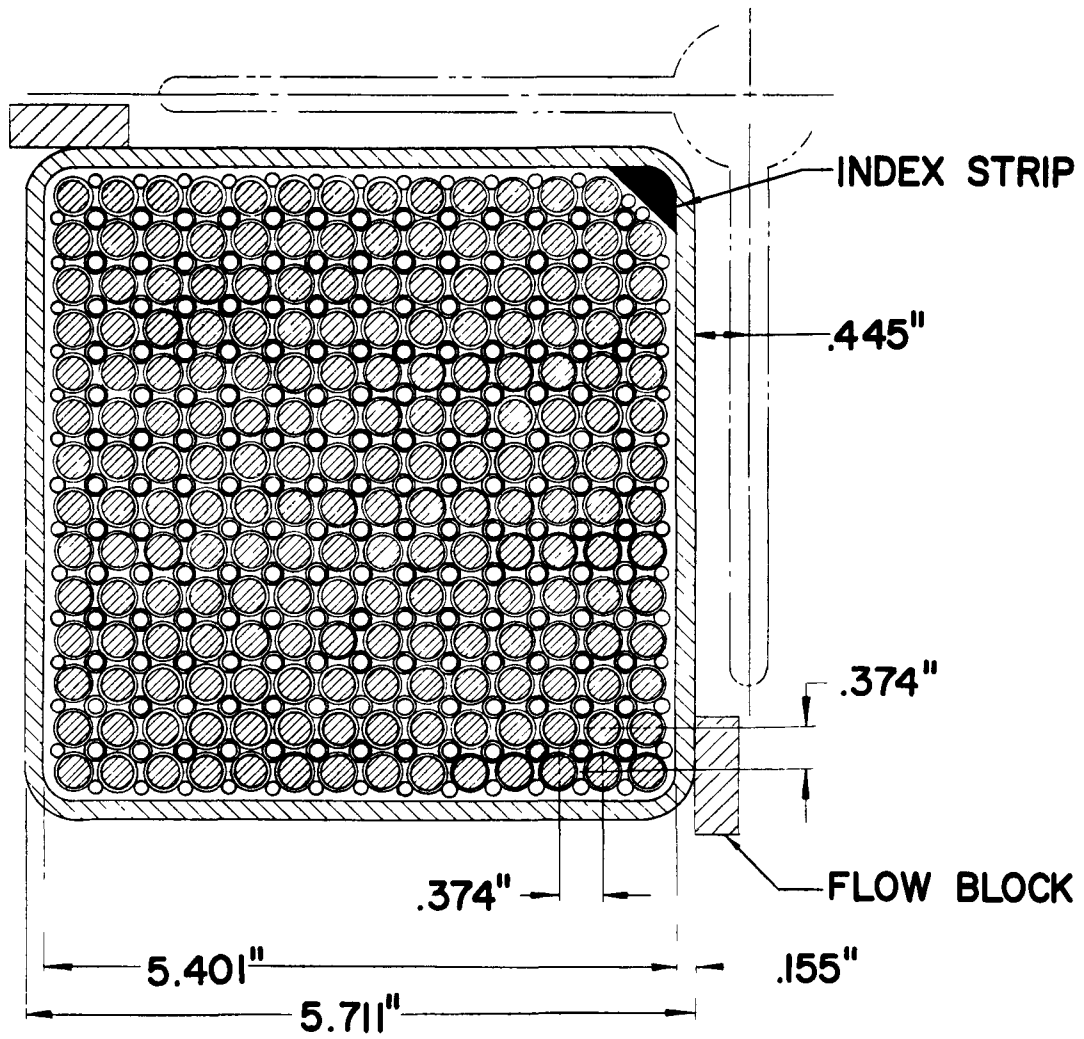
# FIG. 2.3: FUEL ELEMENT LOADING PATTERNS
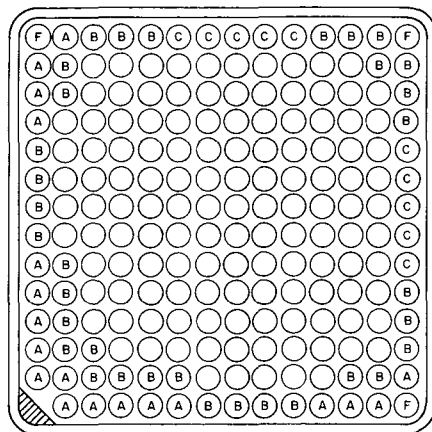
ZONE I
(ALL UNMARKED RODS ARE CONCENTRATION C)
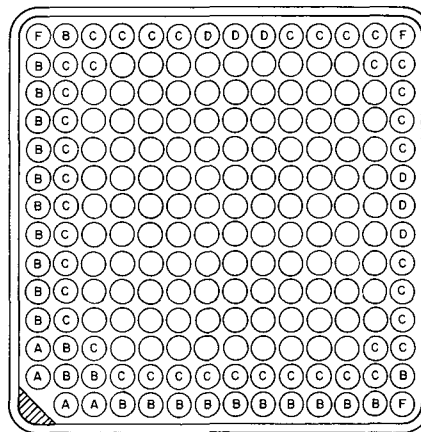
ZONE II
(ALL UNMARKED RODS ARE CONCENTRATION D)
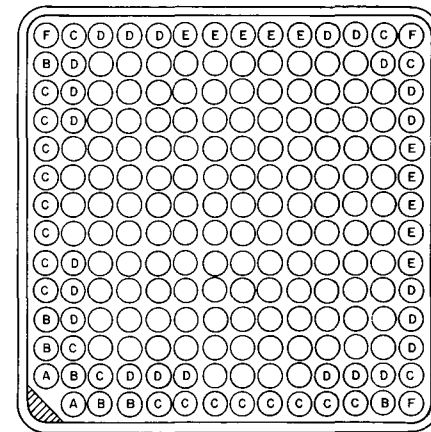
ZONE III
(ALL UNMARKED RODS ARE CONCENTRATION E)

LEGEND

A — LOWEST U-235 CONCENTRATION
B — SECOND LOWEST U-235 CONCENTRATION
C — THIRD LOWEST U-235 CONCENTRATION
D — FOURTH LOWEST U-235 CONCENTRATION
E — HIGHEST U-235 CONCENTRATION
F — 1/3 $THO_2$ + 2/3 CONCENTRATION A

FIG. 3.1: RADIAL MULTIPLICATION CONSTANT VERSUS TIME IN LIFE
WITH UNIFORM AXIAL BURNUP
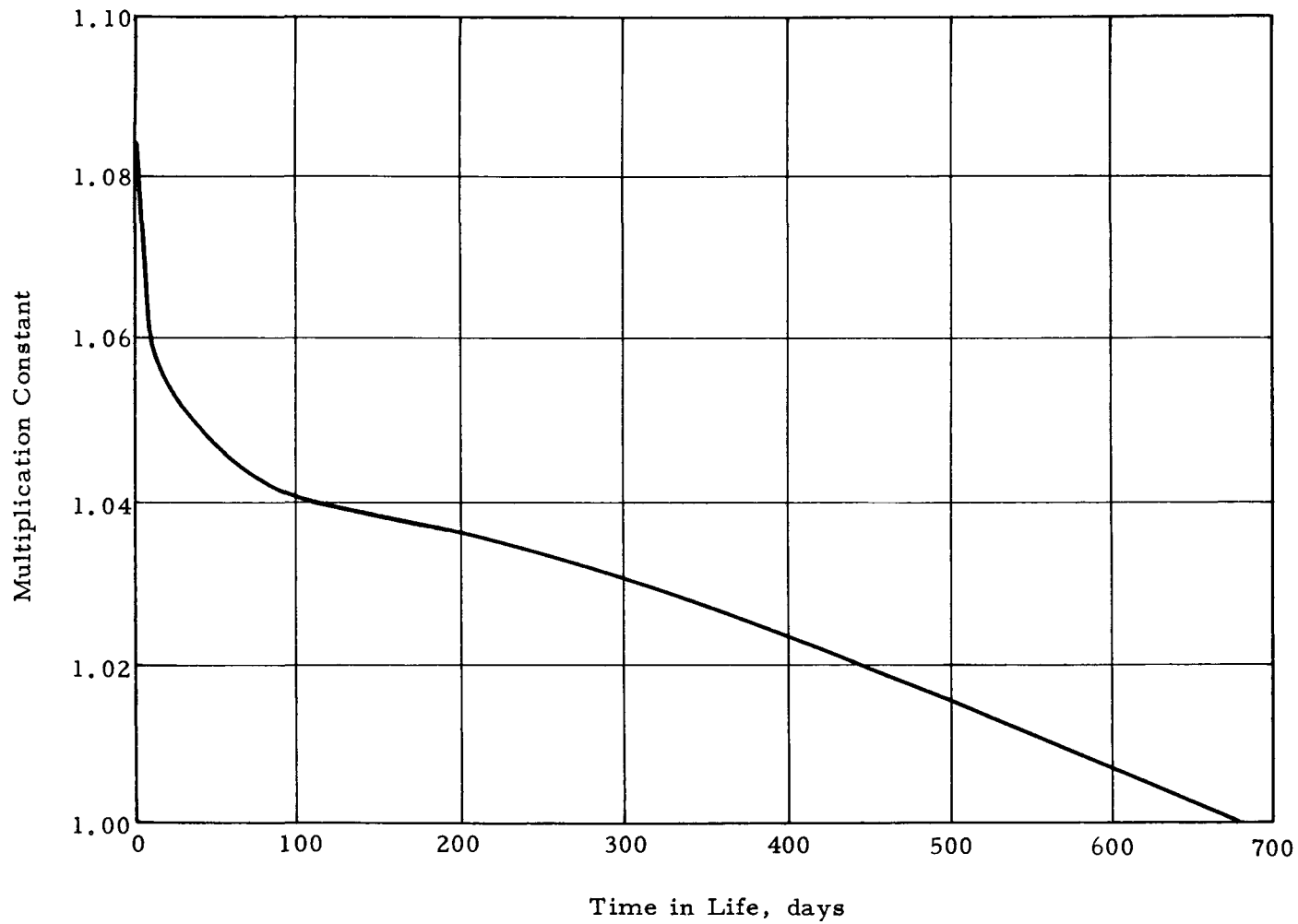
FIG. 3.2: AXIAL MULTIPLICATION CONSTANT VS TIME IN LIFE WITH
UNIFORM RADIAL BURNUP
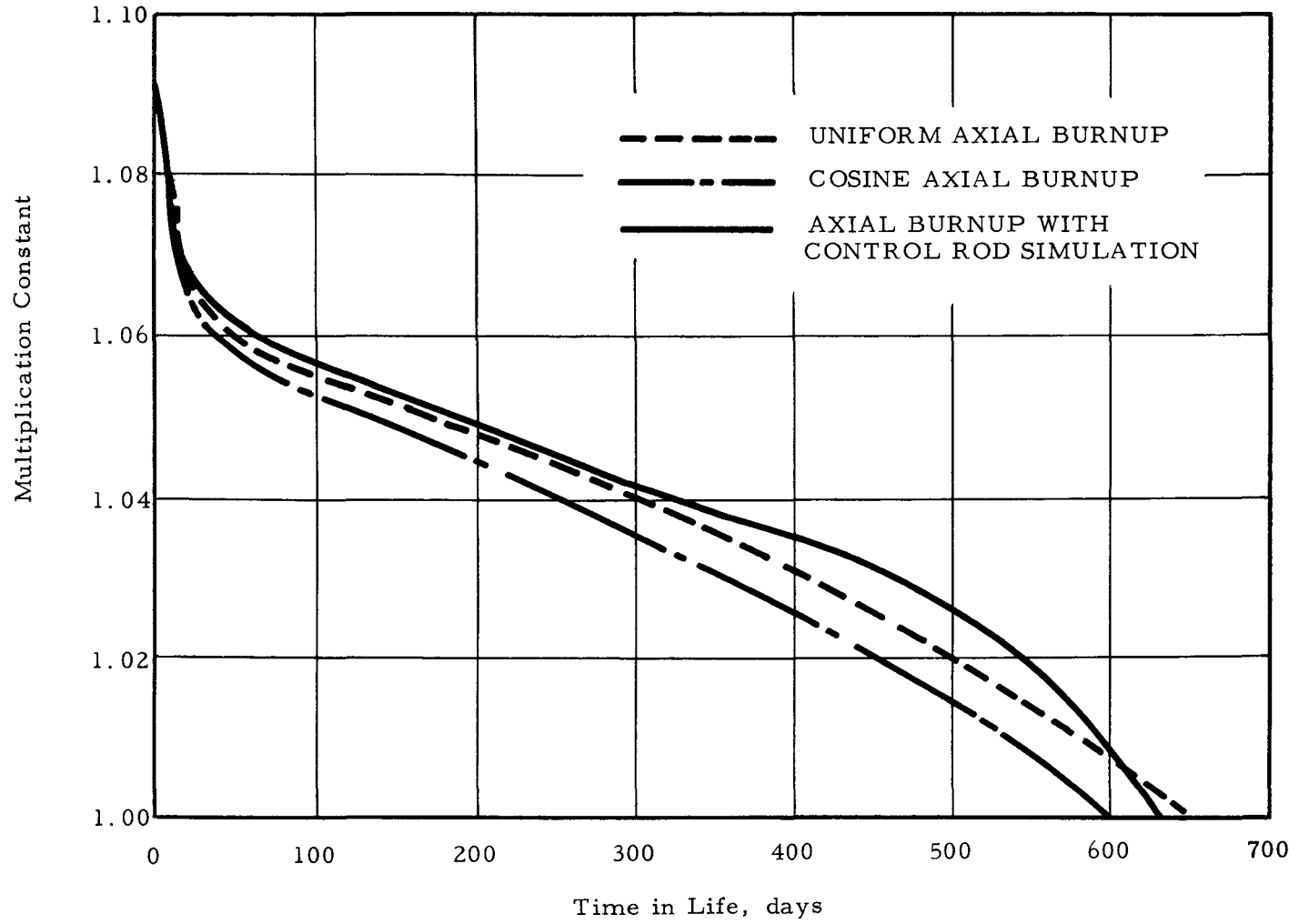
FIG. 3.3: MULTIPLICATION CONSTANT VS TIME IN LIFE WITH THE
CORRECTED AXIAL BURNUP
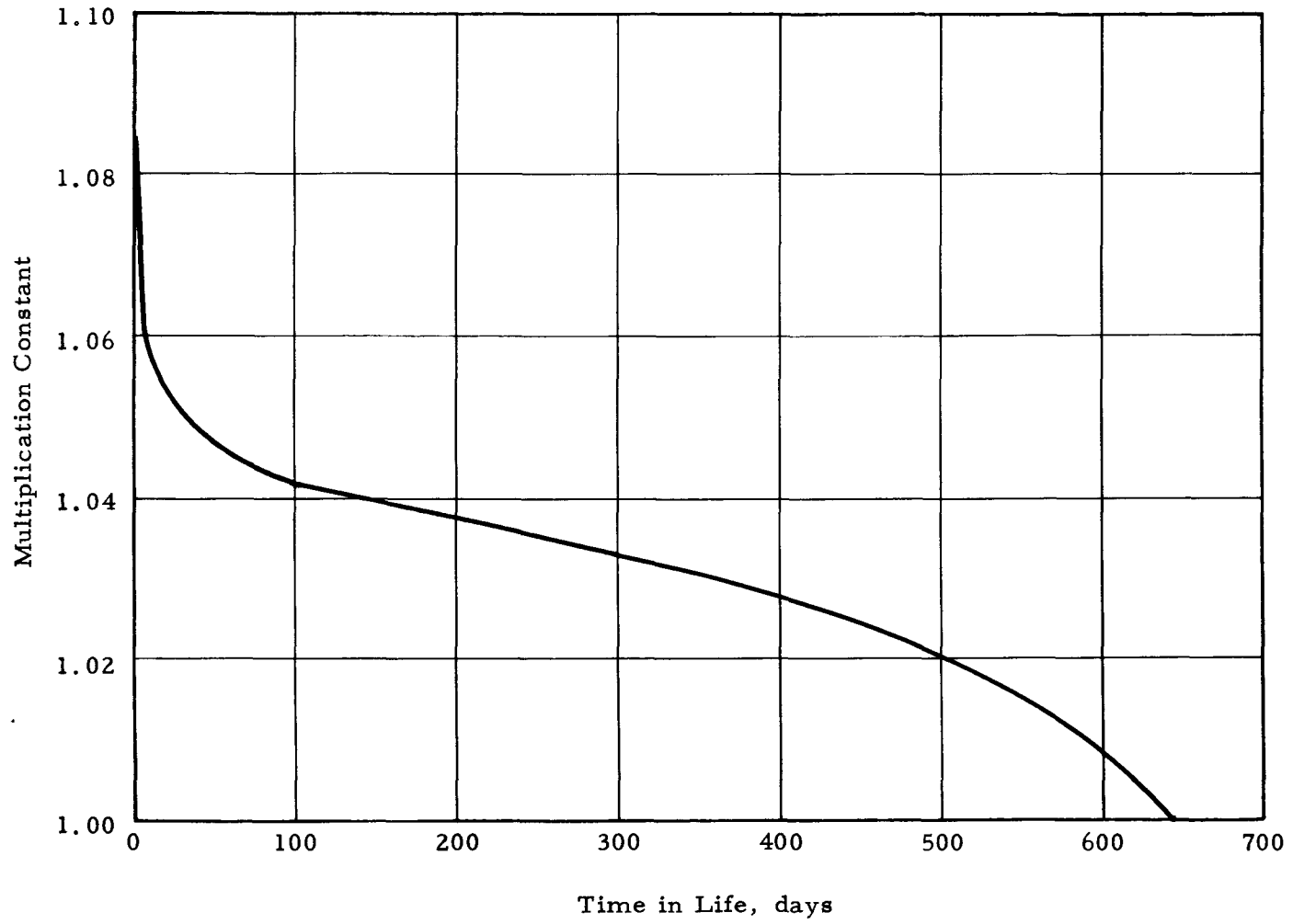
FIG. 3.4:  CETR CORE REACTIVITY AND ROD WORTH VS OPERATING CONDITIONS
(NOMINAL CASE .01 ΔK IN FIXED SHIMS)
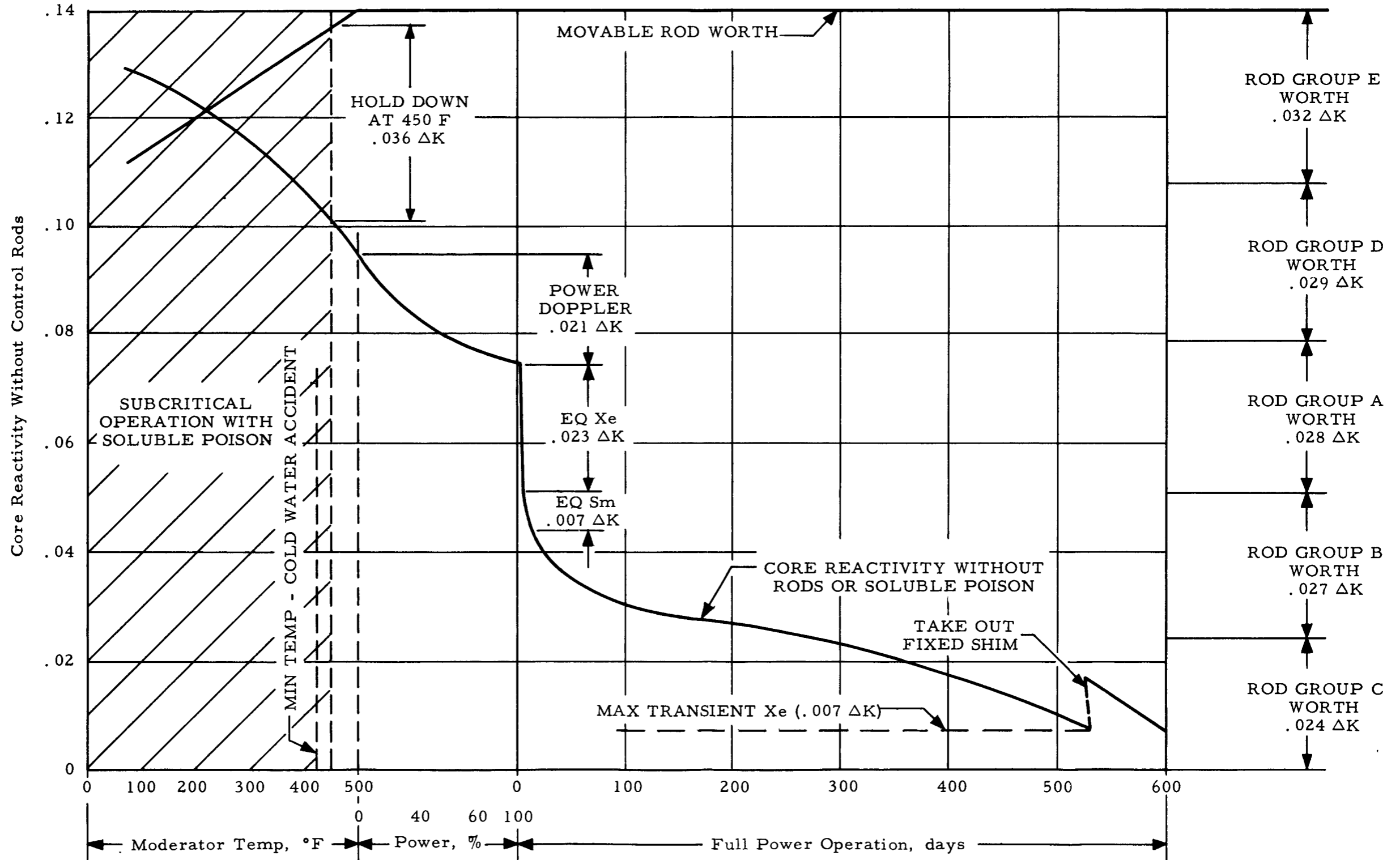
FIG. 3.5: MATERIAL BUCKLING CHANGE VS BORON CONCENTRATION
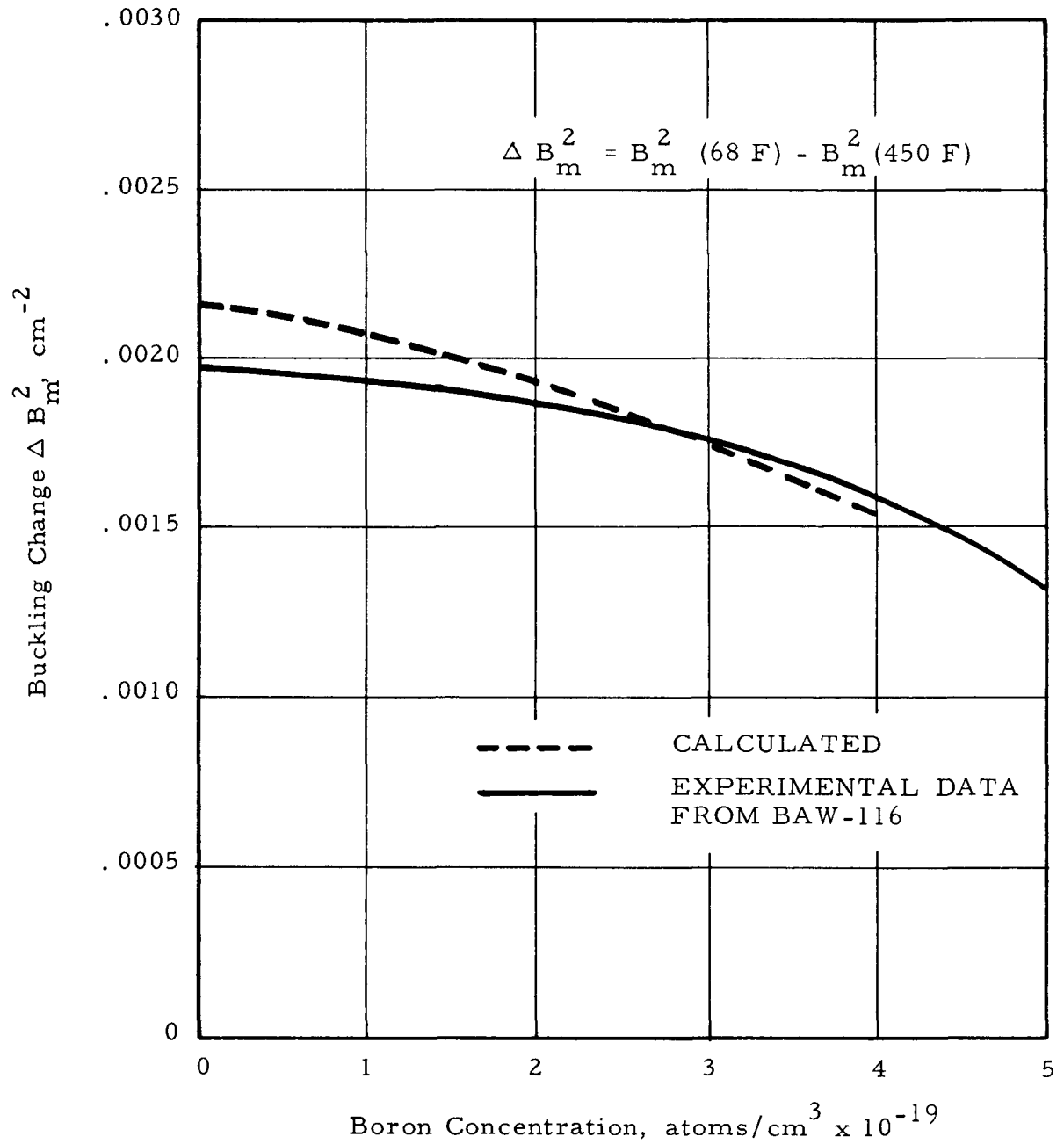
FIG. 3.6: EFFECTIVE MULTIPLICATION AS A FUNCTION OF TEMPERATURE
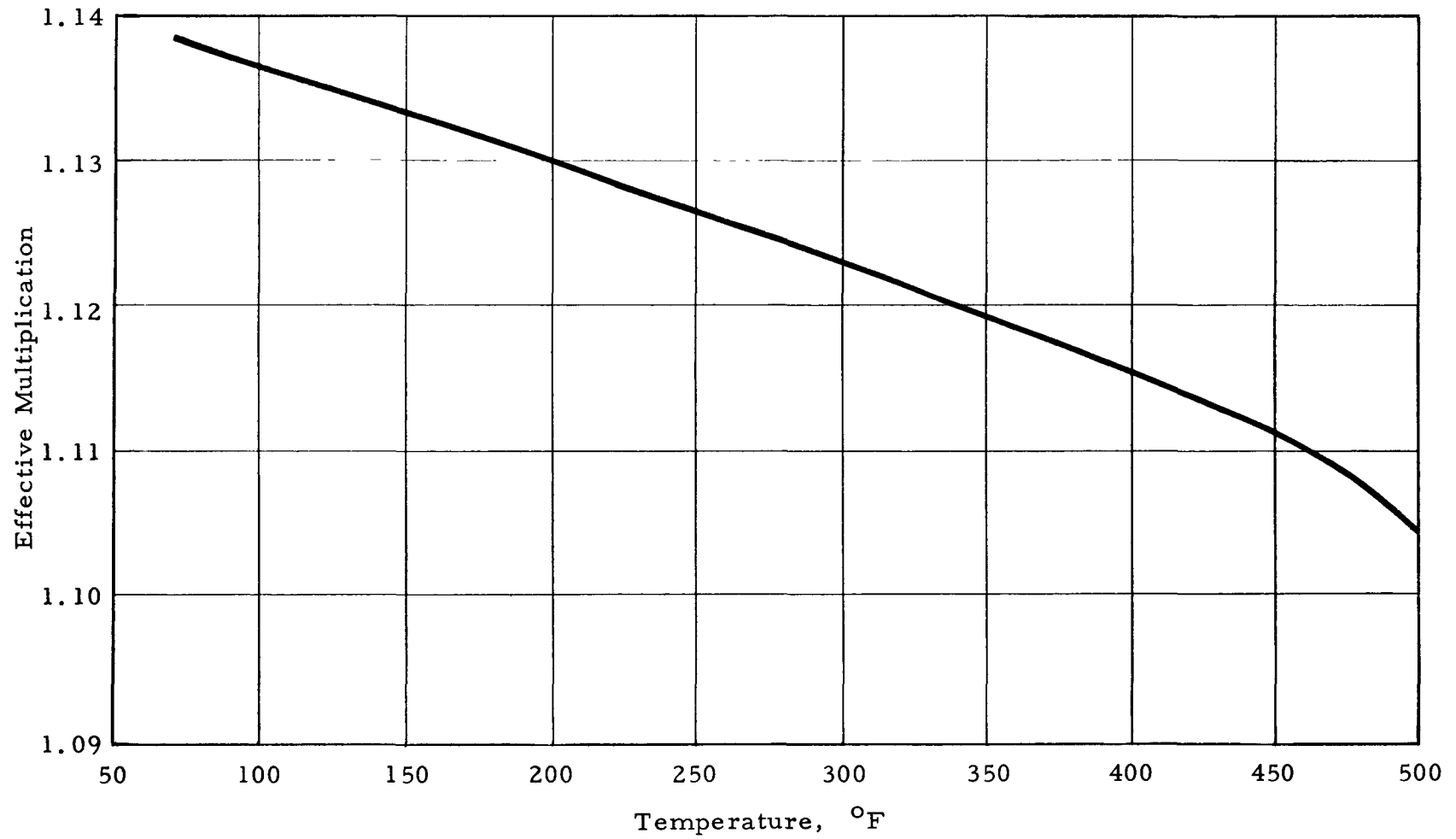
# FIG. 3.7: FUEL TEMPERATURE VARIATION WITH POWER DENSITY



Y-axis: Average Temperature in Fuel Pellet, °F

X-axis: Pellet Power, Fraction of Average Reactor Power Density

COLD GAP 0.0050"

COLD GAP 0.0035"

COLD GAP 0.0020"

COLD GAP 0.0000"

| MATERIAL | THERMAL CONDUCTIVITY BTU HR$^{-1}$ Ft$^{-1}$ °F$^{-1}$ |
|---|---|
| FUEL | 1.10 |
| GAP | 0.01 |
| CLAD | 12.0 |

REACTOR POWER 585 MW

NOTE: ALL COLD GAP DIMENSONS ARE DIAMETRAL
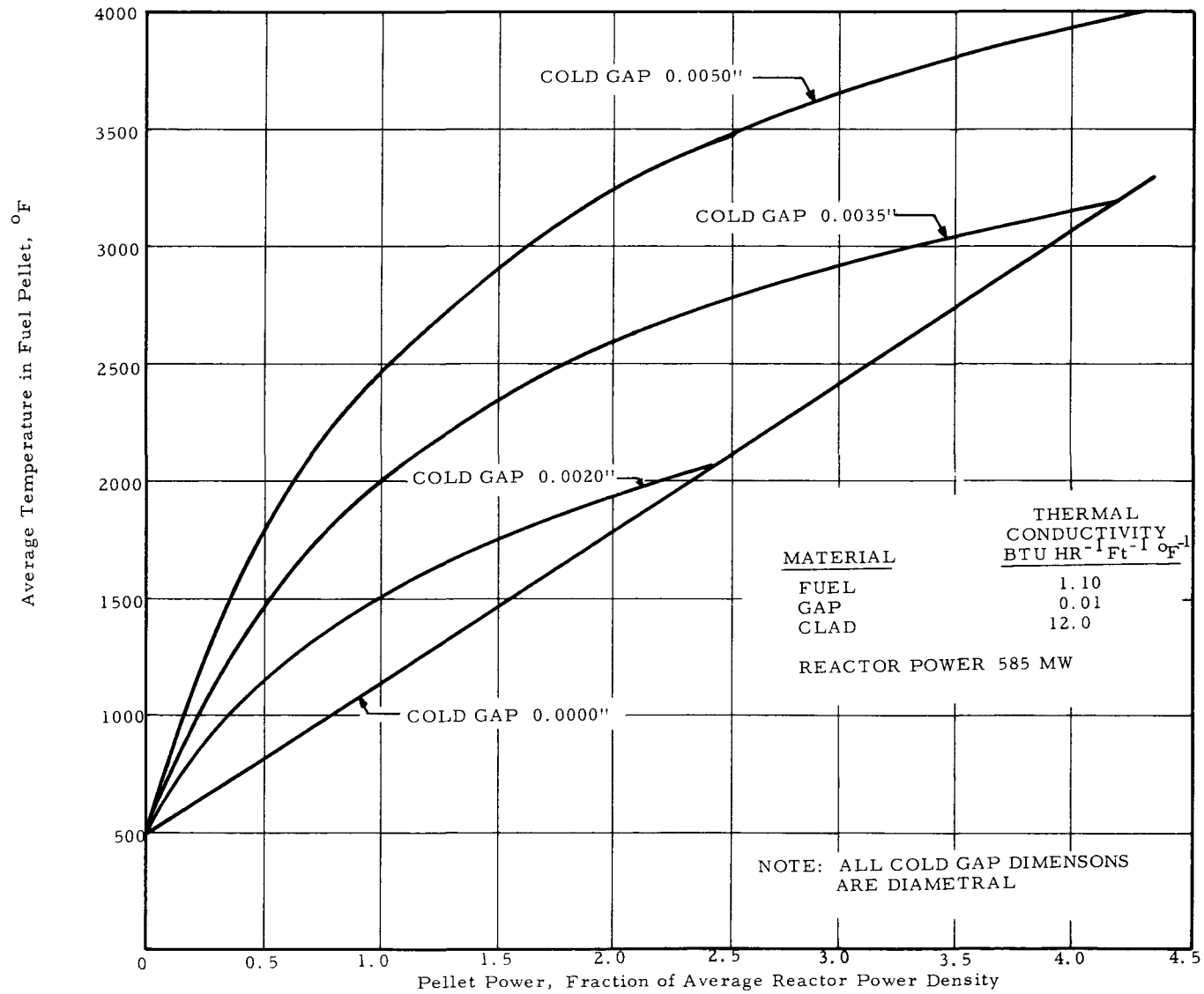
FIG. 3.8: GEOMETRY FOR CALCULATING
RELATIVE IMPORTANCE OF U-235
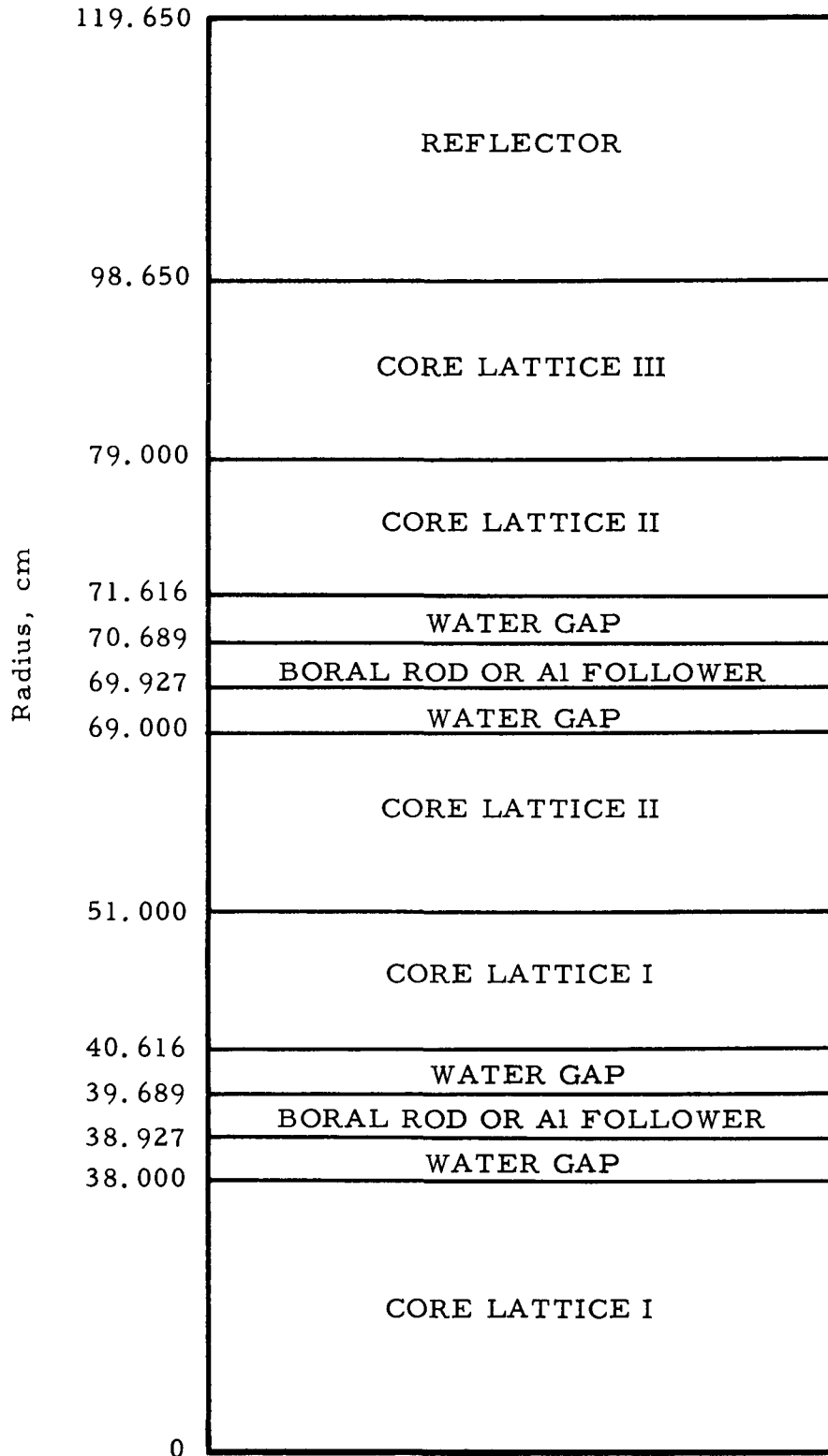
FIG. 3.9: FLUX WITH BORAL CONTROL RODS INSERTED
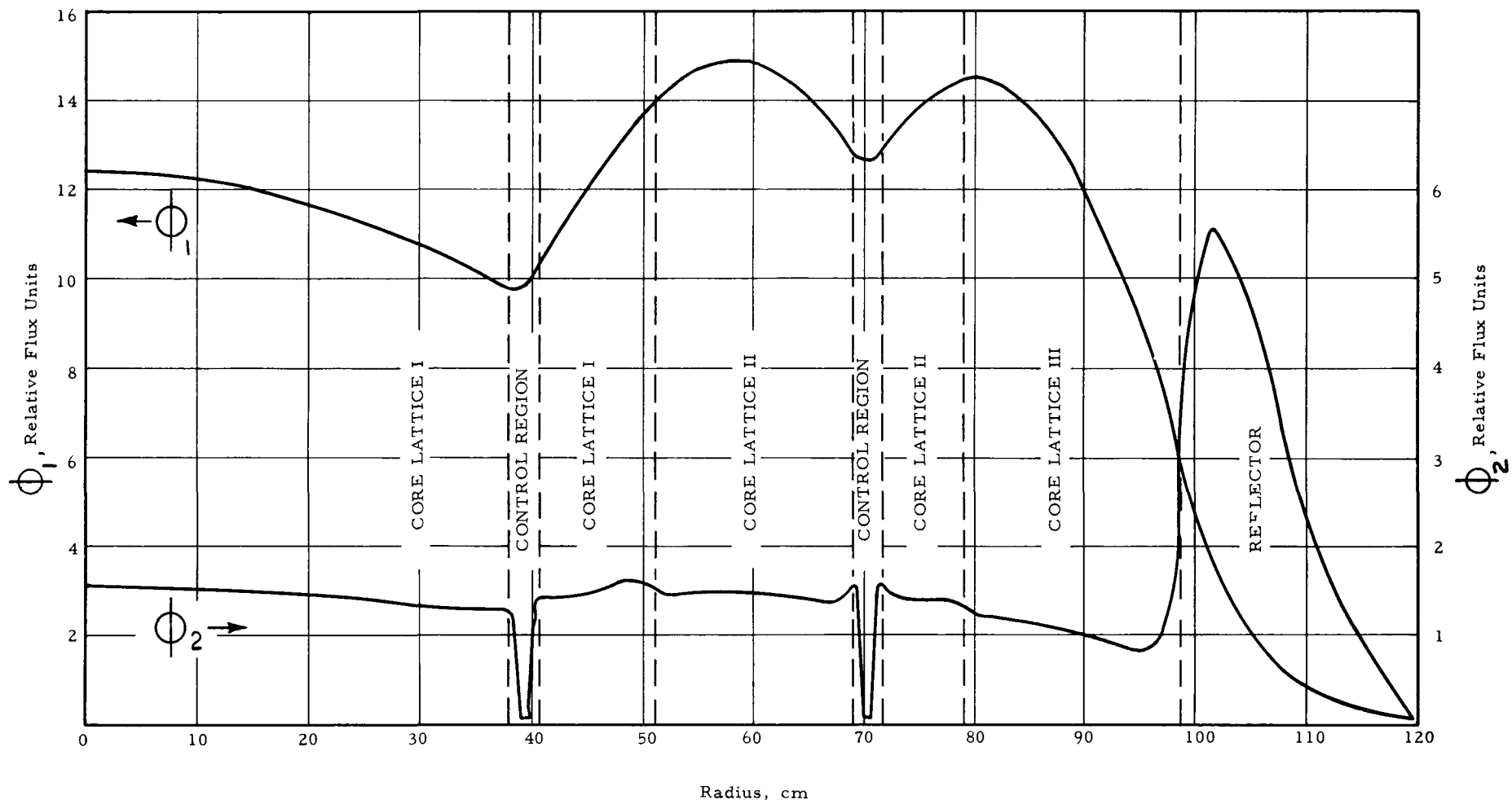
FIG. 3.10: ADJOINT FLUX WITH BORAL CONTROL RODS INSERTED
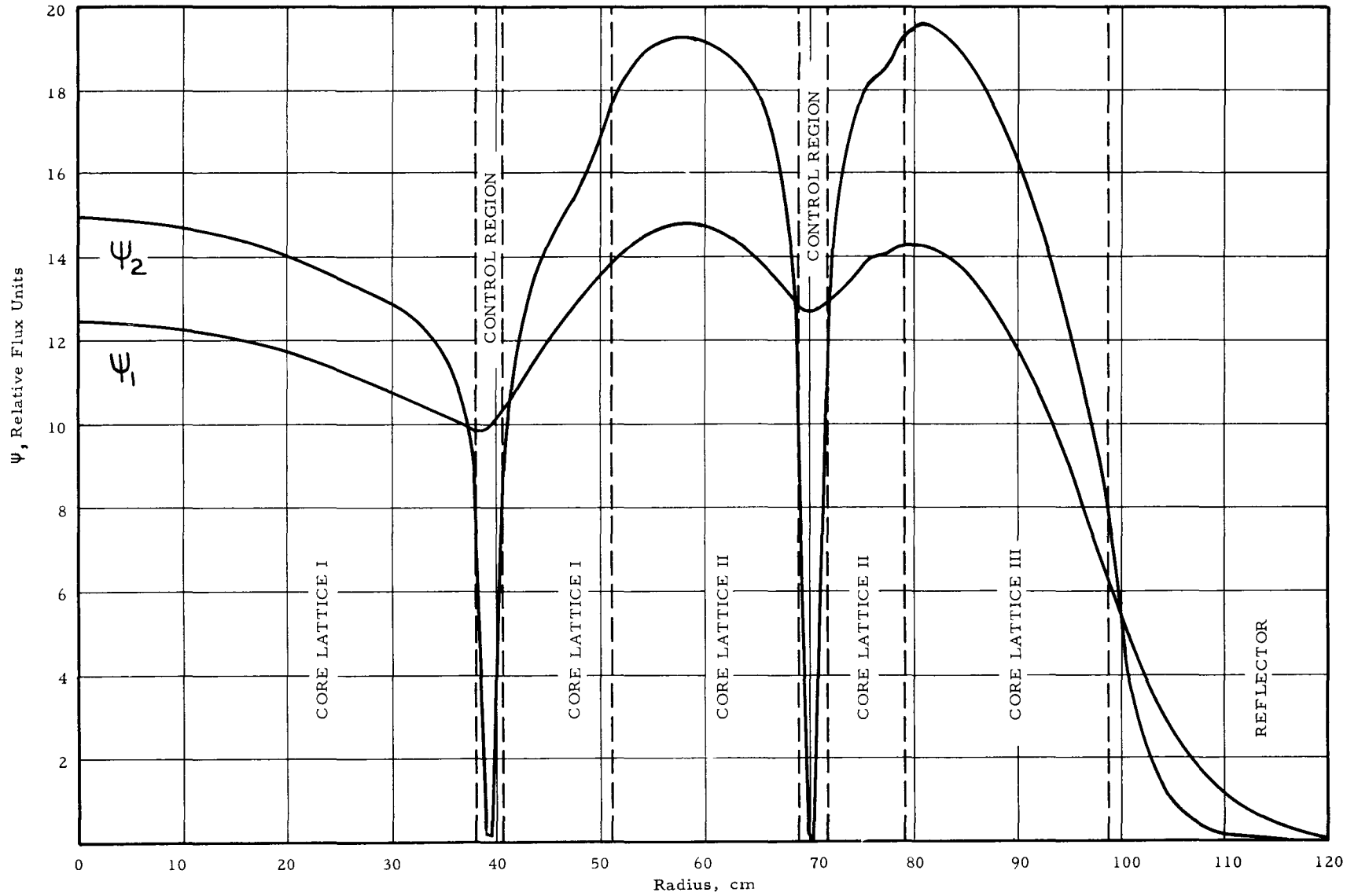
FIG. 3.11: FLUX WITH ALUMINUM FOLLOWERS INSERTED
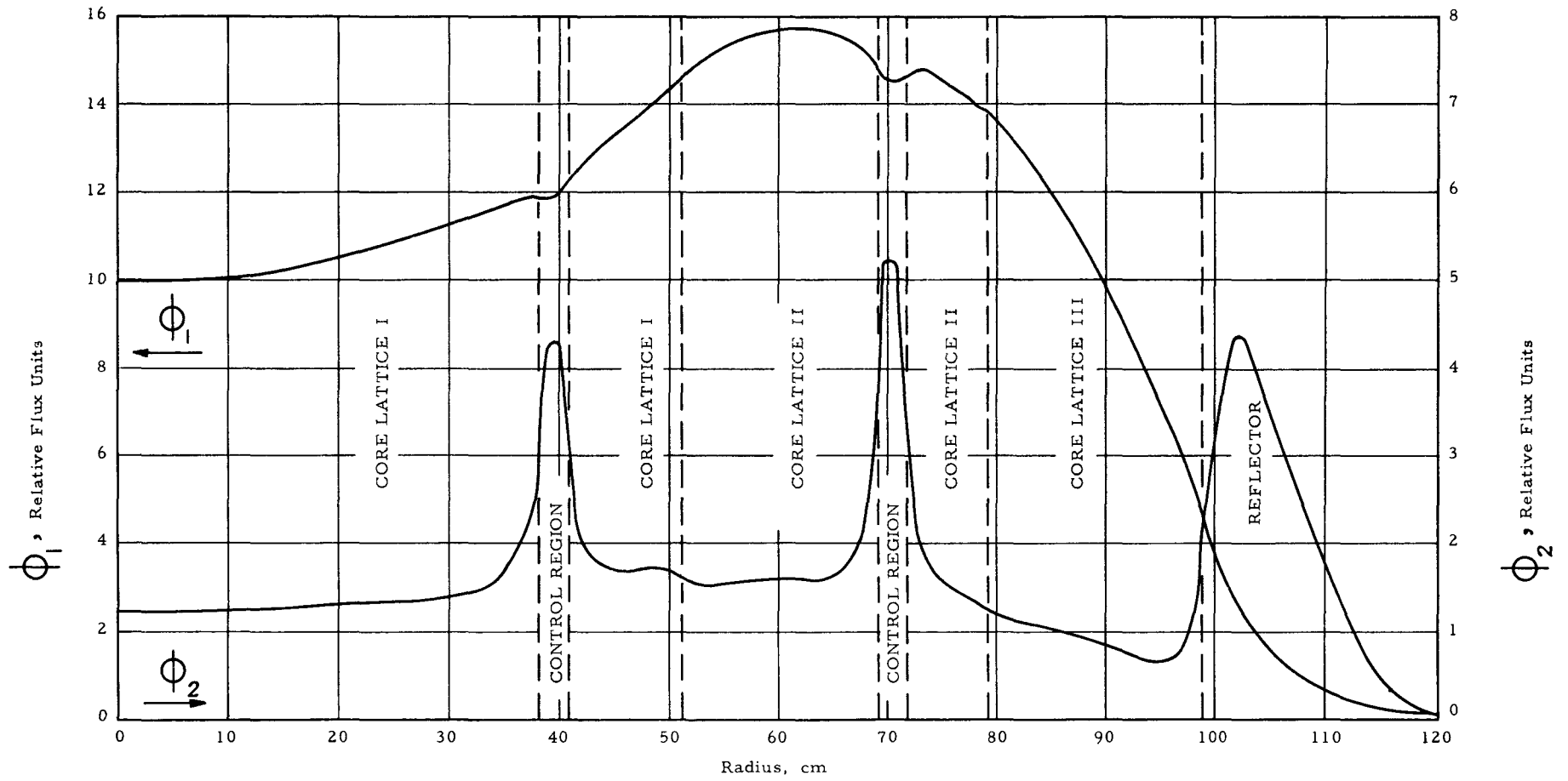
FIG. 3.12: ADJOINT FLUX WITH ALUMINUM FOLLOWERS INSERTED
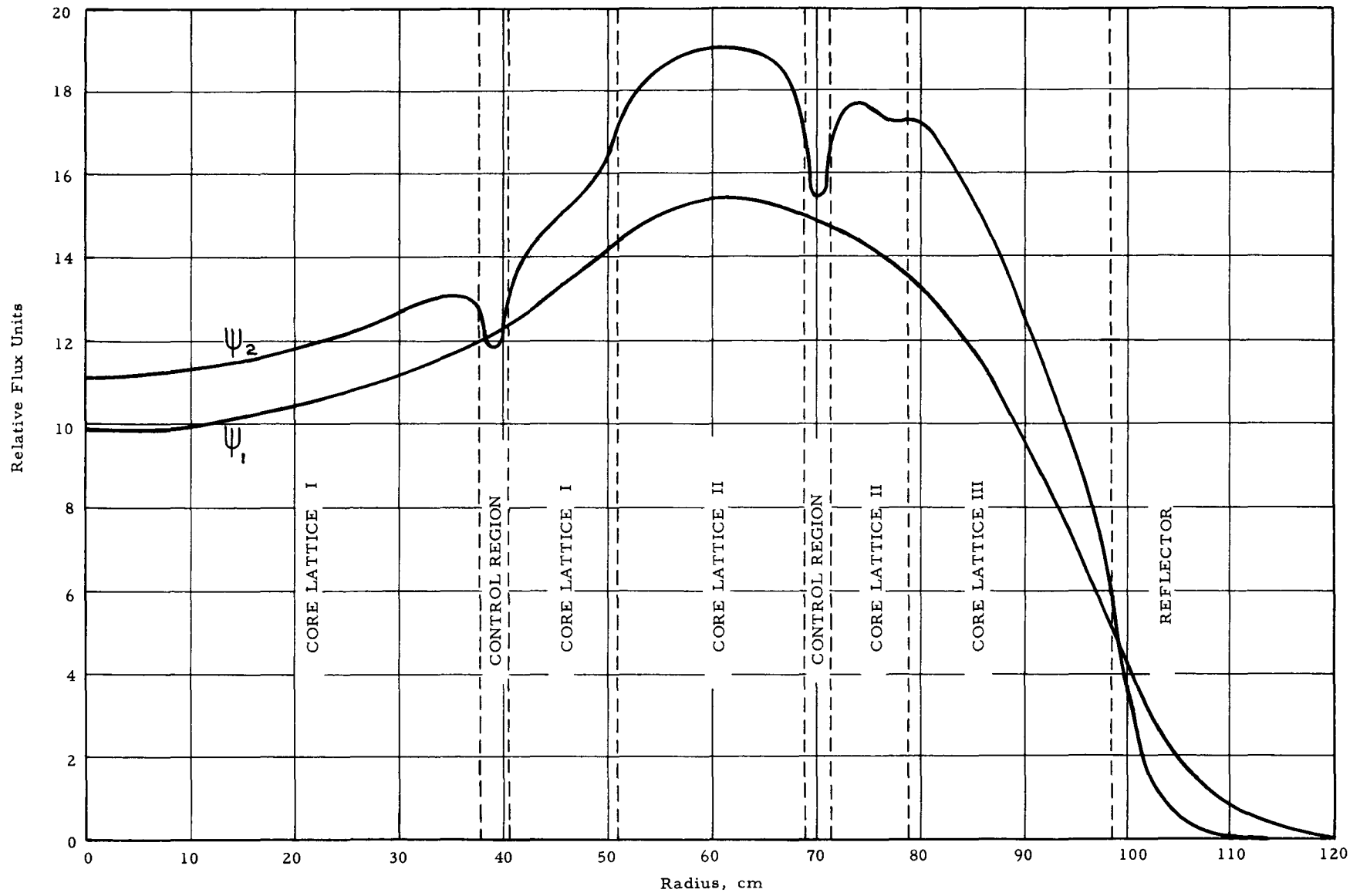
FIG. 3.13:  RADIAL DEPENDENT IMPORTANCE FACTOR
WITH BORAL CONTROL RODS INSERTED
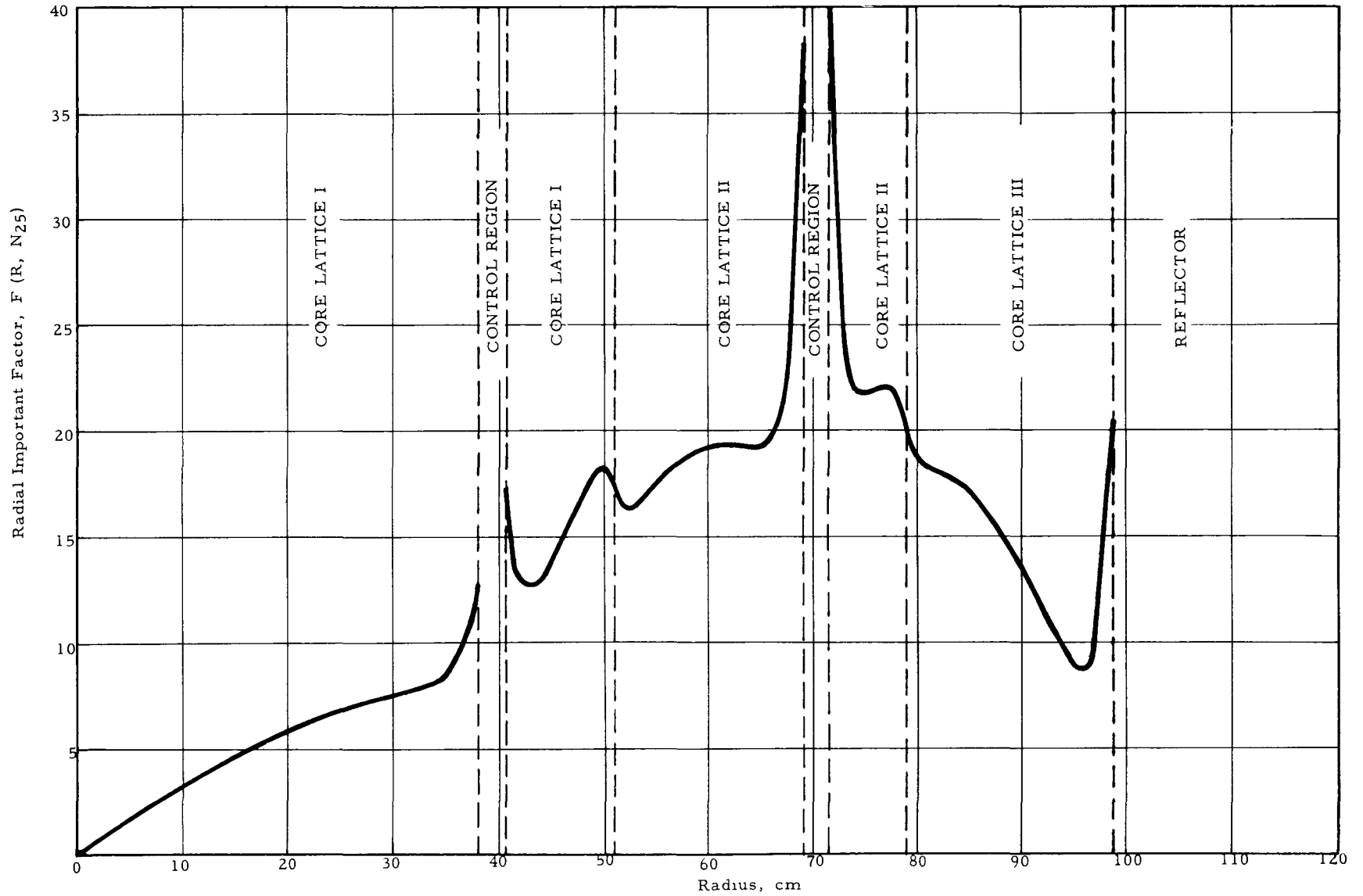
FIG. 3.14:  VOLUME DEPENDENT IMPORTANCE FACTOR
WITH BORAL CONTROL RODS INSERTED
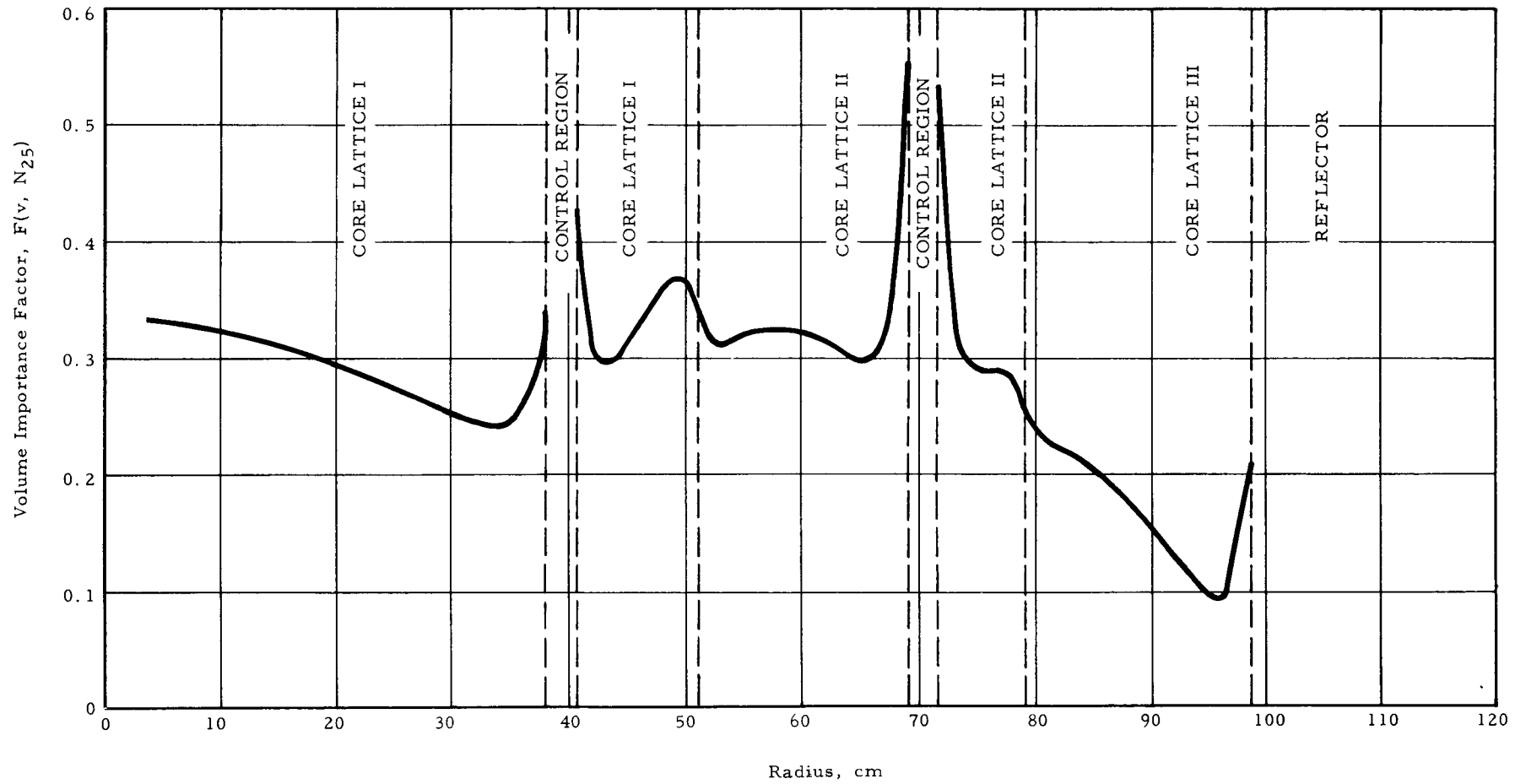
# FIG. 3.15: RADIAL DEPENDENT IMPORTANCE FACTOR WITH ALUMINUM FOLLOWERS INSERTED
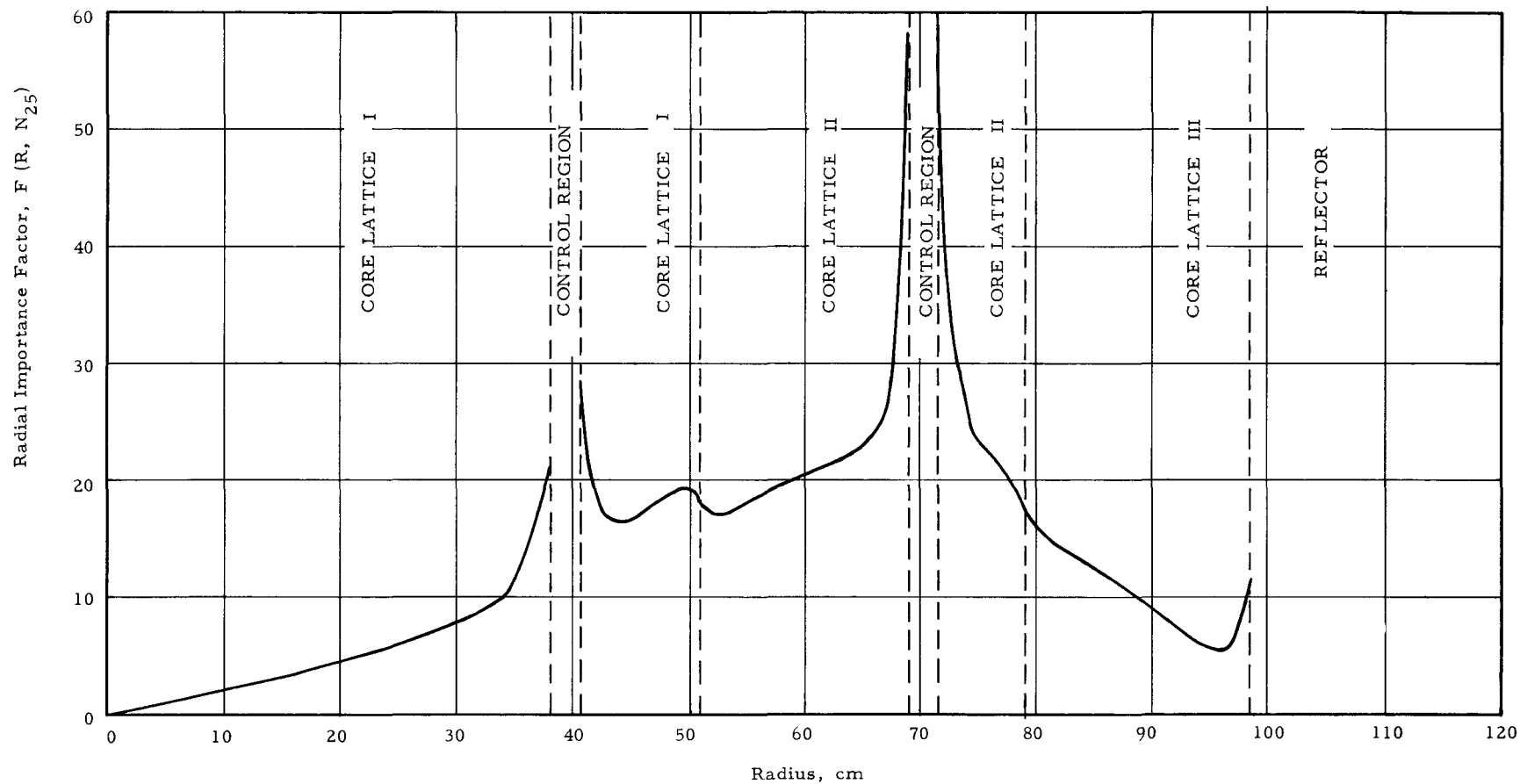
FIG. 3.16: VOLUME DEPENDENT IMPORTANCE FACTOR WITH ALUMINUM FOLLOWERS INSERTED
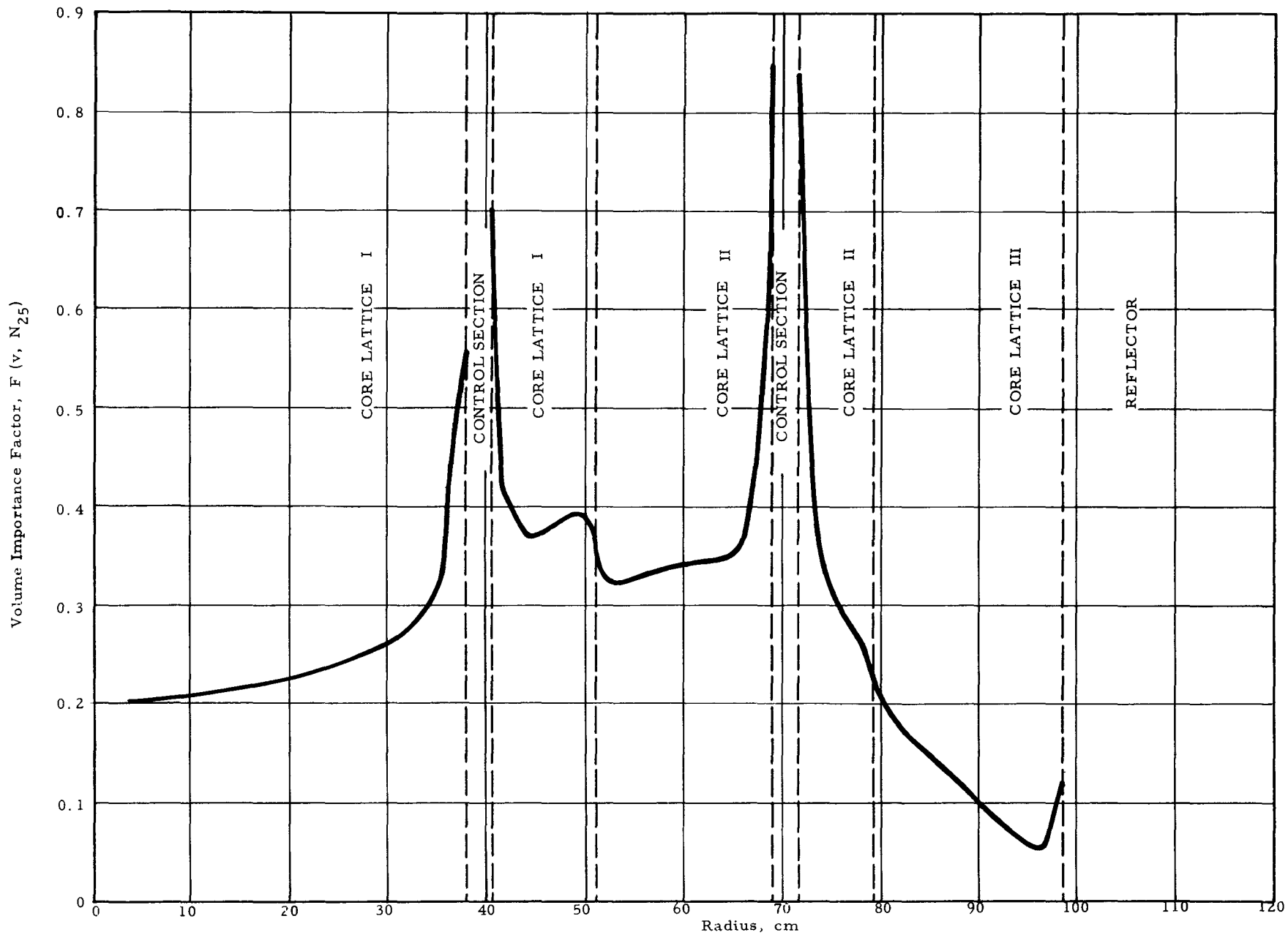
FIG. 3.17: TRANSIENT EFFECTS OF XE-135 AND SM-149
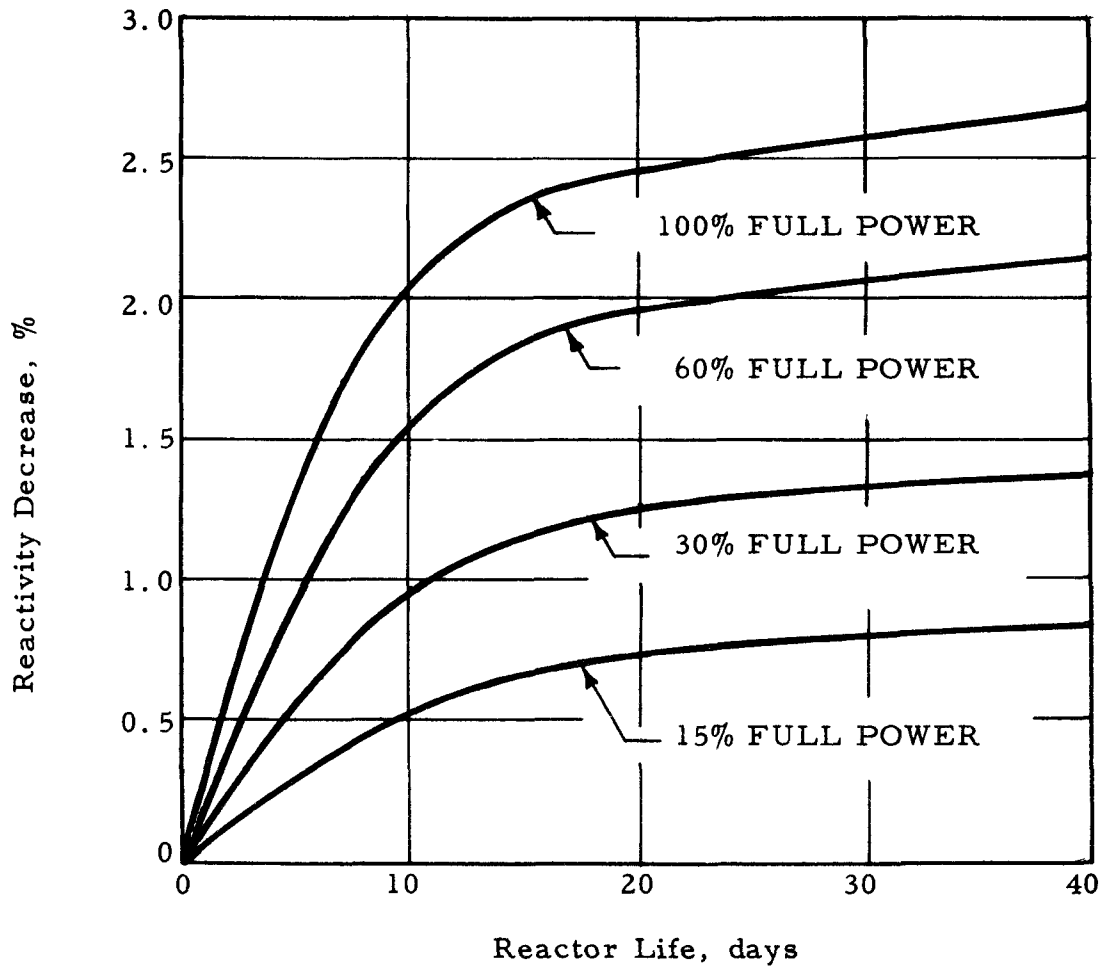
FIG. 3.18: BUILDUP OF XE-135 AT FULL POWER OPERATION
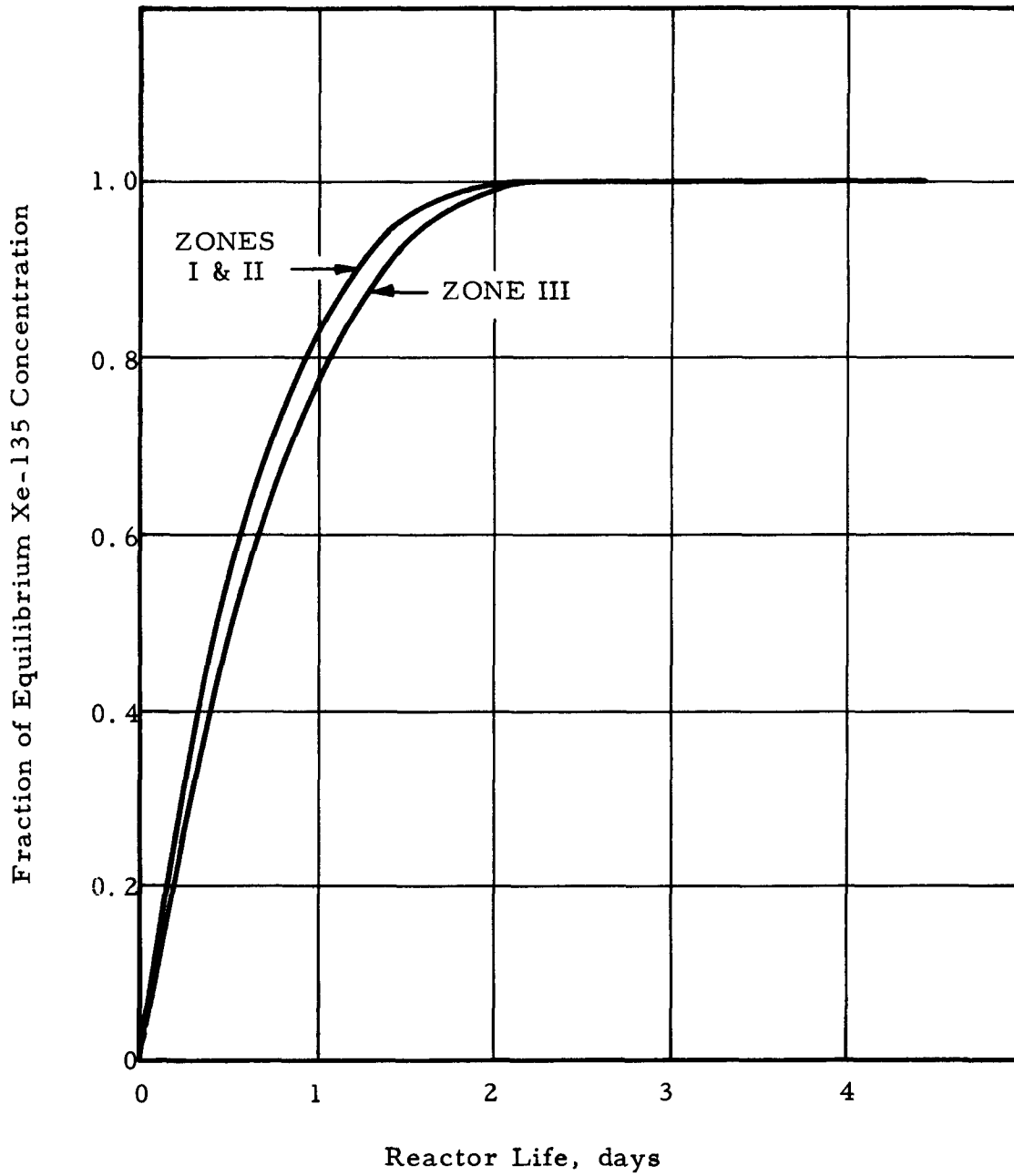
# FIG. 3.19: TRANSIENT EFFECTS OF XE-135



Reactivity Decrease, %

Reactor Life, days

100% FULL POWER

60% FULL POWER

30% FULL POWER
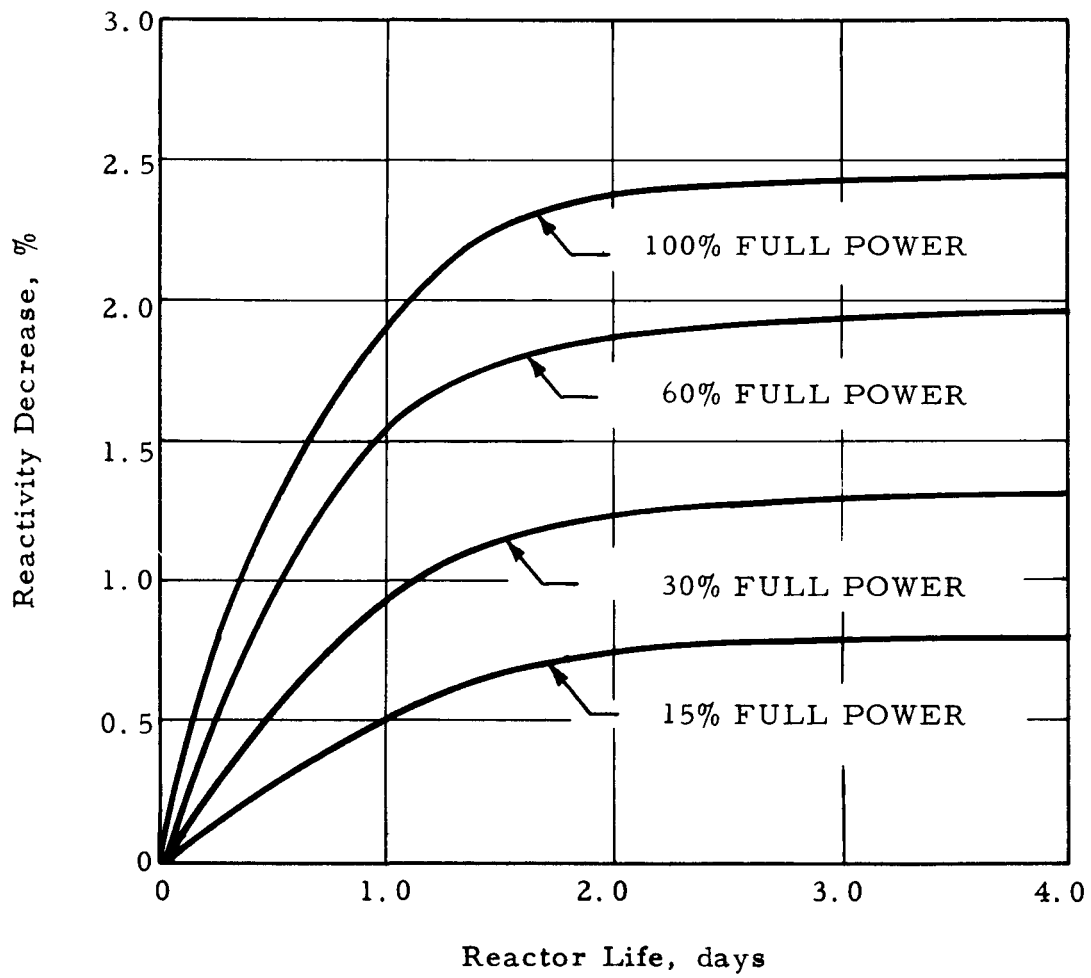
15% FULL POWER

FIG. 3.20:  REACTIVITY EFFECT OF EQUILIBRIUM XE-135



Power Level, % of Full Power
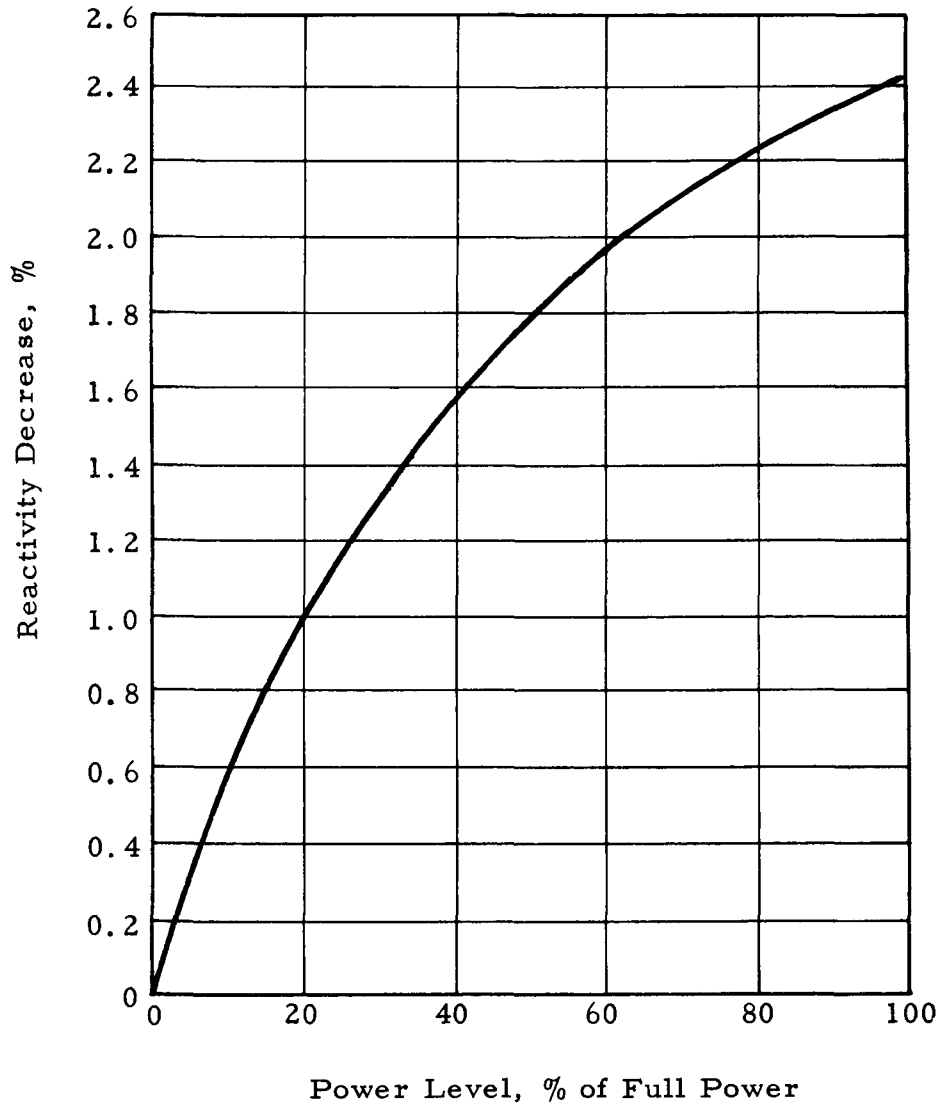
FIG. 3.21: XENON TRANSIENT, FULL POWER TO 15% FULL POWER



$t \leq$ 10 days, P = 585 MW

$t \geq$ 10 days, P = 87.75 MW

Time, days
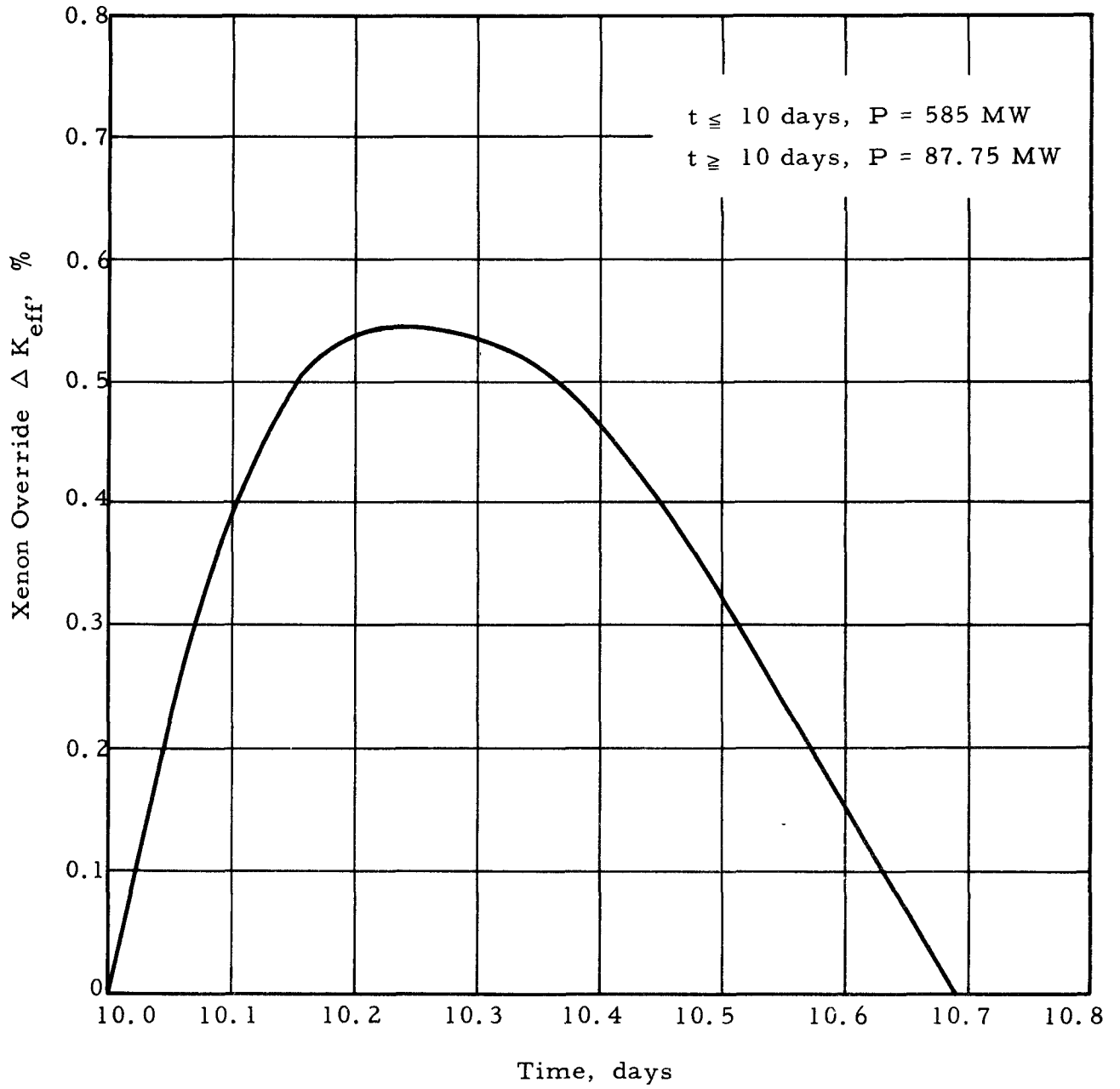
FIG. 3.22:   XENON TRANSIENT,  FULL POWER TO ZERO POWER



t ≤ 10 days,  P = 585 MW

t ≥ 10 days,  P = 0

Time, days

Xenon Override  $\Delta K_{eff}$, %
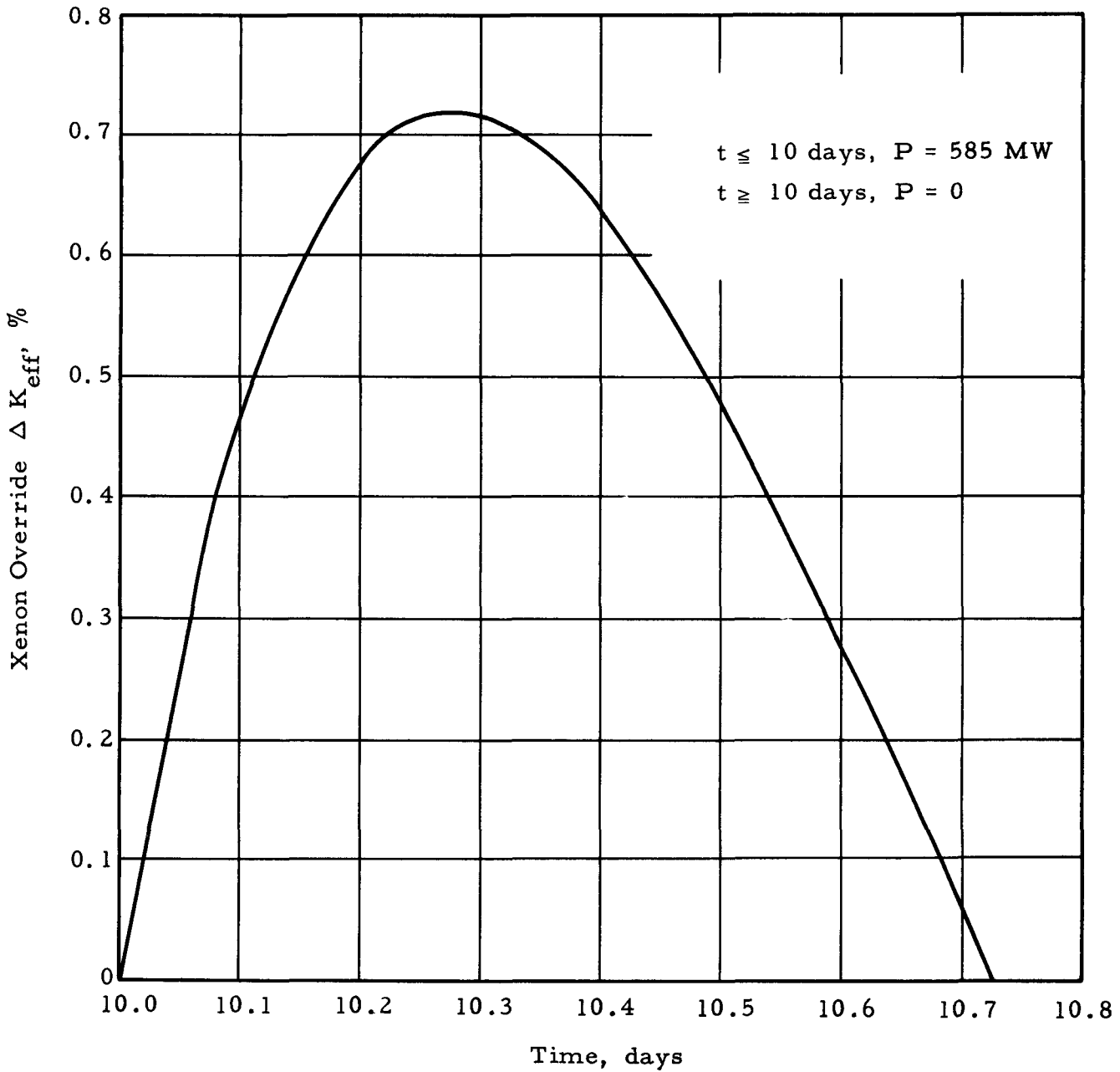
FIG. 3:23: WINDOW SHADE POWER PROFILE: STEADY STATE AT 11 DAYS IN LIFE
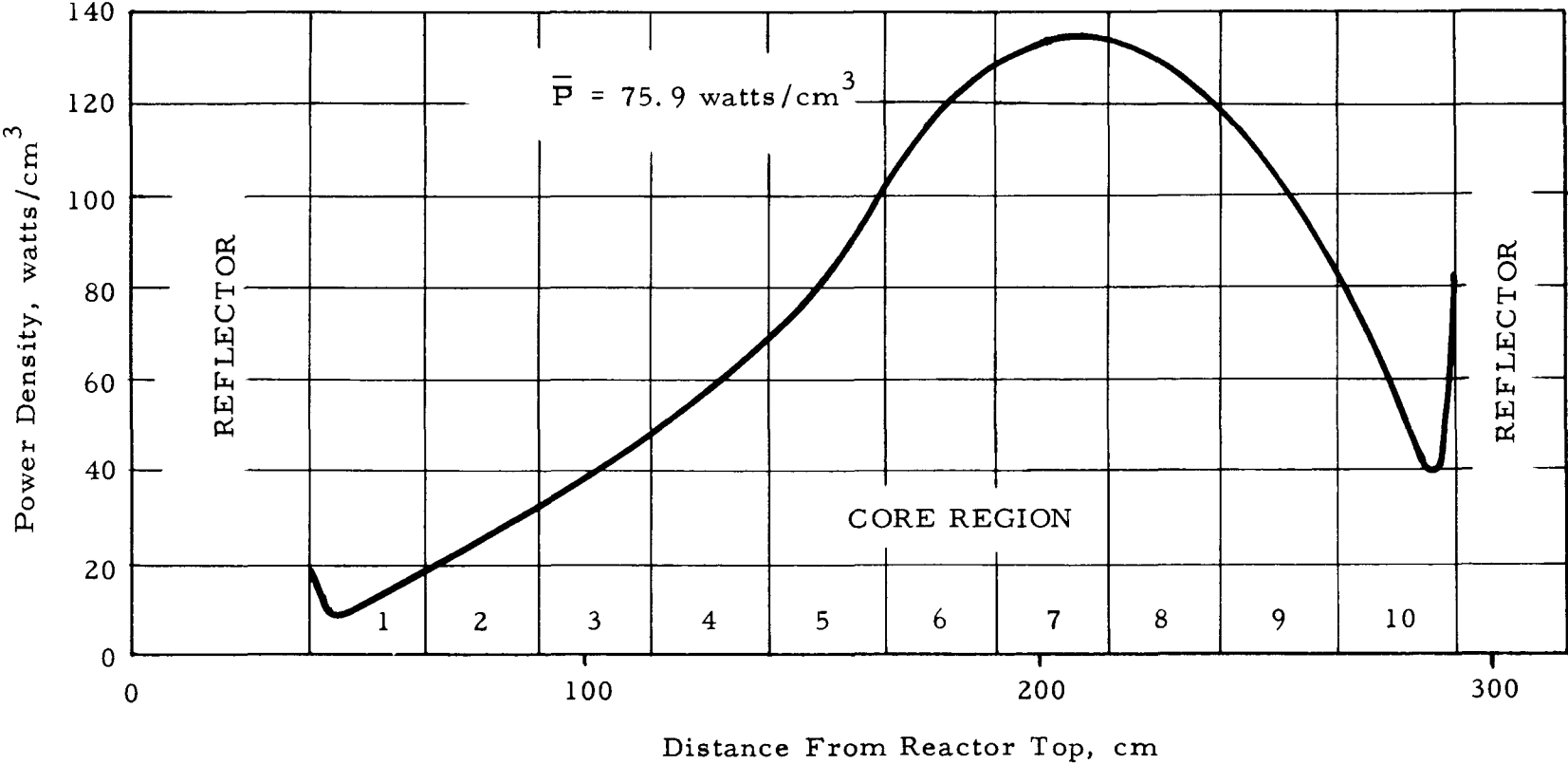
FIG. 3.24: WINDOW SHADE POWER PROFILE: PERTURBED STATE AT 11 DAYS IN LIFE
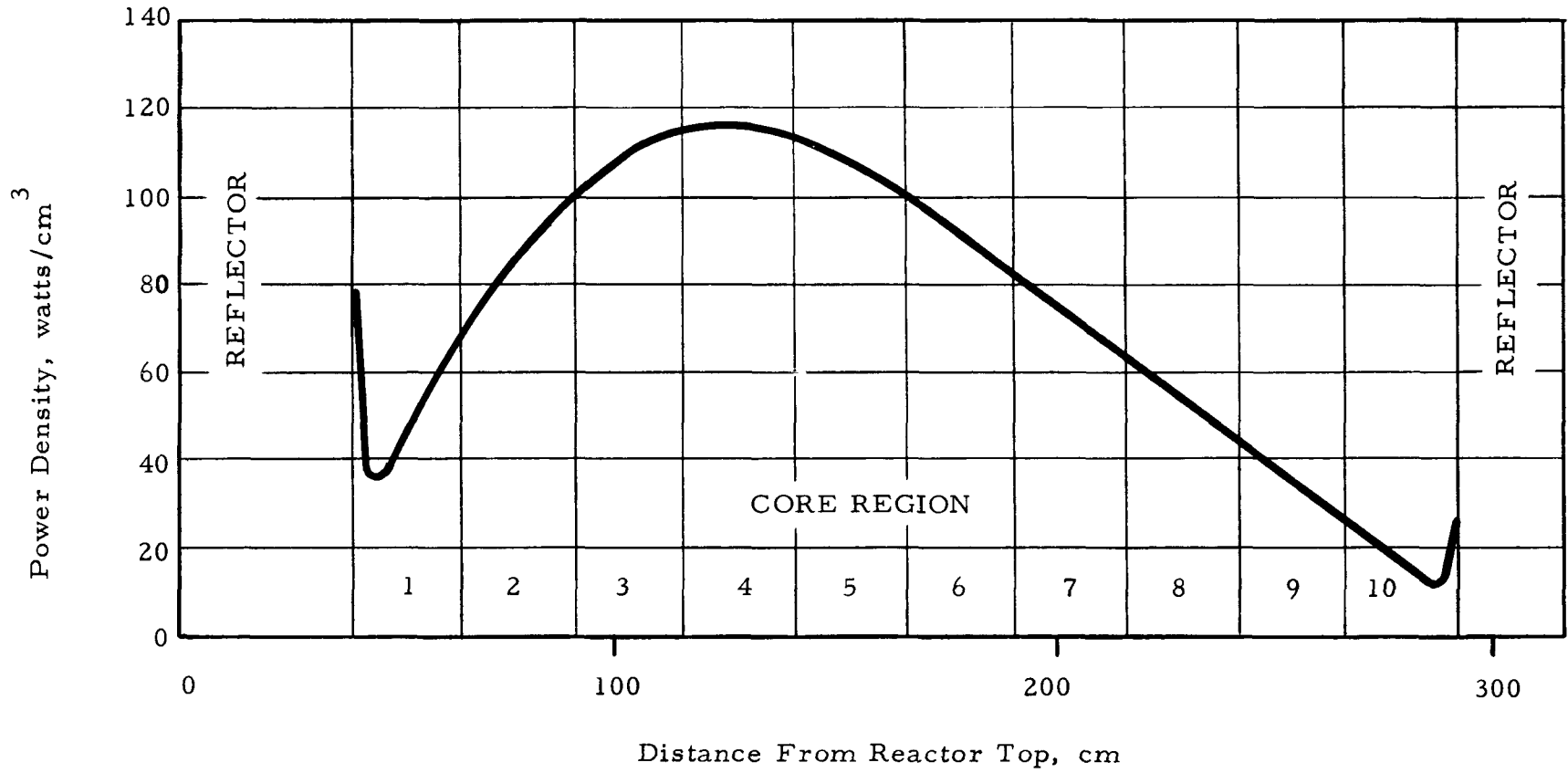
FIG. 3.25: WINDOW SHADE POWER PROFILE: 0.75 DAYS AFTER PERTURBATION
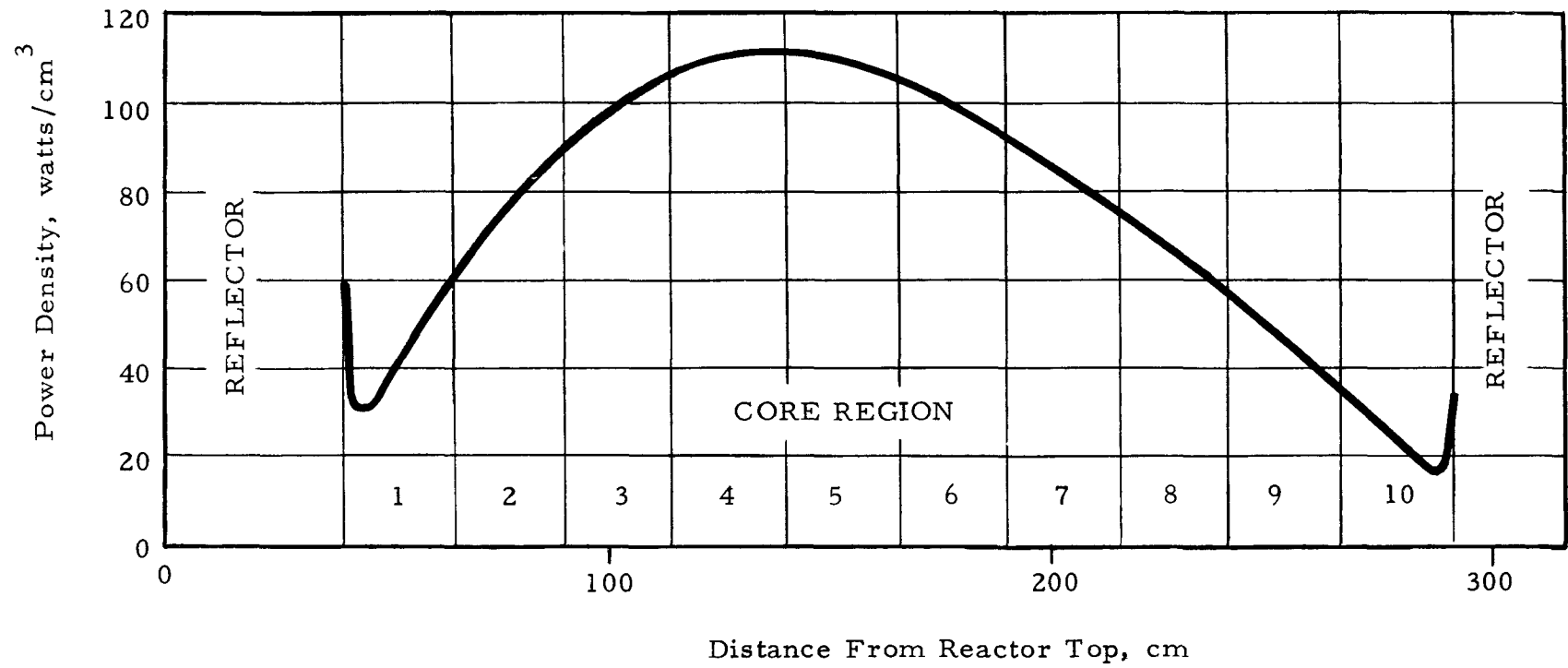
FIG. 3.26: WINDOW SHADE POWER PROFILE: 1.25 DAYS AFTER PERTURBATION
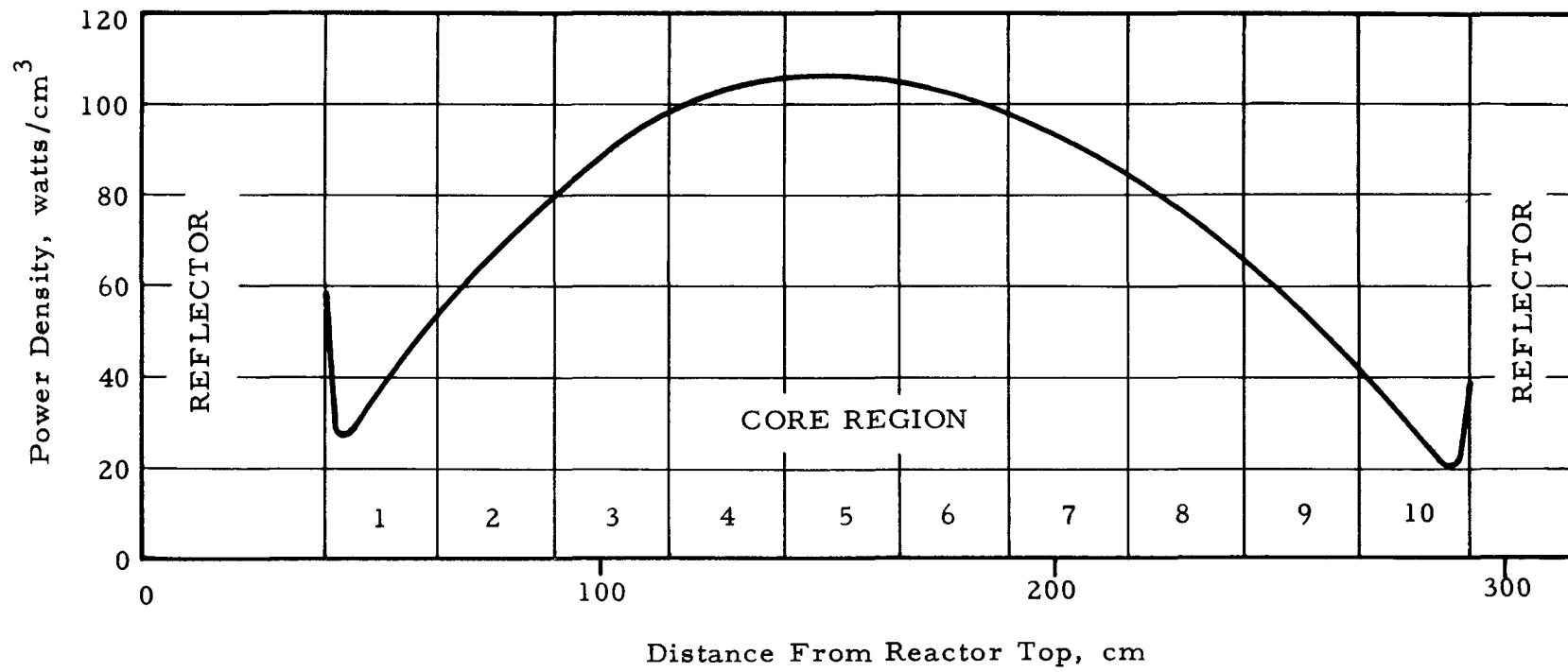
FIG. 3.27: WINDOW SHADE POWER PROFILE: 1.75 DAYS AFTER PERTURBATION
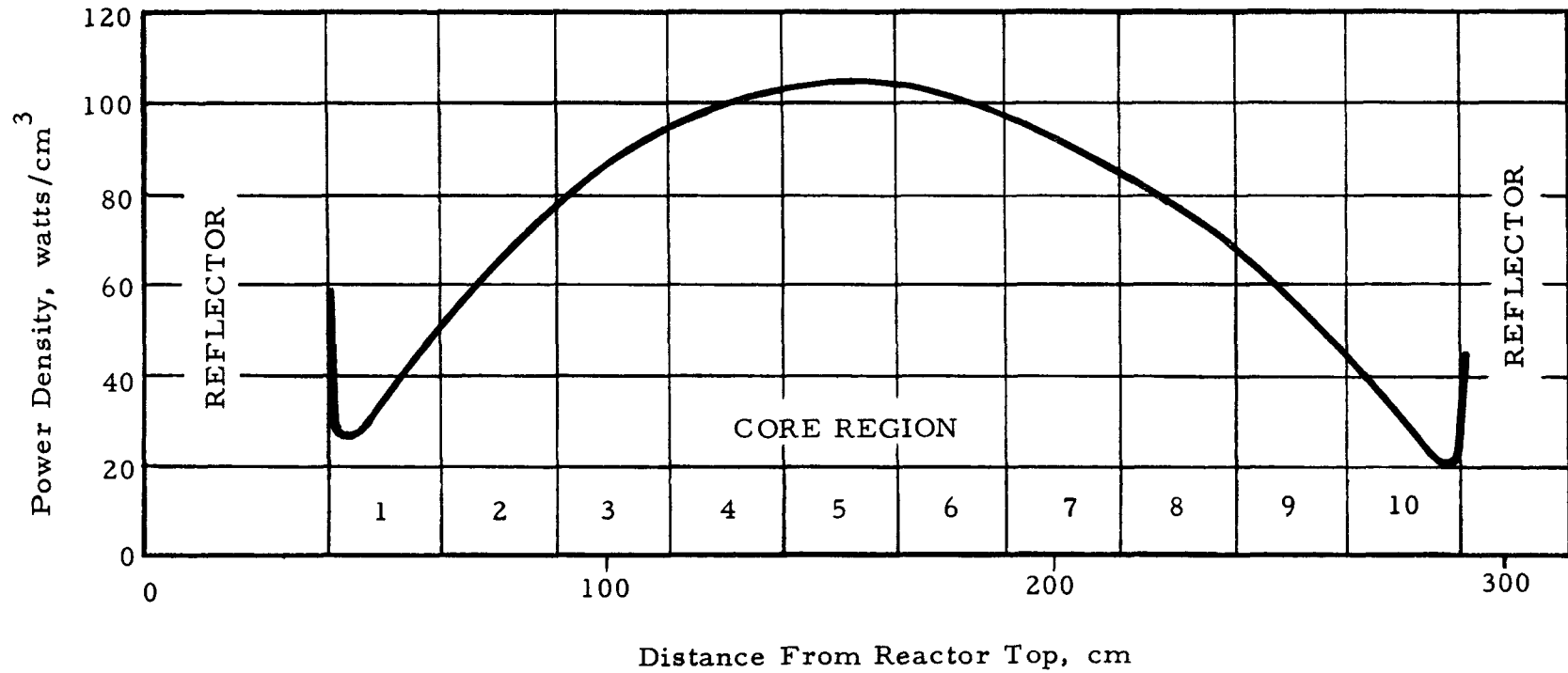
FIG. 4. 1: COMPARISON OF MULTIGROUP AND FOUR GROUP CODES



| CODE | $K_{eff}$ OF HAFNIUM SLAB |
|---|---|
| MULTIGROUP | .0783 |
| FOUR GROUP WITH PSEUDO COEFFICIENTS | .0675 |
| FOUR GROUP WITH SPECTRAL COEFFICIENTS | .0324 |

A - HAFNIUM
B - WATER
C - ALUMINUM
D - 9B CORE

Thermal Flux, Arbitrary Units

Distance From Control Slab Centerline, cm
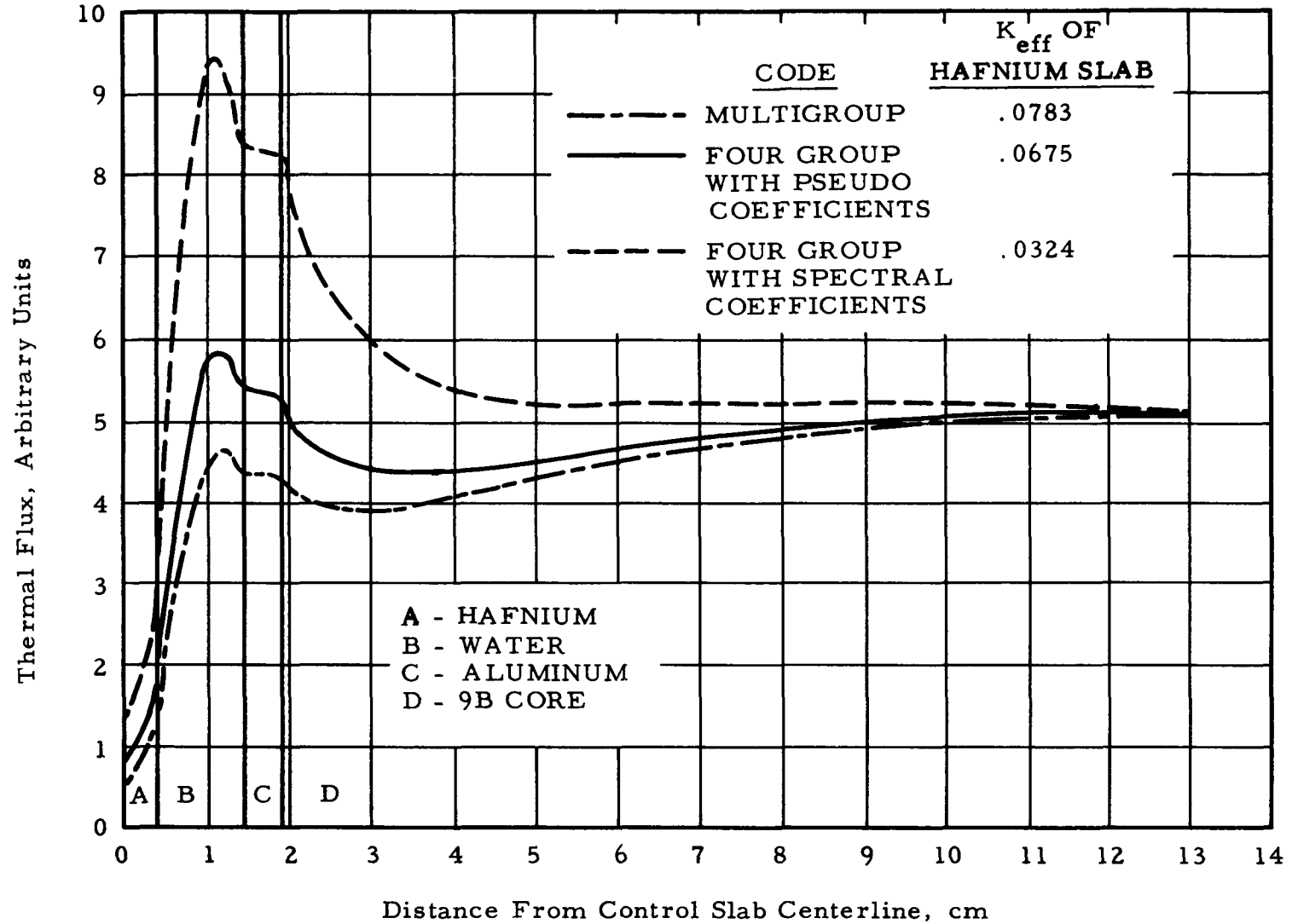
FIG. 4.2: LOCATION OF SPECIAL PINS
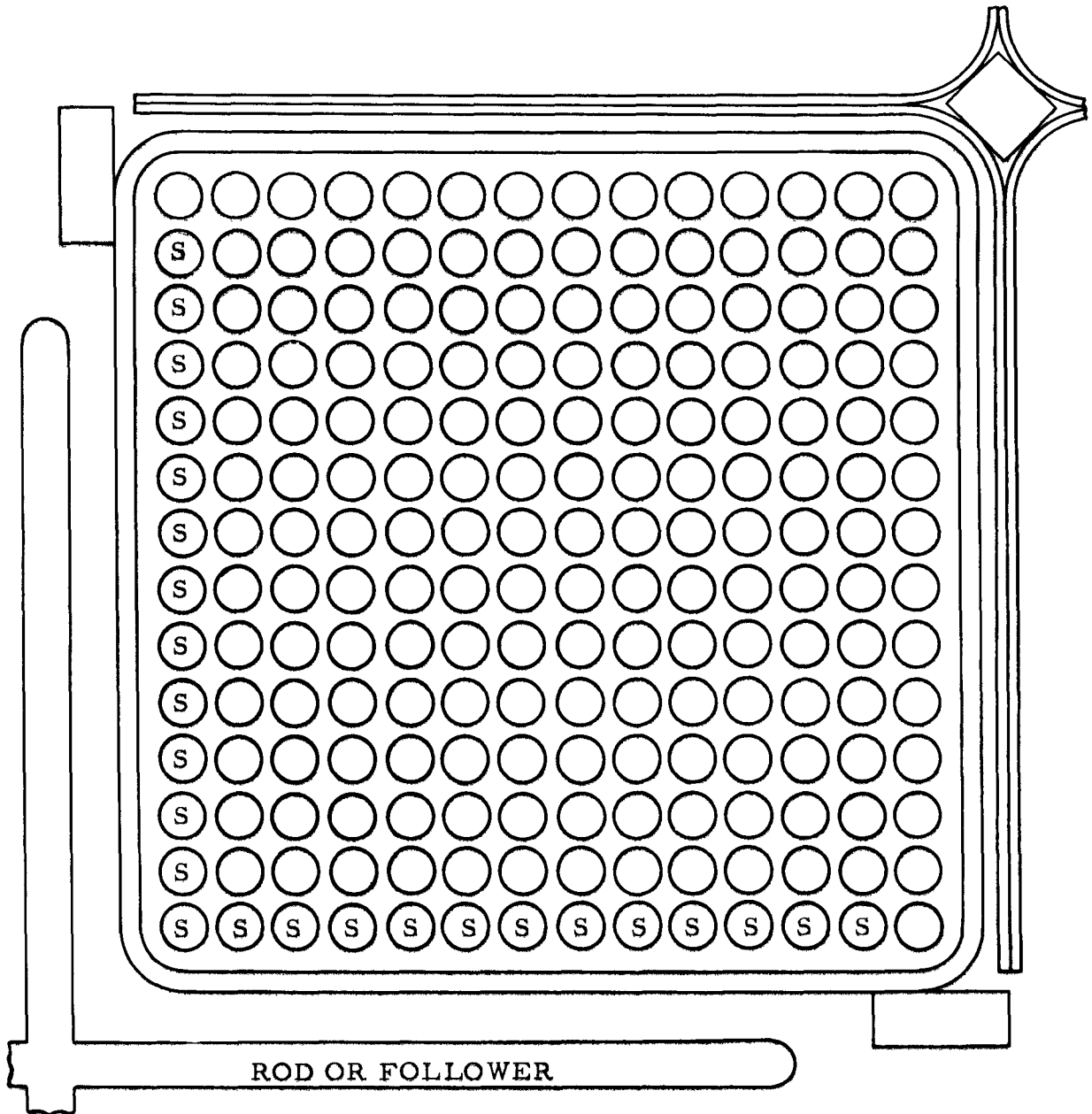


ROD OR FOLLOWER

FIG. 4.3: ROD WORTH AS FUNCTION
OF % INSERTION FOR TWO DIFFERENT
ROD GROUPS
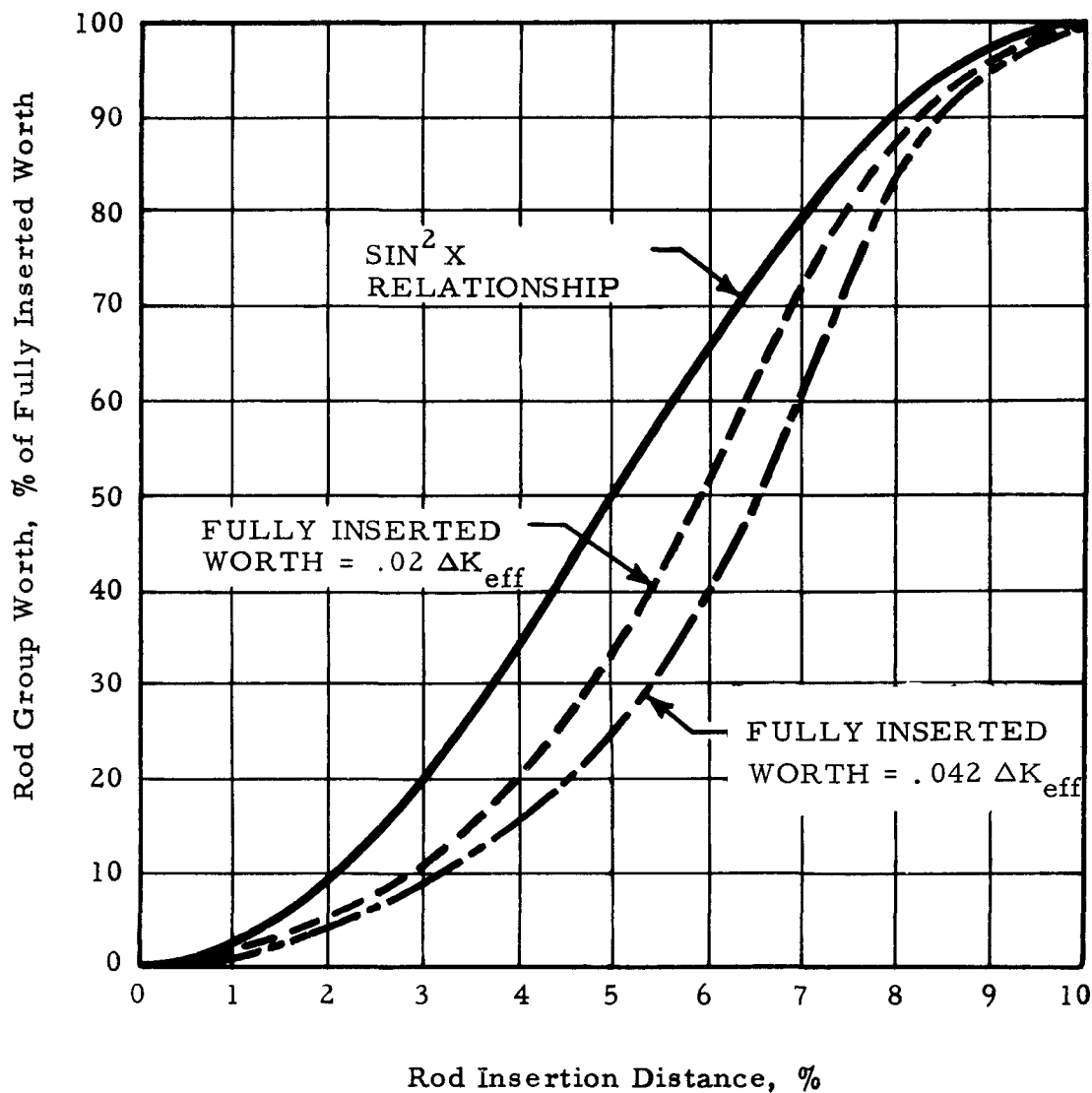
FIG. 5.1:   COMPARISON OF MEASURED AND CALCULATED
THERMAL FLUX NEAR CONTROL ROD
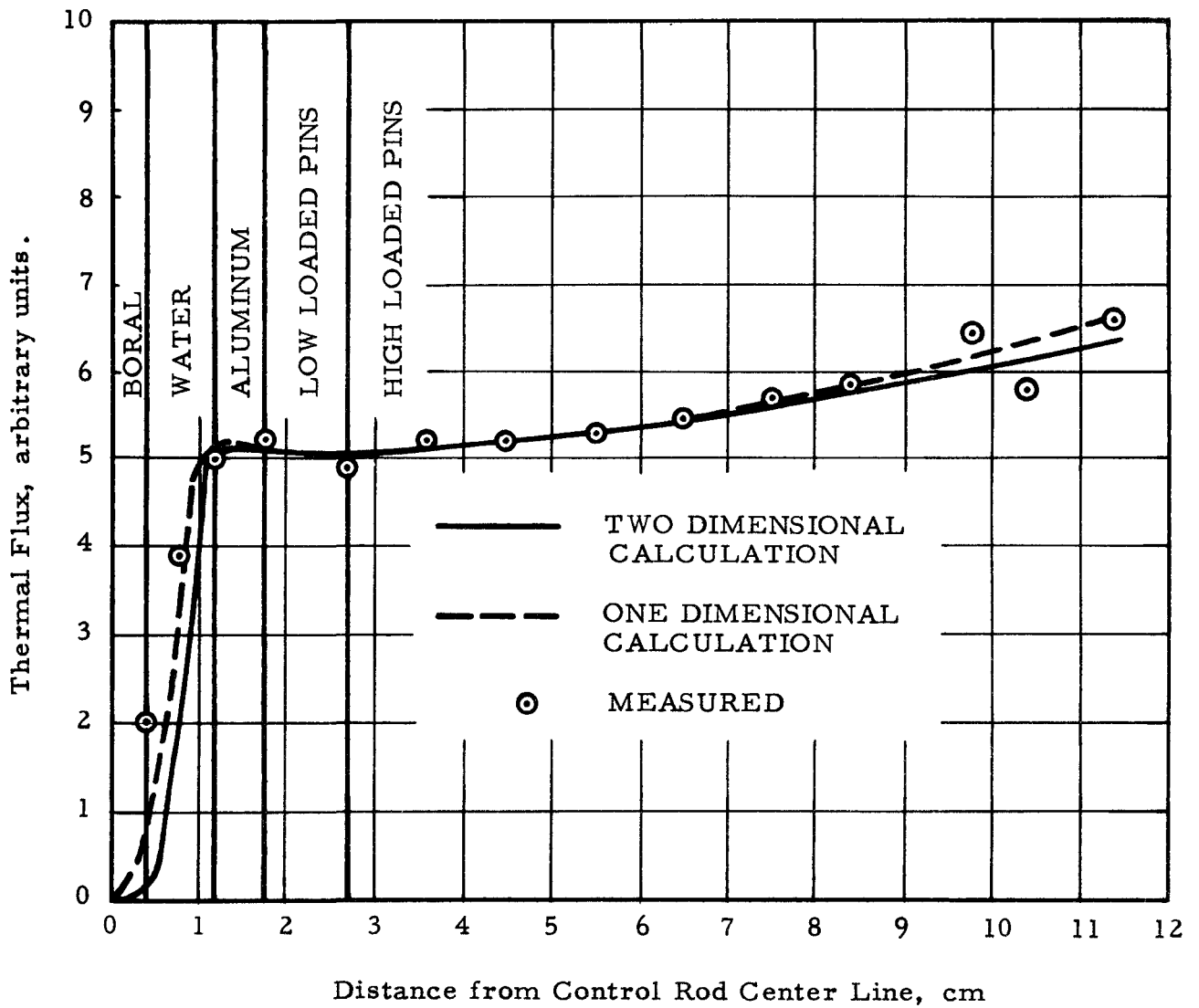
FIGURE 5-2   COMPARISON OF MEASURED
& CALCULATED THERMAL FLUX
(NEAR FOLLOWER)
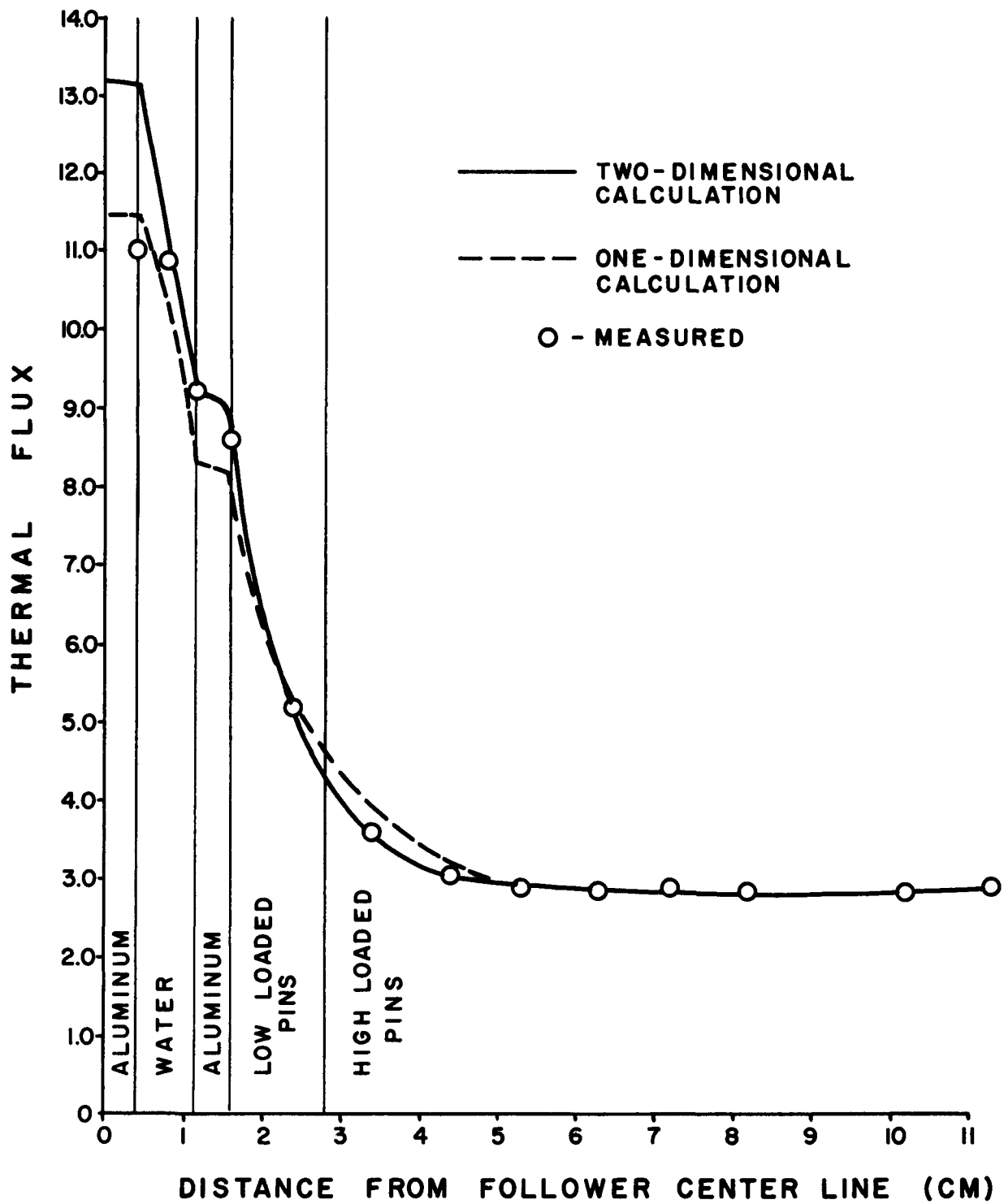
FIGURE 5-3    COMPARISON OF MEASURED & CALCULATED POWER



O — CALCULATED
X — MEASURED (HIGH LOADED PINS)
Δ — MEASURED (LOW LOADED PINS)
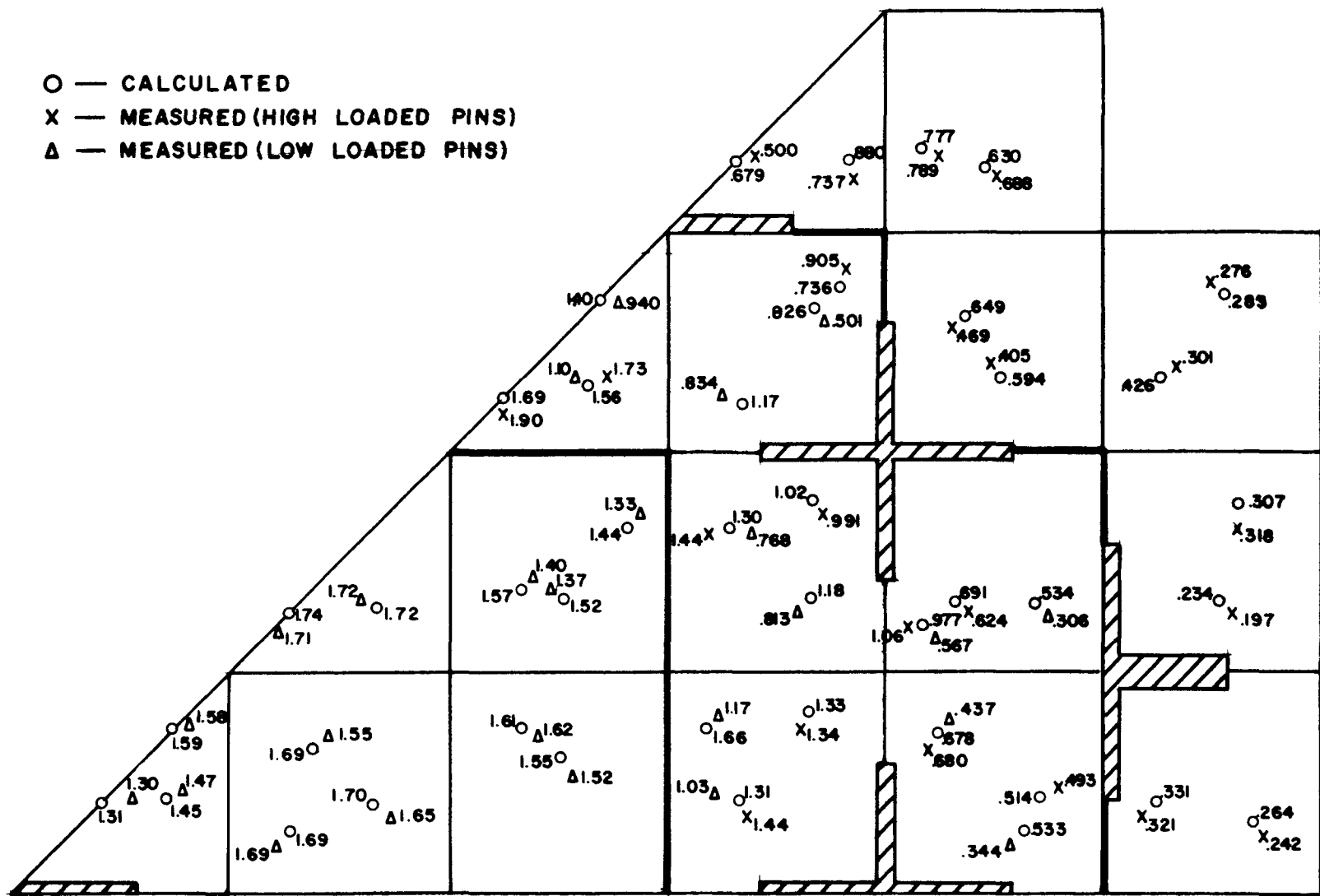
FIG. 5.4: GEOMETRY OF THE EXPONENTIAL ASSEMBLY AND
CHANGE OF FLUX SHAPE BETWEEN 68 F AND 495 F
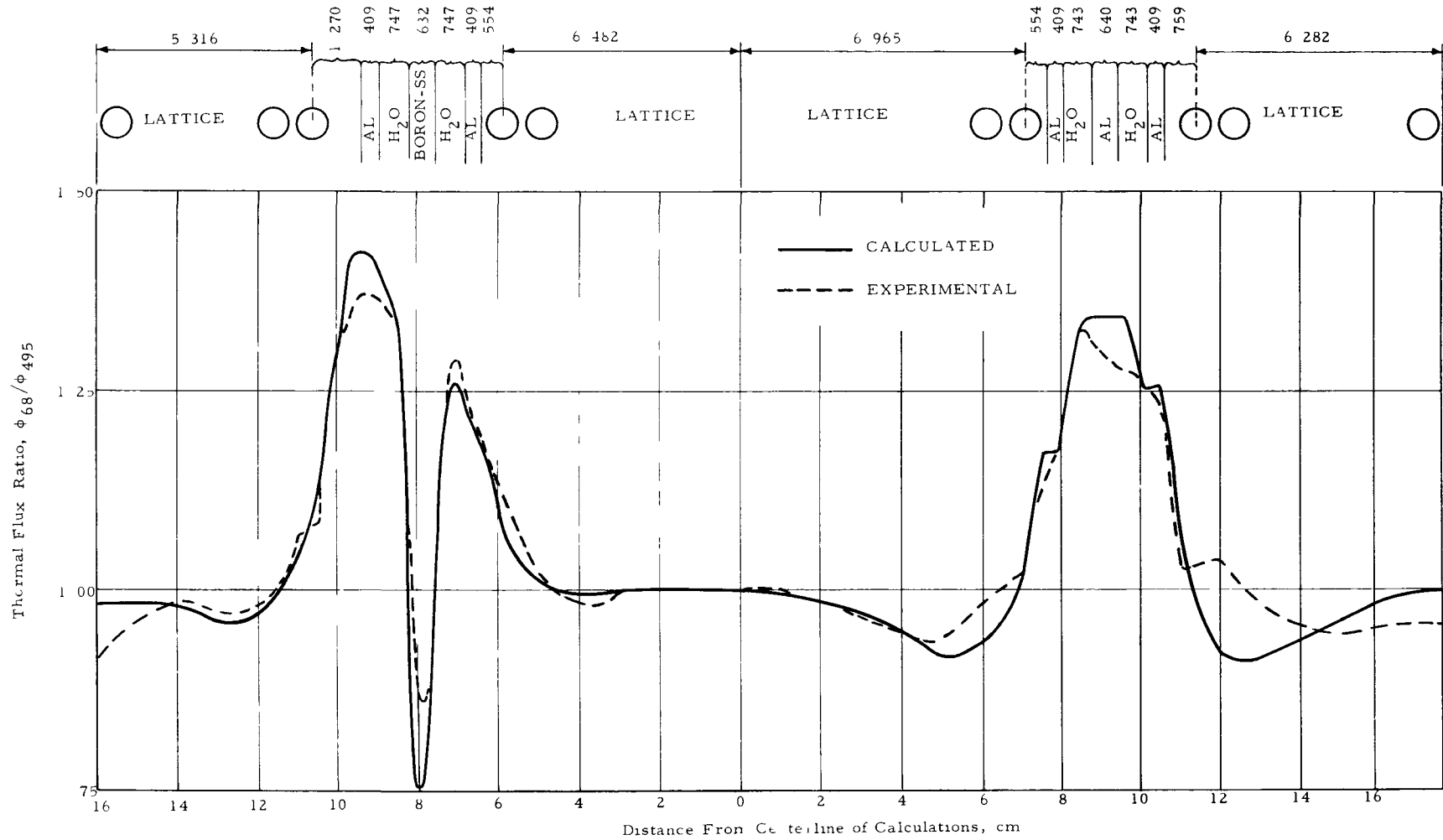
FIG. 5.5:  MEASURED AND CALCULATED FLUXES IN THE EXPONENTIAL
ASSEMBLY AT 68 F
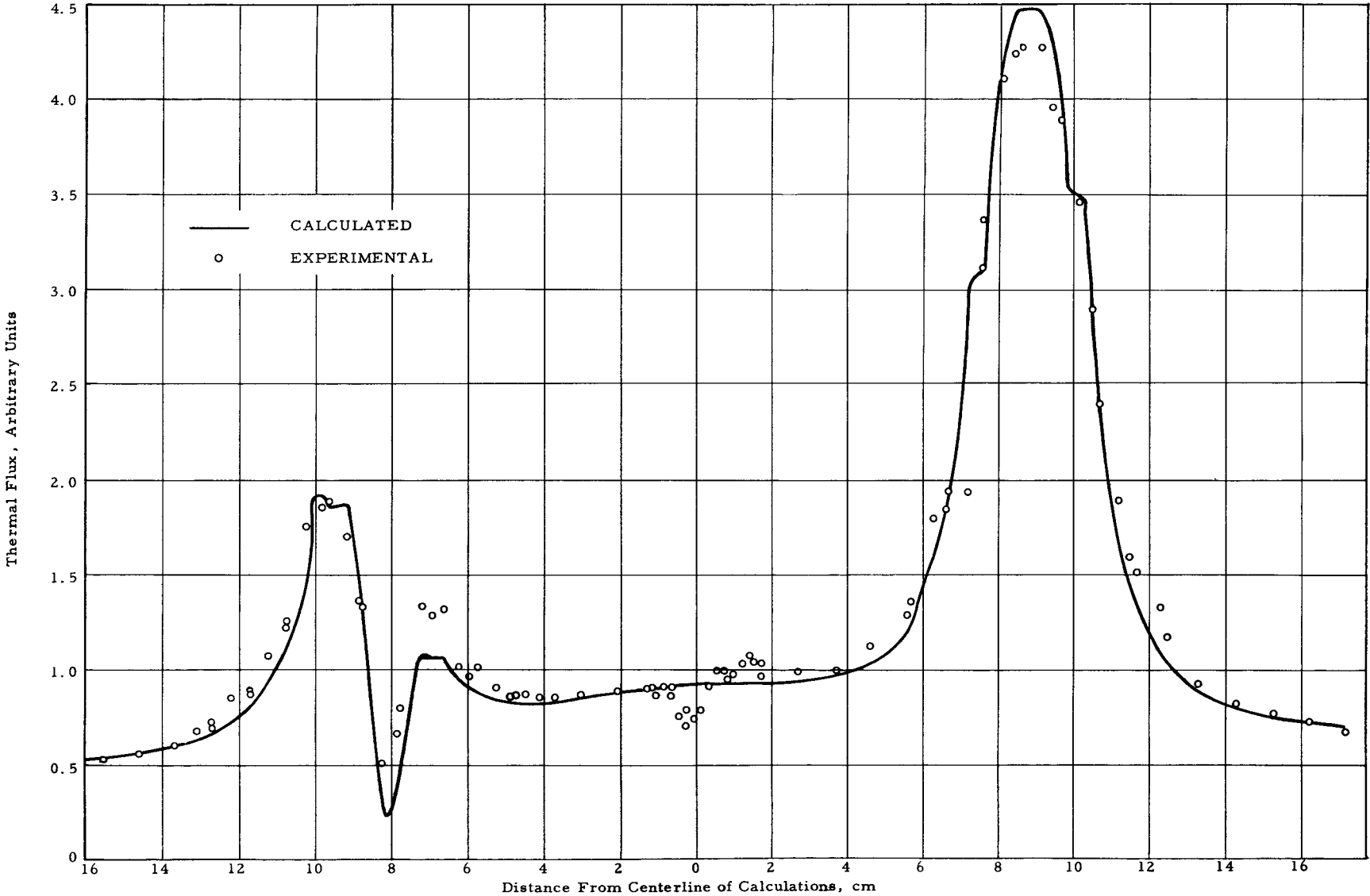
FIG 5.6: MEASURED AND CALCULATED FLUXES IN THE EXPONENTIAL ASSEMBLY AT 495 F
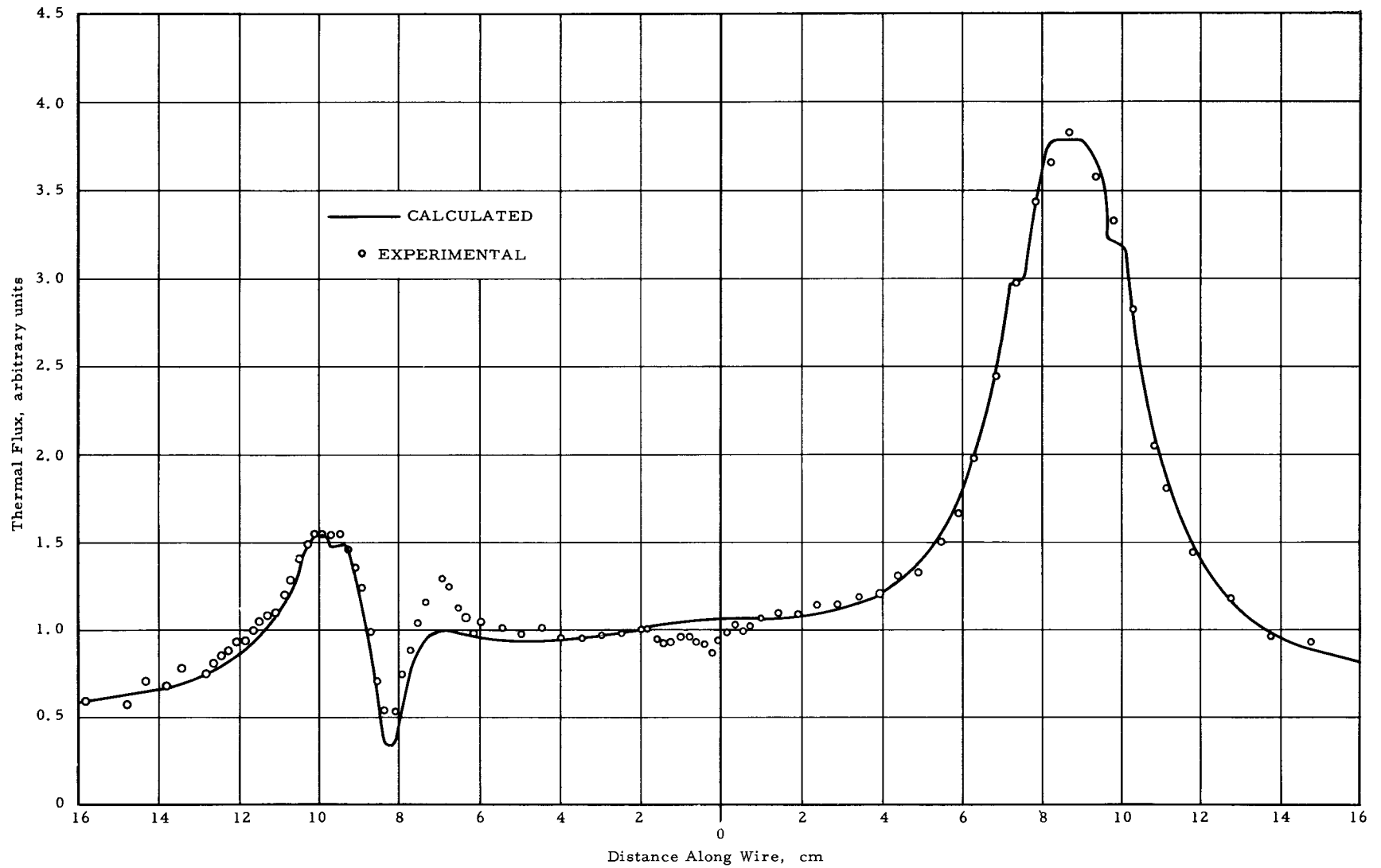
# FIGURE 5-7   GROSS RADIAL POWER DISTRIBUTION
## (TWO-DIMENSIONAL, PDQ CALCULATIONS)

**FIG. A**

| .73 | .65 | .48 | | | |
| 1.14 | 1.07 | .95 | .56 | | |
| 1.34 | 1.30 | 1.20 | .99 | .56 | |
| 1.14 | 1.17 | 1.32 | 1.20 | .95 | .48 |
| 1.07 | 1.10 | 1.17 | 1.30 | 1.07 | .65 |
| 1.03 | 1.07 | 1.14 | 1.34 | 1.14 | .73 |

**FIG. B**

| .54 | .60 | .51 | | | |
| .70 | .99 | 1.05 | .41 | | |
| .97 | 1.32 | 1.39 | 1.19 | .41 | |
| 1.20 | 1.32 | 1.56 | 1.39 | 1.05 | .51 |
| 1.31 | 1.33 | 1.32 | 1.32 | .99 | .60 |
| 1.26 | 1.31 | 1.20 | .97 | .70 | .54 |

**FIG. C**

| .75 | .84 | .69 | | | |
| .88 | 1.24 | 1.32 | .86 | | |
| .98 | 1.37 | 1.47 | 1.41 | .86 | |
| .97 | .86 | 1.15 | 1.47 | 1.32 | .69 |
| .85 | .72 | .86 | 1.37 | 1.24 | .84 |
| .64 | .85 | .97 | .98 | .88 | .75 |

**FIG. D**

| .85 | .96 | .81 | | | |
| .94 | 1.37 | 1.53 | 1.00 | | |
| .88 | 1.37 | 1.64 | 1.62 | 1.00 | |
| .58 | .75 | 1.20 | 1.64 | 1.53 | .81 |
| .42 | .48 | .75 | 1.37 | 1.37 | .96 |
| .50 | .42 | .58 | .88 | .94 | .85 |
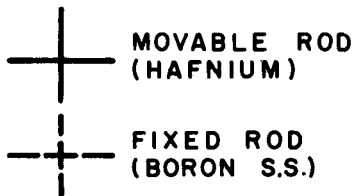
MOVABLE ROD
(HAFNIUM)

FIXED ROD
(BORON S.S.)

1. DRAWINGS REPRESENT A CORE QUADRANT.

2. NUMBERS ON DRAWING REPRESENT AVERAGE BUNDLE POWER TO AVERAGE CORE POWER.

# FIGURE 5—8 GROSS RADIAL POWER DISTRIBUTION
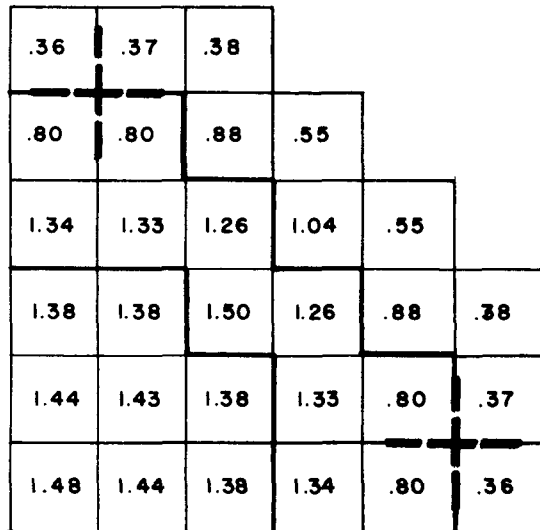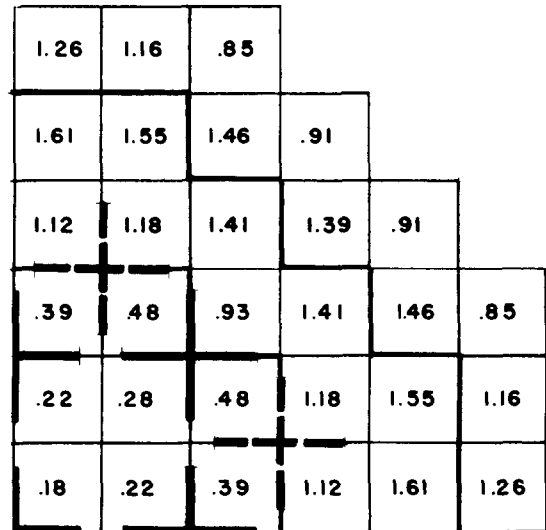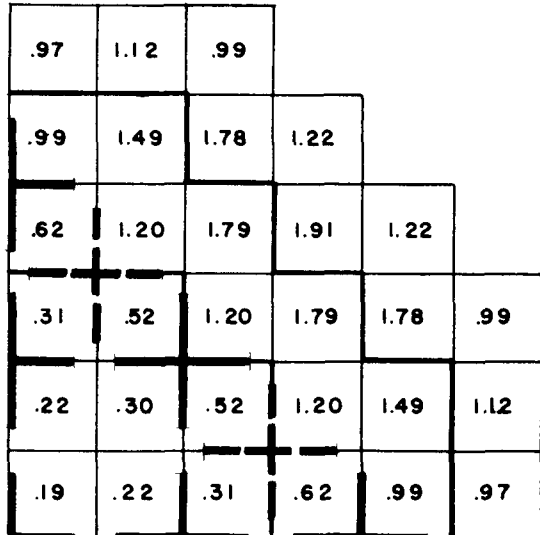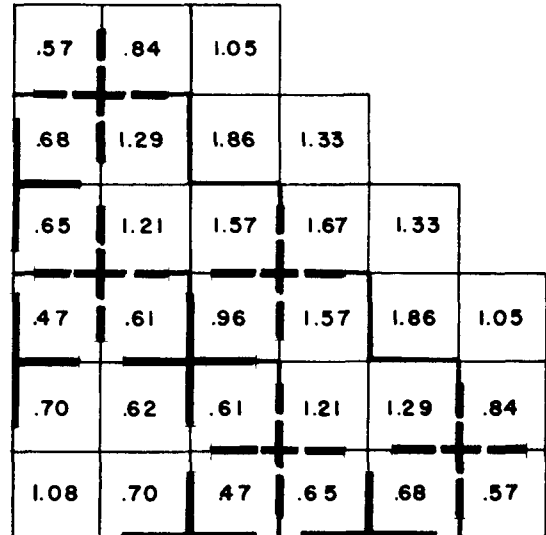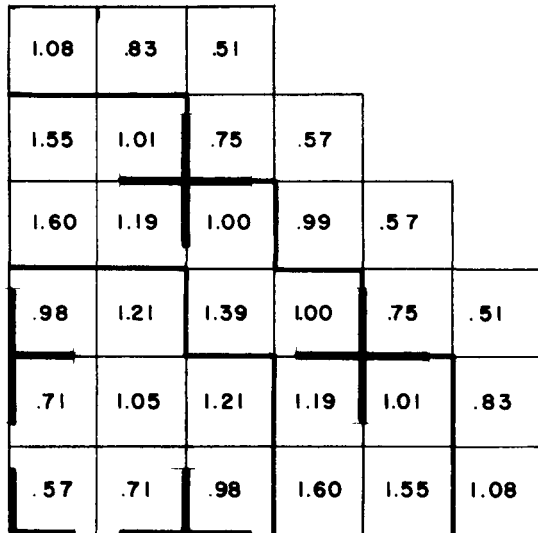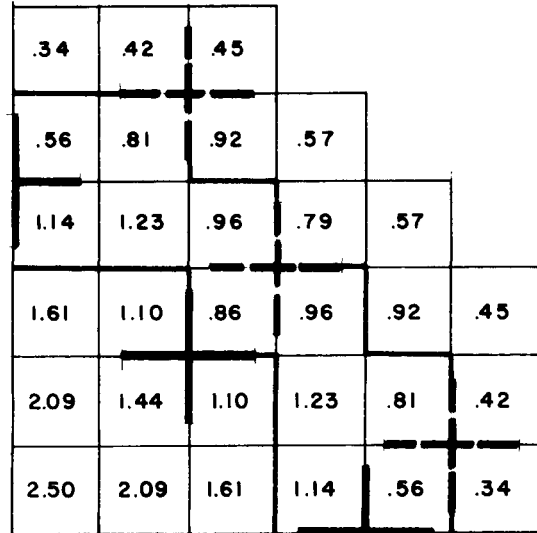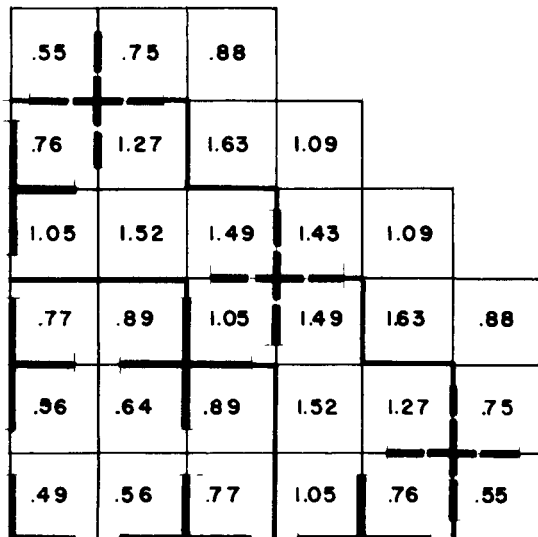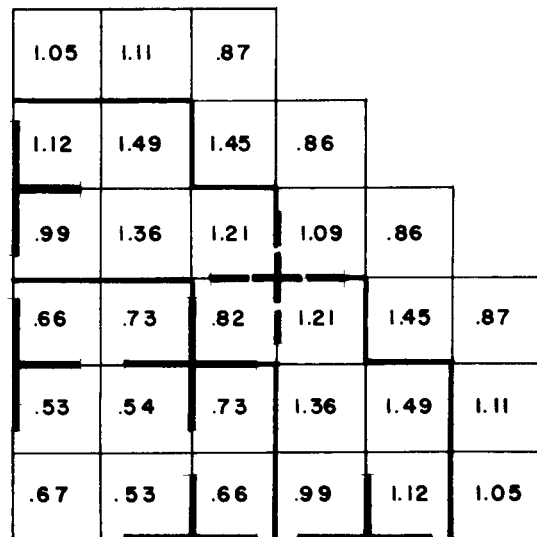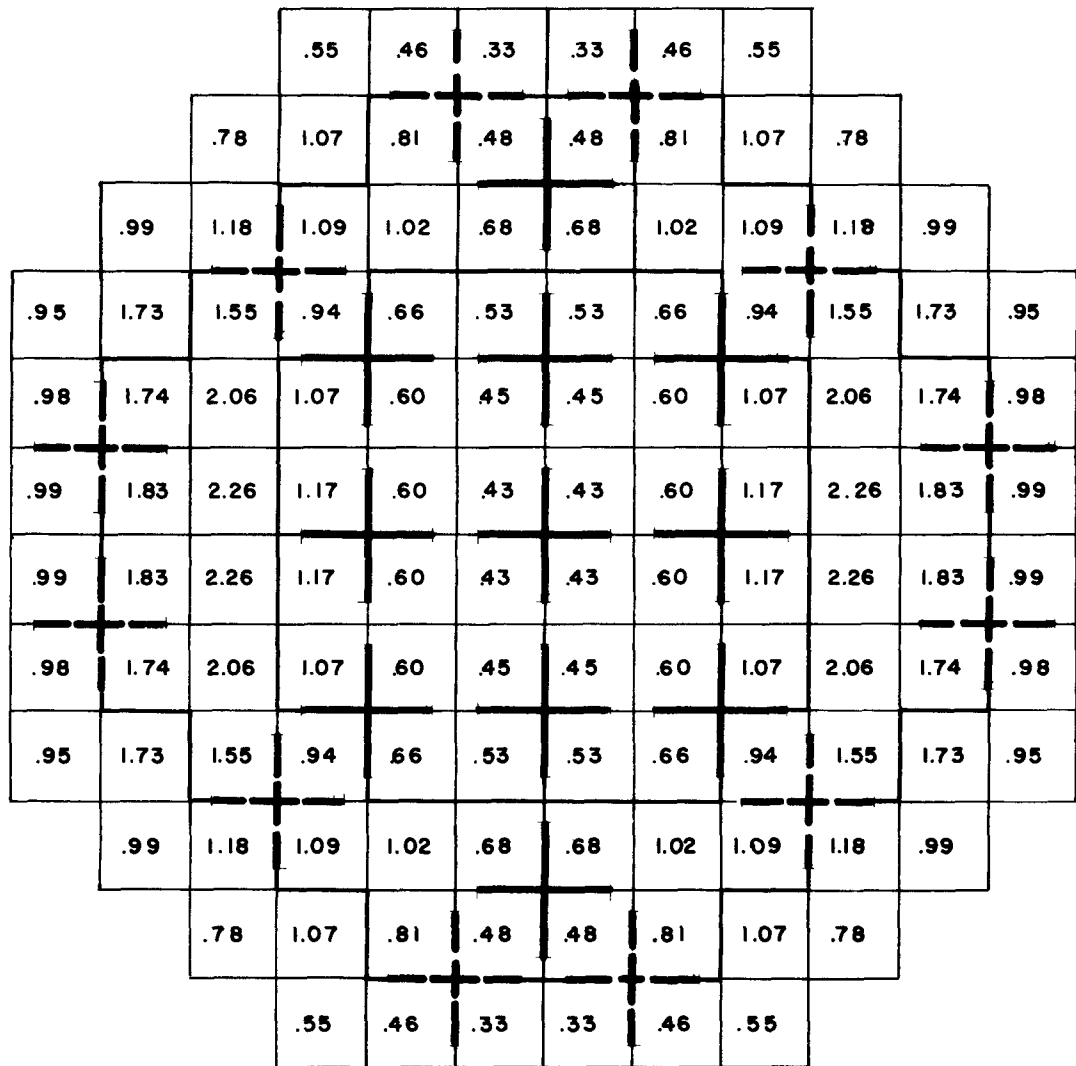## (TWO-DIMENSIONAL, P D Q CALCULATIONS)

**FIG. A**

| .39 | .38 | .37 |      |     |     |
|-----|-----|-----|------|-----|-----|
| .89 | .80 | .76 | .42  |     |     |
| 1.51| 1.32| .94 | .65  | .42 |     |
| 1.57| 1.41| 1.23| .94  | .76 | .37 |
| 1.64| 1.58| 1.41| 1.32 | .80 | .38 |
| 1.73| 1.64| 1.57| 1.51 | .89 | .39 |

**FIG. B**

| .55 | .55 | .54 |      |      |     |
|-----|-----|-----|------|------|-----|
| 1.08| 1.07| 1.08| .65  |      |     |
| 1.51| 1.50| 1.19| .93  | .65  |     |
| 1.01| 1.28| 1.32| 1.19 | 1.08 | .54 |
| .87 | 1.15| 1.28| 1.50 | 1.07 | .55 |
| 1.03| .87 | 1.01| 1.51 | 1.08 | .55 |

**FIG. C**

| .71 | .71 | .70 |      |      |     |
|-----|-----|-----|------|------|-----|
| 1.31| 1.27| 1.31| .80  |      |     |
| 1.65| 1.54| 1.23| 1.07 | .80  |     |
| .89 | .87 | .90 | 1.23 | 1.31 | .70 |
| .52 | .59 | .87 | 1.54 | 1.27 | .71 |
| .42 | .52 | .89 | 1.65 | 1.31 | .71 |

**FIG. D**

| .50 | .68 | .79 |      |      |     |
|-----|-----|-----|------|------|-----|
| .72 | 1.19| 1.49| .98  |      |     |
| 1.03| 1.45| 1.38| 1.30 | .98  |     |
| .84 | .92 | 1.00| 1.38 | 1.49 | .79 |
| .87 | .78 | .92 | 1.45 | 1.19 | .68 |
| 1.21| .87 | .84 | 1.03 | .72  | .50 |

MOVABLE ROD
(HAFNIUM)

FIXED ROD
(BORON S.S.)

1. DRAWINGS REPRESENT A CORE QUADRANT.

2. NUMBERS ON DRAWING REPRESENT AVERAGE BUNDLE POWER TO AVERAGE CORE POWER.

# FIGURE 5—9 GROSS RADIAL POWER DISTRIBUTION
## (TWO—DIMENSIONAL , P D Q CALCULATIONS)

**FIG. A**

| .36 | .37 | .38 | | | |
|---|---|---|---|---|---|
| .80 | .80 | .88 | .55 | | |
| 1.34 | 1.33 | 1.26 | 1.04 | .55 | |
| 1.38 | 1.38 | 1.50 | 1.26 | .88 | .38 |
| 1.44 | 1.43 | 1.38 | 1.33 | .80 | .37 |
| 1.48 | 1.44 | 1.38 | 1.34 | .80 | .36 |

**FIG. B**

| 1.26 | 1.16 | .85 | | | |
|---|---|---|---|---|---|
| 1.61 | 1.55 | 1.46 | .91 | | |
| 1.12 | 1.18 | 1.41 | 1.39 | .91 | |
| .39 | 48 | .93 | 1.41 | 1.46 | .85 |
| .22 | .28 | .48 | 1.18 | 1.55 | 1.16 |
| .18 | .22 | .39 | 1.12 | 1.61 | 1.26 |

**FIG. C**

| .97 | 1.12 | .99 | | | |
|---|---|---|---|---|---|
| .99 | 1.49 | 1.78 | 1.22 | | |
| .62 | 1.20 | 1.79 | 1.91 | 1.22 | |
| .31 | .52 | 1.20 | 1.79 | 1.78 | .99 |
| .22 | .30 | .52 | 1.20 | 1.49 | 1.12 |
| .19 | .22 | .31 | .62 | .99 | .97 |

**FIG. D**

| .57 | .84 | 1.05 | | | |
|---|---|---|---|---|---|
| .68 | 1.29 | 1.86 | 1.33 | | |
| .65 | 1.21 | 1.57 | 1.67 | 1.33 | |
| .47 | .61 | .96 | 1.57 | 1.86 | 1.05 |
| .70 | .62 | .61 | 1.21 | 1.29 | .84 |
| 1.08 | .70 | 47 | .65 | .68 | .57 |

MOVABLE ROD (HAFNIUM)

FIXED ROD (BORON S.S.)

1. DRAWINGS REPRESENT A CORE QUADRANT.

2. NUMBERS ON DRAWING REPRESENT AVERAGE BUNDLE POWER TO AVERAGE CORE POWER.

# FIGURE 5—10 GROSS RADIAL POWER DISTRIBUTION
## (TWO—DIMENSIONAL, P D Q CALCULATIONS)



FIG. A

FIG. B

FIG. C

FIG. D

MOVABLE ROD
(HAFNIUM)

FIXED ROD
(BORON S.S.)

1. DRAWINGS REPRESENT A
   CORE QUADRANT.

2. NUMBERS ON DRAWING REPRESENT
   AVERAGE BUNDLE POWER TO
   AVERAGE CORE POWER.

# FIGURE 5-11 GROSS RADIAL POWER DISTRIBUTION

## (TWO-DIMENSIONAL, PDQ CALCULATION)

|      |      | .55  | .46  | .33  | .33  | .46  | .55  |      |      |      |
|------|------|------|------|------|------|------|------|------|------|------|
|      | .78  | 1.07 | .81  | .48  | .48  | .81  | 1.07 | .78  |      |      |
|      | .99  | 1.18 | 1.09 | 1.02 | .68  | .68  | 1.02 | 1.09 | 1.18 | .99  |
| .95  | 1.73 | 1.55 | .94  | .66  | .53  | .53  | .66  | .94  | 1.55 | 1.73 | .95 |
| .98  | 1.74 | 2.06 | 1.07 | .60  | .45  | .45  | .60  | 1.07 | 2.06 | 1.74 | .98 |
| .99  | 1.83 | 2.26 | 1.17 | .60  | .43  | .43  | .60  | 1.17 | 2.26 | 1.83 | .99 |
| .99  | 1.83 | 2.26 | 1.17 | .60  | .43  | .43  | .60  | 1.17 | 2.26 | 1.83 | .99 |
| .98  | 1.74 | 2.06 | 1.07 | .60  | .45  | .45  | .60  | 1.07 | 2.06 | 1.74 | .98 |
| .95  | 1.73 | 1.55 | .94  | .66  | .53  | .53  | .66  | .94  | 1.55 | 1.73 | .95 |
|      | .99  | 1.18 | 1.09 | 1.02 | .68  | .68  | 1.02 | 1.09 | 1.18 | .99  |
|      | .78  | 1.07 | .81  | .48  | .48  | .81  | 1.07 | .78  |      |      |
|      |      | .55  | .46  | .33  | .33  | .46  | .55  |      |      |      |

┼ MOVABLE ROD (HAFNIUM)

┿ FIXED ROD (BORON S.S)

NUMBERS ON DRAWING REPRESENT BUNDLE POWER TO AVERAGE CORE POWER.

# FIGURE 5-12  LOCAL POWER DISTRIBUTION
## (ZONE I ELEMENT)
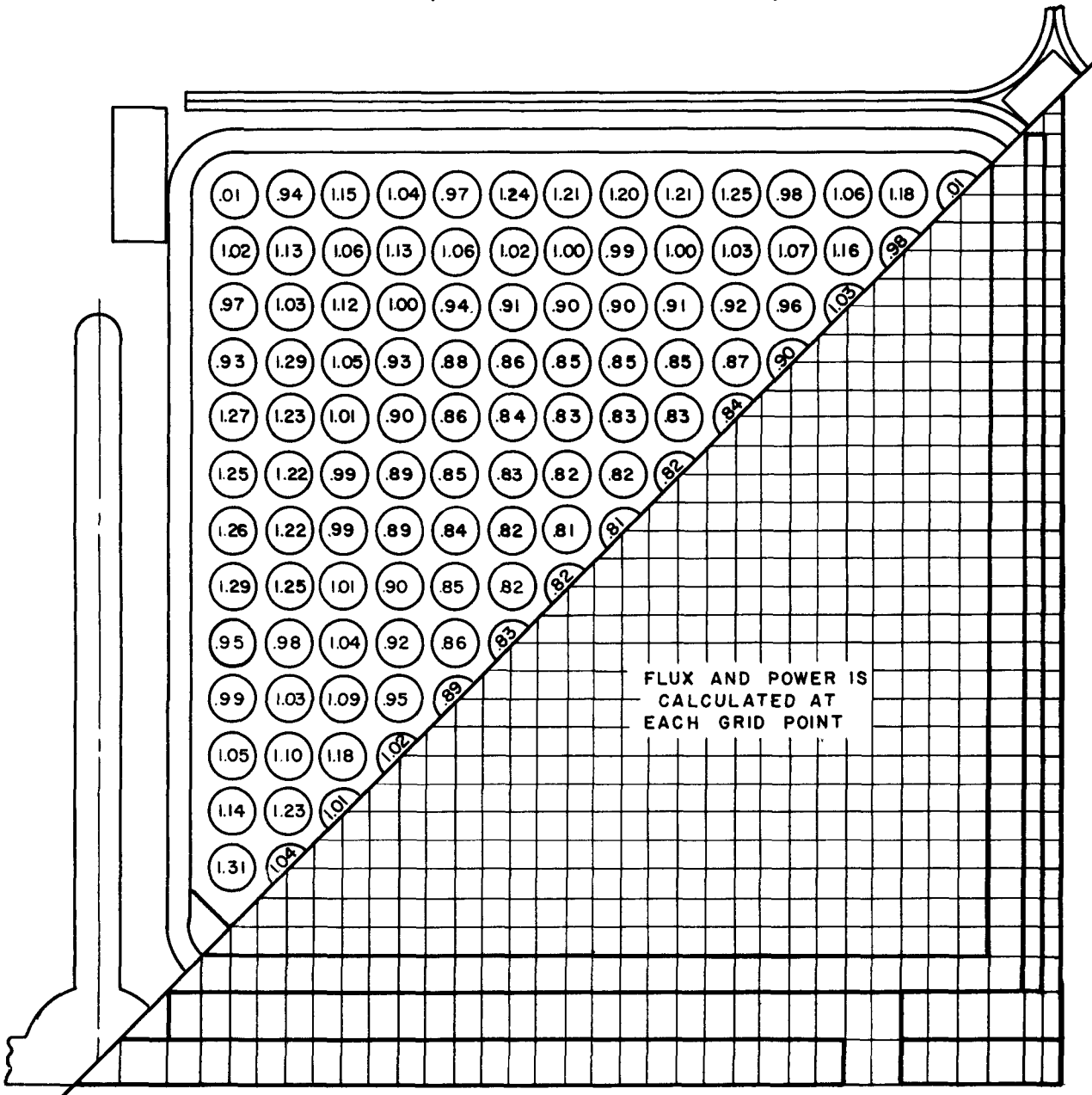


FLUX AND POWER IS
CALCULATED AT
EACH GRID POINT

NOTE:
1. LOWER RIGHT —— CALCULATION MODEL
2. UPPER LEFT —— PHYSICAL MODEL
3 NUMBER IN PIN IS AVERAGE PIN POWER
   TO AVERAGE BUNDLE POWER.

PDQ CALCULATION

# FIGURE 5-13 LOCAL POWER DISTRIBUTION
## (ZONE II ELEMENT)
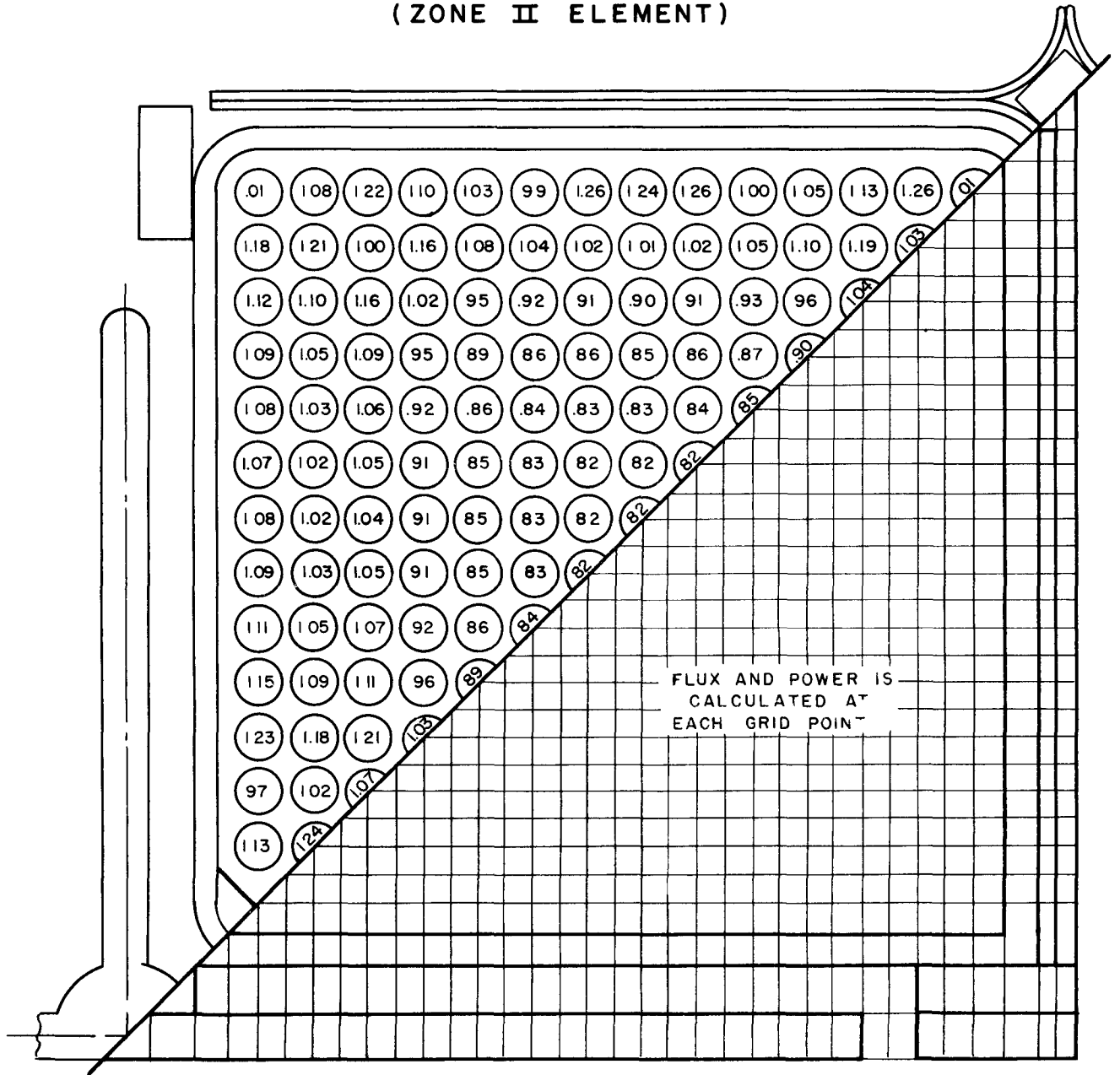


FLUX AND POWER IS
CALCULATED AT
EACH GRID POINT

NOTE.
1 LOWER RIGHT — CALCULATION MODEL
2 UPPER LEFT — PHYSICAL MODEL
3 NUMBER IN PIN IS AVERAGE PIN POWER
  TO AVERAGE BUNDLE POWER

PDQ CALCULATION

# FIGURE 5-15 LOCAL POWER DISTRIBUTION
## (ZONE II ELEMENT WITH HAFNIUM ROD)



FLUX AND POWER IS
CALCULATED AT
EACH GRID POINT
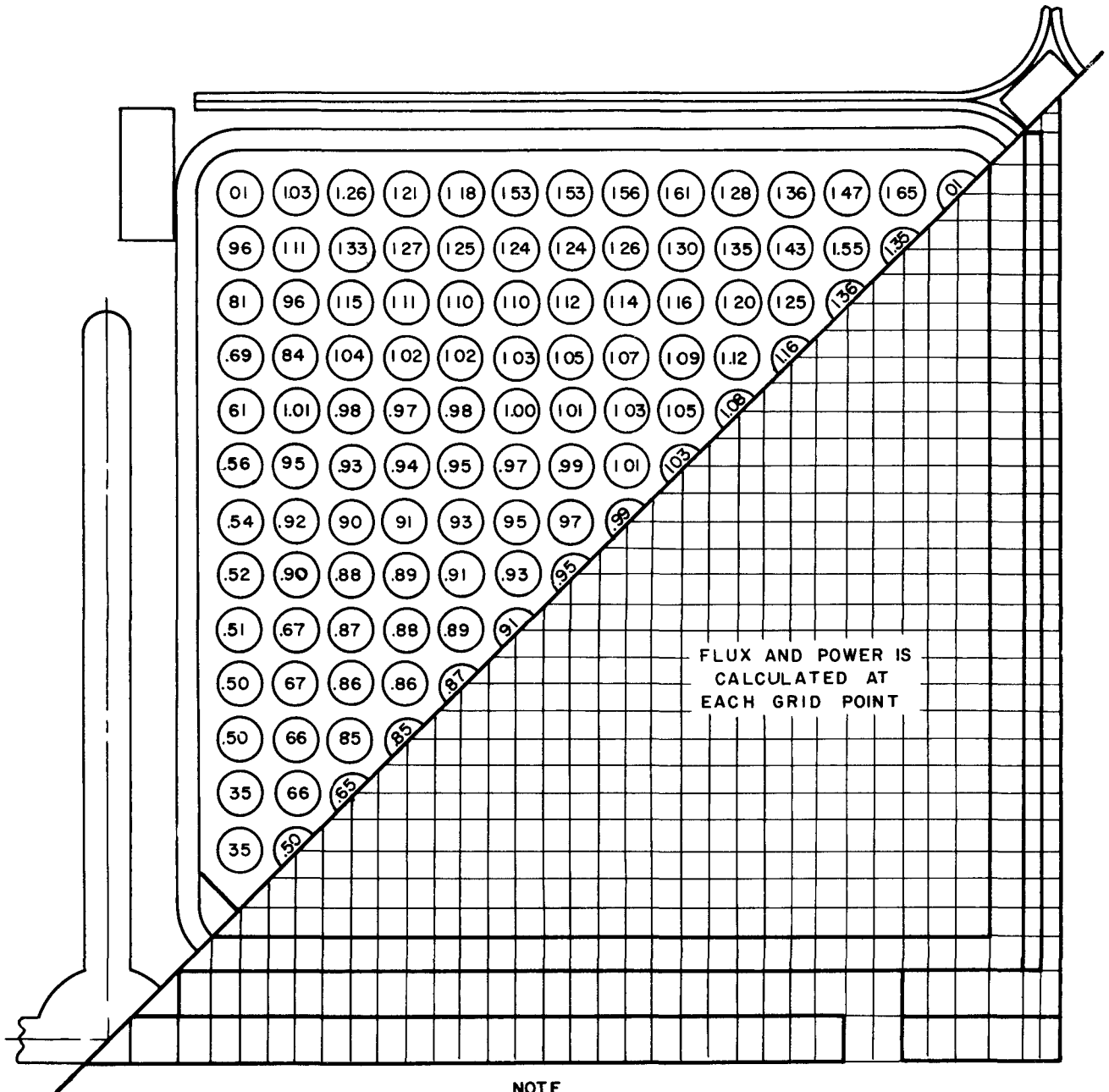
NOTE.
1 LOWER RIGHT — CALCULATED MODEL
2 UPPER LEFT — PHYSICAL MODEL
3 NUMBER IN PIN IS AVERAGE PIN POWER
TO AVERAGE BUNDLE POWER.

PDQ CALCULATION

# FIG. 5.16: AXIAL POWER DISTRIBUTION



Fully Inserted Rod Group Worth = 042 $\Delta K_{eff}$ ──────────

Fully Inserted Rod Group Worth = 020 $\Delta K_{eff}$ ▬ ▬ ▬ ▬ ▬

| | | | | | |
|---|---|---|---|---|---|
| .611 | .699 | .769 | .785 | .754 | .716 |
| 2.52 | 2.28 | 2.04 | 1.81 | 1.63 | 1.58 |
| .699 | .705 | .853 | 1.181 | 1.146 | .864 |
| 2.28 | 2.45 | 2.22 | 1.82 | 1.64 | 1.59 |
| .769 | .853 | 1.248 | 1.513 | 1.472 | .891 |
| 2.04 | 2.22 | 2.06 | 1.75 | 1.62 | 1.59 |
| .785 | 1.181 | 1.513 | 1.670 | 1.241 | |
| 1.81 | 1.82 | 1.75 | 1.66 | 1.60 | |
| .754 | 1.146 | 1.472 | 1.241 | | |
| 1.63 | 1.64 | 1.62 | 1.60 | | |
| .716 | .864 | .891 | | | |
| 1.58 | 1.59 | 1.59 | | | |

TOTAL POWER OF BUNDLE NORMAL-IZED TO AVERAGE BUNDLE POWER

.000

AXIAL PEAK TO AVERAGE POWER IN THE BUNDLE

0.00

FIGURE 5-18  CETR GROSS
POWER DISTRIBUTION

DISTANCE FROM TOP OF CORE (CM.)

0

30

60

90

120

150

168

180

192

204

216

230

247
250
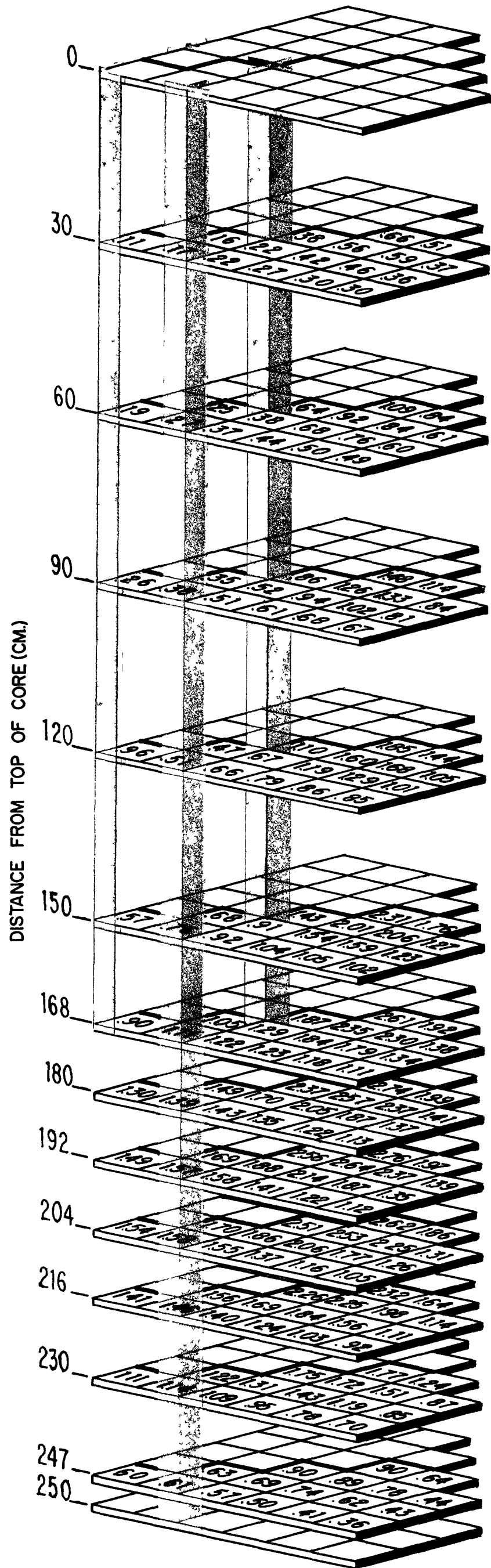
FIG. 5.19: EFFECT OF CONTROL ROD REMOVAL ON XE-135 CONCENTRATION

CONTROL ROD IN

ZR FOLLOWER IN

REGION

A    B    C    D    E    F    G

Xe-135 Concentration, atoms/cm$^3$ x 10$^{-15}$

Distance From Center of Control Rod Channel, cm
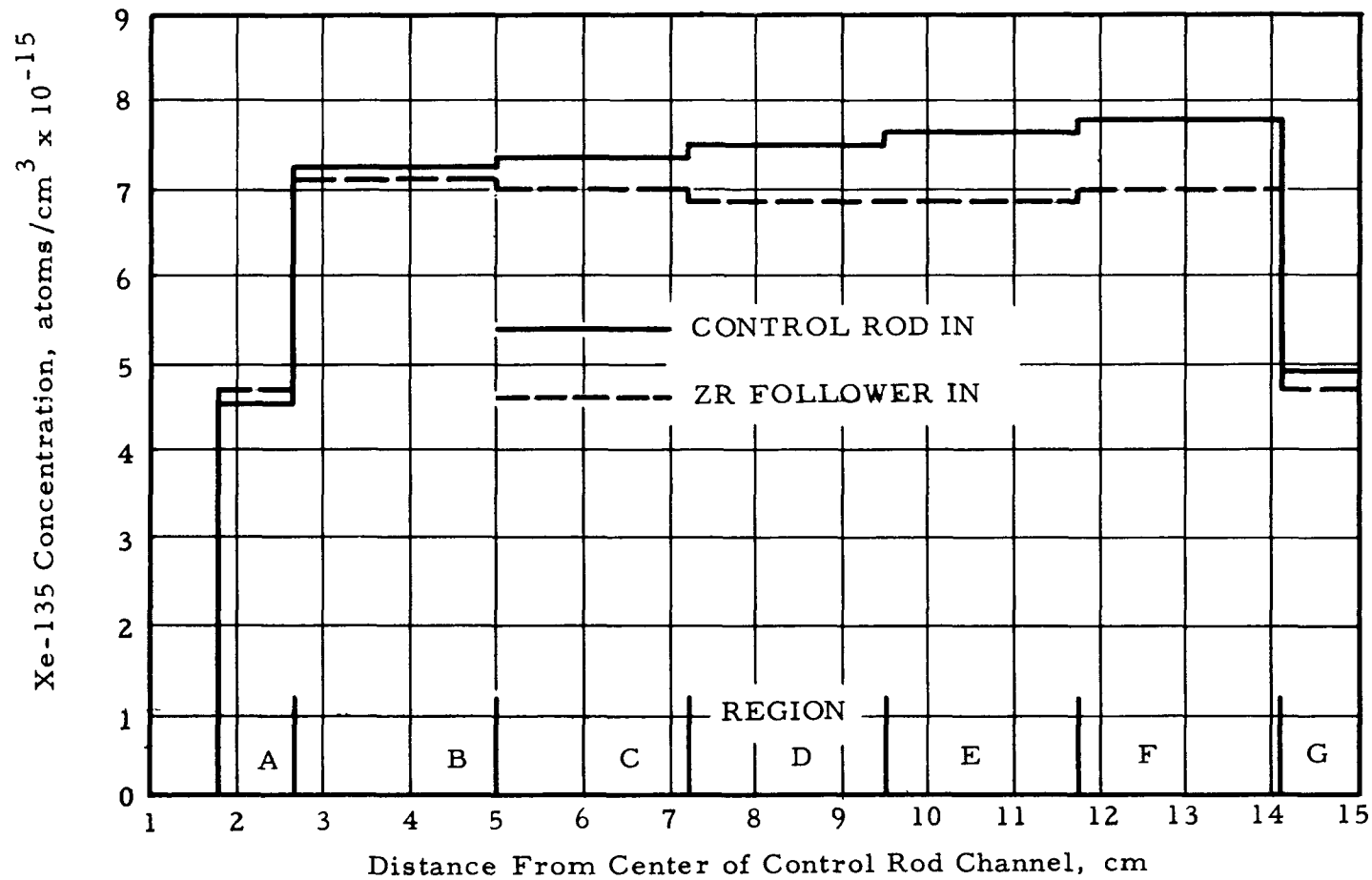
FIG. 5.20: EFFECT OF CONTROL ROD REMOVAL ON LOCAL POWER DISTRIBUTION
AT BEGINNING OF LIFE
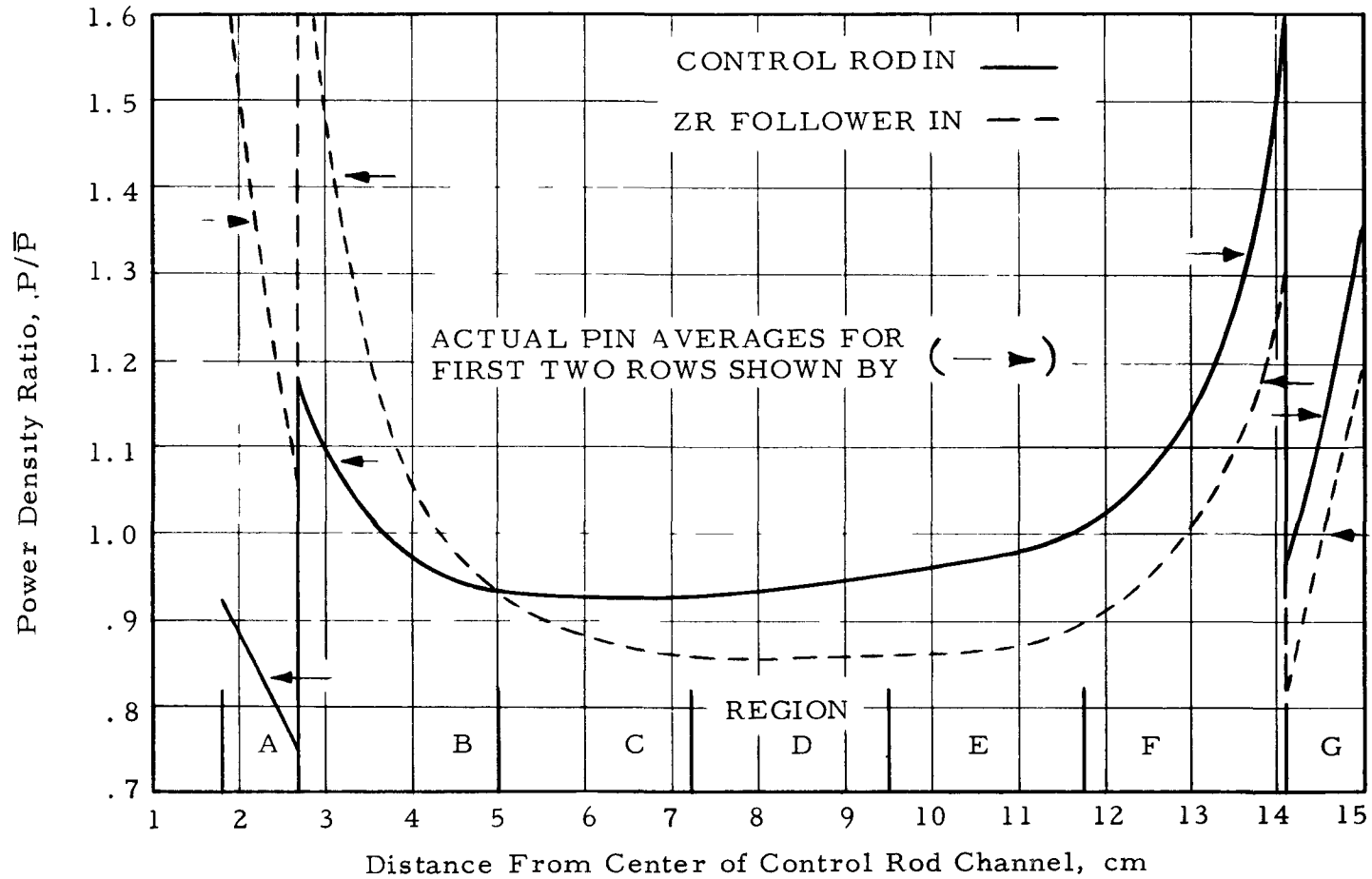
FIG. 5.21: EFFECT OF CONTROL ROD REMOVAL ON LOCAL POWER DISTRIBUTION AFTER 200 DAYS OPERATION
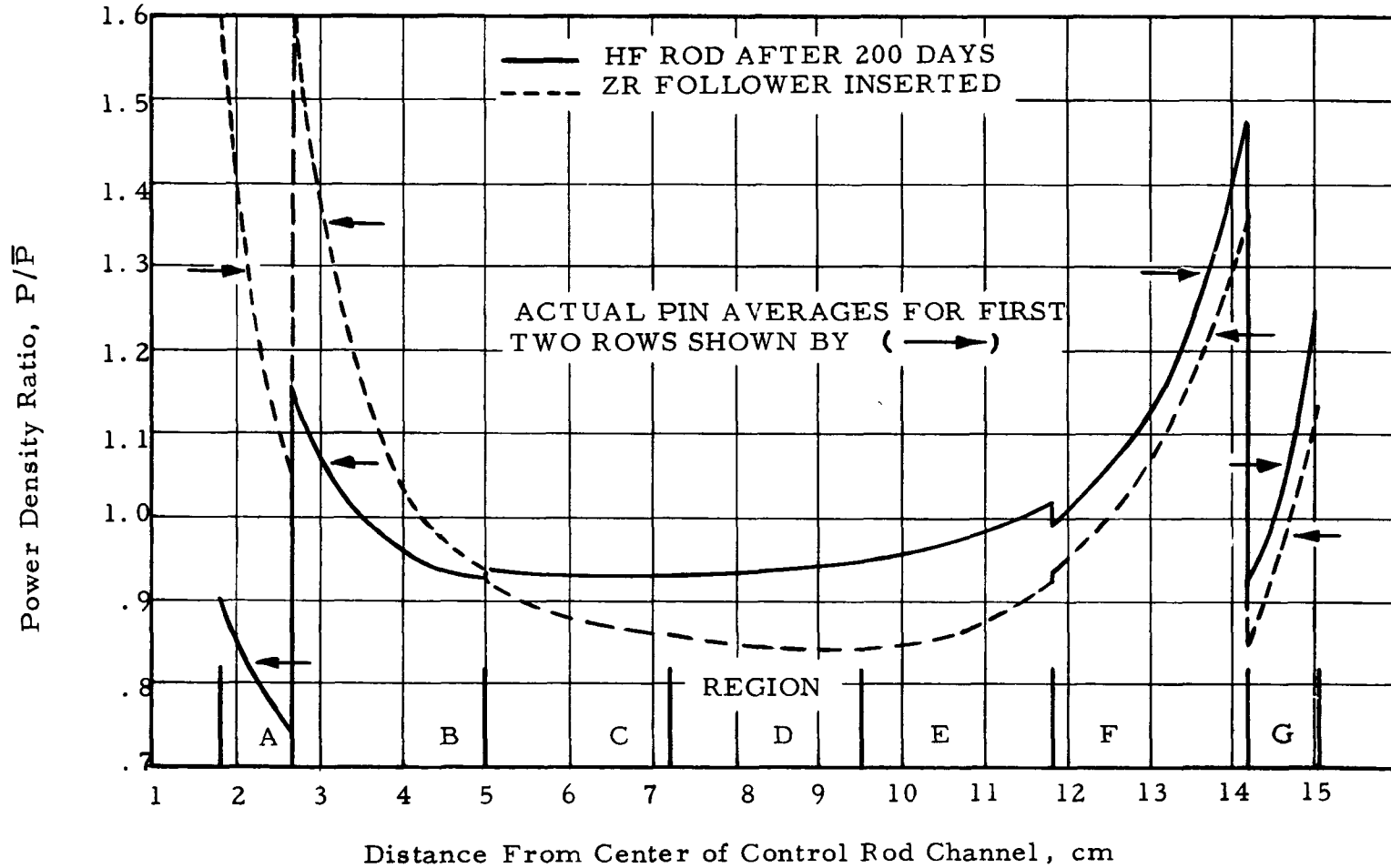
FIG. 5.22: EFFECT OF CONTROL ROD REMOVAL ON LOCAL POWER DISTRIBUTION AFTER 700 DAYS OPERATION
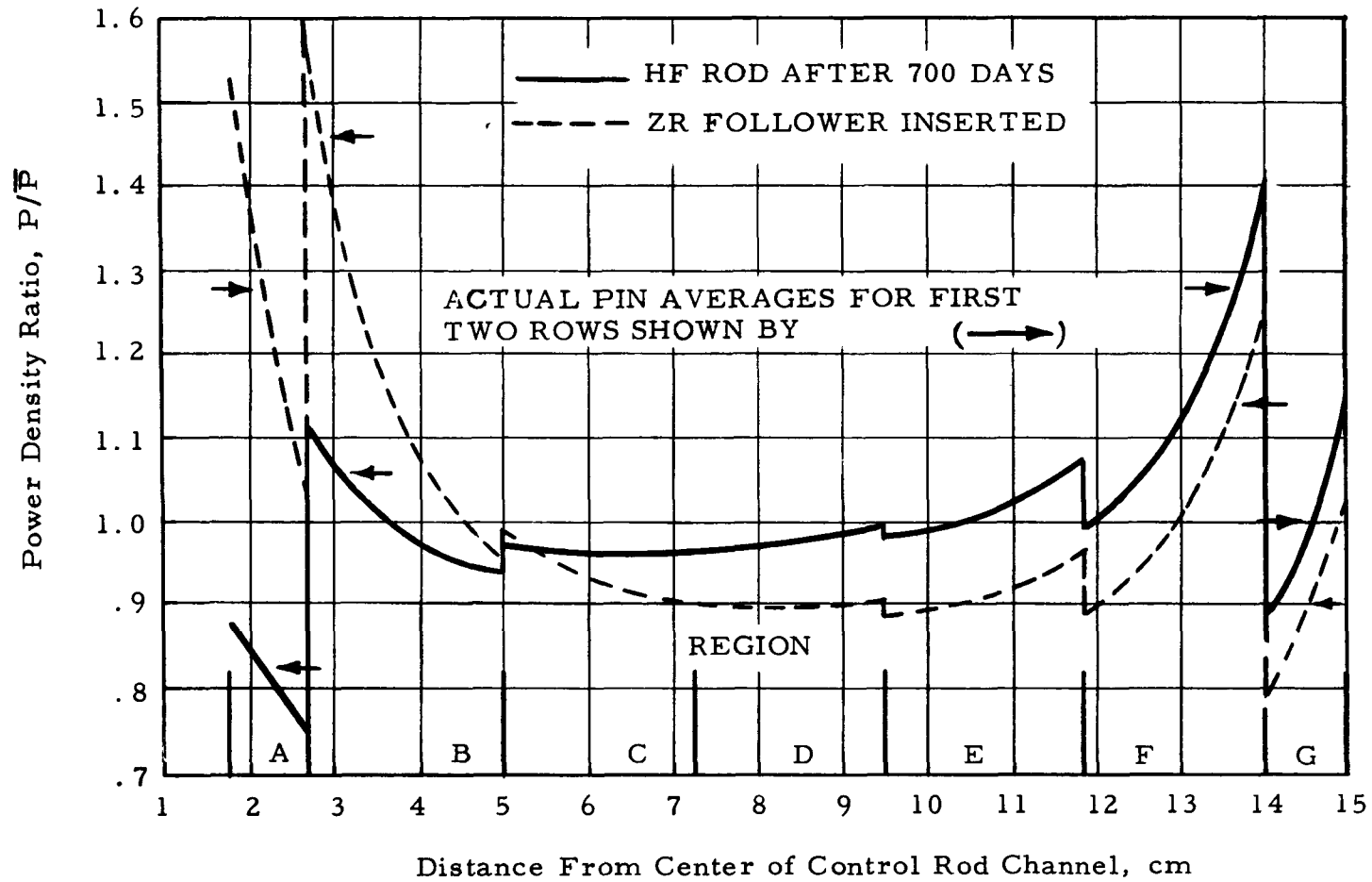
FIG. 5.23: LOCAL POWER DISTRIBUTION THROUGH LIFE WITH CONTROL ROD REMOVED
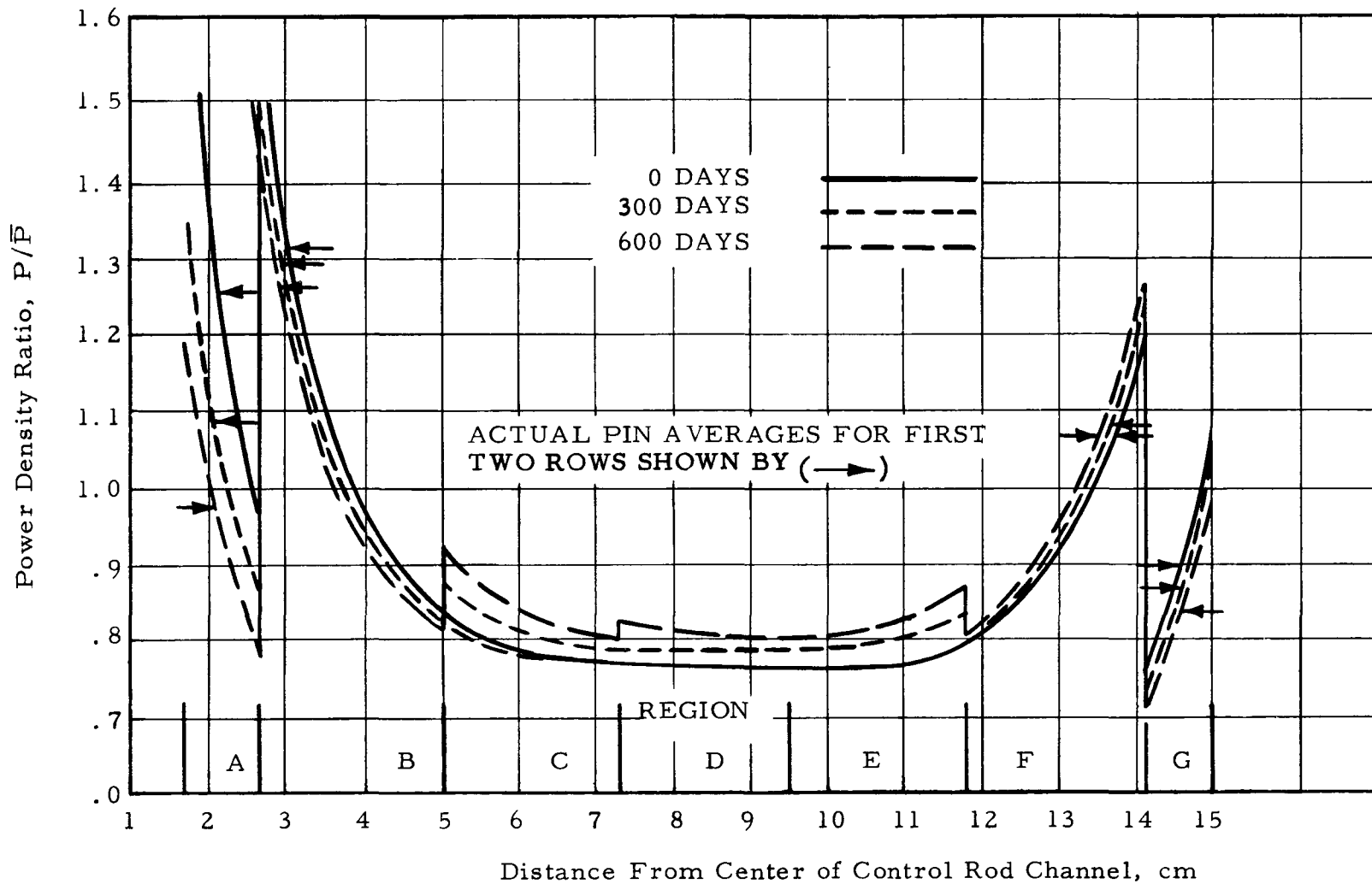
FIG. 5.24: AXIAL POWER PROFILE AT START OF LIFE

$P / \bar{P} = 1.45$

CORE REGION

Power Density, watts/cm³

1  2  3  4  5  6  7  8  9  10

100    200

Distance From Core Top, cm
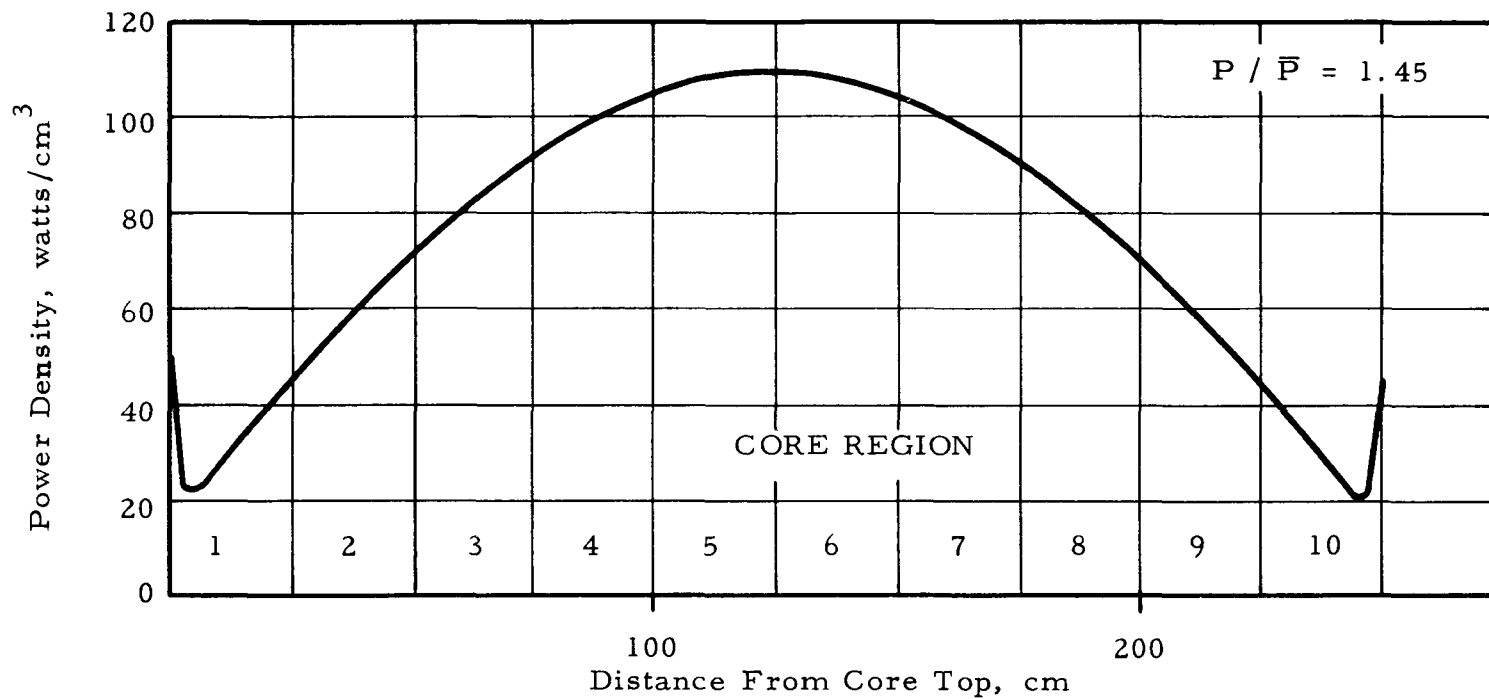
| GROUP I | |
|---|---|
| GROUP II | |
| GROUP III | |

ROD GROUP POSITION

FIG. 5.25:  AXIAL POWER PROFILE AT ONE DAY OF LIFE

$P / \bar{P} = 1.83$

CORE REGION

Power Density,  watts/$cm^3$

Distance From Core Top,  cm
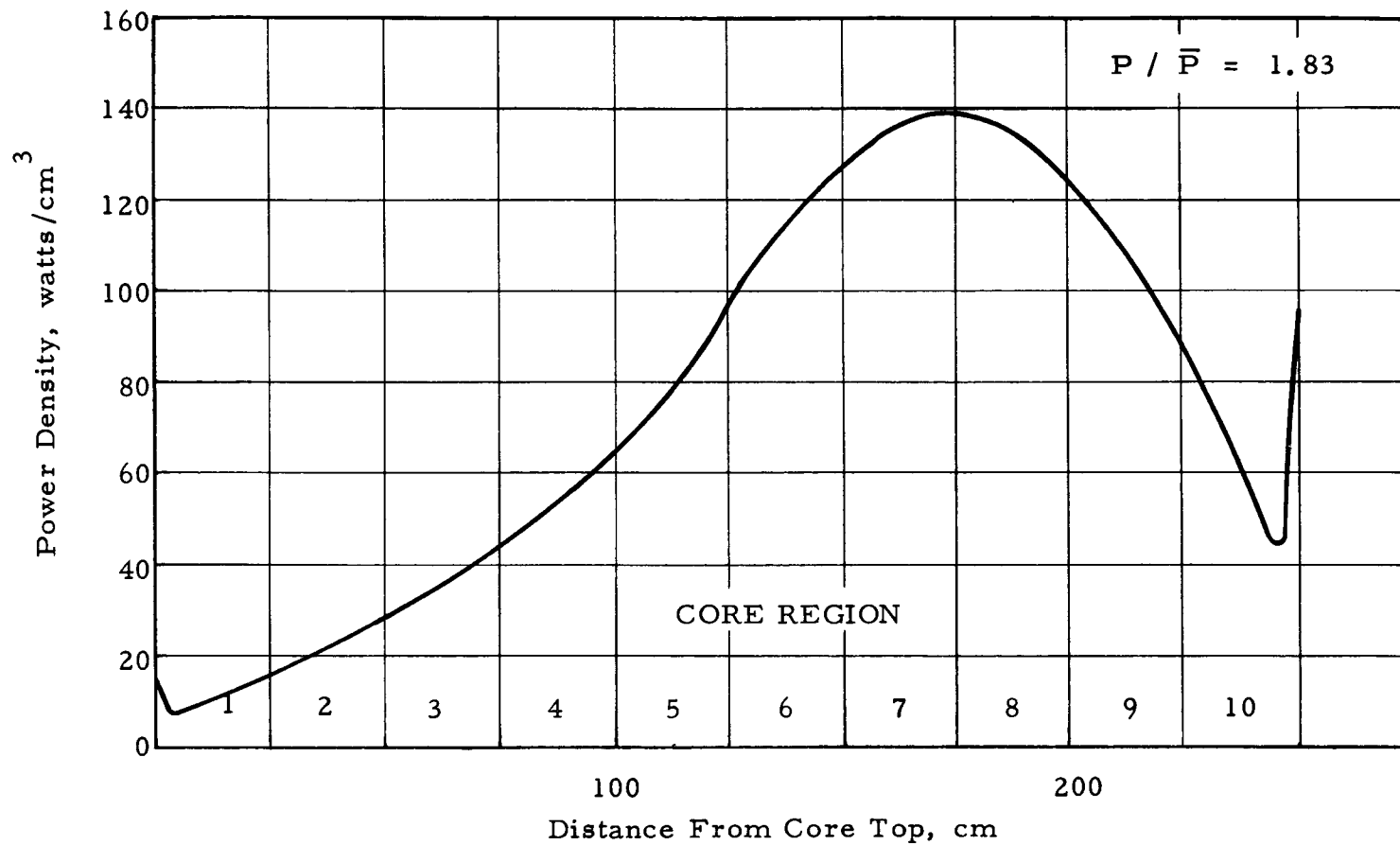
| GROUP I | |
| GROUP II | |
| GROUP III | |

ROD GROUP POSITION

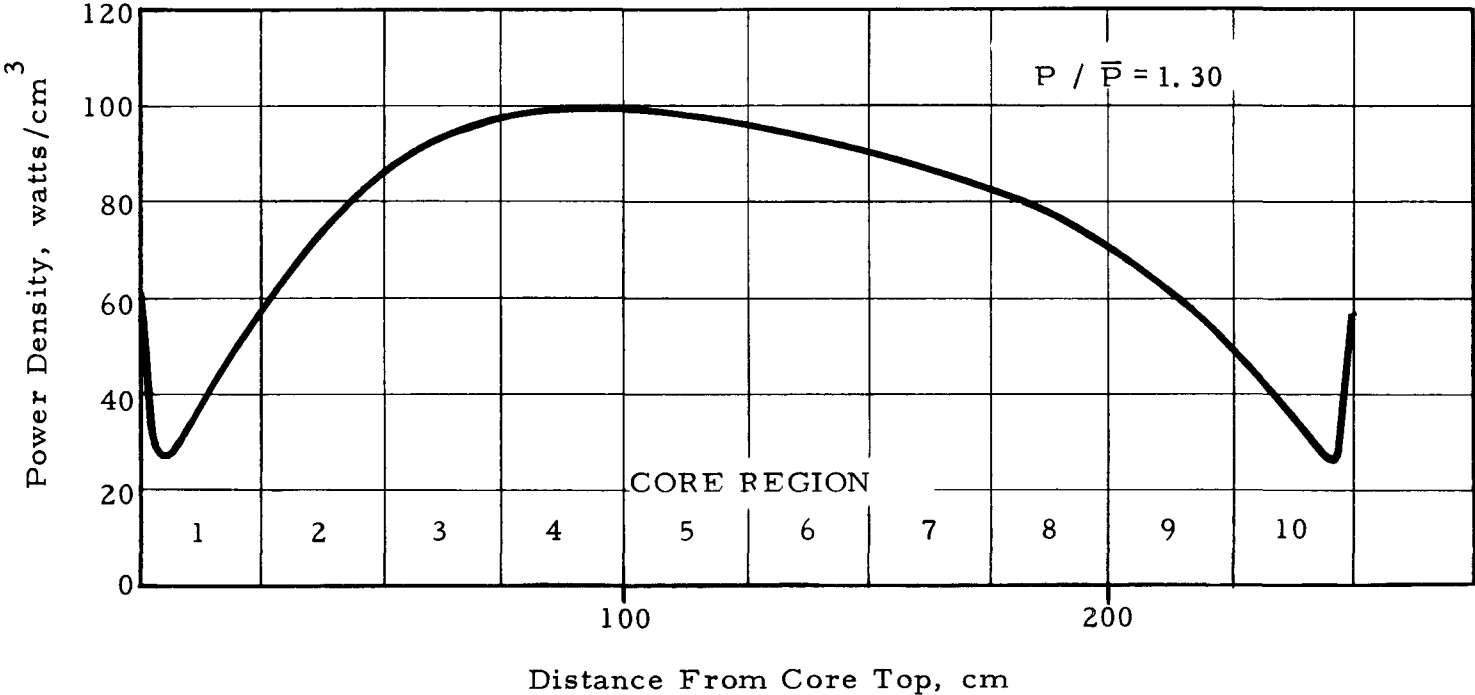## FIG. 5.26: AXIAL POWER PROFILE AT 5 DAYS OF CORE LIFE
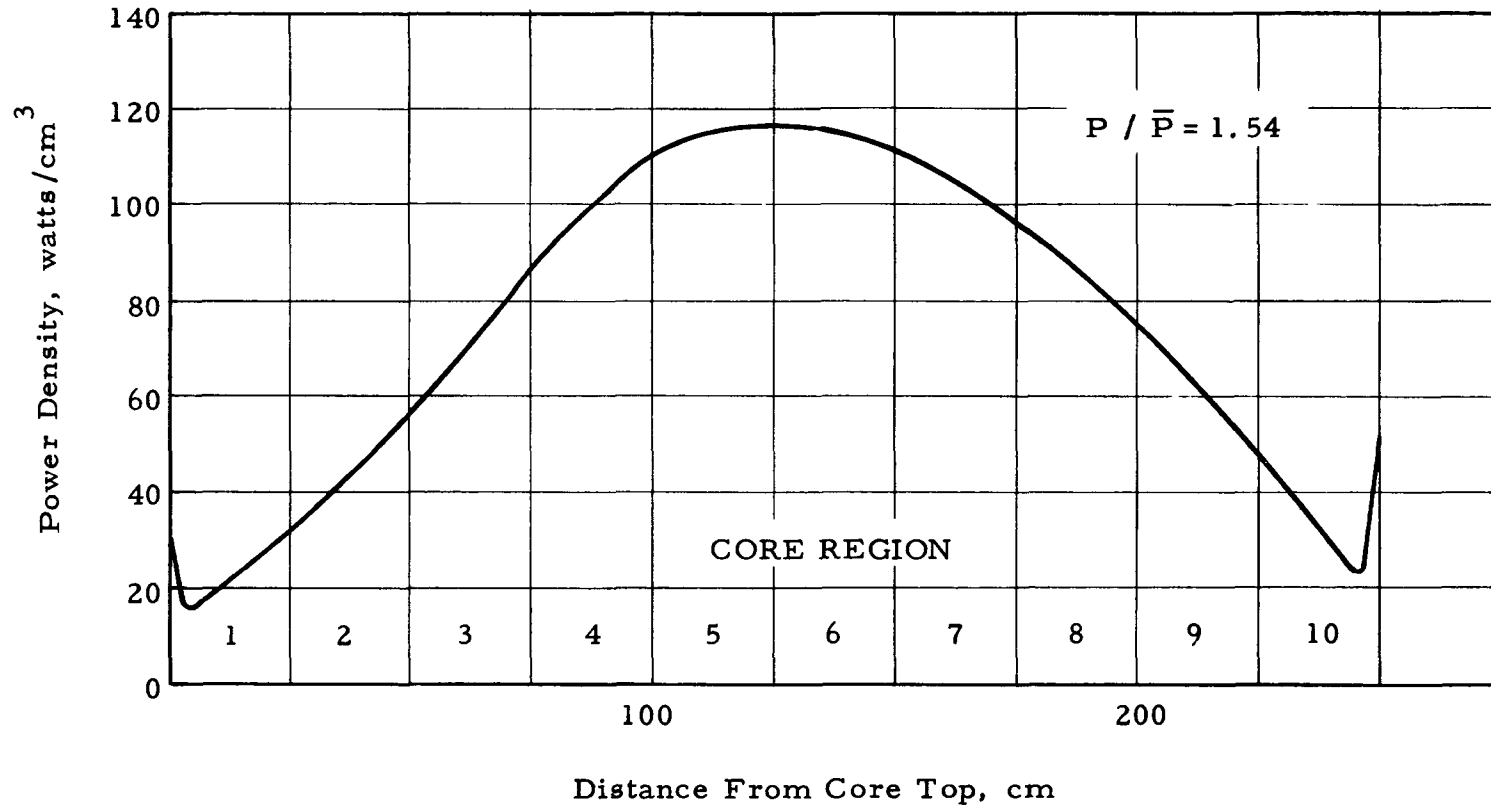


ROD GROUP POSITION

FIG. 5.27: AXIAL POWER PROFILE AT 10 DAYS OF CORE LIFE



P / $\bar{P}$ = 1.43

CORE REGION

Power Density, watts/cm³

Distance From Core Top, cm
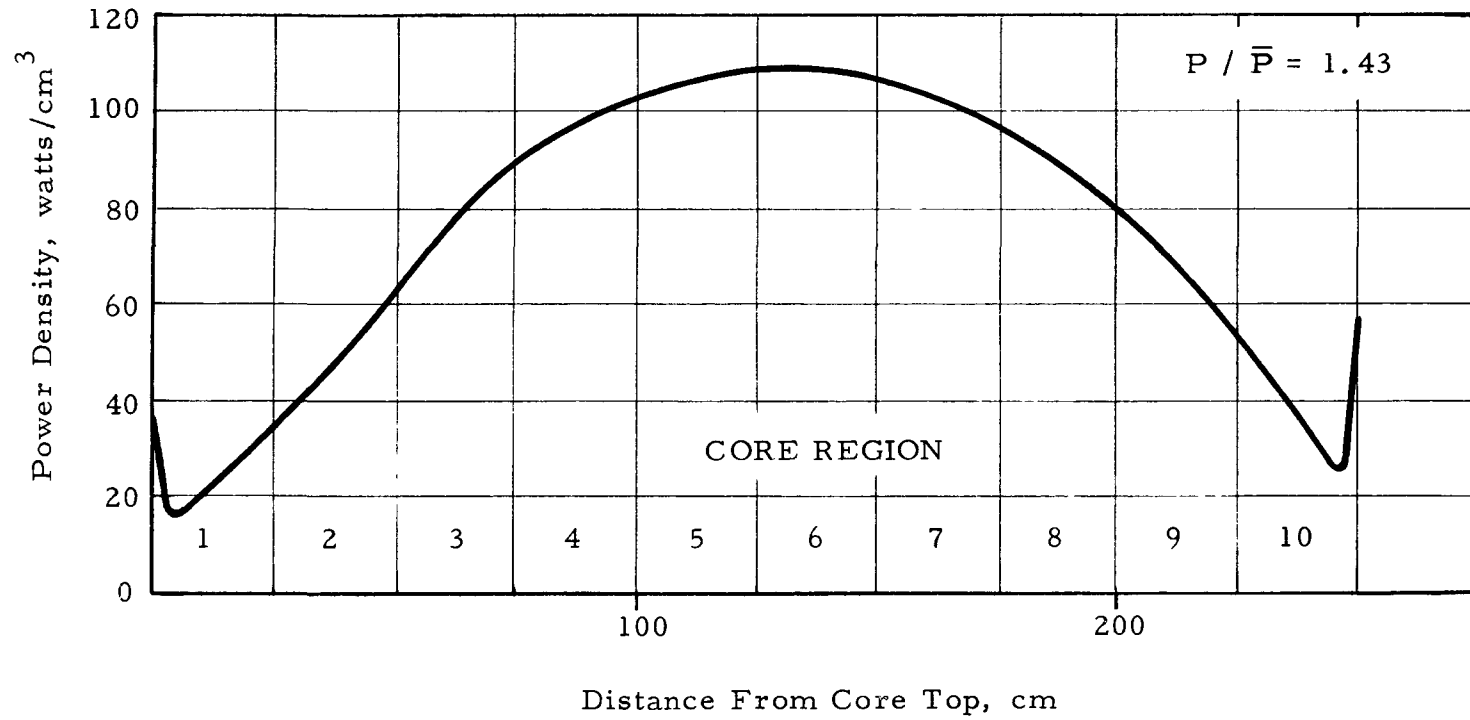
| GROUP I | |
| GROUP II | |
| GROUP III | |

ROD GROUP POSITION

FIG. 5.28: AXIAL POWER PROFILE AT 25 DAYS OF CORE LIFE



$P / \bar{P} = 1.88$
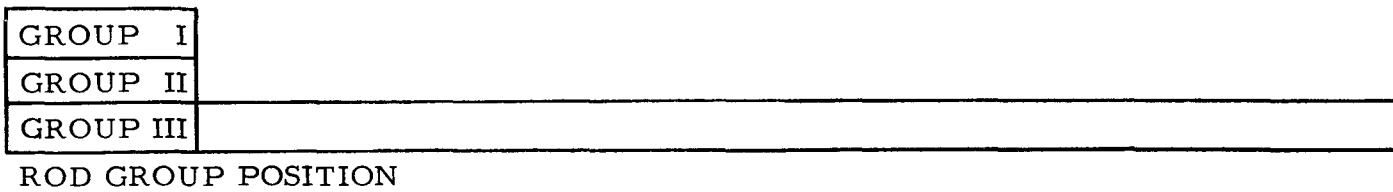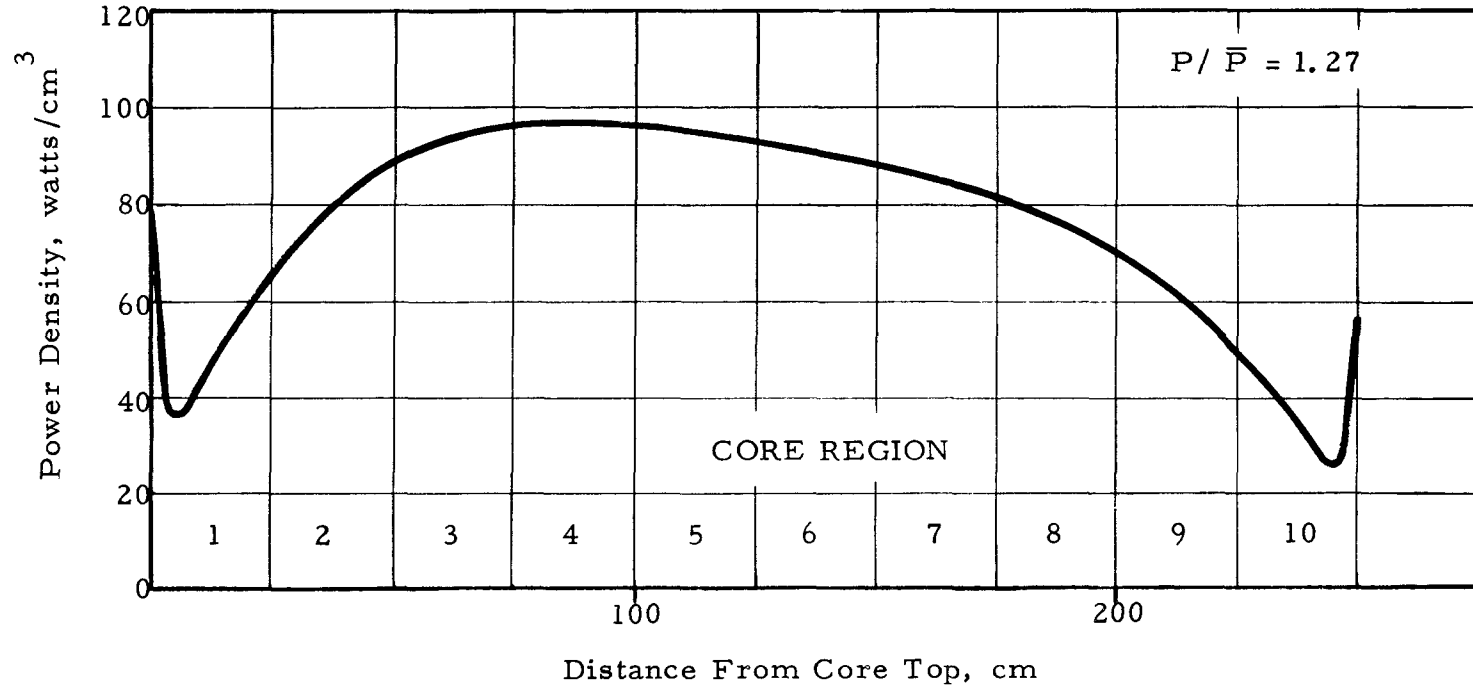
CORE REGION

Power Density, watts/cm$^3$

Distance From Core Top, cm
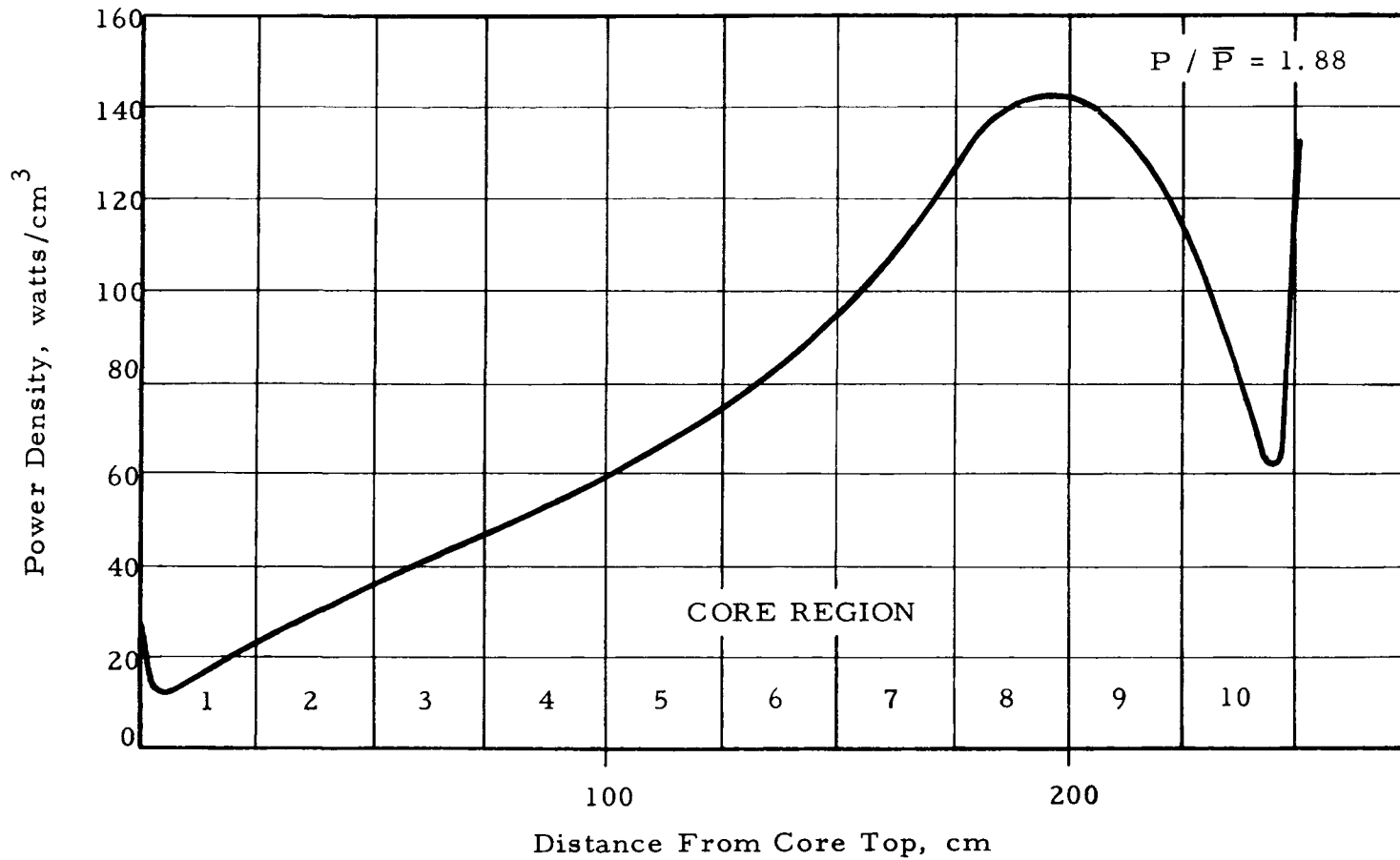
| GROUP I | | |
| GROUP II | | |
| GROUP III | | |

ROD GROUP POSITION

FIG. 5.29: AXIAL POWER PROFILE AT 50 DAYS OF CORE LIFE



Distance From Core Top, cm
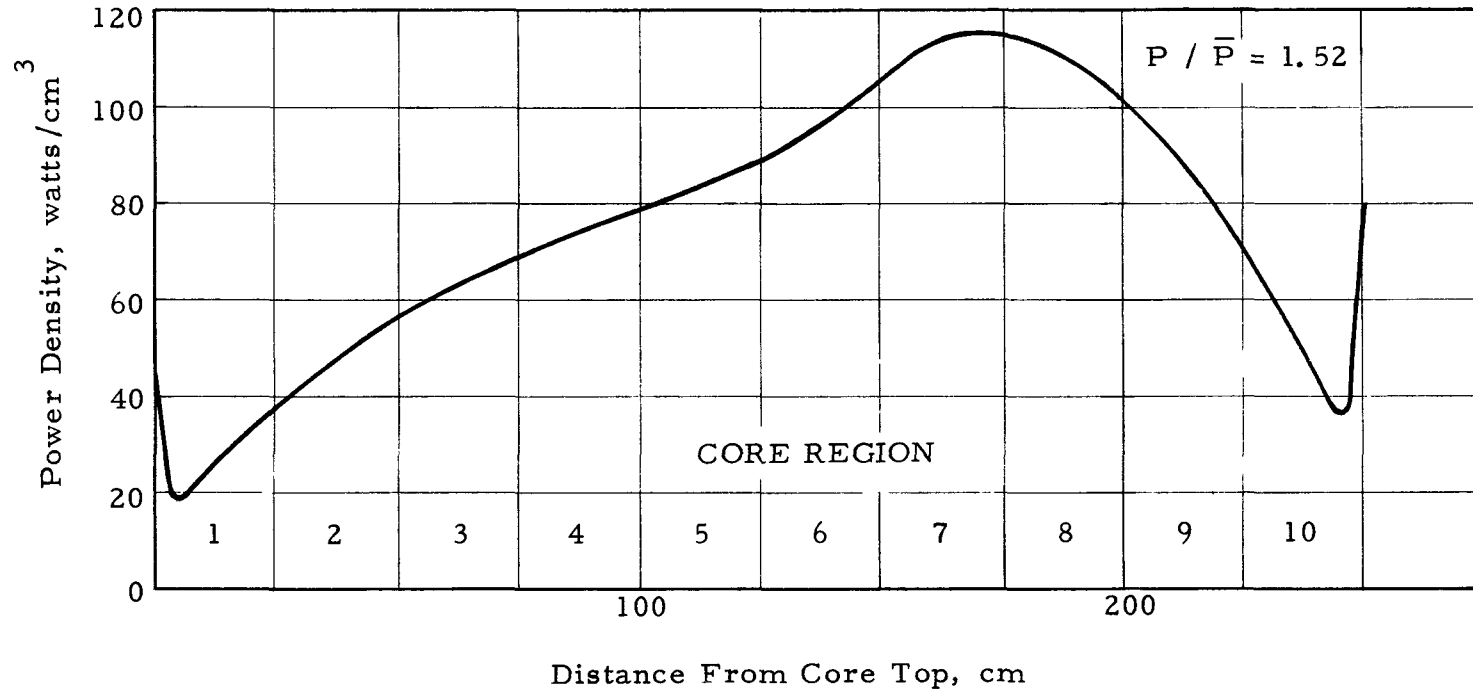
ROD GROUP POSITION

FIG. 5.30: AXIAL POWER PROFILE AT 75 DAYS OF CORE LIFE

$P / \bar{P} = 1.64$

CORE REGION

Power Density, watts/cm$^3$

1  2  3  4  5  6  7  8  9  10

100    200

Distance From Core Top, cm

GROUP    I
GROUP   II
GROUP  III
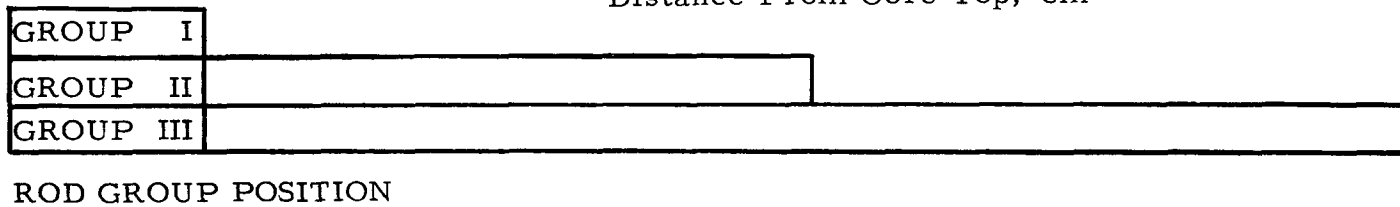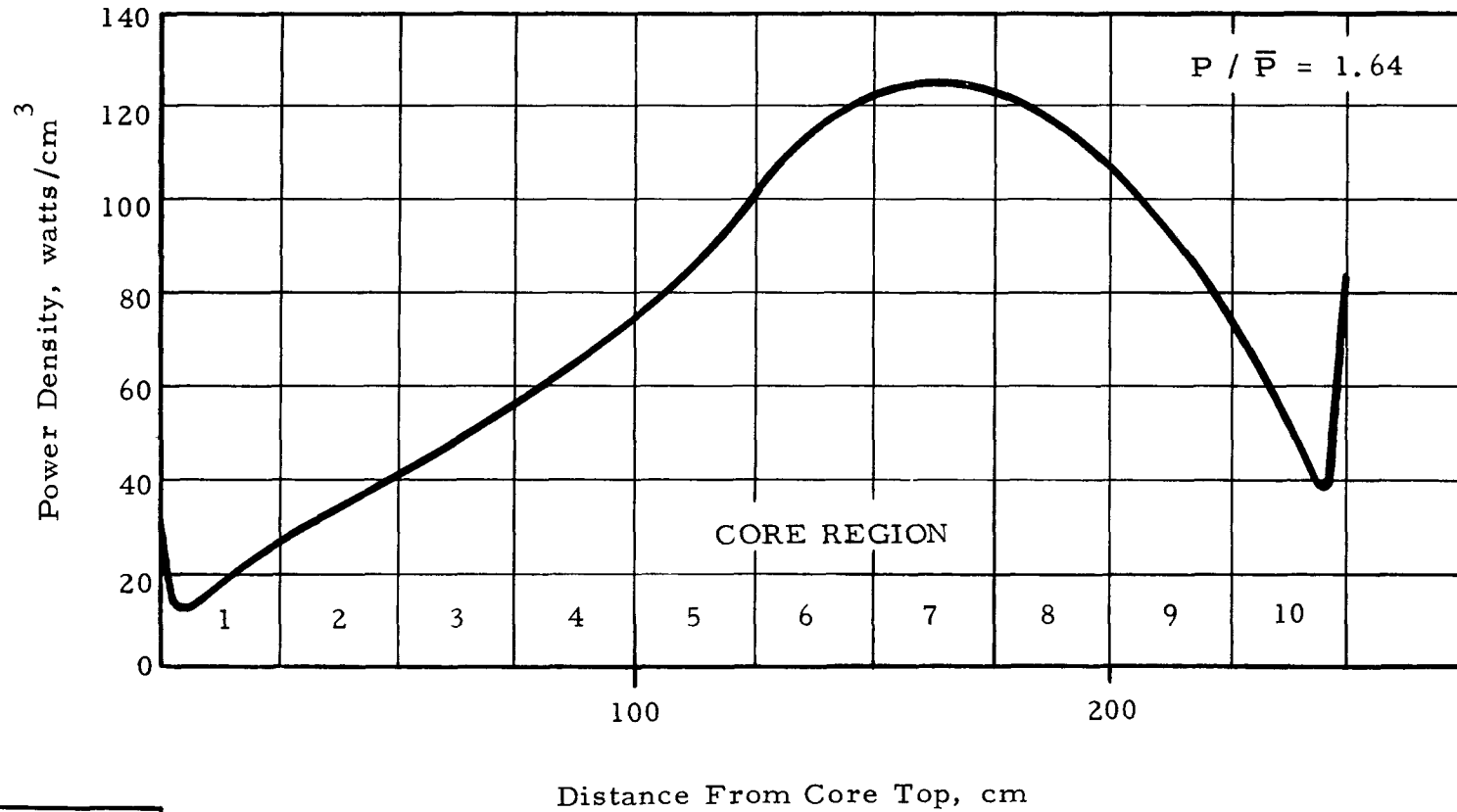
ROD GROUP POSITION

FIG. 5.31: AXIAL POWER PROFILE AT 100 DAYS OF CORE LIFE



$P / \overline{P} = 1.52$

Power Density, watts/cm$^3$

CORE REGION

1  2  3  4  5  6  7  8  9  10

100                    200

Distance From Core Top, cm
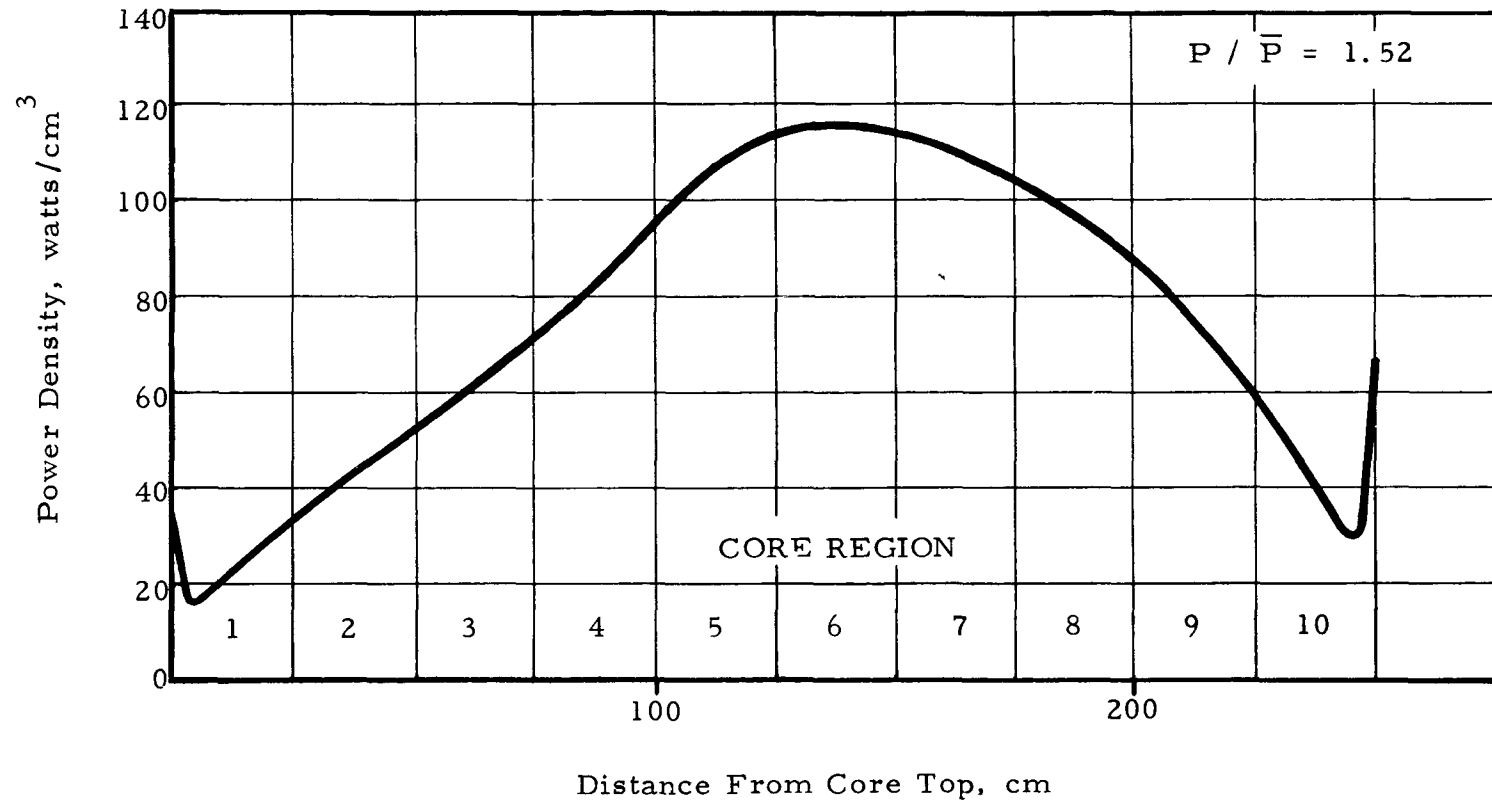
GROUP  I
GROUP  II
GROUP III

ROD GROUP POSITION

FIG. 5.32: AXIAL POWER PROFILE AT 130 DAYS OF CORE LIFE
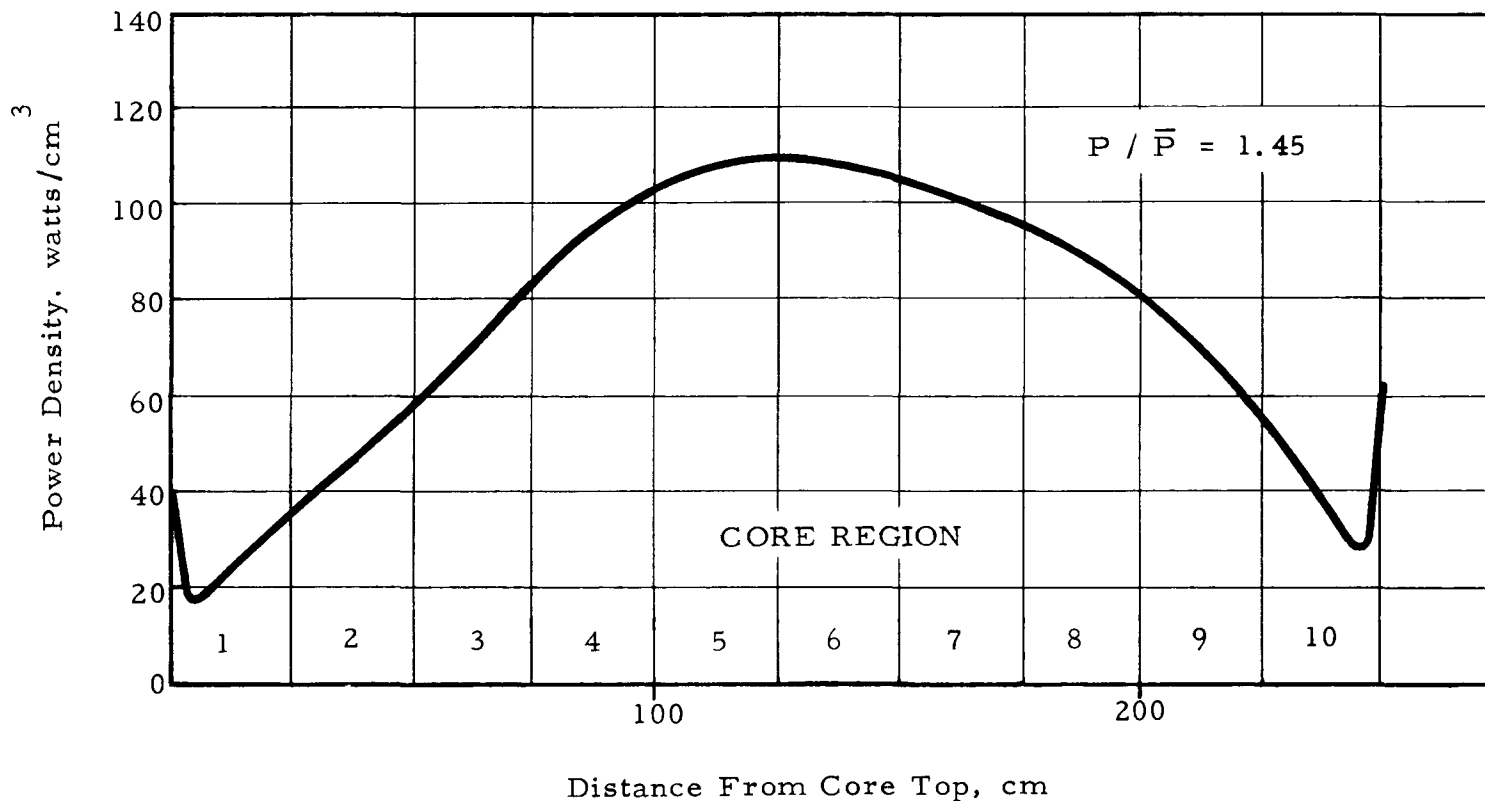
FIG. 5.33: AXIAL POWER PROFILE AT 170 DAYS OF CORE LIFE



Distance From Core Top, cm
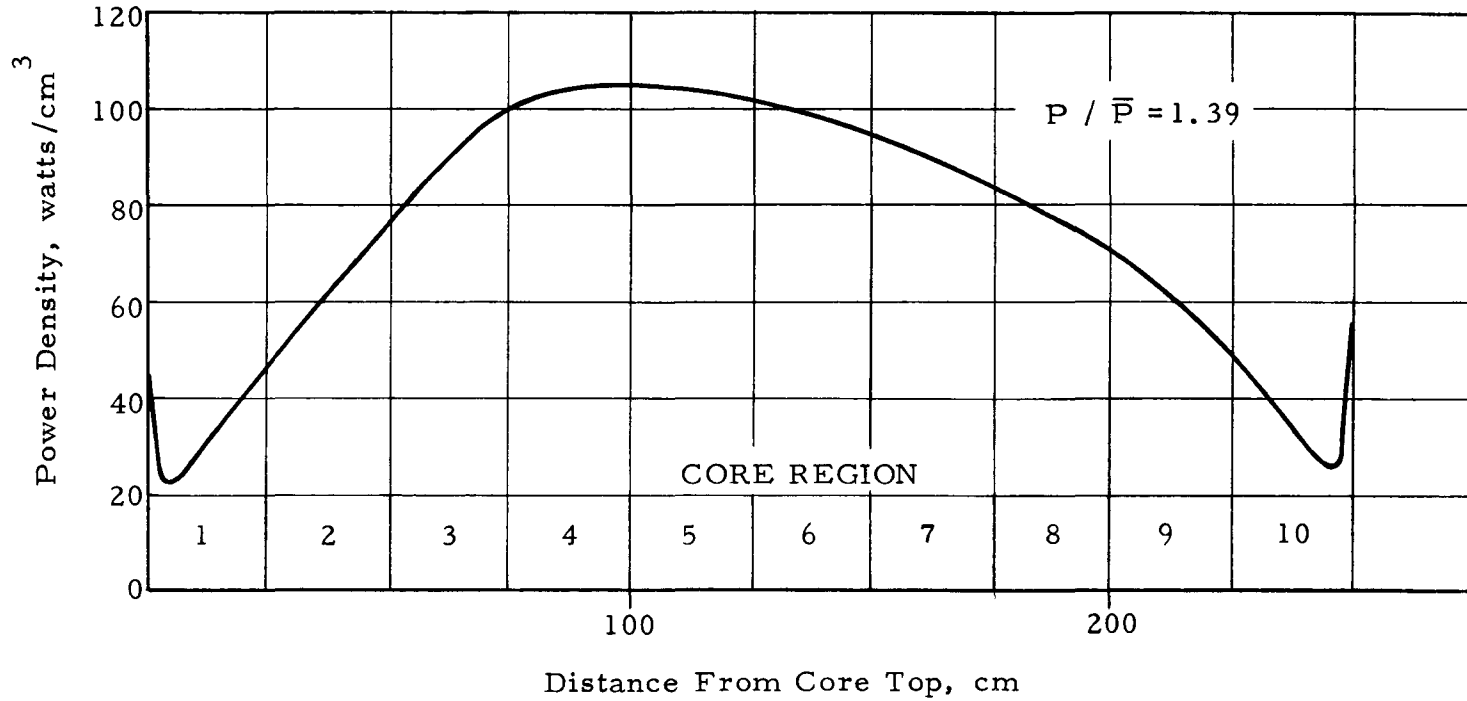
| GROUP   I |
| GROUP  II |
| GROUP III |

ROD GROUP POSITION

FIG. 5.34: AXIAL POWER PROFILE AT 200 DAYS OF CORE LIFE

$P / \overline{P} = 1.30$

CORE REGION

Distance From Core Top, cm

GROUP I
GROUP II
GROUP III

ROD GROUP POSITION
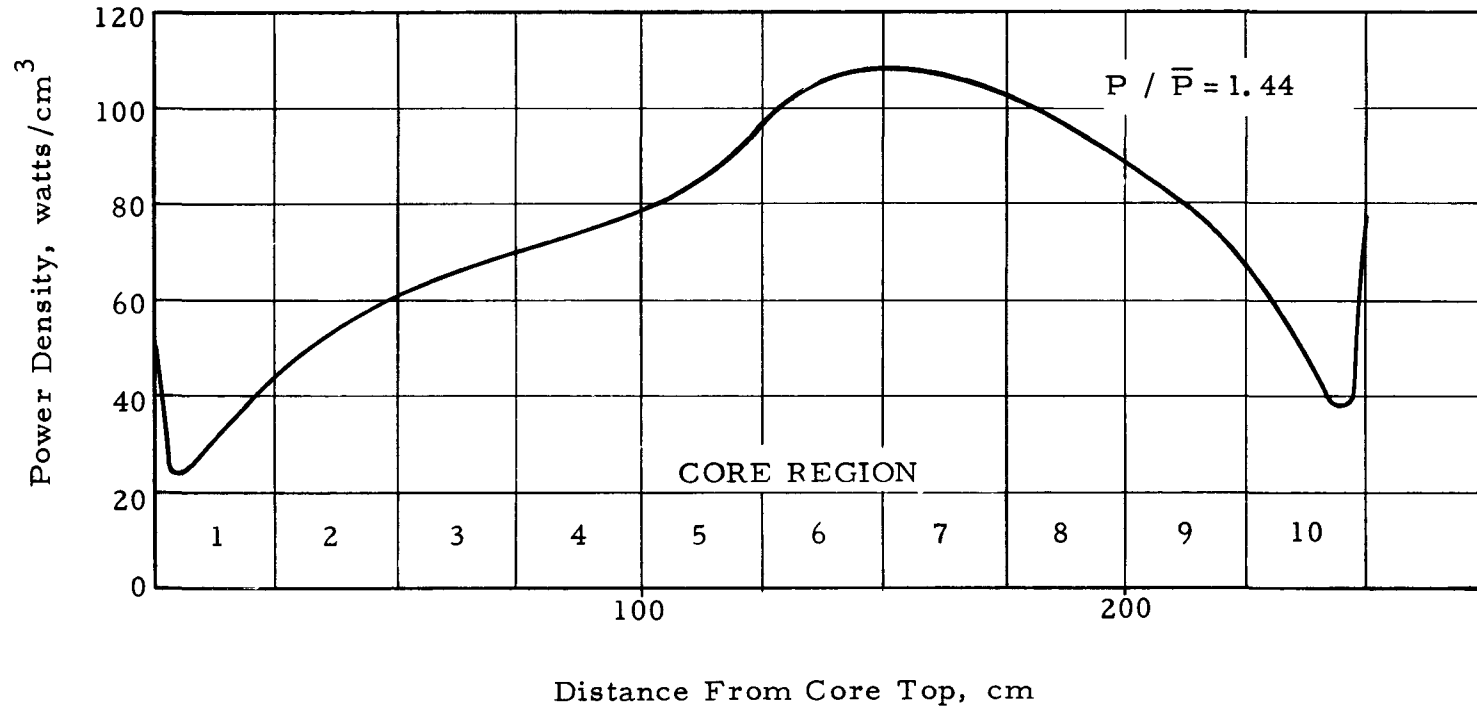
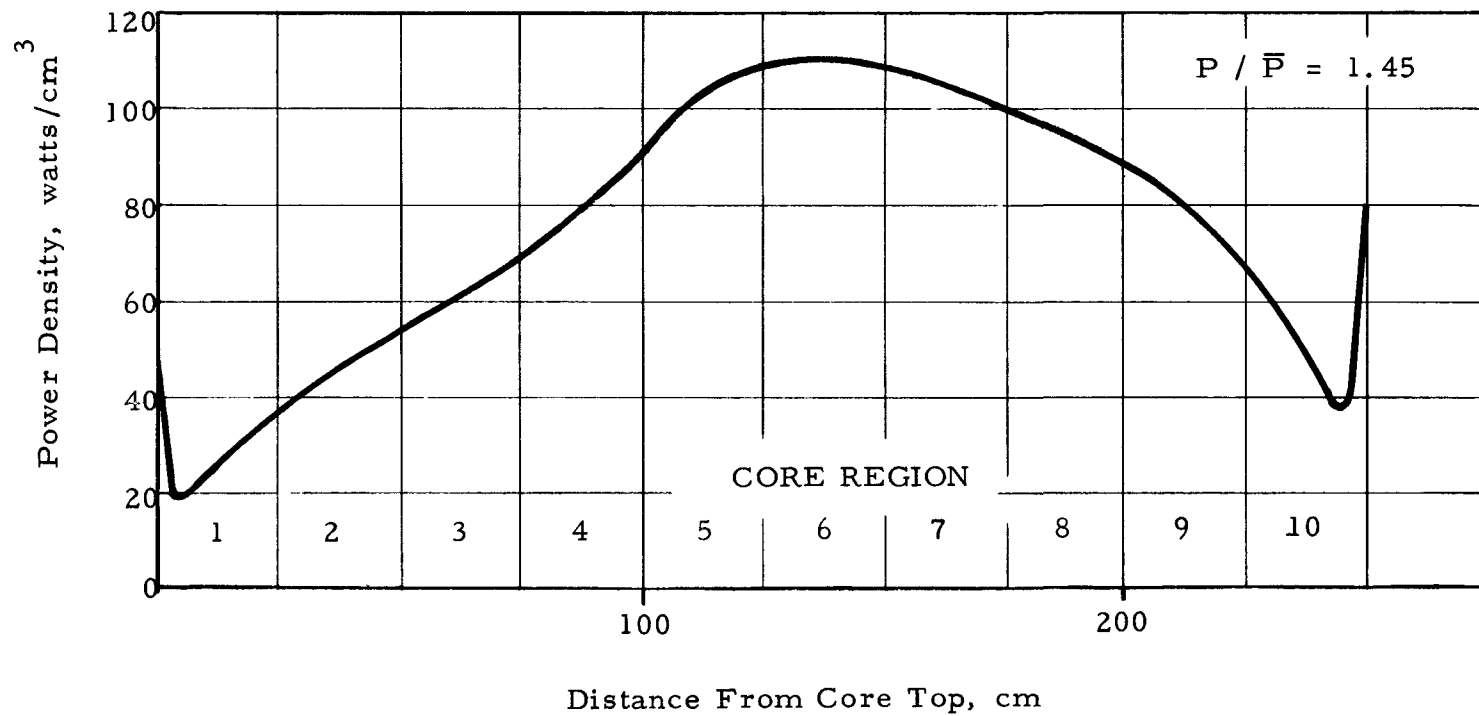FIG. 5.35: AXIAL POWER PROFILE AT 240 DAYS OF CORE LIFE



ROD GROUP POSITION

FIG. 5.36: AXIAL POWER PROFILE AT 270 DAYS OF CORE LIFE



$P / \overline{P} = 1.21$

Power Density, watts/cm$^3$

CORE REGION

1  2  3  4  5  6  7  8  9  10

Distance from Core Top, cm
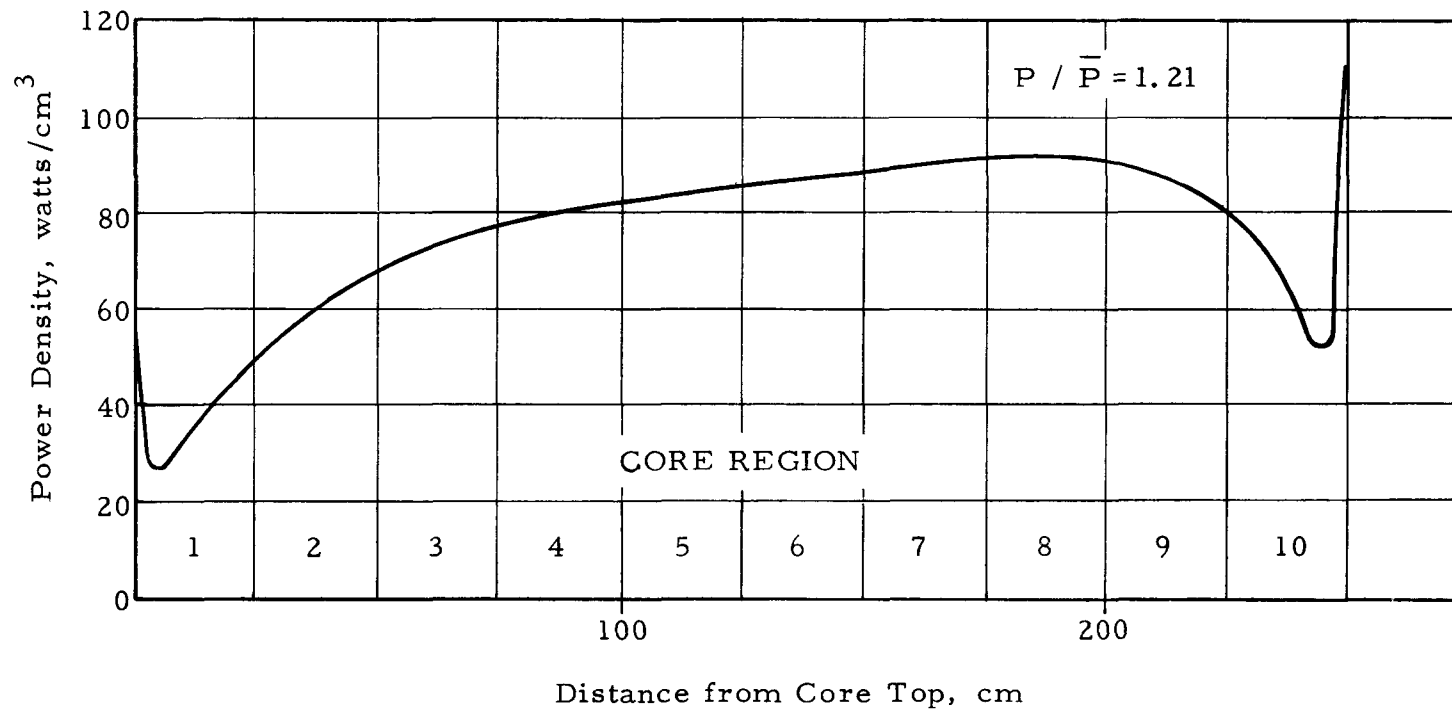
| GROUP   I |
| GROUP  II |
| GROUP III |

ROD GROUP POSITION

FIG. 5.37: AXIAL POWER PROFILE AT 300 DAYS OF CORE LIFE



P / $\overline{P}$ = 1.73

CORE REGION

Power Density, watts/cm$^3$

Distance From Core Top, cm
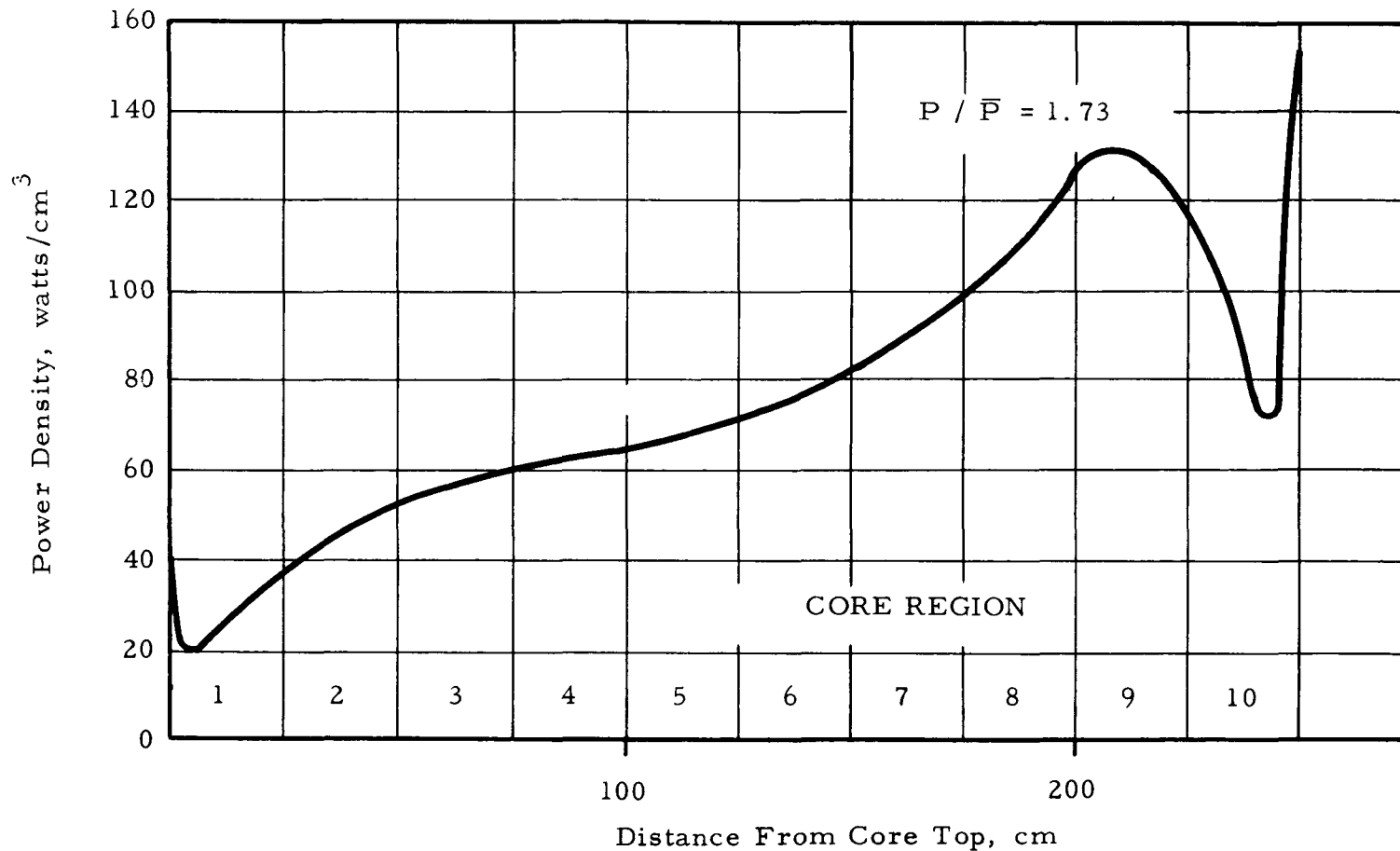
| GROUP I |
| GROUP II |
| GROUP III |

ROD GROUP POSITION

# FIG. 5.38: AXIAL POWER PROFILE AT 340 DAYS OF CORE LIFE

$P / \bar{P} = 1.62$

CORE REGION

| 1 | 2 | 3 | 4 | 5 | 6 | 7 | 8 | 9 | 10 |

Power Density, watts/cm$^3$

Distance From Core Top, cm
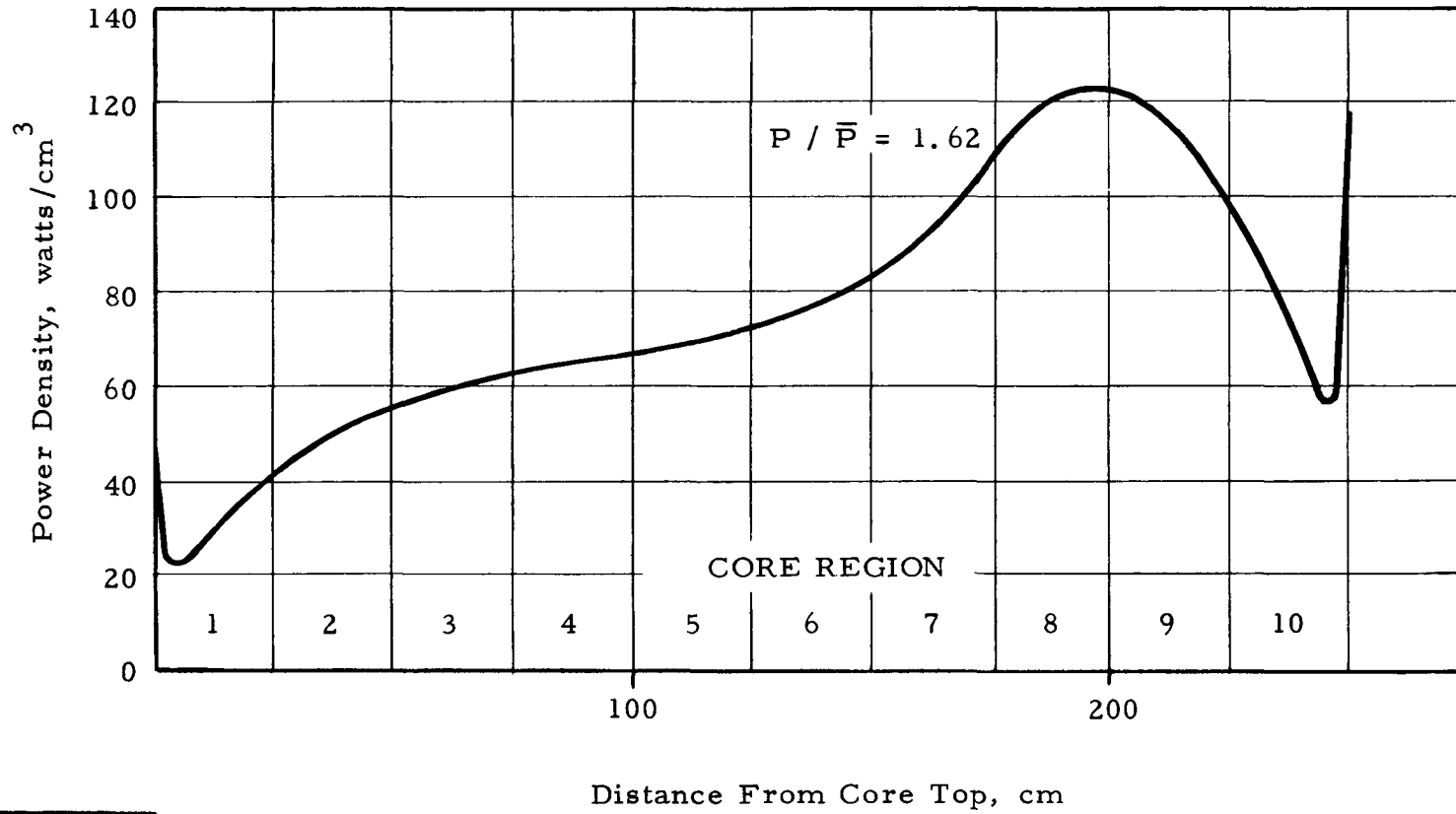
| GROUP I | |
| GROUP II | |
| GROUP III | |

ROD GROUP POSITION

# FIG. 5.39: AXIAL POWER PROFILE AT 370 DAYS OF CORE LIFE



$P / \overline{P} = 1.71$

CORE REGION

Power Density, watts/cm$^3$

Distance From Core Top, cm

| GROUP I | |
|---|---|
| GROUP II | |
| GROUP III | |
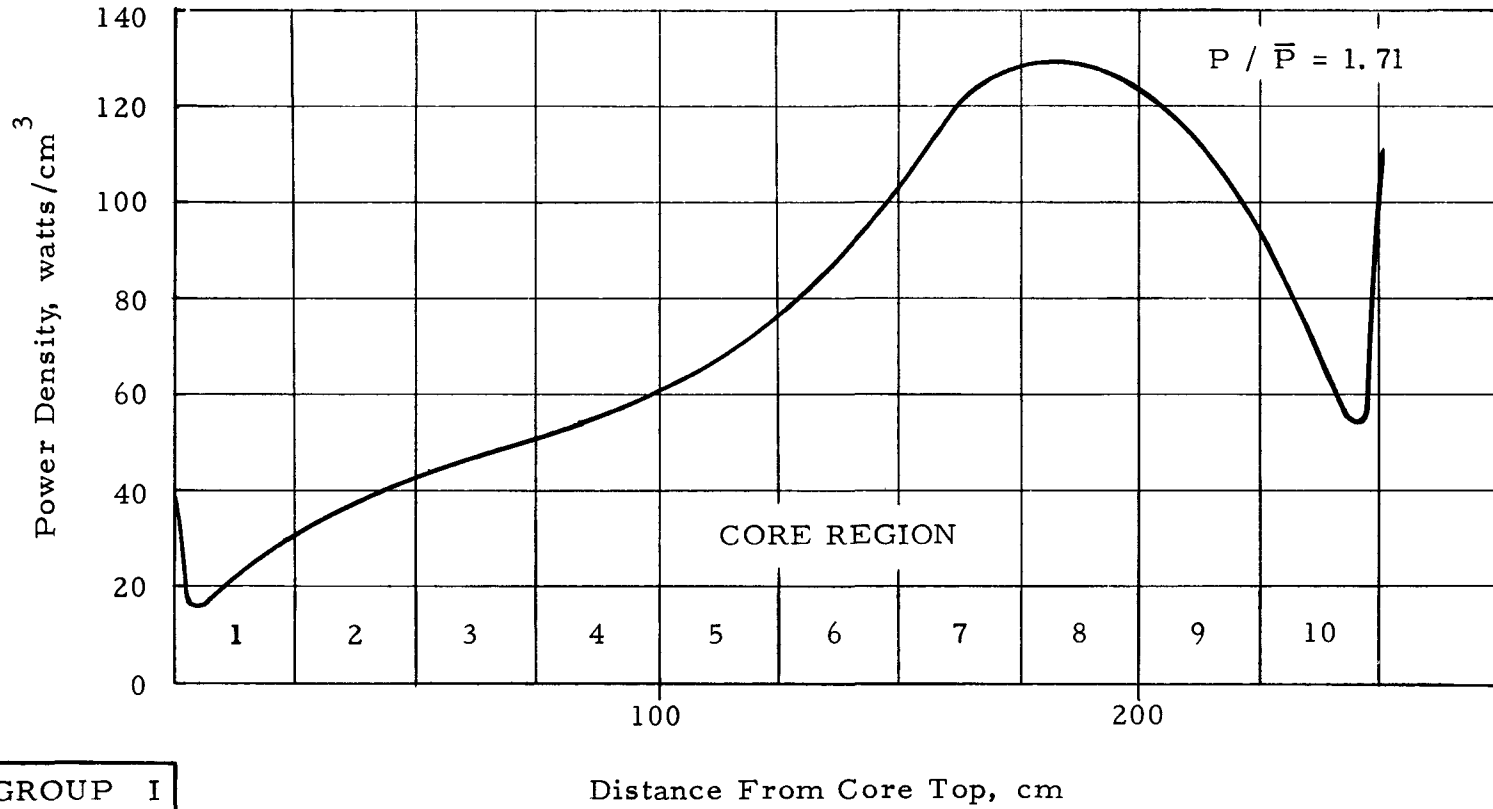
ROD GROUP POSITION

FIG. 5.40: AXIAL POWER PROFILE AT 420 DAYS OF CORE LIFE



Distance From Core Top, cm

| GROUP | I |
|-------|---|
| GROUP | II |
| GROUP | III |

ROD GROUP POSITION

FIG. 5.41: AXIAL POWER PROFILE AT 460 DAYS OF CORE LIFE

FIG. 5.42: AXIAL POWER PROFILE AT 500 DAYS OF CORE LIFE
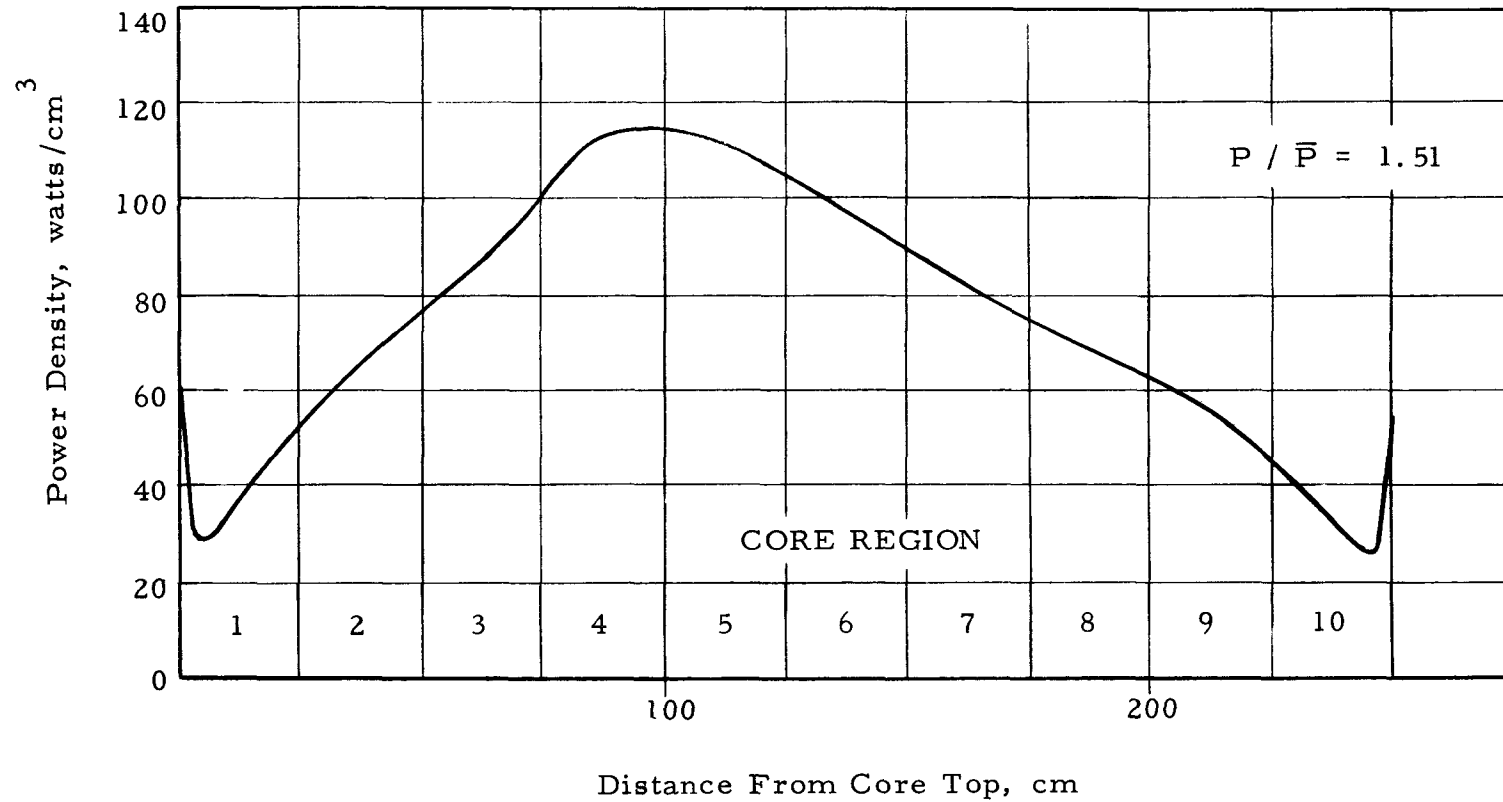
FIG. 5.43: AXIAL POWER PROFILE AT 540 DAYS OF CORE LIFE



$P / \overline{P} = 1.44$

Power Density, watts/cm$^3$

CORE REGION

| 1 | 2 | 3 | 4 | 5 | 6 | 7 | 8 | 9 | 10 |

100    200

Distance From Core Top, cm
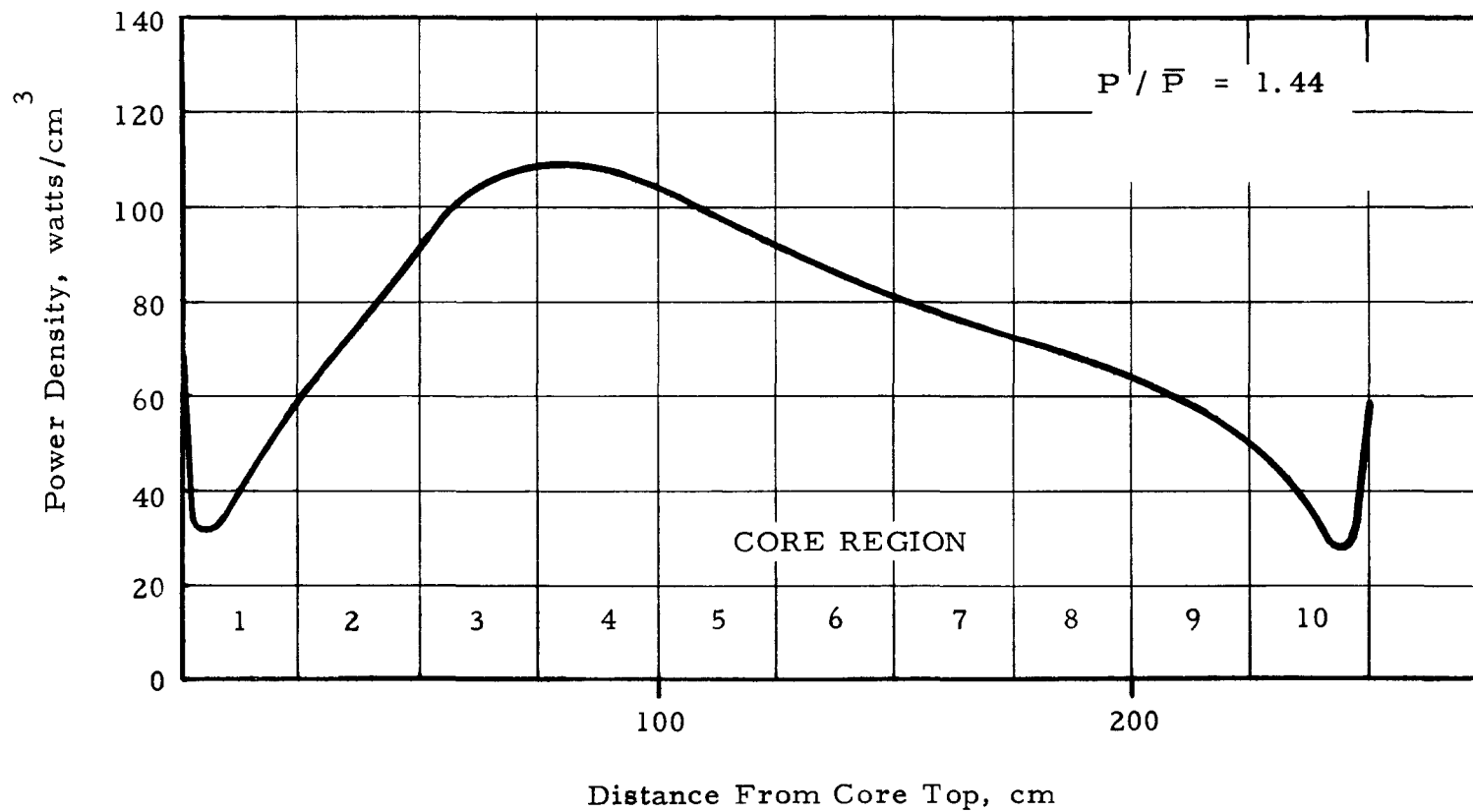
| GROUP I |
|---|
| GROUP II |
| GROUP III |

ROD GROUP POSITION

# FIG. 5.44: AXIAL POWER PROFILE AT 590 DAYS OF CORE LIFE

$P / \bar{P} = 1.63$

CORE REGION

1  2  3  4  5  6  7  8  9  10

Power Density, watts/cm$^3$

Distance From Core Top, cm
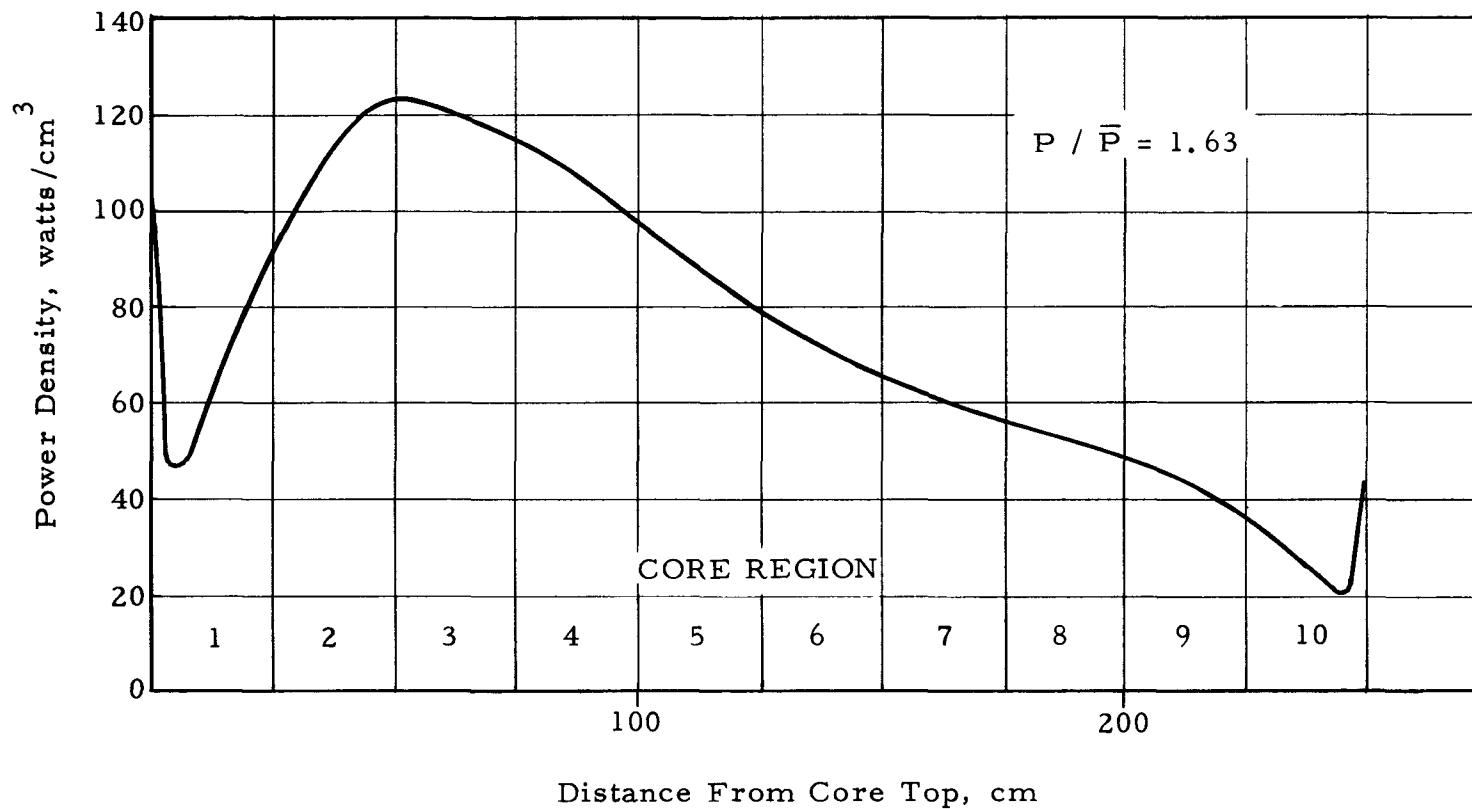
| GROUP I |
| GROUP II |
| GROUP III |

ROD GROUP POSITION

FIG. 5.45: AXIAL POWER PROFILE AT 630 DAYS OF CORE LIFE



$P \ / \ \overline{P} = 1.32$

CORE REGION

| 1 | 2 | 3 | 4 | 5 | 6 | 7 | 8 | 9 | 10 |

Distance From Core Top, cm
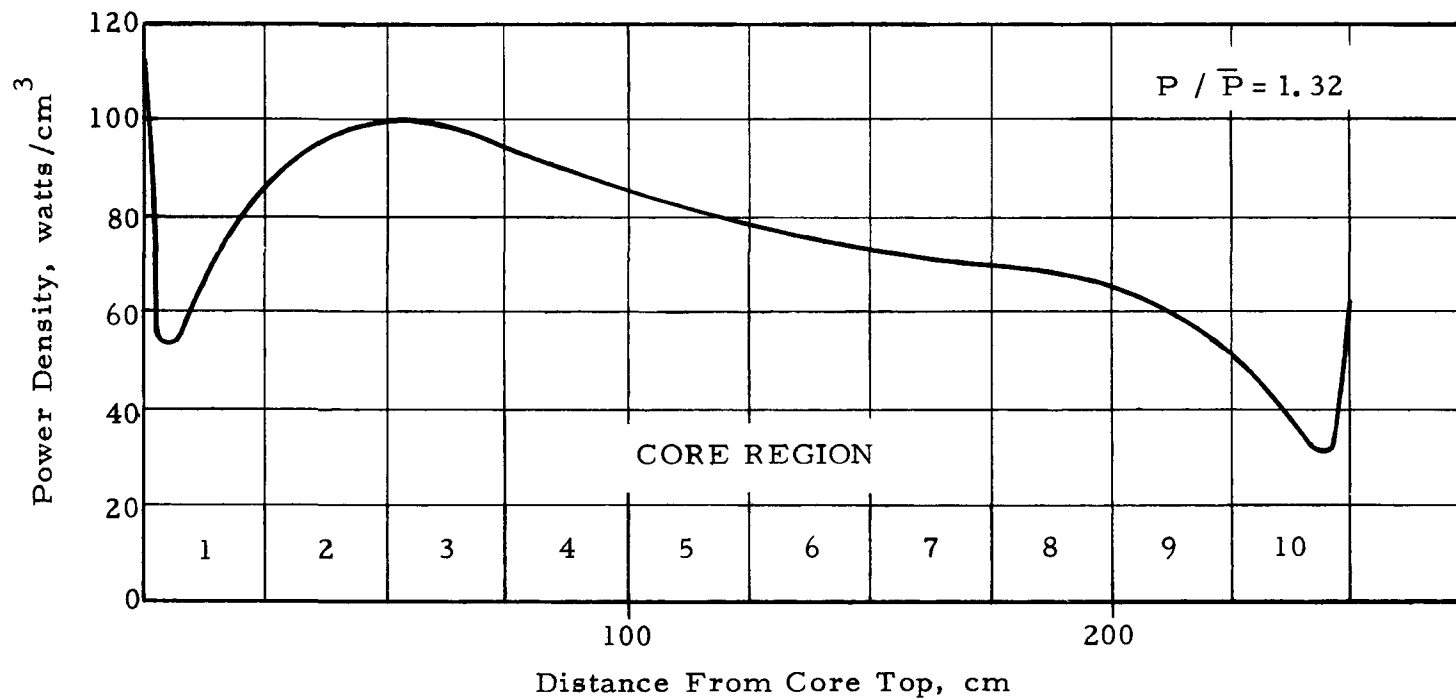
| GROUP I |
| GROUP II |
| GROUP III |

ROD GROUP POSITION

FIGURE B-1
TYPICAL GEOMETRY AND POWER DISTRIBUTION RESULTS
FOR TWO-DIMENSIONAL PDQ CALCULATIONS

540 - 170